3*H*-1,2,3,4-Triazaphospholes -Tuned 1*H*-1,2,3-Triazoles or Independent Ligand Class

Dissertation zur Erlangung des akademischen Grades des Doktors der Naturwissenschaften (Dr. rer. nat.)

Eingereicht im Fachbereich Biologie, Chemie, Pharmazie der Freien Universität Berlin

Vorgelegt von

## JULIAN ALEXANDER WOLFGANG SKLORZ

Aus Berlin

2016

Diese Arbeit wurde im Mai 2012 am Institut für Anorganische Chemie der Freien Universität Berlin unter Leitung von Herrn Prof. Dr. Christian Müller begonnen und im August 2016 fertiggestellt.

1. Gutachter: Prof. Dr. Christian Müller
2. Gutachter: Prof. Dr. Biprajit Sarkar
Disputation am 20.10.2016

To my parents Wolfgang Sklorz and Gundula Marduns Sklorz

As well as my siblings Christian, Sebastian and Florian Sklorz
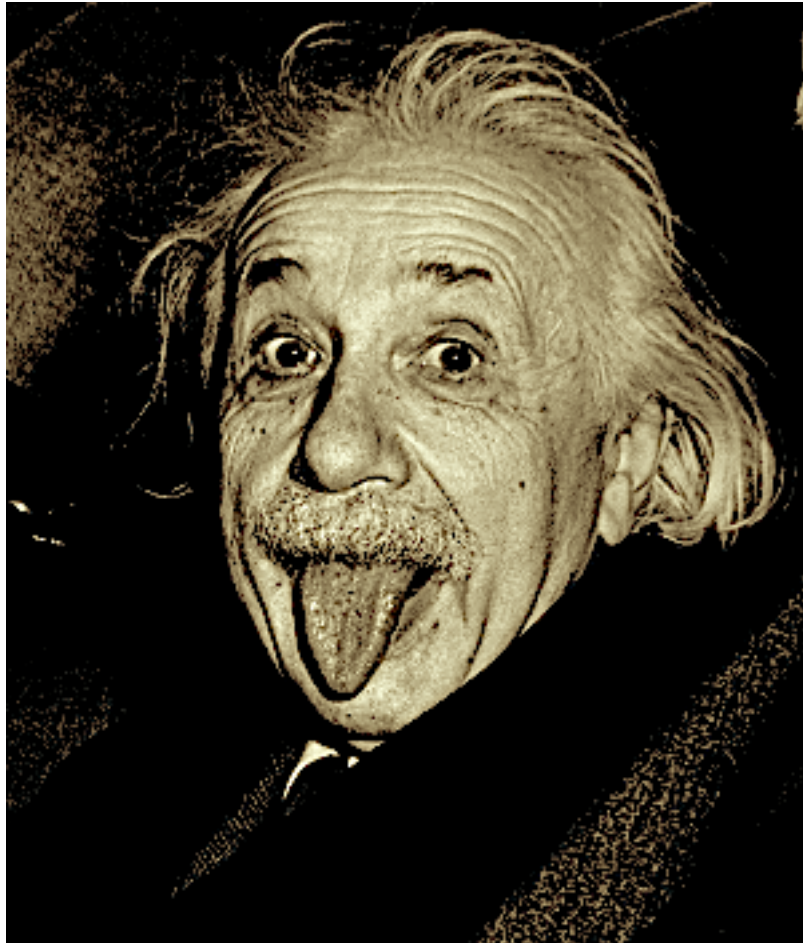
(Albert Einstein)

Declaration

I herewith confirm that I have prepared the present dissertation without the help of any impermissible resources. All citations are marked as references. The present thesis has neither been accepted in any previous doctoral degree procedure nor has it been evaluated as insufficient.

Berlin, August 2016

(Julian Sklorz)

Parts of this work have already been published:

(1)   „*Triazaphospholes versus Triazoles: An Investigation of the Differences between "Click"-Derived Chelating Phosphorus- and Nitrogen-Containing Heterocycles*" **Julian A.W. Sklorz**, Santina Hoof, Michael G. Sommer, Fritz Weißer, Manuela Weber, Jelena Wiecko, Biprajit Sarkar, Christian Müller, *Organometallics* **2014**, *33*, 511-516.

(2)   "*Recent Developments in the Chemistry of Pyridyl-Functionalized, Low-Coordinate Phosphorus Heterocycles*" Christian Müller, **Julian A. W. Sklorz**, Iris de Krom, Antonia Loibl, Marija Habicht, Marlene Bruce, Gregor Pfeifer, Jelena Wiecko, *Chem. Lett.* **2014**, *43*, 1390-1404.

(3)   "*Pyridyl-Functionalized 3H-1,2,3,4-Triazaphospholes: Synthesis, Coordination Chemistry and Photophysical Properties of Low-Coordinate Phosphorus Compounds*" **Julian A. W. Sklorz**, Santina Hoof, Nadine Rades, Nicolas de Rycke, László Könczöl,

Dénes Szieberth, Manuela Weber, Jelena Wiecko, László Nyulászi, Muriel Hissler, Christian Müller, *Chem. Eur J.* **2015**, *21*, 11096-11109*.*

(4)   "*Functionalized 3H-1,2,3,4-Triazaphosphole Derivatives: Synthesis and Structural Characterization of Novel Low-Coordinate Phosphorus Heterocycles*" **Julian A. W. Sklorz**, Maike Schnucklake, Matthias Kirste, Manuela Weber, Jelena Wiecko, Christian Müller, *Phosphorus Sulfur Silicon Relat. Elem.* **2016**, *191*, 558-562.

(5)   "*2,4,6-triphenylphosphinine and 2,4,6-triphenylposphabarrelene revisited: synthesis, reactivity and coordination chemistry*" Massimo Rigo, **Julian A. W. Sklorz**, Nils Hatje, Florian Noack, Manuela Weber, Jelena Wiecko, Christian Müller, *Dalton Trans.* **2016**, *45*, 2218-2226.

(6)   "*Recent developments in the chemistry of 3H-1,2,3,4-triazaphosphole derivatives*" **Julian A. W. Sklorz**, Christian Müller, *Eur. J. Inorg. Chem.* **2016**, *5*, 595-606.

Not included in this dissertation are the following publications, which originated from the authors studies and from joint research collaborations.

(1)   "*Gas-phase H/D-exchange reactions on resorcinarene and pyrogallarene capsules: Proton transport through a one-dimensional Grotthuss mechanism*" Henrik D. F. Winkler, Egor V. Dzyuba, **Julian A. W. Sklorz**, Ngong K. Beye, Kari Rissanen, Christoph A. Schalley, *Chem. Sci.* **2011**, *2*, 615-624.

(2)   "*Synthesis, Structure and Reactivity of Pentamethylcyclopentadienyl 2,4,6-Triphenylphosphinine Iron Complexes*" Rabak Rabak Rezaei Rad, Uttam Chakraborty, Bernd Mühldorf, **Julian A. W. Sklorz**, Michael Bodensteiner, Christian Müller, Robert Wolf, *Organometallics* **2015**, *34*, 622-635.

(3)   *Clicking the Arsenic-Carbon Triple Bond: An Entry into a New Class of Arsenic Heterocycles,* Gregor Pfeifer, Martin Papke, Daniel Frost, **Julian A. W. Sklorz**, Marija Habicht, Christian Müller, *Angew. Chem. Int. Ed.* **2016**, DOI: 10.1002/anie.201605143.

Acknowledgment

First of all, I would like to thank Prof. Dr. Christian Müller for the opportunity and the trust to be part of his Berlin group from the very beginning. I am very grateful for his support, feedback and guiding as well as his literally "policy of an open door". This yielded several (joint) research projects and the realisation of my own ideas and the opportunities to join scientific conferences are to appreciate as well.

Furthermore, I like to thank my co-promoter Prof. Dr. Biprajit Sarkar not only for being reviewer for this dissertation, but also for his expertise on the 1H-1,2,3-triazoles and the joined research projects as well as imbedded fruitful discussions.

I also want to express my gratitude to Prof. Dr. Muriel Hissler for fluorescence spectroscopy and Prof. Dr. László Nyulászi for DFT calculations in joined research collaborations. Here, I want to thank Prof. Dr. Tibor Pasinszki for the photoelectron spectroscopy.

Dr. Jelena Wiecko I want to thank for leading and mastering the starting phase of the group and introducing me into inorganic working techniques, and that I always could count on her support and a sympathetic ear as well as research related discussions. Besides that, I want to thank her for several single crystal X-ray diffraction analyses and first steps into X-ray crystal structure determinations.

Dr. Naina Deibel and Dr. Fritz Weißer I want to thank both for the introduction into cyclic voltammetry measurements and the whole Sarkar group for using their equipment, like their potentiostat, coffee machine, ale-bench and grill, as well as the incorporations into the research of the effects of ethanol and meat on the human body.

The students M. Sc. Santina Hoof, M. Sc. Nadines Rades, M. Sc. Sebastian Brühl, M. Sc. Martin Papke and B. Sc. Maike Schnucklake I want to thank for their help with the experimental work during their research internship in the group as well was my bachelor student B. Sc. Matthias Kirste.
Especially I would like to thank B. Sc. Selina Kaiser for finishing my experimental work in her master thesis.
Markus Peschke and Dorian Reich I am very grateful for carrying out several reactions.

My temporary lab-mate Annet Vliegenthart I want to thank a lot for the hilarious times in the lab and in private life. I liked our bets a lot! Also I want to thank her for cheering me up and supporting me.

Further, I also want to thank my second Dutch lab mate, Johan de Boed for our nice discussions about chemistry.
I am very grateful to M. Sc. Antonia Loibl, whom I also shared a lab for a certain amount of time with. M. Sc. Massimo Rigo and M. Sc. Marlene Bruce (*aka* the kitchen group) for the very nice time in Ireland and for the nice and critical discussions of results and chemical problems, to this also M. Sc. Steven Giese and Dr. Fanni Daruny Sypaseuth contributed.

Dipl.-Chem. Gregor Pfeifer I would like to thank for the collaborations we attempted and carried out.

Dr. Jelena Wiecko, Dr. Mirko Lohse, M. Sc. Antonia Loibl, M. Sc. Steven Giese, M. Sc. Massimo Rigo and M. Sc. Annet Vliegenthart I would like to thank for proofreading this work. For the nice time and chemical discussions I would like to thank the whole group.

Manuela Weber, Dr. Adelheid Hagenbach and Prof. Dr. Dieter Lentz for solving crystal structures and helping in all possible fashions.

Representative for the analytic core facilities I would like to thank Dr. Andreas Springer for the performed mass spectrometric and Dr. Andreas Schäfer for the NMR spectroscopic analysis. However, the contribution of Dipl.-Ing. Fabian Klautzsch and Bettina Zeisig I would like to highlight in this context for special measurements.

Dr. Mirko Lohse Christian Grunewald, Anja Sokolowski, Christian Goroncy, Sabine Reimann Johannes Ulrich my former fellow students I gratitude for finishing the chemistry studies with me as well as good friendships we developed.

Last but not least, I would like to thank my parents for their continuous support over the years.

Abstract

Within this work, a systematic study on the synthesis, coordination chemistry, reactivity and application of 3*H*-1,2,3,4-triazaphospholes has been performed for the first time. Thereby, two different phosphaalkynes have been used to investigate the influence of the substituent in 5-position. However, the assumed influence proved to be only of minor importance, as it was derived from Tolman parameters and cyclic voltammetry measurements. In order to synthesise *tert*-butyl phosphaalkyne **A2** on a large scale, the synthesis protocol of the phosphine source P(TMS)$_3$ has been significantly improved and the origin of long reaction times has been determined. From monodentate ligands **L1**-**L3**, no metal complex could be obtained, although a correlation of electron-withdrawing substituents in 3-position their stability could be shown. An interesting N$_2$ elimination pathway led to a promising synthesis strategy for iminophosphanes starting from readily available precursors.

Different approaches for chelating 1,2,3,4-triazaphospholes have been engaged, showing that non-conjugated compounds - especially the alkoxy binding side - are less promising compared to the conjugated systems. This was nicely demonstrated by the various investigations towards applications in the field of light-emitting phosphorus containing molecular materials. Although the emitted light was shifted too far into the blue regime, no optimisation of the substitution pattern was performed, leaving room for qualitative improvements and a potential application in OLEDs. A first step for improvement is achieved with the investigation of photoelectron spectroscopy experiments, although not all results are available up to this point.

This concept can also be transferred to the electrochemical carbon dioxide reduction. From DFT calculations as well as from the crystallographic characterization regarding the suitability of the ligand properties, an electron accepting ligand is critical since the organic framework acts as a capacitor providing the right potential for the catalytic active metal centre. Although approaches with Mn(I) and Re(I) complexes lack in the right reduction potential, an electronically fine-tuned ligand realised by the right substitution pattern might be suitable for carbon dioxide reduction.

The striking results obtained from the CuAAC reactions might present the potential strength of these concept ligands. The triazaphosphole based complex showed to be much faster compared to the triazole based ones. Further, indications for autocatalysis were found, while the triazole copper complex gets inhibited by product formation.

However, the root of the magnificent enhancement of the catalysis reaction remains unclear since the molecular structure in the crystals does not reveal any influence of the π-accepting ligand and thus might only be attributed structural aspects and intermolecular interactions.

Modification of 1,2,3,4-triazaphospholes revealed interesting results concerning their counterpart. The methylation of triazaphospholes is only possible with monodentate ligands and the resulting triazaphosphole-1-ium salts proved much less stable than the 1,2,3-triazolium salts. Proton and carbon NMR spectra strongly indicate the formation of the desired compounds, although the stability of the compounds prevented investigations by means of mass spectrometry and X-ray diffraction. Metal coordination towards Cu(I) failed.

In the second part of this thesis, cycloreversion reactions were tested since it is known for other diaza-, triazaphospholes and phosphinines. However, the 1,2,3,4-triazaphosphole framework proved much less reactive and only proceeded with perfluorobut-2-yne in very long reaction times. Furthermore, the non-conjugated systems distinguished from the conjugated ones by even higher conversion times. The combination of multicore NMR analysis unequivocally proved the formation of the cycloreversion product. Preparative attempts were only carried out with the conjugated systems **28** and **L12**. Both ligands were employed in metal coordination, although they either underwent decomposition or no hint of coordination could be obtained. At least it was possible to characterise one cycloreversion product by means of X-ray diffraction analysis.

Kurzzusammenfassung

Die vorliegende Dissertation beinhaltet die erste systematische Studie über die Synthese, Koordinationschemie, Reaktivität und Anwendung von 3*H*-1,2,3,4-Triazapospholen. Auf Basis zweier unterschiedlicher Phosphaalkine wurde der Einfluss des Substituenten in 5-Position bestimmt. Mithilfe einer Abwandlung von Tolmans elektronischem Parameter sowie zyklischer Voltammetrie konnte ein Einfluss der gegensätzlich wirkenden Substituenten festgestellt werden, jedoch war dieser gering. Im Rahmen der Hochskalierung der Synthese des *tert*-butyl substituierten Phosphaalkines **A2** konnte die Vorschrift zur Herstellung der Phosphor(III)quelle (P(TMS)$_3$) signifikant verbessert werden. Hauptgrund hierfür war die Identifizierung der Ursache zwischen der berichteten und der tatsächlichen Reaktionszeit.

Die Verwendung der monodentaten Verbindungen **L1-L3** als Liganden ergaben keine Komplexverbindungen mit den ausgewählten Metallen. Ausnahme ist Verbindung **L3**, die interessanterweise unter N$_2$ Abspaltung einen Gold Komplex ergab und als mögliche, neuartige Synthesestrategie für Iminophosphane betrachtet werden kann.

Verschiedene Ansätze zu chelatisierenden 3*H*-1,2,3,4-triazaphospholen ergaben, dass nicht konjugierte Verbindungen, besonders solche mit Alkoxy-Bindungsstellen, weniger nützlich sind. Insbesondere die unterschiedlichen Anwendungen zeigten den klaren Vorteil der konjugierten Verbindungen, beispielsweise im Feld der licht-emittierenden phosphorhaltigen Materialien. Zwar zeigte diese in den Fluoreszenzmessungen eine Emission im UV-Bereich, jedoch wurde bei den Verbindungen nicht das Substitutionsmuster optimiert um eine Verschiebung in den sichtbaren Bereich und damit den Einsatz als OLED zu ermöglichen. Um genauere Informationen über den Aufbau der Molekülorbitale und damit für die Optimierung einen richtungsweisenden Schritt zu machen, wurden ausgesuchte Verbindungen mit Hilfe der Ultraviolett-Elektronenspektroskopie untersucht. Die meisten Ergebnisse stehen jedoch noch aus.

Das Konzept der konjugierten Systeme wurde auf die elektrochemische Reduktion von Kohlenstoffdioxid angewendet. Vorherige DFT Berechnungen sowie die Ergebnisse der Röntgenstrukturanalyse wiesen darauf hin, dass die beiden 2-Pyridyl-subsituierten Verbindungen **L12** und **L14** das Potential bieten, zusätzliche elektronendichte im LUMO aufzunehmen. Da der Ligand in der Metall katalysierten CO$_2$-Reduktion als Kondensator fungiert, wurden zyklovoltammetrische Messungen unter Ar, in gesättigter CO$_2$-Lösung und in gesättigter CO$_2$-Lösung mit 5%-igem Wasserzusatz durchgeführt. Die ermittelten

Potentiale liegen jedoch weit unterhalb für die Katalyse notwenigen Schwelle. Eine Optimierung des Substitutionsmusters am Liganden wurde nicht weiterverfolgt, es ist jedoch anzunehmen, dass dieses erfolgsversprechende Verbindungen hervorbringen könnte.

Im Gegensatz dazu konnte mit dem Einsatz der beiden Triazaphosphole **L12** und **L14** als Liganden in der CuAAC sehr interessante Ergebnisse erzielt werden. Der Triazaphosphol-basierte Komplex zeigte eine sehr schnelle Umsetzung ebenso wie Hinweise auf eine autokatalytische Reaktion – in begrenztem Rahmen. Der Triazol-basierte Cu(I) Komplex hingegen wies sehr hohe Reaktionszeiten auf und zeigte, dass das Produkt oder das Produktadditiv die Reaktion inhibierte. Die Ursache für dieses gegensätzliche Verhalten konnte nicht direkt identifiziert werden. Der Vergleich der Ergebnisse der Röntgenstrukturanalyse ergab keine signifikanten Unterschiede, weshalb nicht das bessere π-Akzeptorvermögen für die höhere Aktivität herangezogen werden kann. Jedoch könnten entweder strukturelle Aspekte und/oder intermolekulare Wechselwirkungen eine Ursache sein.

Zuletzt wurde versucht die Triazaphosphole analog zu 1*H*-1,2,3-Triazolen sowie zu Phosphininen zu modifizieren. Die bei Triazolen bekannte Methylierung wurde bei den Triazaphospholen bisher noch nicht untersucht. Da nach einer literaturbekannten Methode für chelatisierende Triazaphosphoniumsalze keine entsprechenden Erfolge festzustellen waren, wurden lediglich monodentate Verbindungen verwendet. Es zeigte sich jedoch, dass die 3*H*-1,2,3,4-Triazaphospholiumsalze sehr viel (termisch) labiler sind, als die ausschließlich Stickstoff beinhaltenden Heterozyklen. So konnten der Phosphor-Heterozyklus zwar mittels NMR Spektroskopie charakterisiert werden, jedoch gelang es ihn weder massenspektrometrisch noch röntgenkristallographisch nachzuweisen. Die Koordination an ein Kupfer(I) ion misslang ebenfalls.

In zweiten Teil der Modifikationen von 3*H*-1,2,3,4-Triazapospholen wurden diese auf ihr Verhalten in Diels-Alder-Reaktionen untersucht. Die Reaktionsparameter der bereits untersuchten Derivate der 2*H*-1,2,4,3-Triazaphosphole ließen sich nicht übertragen, da ausschließlich bei langen Reaktionszeiten und mittlerer Temperatur ein sauberes Produkt erhalten werden konnte. Hierbei zeigte sich, dass auch zwischen den konjugierten und nicht-konjugierten Verbindugnen differenziert werden muss, da die nicht-konjugierten eine noch längere Reaktionszeit benötigten. Präperative Ansätze wurden daher nur mit den Phenyl- und 2-Pyridyl substituierten Komponenten **28** und **L12** durchgeführt. NMR-spektroskopische Untersuchungen ergaben einen zu

(Di)-Azaphophininen analogen Reaktionsverlauf. Zwar konnte kein Metallkomplex erhalten werden, jedoch das Phenylderivat kristallographisch charakterisiert werden.

Table of Content

Table of Schemes

Table of Figures

Table of Tables

Table of Abbreviations

μW	micro wave irradiation
$\tau_{1/2}$	half-life period
T	Torsion Angle
cm^{-1}	Unit of the wave number
aNHCs	Abnormal N-Heterocyclic Carbenes
atm	Atmosphere
Bn	benzyl
Bu	butyl
BDE	Bond Dissociation Energy
Cp	cyclopentadienyl
Cp*	pentamethyl cyclopentadienyl
CuAAC	Copper Catalysed Alkyne Azide Cycloaddition
CV	Cyclic Voltammetry
bpy	2,2'-Bipyridine
d	doublet
DABCO	1,4-diazabicyclo[2.2.2]octane
DBU	1,8-Diazabicyclo[5.4.0]undec-7-ene
DCM	Dichloromethane
DDQ	2,3-Dichloro-5,6-dicyano-1,4-benzoquinone
DFT	Density Functional Theory
$-d_x$	x-times deuterated solvent
DMSO	dimethyl sulfoxide
E_g	HOMO-LUMO energy gap
Et_2O	diethyl ether
EtOH	Ethanol
EN	Electronegativity
E_{PA}	Proton affinity
EPR	Electron Paramagnetic Resonance
Eq.	Equivalents
EXAFS	Extended X-ray Absorption Fine Structure
f	Oscillator Strength
h	hour

HOMO	Highest Occupied Molecular Orbital
HOMO-#	Molecular Orbital # below the HOMO
HF	Hartree-Fock
IE	Ionisation Energy
ILCT	Inter Ligand Charge Transfer
IR	Infrared
IR-SCE	Infra Red Spectro Electro with Standard Calomel Electrode
LMCT	Ligand to Metal Charge Transfer
LUMO	Lowest Unoccupied Molecular Orbital
m	multiplet
m-CPBA	*Meta*-chloroperoxybenzoic acid
Me	methyl
MeCN	Acetonitrile
Mes	mesityl
Mes*	super-mesityl
min	minute
NBS	*N*-Bromosuccinimide
NHCs	*N*-heterocyclic carbenes
NICS	Nuclear Independent Chemical Shift
n.o.	not observed
nNHCs	N-heterocyclic carbenes
NMR	nuclear magnetic resonance
nm	Nanometer
n.p.	Not Performed
o	ortho
OLED	Organic Light Emitting Diode
OTf	trifluoromethanesulfonate
Q	Electronic Charge in eV
p	para
ppm	Parts Per Million
Ph	phenyl
Py	pyridine
r.t.	room temperature
s	singlet

SCE		Standard Calomel Electrode
sec		Seconds
t		triplet
^{t}Bu		*tert*-butyl
tbta		tris[(1-benzyl-1*H*-1,2,3-triazole-4-yl)methyl]amine
THF		Tetrahydrofuran
TMS		trimethylsilyl
TAP		triazaphosphole
TA		triazole
Ts		tosyl
TOF		Turn Over Frequency
UPS		Ultraviolet Photoelectron Spectroscopy
UV		Ultraviolet
UV/Vis		Ultraviolet–Visible Spectroscopy
vs		versus

1 Introduction

1.1 Low-Coordinate Phosphorus Compounds

Intense research on organophosphorus compounds revealed the phosphorus atom to be a chemical chameleon. The ability to mimic its neighbours (silicon, nitrogen and carbon) in the periodic table of the elements, depending on the oxidative state, was cause for fascination.[1] Especially the low-coordinate phosphorus compounds are very interesting because they mimic the chemical behaviour of the carbon atom (*vide infra*). First, the classification of different coordination states is necessary. "Classical" phosphorus compounds are defined as $\lambda^3\sigma^3$ compounds, where λ corresponds to the valency and σ to the coordination number (Figure 1, **1**). The $\lambda^3\sigma^2$ phosphaalkene (**2**) was synthesised by Gerd Becker and represented the first low-coordinate phosphorus compound with located π-electrons.[2] Previous contributions by Dimroth and Hoffmann as well as Märkl and Ashe dealt with compounds, in which the C=P bond was part of a conjugated system.[3–6] Indication of the successful synthesis of the first phosphaalkyne, a $\lambda^3\sigma^1$ compound (**3**), was reported by Gier (R = H in **3**).[7]
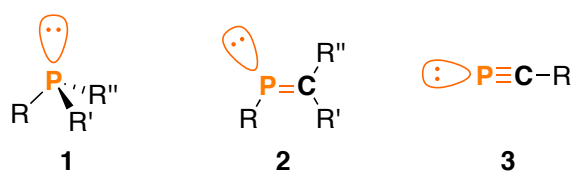
Figure 1: Selected coordination states of phosphorus.

1.1.2 Properties of Phosphaalkenes

Because this work is focuses on aromatic compounds containing C=P bonds, only important information about systems of type **2** will be given. Starting with the electronegativity (EN) according to the Pauling scale, the EN of carbon (2.5) is higher than the EN of phosphorus (2.2) and nitrogen has the highest electronegativity of these elements, causing a slightly negative or positive polarised carbon atom, respectively. The phosphorus atom has a stronger π-accepting capacity than nitrogen, leading to the overall outcome of a relatively apolar C=P system.[8–10] The parent phosphaalkene

methylenephosphane **4** ($H_2C=PH$), ethene **5** ($H_2C=CH_2$) and methanimine **6** ($H_2C=NH$) have been investigated using UV photoelectron spectroscopy. The order of the molecular orbitals, assigned by these experiments, exhibited a higher correlation of the phosphorus-carbon and the carbon-carbon system than with its lower homologue. The HOMO of both compounds consist of the π-bond, while the phosphorus lone pair was determined to contribute to the HOMO-1, while the arrangement in the methanimine is *vice versa* (Figure 2).[11,12] The results predict for the $\lambda^3\sigma^2$ phosphorus compound the tendency to undergo reactions with the C=P bond rather than on the lone pair. In contrast, the nitrogen atom will first provide its lone pair, because it is located in the HOMO and the energy difference between the HOMO and HOMO^{-1} is large.

	4	5	6
HOMO	-10.30 eV	-10.51 eV	-10.62 eV
HOMO-1	-10.70 ev		-12.49 ev
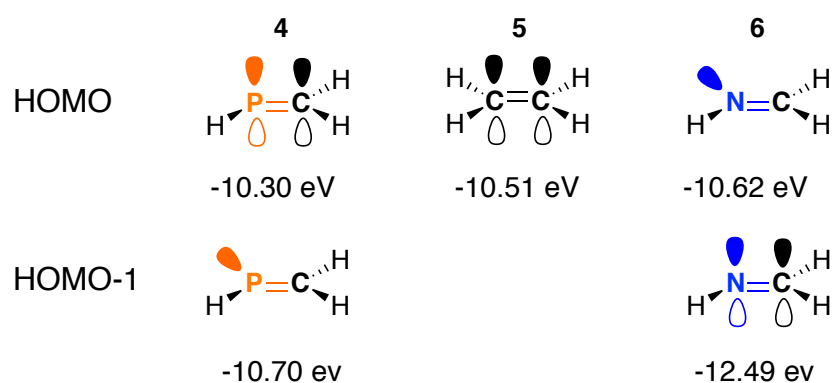
Figure 2: Molecular orbital arrangement in methylenephosphane **4**, ethene **5** and methanimine **6**.

Natural bond analysis (B3PW91/6-311++G(3df,2p)) of the geometry optimised structures exposed further differences. The 3*s* atom orbital of the phosphorus atom contributes 66% to its lone pair and the 3*p* only 34%. In methanimine, an almost inverted situation was found, as the nitrogen lone pair showed significant 2*p* (61%) and correspondingly less 2*s* character (39%). Moreover, the calculated strength of the C=P π-bond was determined to be 43 kcal mol^{-1} while the C=C π-bond is 65 kcal mol^{-1} strong.[12,13] The setup of the molecular orbitals causes a unique orientation of the lone pair. The C-P-lone pair angle is around 20 ° below the corresponding one in the nitrogen based system. The overall outcome of these results demonstrates the weak hybridisation ability of the phosphorus atom, caused by a weak 3*s*-3*p* overlap.[10] Another important structural aspect is the C=P bond distance with an average length of 1.60-1.70 Å.[1]

Besides the UPS experiments and the DFT calculations, the high similarity between carbon phosphorus double (and triple) bonds were confirmed by NMR investigations[14]

and led to the conclusion that phosphorus can "copy" the chemical behaviour of carbon.[15]

1.1.3 Coordination Chemistry of Phosphaalkenes

As a consequence of the energetically small differences between the phosphorus carbon π-bond and the phosphorus lone pair, metal coordination proceeded in different fashions. η^2-metal coordination of the double bond (Figure 3, **7**) results in elongation of the carbon phosphorus bond due to ligand metal π-bonding and metal ligand π-backbonding.[1] The σ-coordination of a metal centre of type **8** through the phosphorus lone pair is also possible. Even a complex equilibrating between both modes was observed.[16] Therefore, the bimetallic η^1-η^2-metal complexes of type **9** are plausible.[17] Other bimetallic complexes are increasing the coordination number of the phosphorus atom from three to four with resembling to structure **10**.[18] The coordination of three metal centres was shown as well. The phosphorus atom lone pair coordinate two while the third is coordinated by the phosphorus atom and one binds *via* the C=P bond (Figure 3, **11**).[17,19]
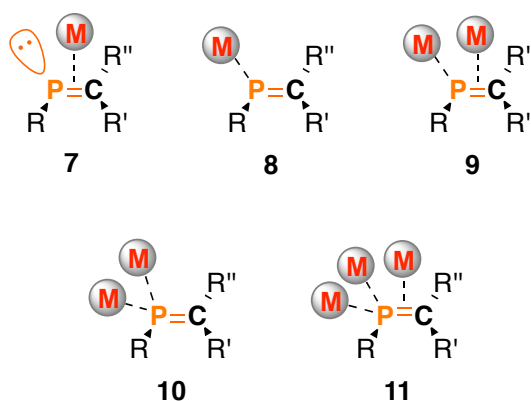
Figure 3: Coordination modes of phosphaalkenes.

1.1.4 Reactivity of Phosphaalkenes

The similarities in the energy levels of the first two occupied molecular orbitals resembled by the chemical behaviour of these compounds. Most interestingly, no protonation of the phosphorus lone pair is possible, but the compound undergoes

selective addition and, due to the apolar nature of the C=P bond, the regioselectivity is controlled by the substituents (Scheme 1). The addition of hydrogen chloride to a positive polarised phosphorus atom yielded the phosphorus dichloride (**Eq. 1**).[20] The variation of the substitution pattern results in a change of the regioselectivity (**Eq. 2**).[21] While these two reactions proceeded without any interaction to the phosphorus lone pair, some reactions on the C=P bond do not work, because of interferences with the lone pair.[15]
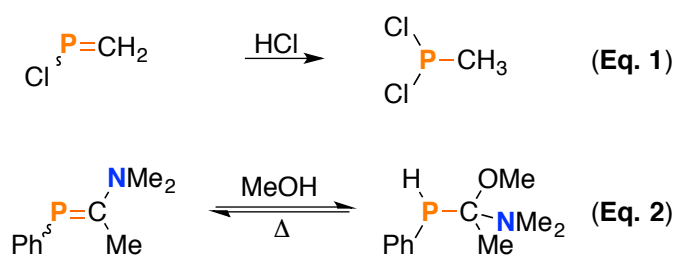
Scheme 1: Control of regioselectivity by substituent effects.

Epoxidation with *m*-CPBA and *cis*-hydrogenation are only possible, if the phosphorus lone pair is coordinated, e.g. to a **W**(CO)$_5$ fragment (Scheme 2, **Eq. 3**). Also the hydrogenation is only possible, if interferences with the lone pair are inhibited by coordination (**Eq. 4**).[22,23]
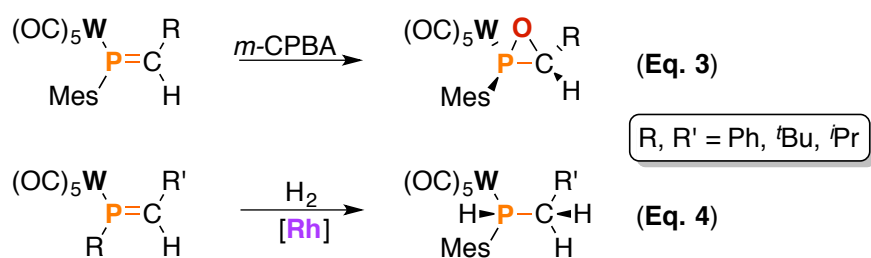
Scheme 2: Examples for C=P addition reactions showing phosphorus lone pair interference.

1.2 Phosphaalkynes[24]

Phosphaalkynes are, as mentioned before, $\lambda^3\sigma^1$ phosphorus compounds and the phosphorus carbon triple bond is a good example to demonstrate that the "double bond rule" is outdated. Already in 1961 Gier was able to electrochemically synthesise the parental phosphaalkyne (HCP, **1**) from phosphane.[7] This compound is very reactive and tends to polymerise above T = -70 °C, but can be stored at room temperature under reduced pressure. Later, a more convenient method for the synthesis of **1** was established. The reaction is based on hydrogen halide elimination by flash pyrolysis. The reaction procedure was transferred to several phosphaalkynes, which were all thermally and kinetically instable (**2**-**8**, Figure 4).[25-29] "Medium stable" phosphaalkynes were also discovered, but the half-life times are still unpleasantly short. For example, the phenyl substituted phosphaalkyne **9** has a $\tau_{1/2}$ = 7 min at T = 0 °C.[30] The TMS-CP **10** compound shows with $\tau_{1/2}$ = 50 min at T = 20 °C even a higher stability. Russell *et al.* developed a synthesis, yielding **10** as a temperature stable adduct with aromatic solvents.[31]

1.2.1 Kinetically and Thermally Instable and Stable Phosphaalkynes

The first kinetically stable phosphaalkyne was prepared in 1981 by Becker and co-workers with the *tert*-butylphosphaacetylene (Figure 4, **11**).[32] Within this decade, other stable phosphaalkynes were discovered **12**-**14**.[33-35] They all share in common a sterical demanding substituent, providing kinetic stabilisation. In the late 1990s and beginning of the 21st century, an adamantyl-based bisphosphaalkyne **15** was reported by Veek[36] and the triptylene-based bisphosphaalkyne **16**.[37]
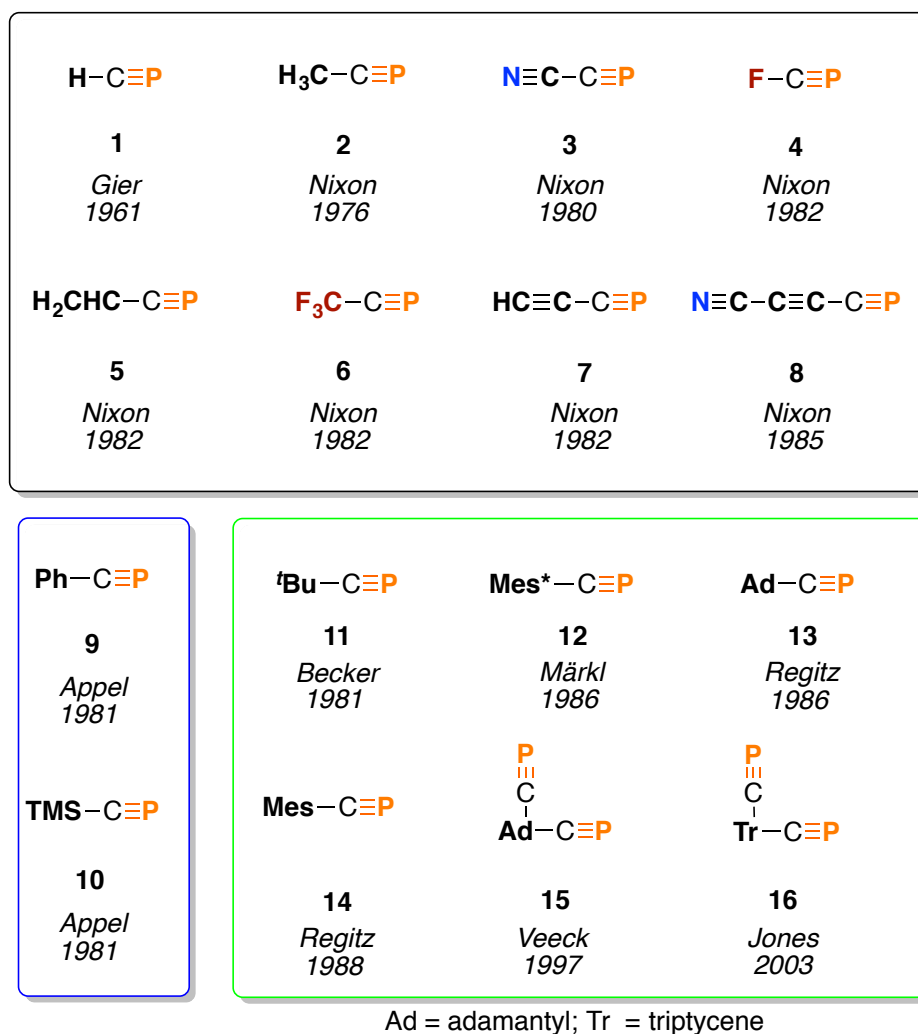
Figure 4: Overview of the unstable (black box), medium stable (blue box) and stable (green box) phosphaalkynes.

1.2.2 Synthesis of Phosphaalkynes

The synthetic pathways of phosphaalkynes are as various as their substitution pattern. As mentioned at the beginning, the conversion of PH_3 at a graphite electrode[38] (**Eq. 1**, Scheme 3) and the hydrogen halide elimination by flash pyrolysis at high temperatures up to T = 1000 °C (**Eq. 2**) were reported.[39] This can also be achieved by the usage of potassium hydroxide at room temperature (**Eq. 3**).[40-44] In this context, the elimination of trimethylsilyl chloride became a useful approach (**Eq. 4**).[30,45] Further reactions are bases on induced rearrangements with triethylamine or DBU at low temperatures (**Eq. 5**),[46] elimination reactions (**Eq. 6**)[47,48] and other hydrogen halide elimination with other based at ambient temperature were reported (**Eq. 7**).[15,49]

$$PH_3 + C(s) \xrightarrow{\ -||+\ } H\!\!-\!\!\!\equiv\!\!P \qquad \text{(Eq. 1)}$$

$$H_3C\!\!-\!\!PH_2 \xrightarrow{\ \Delta\ } H\!\!-\!\!\!\equiv\!\!P \qquad \text{(Eq. 2)}$$

$$F_3C\!\!-\!\!PH_2 \xrightarrow{\ KOH\ } F\!\!-\!\!\!\equiv\!\!P \qquad \text{(Eq. 3)}$$

$$(TMS)_3C\!\!-\!\!PCl_2 \xrightarrow{\ \Delta\ } TMS\!\!-\!\!\!\equiv\!\!P \qquad \text{(Eq. 4)}$$

$$\underset{PH_2}{\overset{Cl_2}{R-C}} \xrightarrow{\ K_2CO_3\ } R\!\!-\!\!\!\equiv\!\!P \qquad \text{(Eq. 5)}$$

$$R\!\!-\!\!\!\equiv\!\!C\!\!-\!\!PH_2 \longrightarrow \underset{R}{\overset{H}{>}}\!\!C\!\!=\!\!PH \longrightarrow \underset{R}{\overset{H}{\vee}}\!\!C\!\!\equiv\!\!P \qquad \text{(Eq. 6)}$$

$$\underset{H}{\overset{}{H_2C\!\!=\!\!C}}\!\!-\!\!P\!\triangleleft \xrightarrow{\ -C_2H_4\ } \left[\underset{H}{\overset{}{H_2C\!\!=\!\!C}}\!\!-\!\!P \right] \longrightarrow H_3C\!\!-\!\!C\!\!\equiv\!\!P \qquad \text{(Eq. 7)}$$
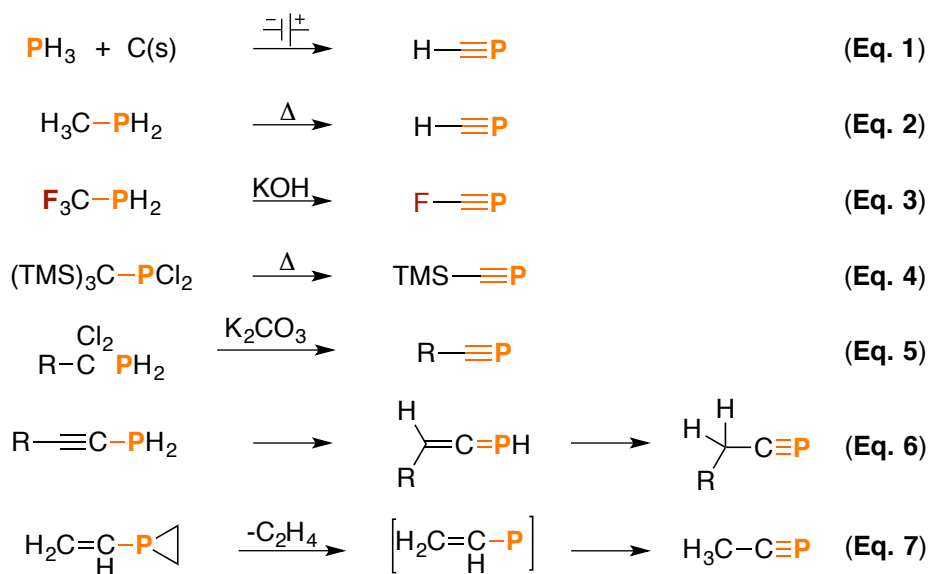
Scheme 3: Overview on selected synthesis strategies for phosphaalkynes.

A remarkable synthesis strategy was the elimination of hexamethyldisiloxane from phosphaalkenes. This breakthrough approach by Becker and co-workers paved the way to numerous phosphaalkynes. Tris-(trimethylsilyl) phosphane **17** was reacted with an organic acid chloride **18**. A nucleophilic substitution of the chloride by phosphorus can be assumed, followed by loss of a trimethylsilyl group, yielding trimethylsilyl chloride and the phosphanyl-alkyl-one **19**. Above T = 0 °C a 1,2-trimethylsilyl-shift from the phosphorus to the oxygen atom was observed. The phosphaalkenes **20**, obtained in this way, were transferred into their corresponding phosphaalkyne **21** using sodium hydroxide as catalyst (Scheme 4).[32]
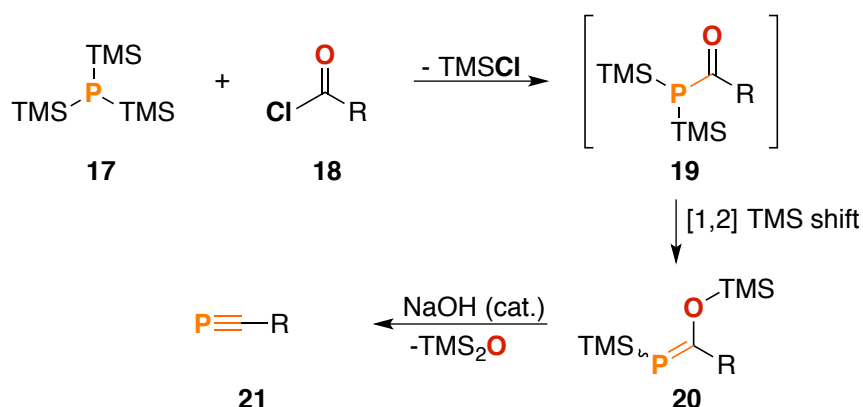
Scheme 4: Reaction steps for phosphaalkyne synthesis by hexamethyldisiloxane elimination.

1.2.3 Reactivity of Phosphaalkynes

The carbon-phosphorus triple bond resembles in many aspects the carbon-phosphorus double bond. Starting with the arrangement of the molecular orbitals in phosphaalkynes, it was found that their HOMO has π-symmetry and the HOMO^{-1} was determined to be the phosphorus lone pair. The difference in the ionisation energies is around $\Delta E = 1.8$ eV.[50] The phosphorus atom is positively polarised to the extent, that reaction with HSO$_3$F lead to selective protonation of the carbon rather than at the phosphorus lone pair.[51] The lone pair itself is located more closely to the phosphorus atom than in phosphaalkenes.[52,53]

Consequently, the chemistry of the phosphaalkynes is predominated by a broad variation of addition and cycloaddition reactions. To give another example for the polarisation of the carbon phosphorus triple bond, the 1,2-addition reaction with methyl lithium proceeds selectively and the lithium is located at the carbon atom (Scheme 5).[54]
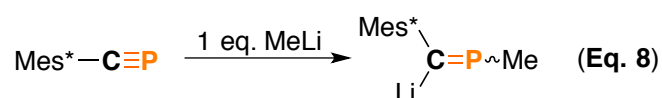
Scheme 5: 1,2-Addition reaction with methyl lithium.

[2+1] cycloaddition reactions involving phosphaalkynes provide a suitable approach in the synthesis of three membered ring systems, the so-called phosphirene derivatives, as they are obtained from reactions of phosphaalkynes and carbenes. Isomerisation with chloro-substituent on the carbene was observed.[55,56] Besides carbenes, also reactions with sterical shielded silylenes and germylenes were observed (Scheme 6).[57,58] Noteworthy is the cycloaddition reaction of carbon phosphorus triple bonds with iminophosphanes, because they yield the [2+1] cycloaddition product.[15,59]

R = ^{t}Bu; **X** = Si; R'/ R" = ^{t}Bu   R = ^{t}Bu; **X** = C; R" = Cl
X = Ge; R'/R" = TMS
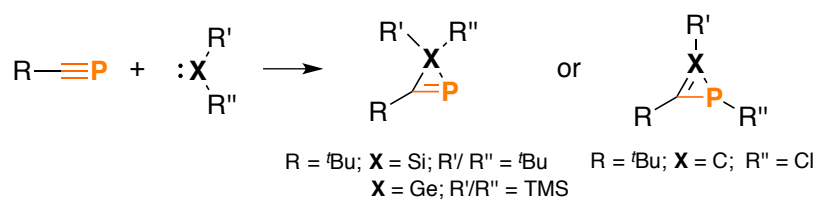
Scheme 6: Selected [2+1] cycloaddition reactions.

In a solvent-free environment the *tert*-butyl phosphaalkyne can undergo a heat induced cascade of cyclodimerisation reactions, yielding a heterocubane, involving three different steps of [2+2] cycloaddition reactions (Scheme 7).[60]
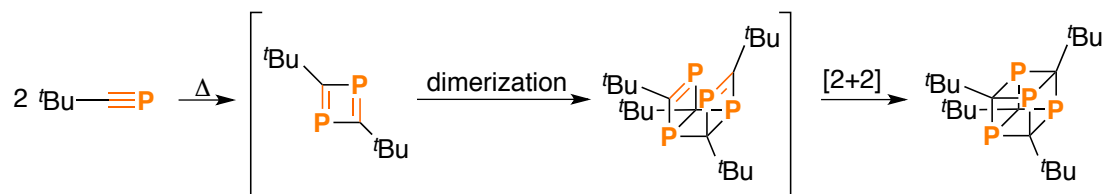
Scheme 7: Cascade [2+2] cyclodimerisation of (2,2-dimethylpropylidyne)phosphane.

Furthermore, there are different [3+2] cycloaddition reactions known for phosphaalkynes. To give an example, the formation of diazaphospholes with cyclic backbones is reported to undergo an rearrangement of the backbone rearranges in order to form an aromatic compound (Scheme 8).[60–62] The cycloaddition reaction are not only limited to these type of heterocycles. Nitrile oxides and their corresponding sulfides can also be converted into various heterocycles.[63–68]
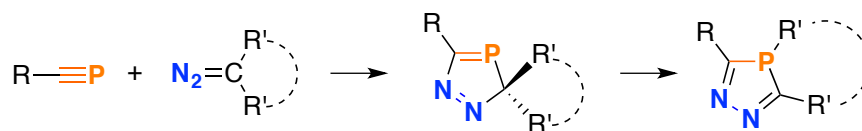
Scheme 8: [3+2] Cycloaddition with diazo-alkanes.

The cycloaddition reaction of phosphaalkynes and nitrile oxides, yielding the oxazaphosphole, is shown in Scheme 8. The C=P double bond is still reactive and can undergo a further reaction with a second equivalent. Although phosphorus-oxygen attractions and the polarisation of the carbon-phosphorus triple bond gave rise to the expectation to form the *cis* regioisomer, only the *trans* is obtained (Scheme 9). Grundmann showed, that the electronic influence in for cycloaddition reaction with nitrile oxides on the dipolarophile is low.[69] Cycloaddition reactions between phosphaalkynes and azides will be discussed in the synthesis of triazaphospholes (*vide infra*).
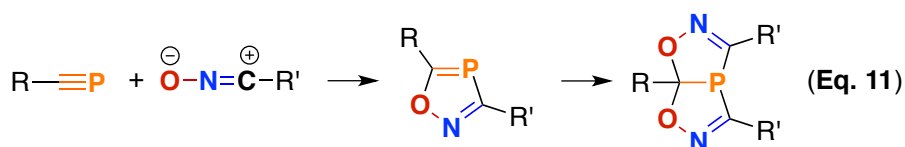
Scheme 9: [3+2] Cycloaddition with nitrile oxides.

Last to be mentioned are the [4+2] cycloadditions. Reactions yielding phosphinines are excluded (*vide infra*). Diels-Alder reactions with five- and six-membered rings were reported, including anthracenes. Other reactions of phosphaalkynes with aromatic systems are unknown and explained by the formation of unstable phosphabarrelenes.[24,70–74]
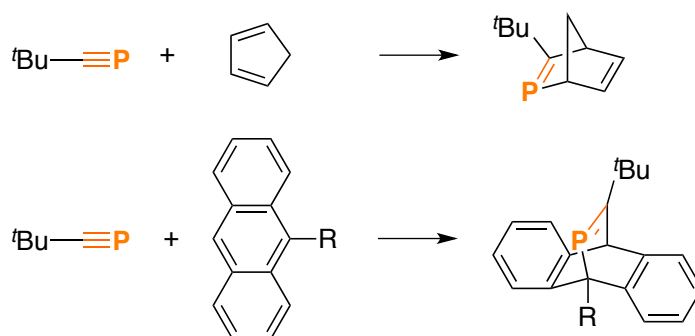
Scheme 10: Selected [4+2] cycloaddition reactions.

1.2.4 Coordination Chemistry of Phosphaalkynes

The modes in coordination chemistry of phosphaalkynes strongly resemble the ones observed in phosphaalkenes (Figure 5). The η^1-coordination mode (**22**) is rarely observed and only found in special designed metal complexes,[75] because of the low-lying phosphorus lone pair. Therefore, the first phosphaalkyne metal complex, reported by Nixon in 1981, showed an η^2-coordination mode (**23**) and they were frequently reported.[76–79] The bimetallic complexes are also known and are either formed with a σ- and a π-bond (**24**) or exclusively by the π-bonds (**25**), and both can be extended to the fully "saturated" coordinative form of type **26**.[39,40,80,81] Phosphanylidynemethanide complexes, the higher homologues of the cyanides, were first established in the 2014 by Crossley *et al.*[82] of type **27** while Grützmacher and co-worker used a different approach and generated a boron adduct **28**.[83]
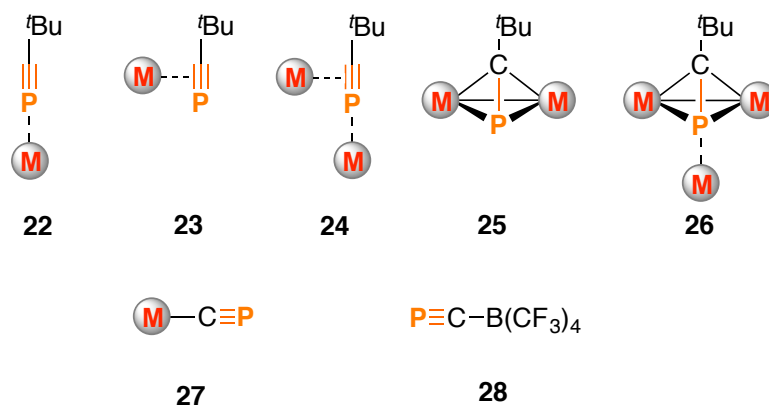
Figure 5: Coordination modes of phosphaalkynes.

1.3   Aromatic $\lambda^3\sigma^2$-Phosphorus Compounds

Implementing the C=P bond into an aromatic system provides a certain degree in kinetically and thermodynamic stabilisation, as they are less sensitive towards water or oxygen as well as acids and bases, depending on the substitution pattern.[84,85] The following part will only take the phosphinines into account. Besides this compound class, also (poly-)phospholes,[86–88,89] aza-phosphinines[90,91] are known. The first time such an aromatic system was described, was in 1966 by Märkl (Scheme 11, **1**).[92,93] The parent compound (**2**) to Märkl's triphenyl phosphinine was contributed by Ashe III in 1971.[6] While Märkl's synthetic pathway started from the pyrylium salt **3**, Ashe's approach proceeded *via* a tin cycle **4**.
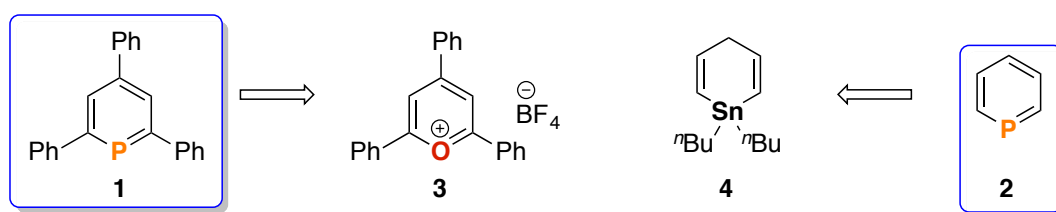
Scheme 11: Retro synthesis of the first phosphinine and its parent compound.

1.3.1   Synthesis of Phosphinines

Nowadays several different synthetic pathways to phosphinines with different substitution pattern are known, including ring extension reactions starting from acylpholium salts (Scheme 12, **Eq. 1**),[94–99] reactions with phosphorus heterocycles with diazocompounds (**Eq. 2**)[100] and dichlorocarbenes (Scheme 13, **Eq. 3**),[101–103] electrocyclisation (**Eq. 4**)[104] and Diels-Alder reactions (**Eq. 5** and **Eq.6**)[24,70,73,105,106] as well as modification of the tin route (**Eq. 7**).[107,108] Also palladium catalysed C-C formation for past-synthesis functionalisation were reported.[109–111]
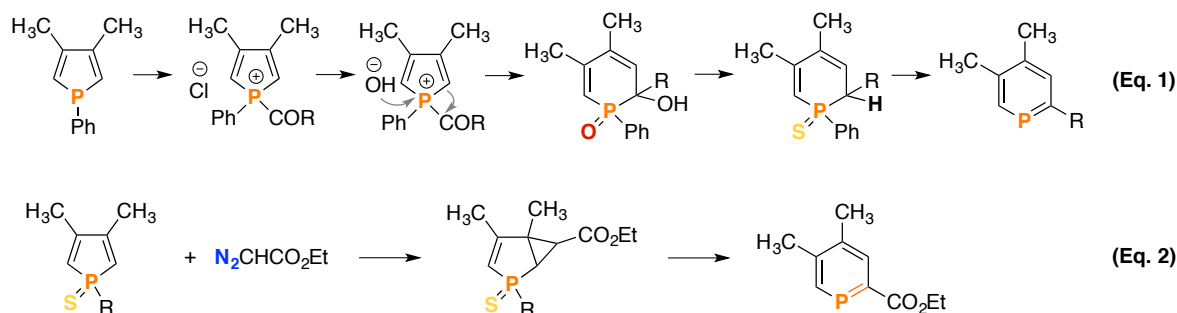
Scheme 12: Different approaches towards phosphinine synthesis.

(Eq. 3)

(Eq. 4)

(Eq. 5)

(Eq. 6)

(Eq. 7)
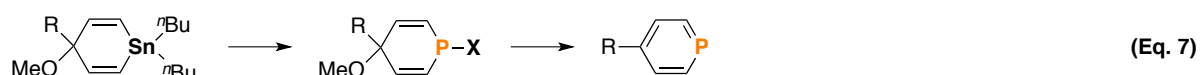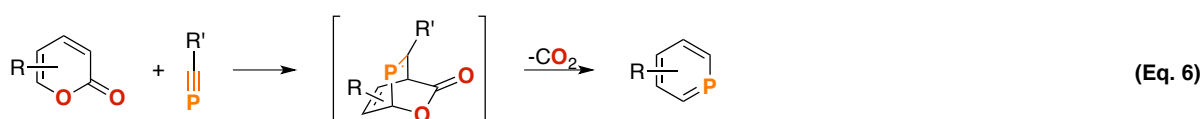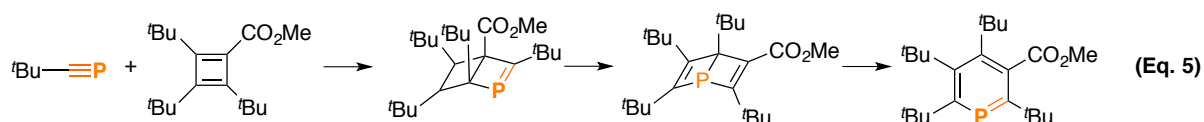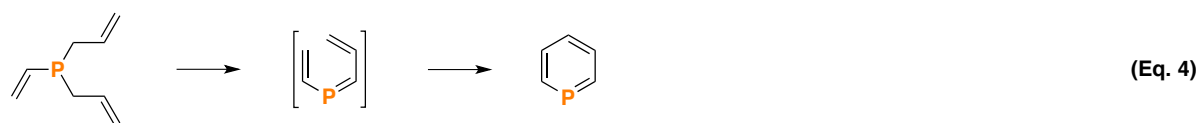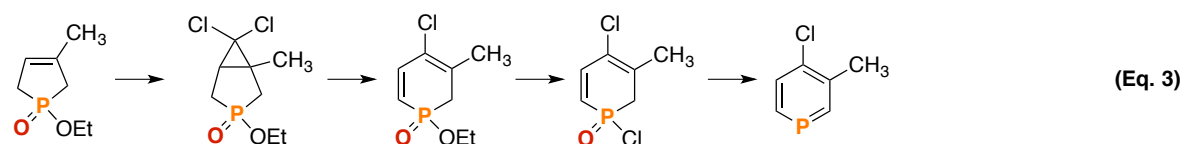
Scheme 13: Further approaches towards phosphinine synthesis.

The pyrylium salt route will be highlighted, because the modular approach provides an easy pathway to differently substituted phosphinines (Scheme 14), including P,N- and even P,N,P-compounds as well as bipyridines.[112–115] Starting from aryl aldehydes **5** and aryl ketones **6** under basic conditions, chalcone **7** is generated. Applying the previous conditions again with another (equivalent) of aryl ketone **8**, the diketone **9** is obtained. Treatment with HBF_4- or BF_3-etherate yields triaryl-pyrylium salts **10**. Depending on the substitution pattern, the reaction can also be applied as one-pot-synthesis. Conversion with either a phosphorus(III) source or NH_3 yields phosphinines or pyridines **11**.
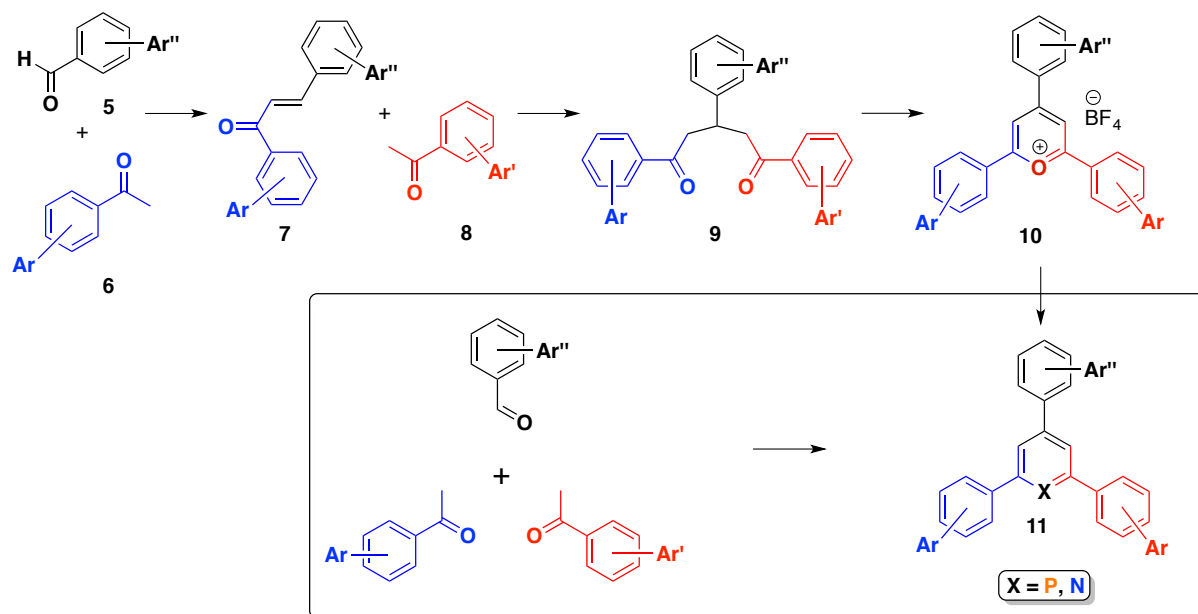
Scheme 14: Pyrylium salt route, starting from aryl-aldehyde and –ketone. (**Box**): overall modular synthesis.

Different suitable phosphorus(III) sources are described. In the original report, Märkl used $P(CH_2OH)_3$.[93,116] The highest yields are obtained with PH_4I but the precursor is quite instable.[117] A more convenient compound is $P(TMS)_3$[5] or as recently reported the lithium-salt of type $Li^+P(TMS)_2^-$.[118]

1.3.2   Properties of Phosphinines

Phosphinines are aromatic compounds, as it was derived from Nucleus-Independent Chemical Shifts (NICS), but compared to the C=C building block the C=P double bond is less stabilised and the resonance energy was determined to be 88% of the benzene value.[119–123] The calculated bond length of the carbon-carbon bonds are in line with the values of the X-ray structure analysis and very similar to the C-C bonds in benzene.[124,125] A combinatorial study investigating the parent phosphinine structure by means of photoelectron spectroscopy and DFT calculations exhibit results close to the ones observed in phosphaalkenes. The HOMO showed π-symmetry and the phosphorus lone pair contributed with larger coefficient to the molecular orbital. Further, the phosphorus lone pair was located in the HOMO^{-2}, while in the corresponding pyridine the nitrogen lone pair was located in the HOMO.[124,126,127] As a consequence, the phosphorus lone pair is only poorly nucleophilic. Protonation in the gas phase revealed a difference of ΔE_{PA} = 23.6 kcal mol^{-1} in proton affinity to the pyrdinium species.[128–131]

The charge distribution in the C_5H_5P was determined by Mulliken population analysis, showing a positive charge located at the phosphorus atom (Q = + 0.55 e), while the carbon atoms are negatively charged ($Q_{C\alpha}$ = -0.54 e, $Q_{C\beta}$ = -0.22 e and $Q_{C\gamma}$ = -0.25 e).[127] These results are in line with the chemical shifts obtained by ^{13}C NMR spectroscopy.[132] The charge distribution in phosphinines with the electropositive charged phosphorus atom causes interesting chemical interactions with strong nucleophiles. Organo-lithium compounds led to akylation[133–135] as well as arylation[136] at the phosphorus atom, yielding λ^4-phosphinines. These compounds are manifold in their chemistry and oxidation with alkyl halogens[137,138] and a combination of alcohols and diazo compounds[139] as well as hydrolysis[140] reactions were reported. Recently, the coordination chemistry of λ^4-phosphinines was explored.[141]

Phosphinines show in coordination chemistry unique chemical properties. The low-lying phosphorus lone pair causes weak sigma-donation ability (Figure 6). These findings are approved by molecular orbitals plots obtained from DFT calculations. The phosphorus lone pair is found in HOMO[-2]. However, the LUMO in phosphinines is lower in energy as the one in pyridines and the large coefficient at the phosphorus atom lone pair is responsible for strong metal-ligand back bonding. The location of the phosphorus lone-pair and its low nucleophilicity predestine phosphinines to bind to electron rich metal centres.
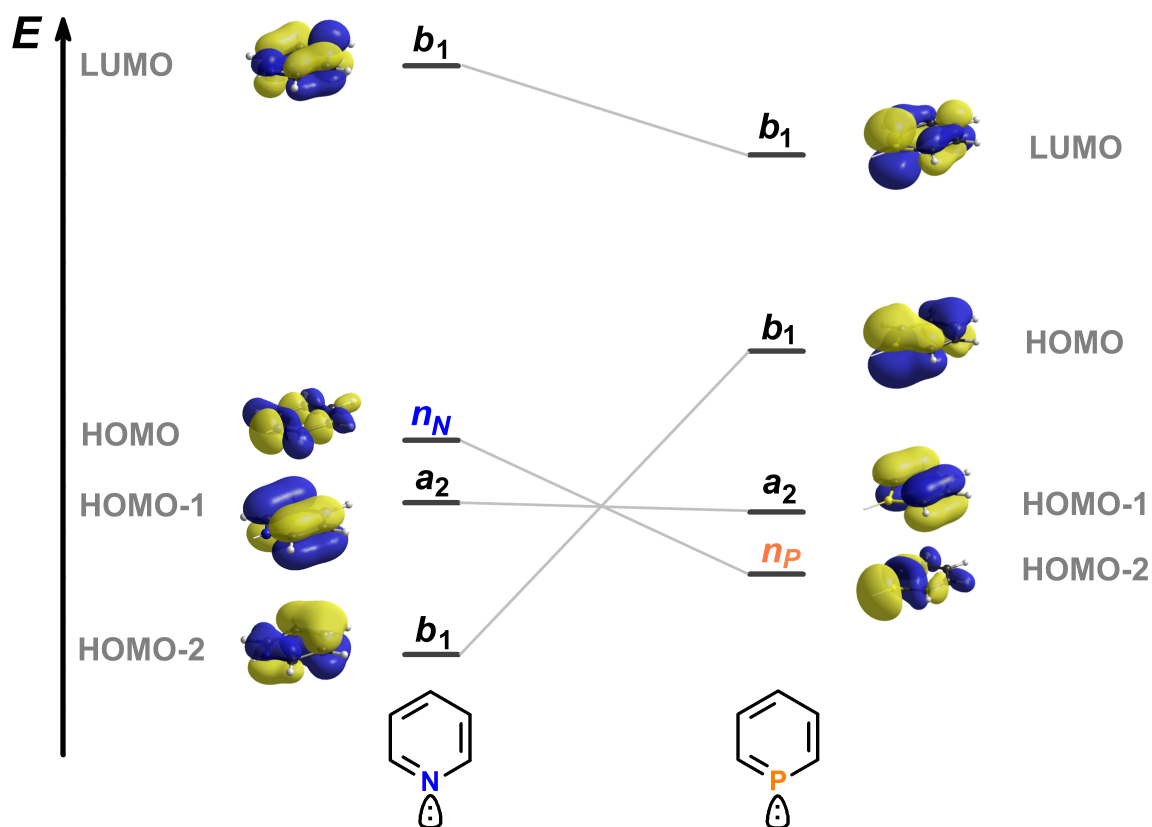
Figure 6: Selected molecular orbitals of pyridine and phosphinine.

Comparing the phosphinine with one of the most known classic trivalent phosphorus compounds, the triphenylphosphine, are good examples for illustrating the variances in the steric demand of these two types of molecules. A general procedure to quantify the steric demand of ligands in metal complexes was suggested by Chadwick Tolmans.

Excursion 1: Tolman Cone Angle[142–144]

In (transition) metal catalysis steric effects were determined to play an important role and might enhance the outcome (yield or/and *ee*) of the catalysis.[145] Consequently, quantification is required. Chadwick Tolman suggested measuring the angle of a fixed point with a distance of 2.28 Å in molecular structures or 2.57 cm using a model kit from the centre of the phosphorus atom, inspired by the Ni-P-distance. The apex angle Θ, open between this line and the outer sphere of the van-der-Waals radius of the ligand, can be determined for symmetrically substituted phosphines by measuring (Figure 7, **I**). For unsymmetrically substituted phosphines Θ comply with a model minimising the

half-angle sum by equation $\Theta = \left(2/3\right)\sum_i^3 \Theta_i/2$ **(II)**. Ligands with high steric demand, $\Theta > 180°$ can also be determined by trigonometry, $\tan \alpha = h/d$ and $\Theta = 180 + 2\alpha$ **(III)**.
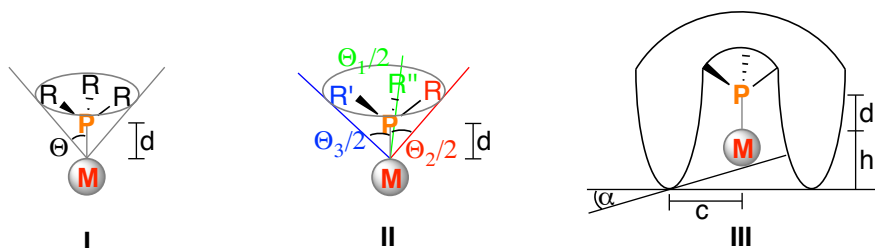
Figure 7: Approaches to determine the cone angle in different steric demanding substituents, d = 2.28 Å.

However, phosphinines are, like pyridines or benzenes, planar molecules due to their aromaticity. Their steric demand will mainly be located in the x/y-plane rather than in any z-plane. Hence, Tolmans concept lacks the potential to describe these molecules and a more convenient way is the use of occupancy angles α and β (Figure 8).[146] With all the electronically differences, the structures of phosphinine and the pyridine correlate more than with the one of classical phosphines.[147] The C-C bond length in both heterocycles remain the same and in case of the phosphorus heterocycle, the C_α-P bond length shows alternation and is with ~1.75 Å in between the distances in triphenylphosphine (1.83 Å) and diphenylmethylenephosphaalkene (1.66 Å). This can be attributed to the delocalised π-bond and indicates participation in the aromatic system (*vide supra*).[148,149] Comparing the molecular structure in detail, the reluctance of phosphorus to hybridise becomes obvious, as the C-P-C angle value is around 100° while the corresponding angle in the nitrogen heterocycle shows a value around 117°. Consequently, the six-membered phosphorus heterocycle is distorted (Figure 8, Box).[85,147]
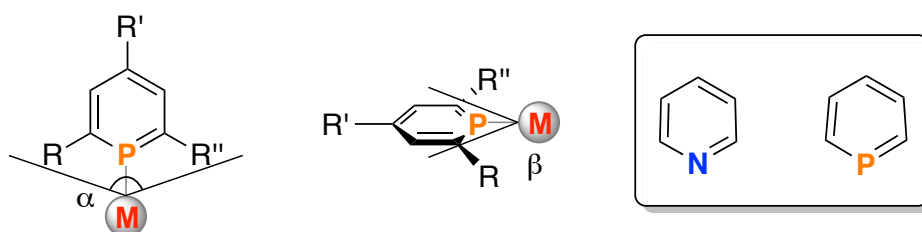
Figure 8: Determination of the steric demand in phosphinines. (**Box**): overstated molecular structures of pyridine and phosphinine.

1.3.3 Coordination Chemistry of Phosphinines

Phosphinines can coordinate to metal centres in different fashions and these resemble strongly the coordination modes observed in phosphaalkenes. The delocalisation of the π-system has without any doubt a strong influence and therefore no η²-complexes *via* the C=P bond were observed so far, but the η⁶-coordination *via* the π-system was observed (Figure 9, **12**). Nöth and co-worker reported the successful transformation of triphenylphosphinine with hexacarbonylchrome[150] and later its X-ray diffraction structure was complemented by the same group.[151] Further, the authors contributed the first η¹-bond carbonyl complexes of molybdenum and tungsten (**13**).[152] Soon after, the first heterobimetallic complex in η¹-η⁶ fashion (**14**) was synthesised.[153,154] Also the η²-complexes, where the phosphorus atom binds to osmium carbonyl fragments, are known **15**.[155]

More exotic coordination modes are also found in phosphinines. Mathey reported the oxidative addition of a zirconium into bromine-C_α bond, followed by the deprotonation of the C_β, yielded phosphabenzyne-zirconocene complex. Without the addition of PMe₃ the complex dimerises and the coordination mode of one subunit corresponds to structure **16**.[156] More curious is the structure of type **17**, also reported by Manzur *et al.*.[155]
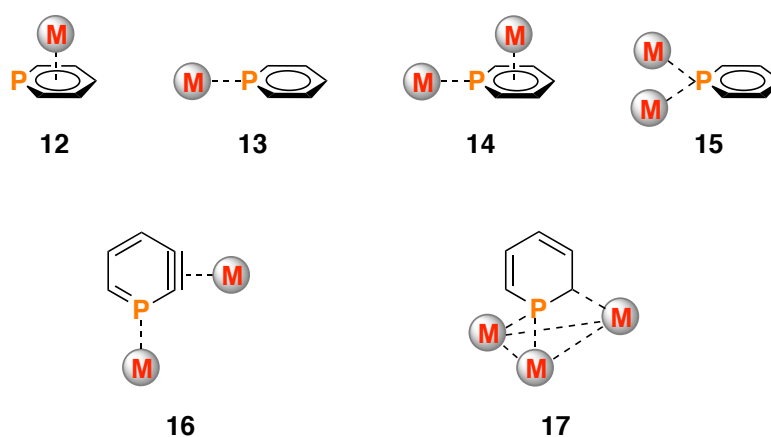
Figure 9: Coordination modes of phosphinines.

The final presented coordination mode **17** shows an interesting chemical behaviour of phosphinines. Metal coordination *via* the phosphorus atom lone pair causes obviously a destabilisation of the resonance structure. Similar behaviour was observed in cyclometalated triphenylphosphinine. Treating the cyclometalated complex with water

yielded addition on the phosphorus and C_α atom.[157] But not only do metal complexes enhance the reactivity of the delocalised $C=P$ bond; the lone pair of the phosphorus atom in phosphinines **18** can also be oxidised with hydrogen peroxide. In contrast to the oxidation with sulphur, the oxide was not obtained, but rather the hydroxyl phosphine oxide **19**.[158–160] This might imply a higher stability of the phosphinine sulfide **20**, but treatment with protic solvents such as methanol lead to the corresponding alkoxy addition products **21**.[161] For the sake of completeness the oxidation of phosphinines by halogens was also reported (Scheme 15, **22**).[162] However, Märkl found the addition of carbenes to the $C=P$ bond in phosphinines and no metal was required.[163] Here, the phosphinine mimics some chemical behaviour found in carbon double and triple bonds (*vide supra*).

1.3.4   Reactivity and Selected Applications of Phosphinines

Phosphinine based complexes are by far no laboratory curiosities anymore and can e.g. be used as ligands in homogenous catalysis. In 1996, Berhand Breit reported on the hydroformylation reaction using low-coordinate phosphorus compounds as ligands.[164] More recently, a tandem reaction including hydroformylation as well as cyclisation of N-allyl-imidazole was catalysed with a chiral phosphinine-based **Rh**(I) complex (Scheme 16).[165,166]
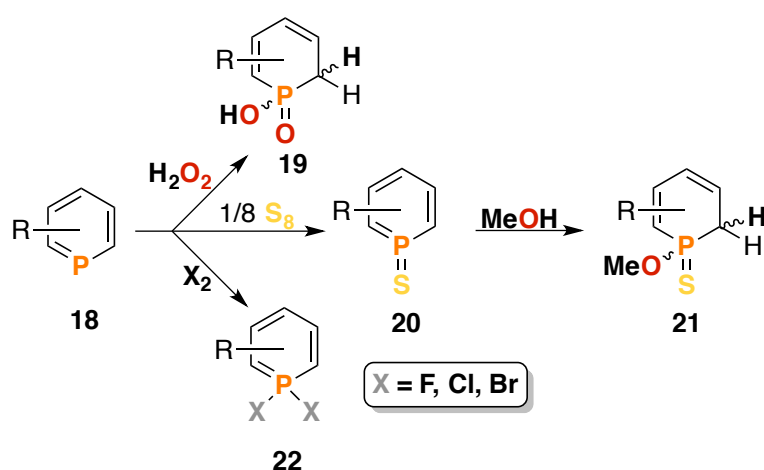
Scheme 15: Selected oxidation reactions for phosphinines.

More recently discovered applications are the cyclometalation of triphenylphosphinine, the **Ir**(III) complex and the **Ce⁴⁺** assisted water oxidation by the group of Müller.[167,168] Further, phosphinines were investigated towards luminescent materials.[169]
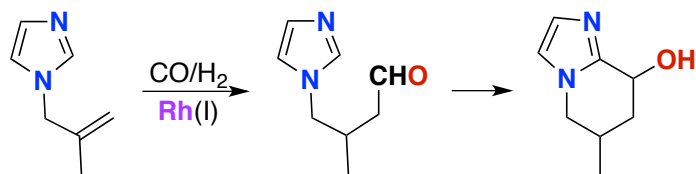
Scheme 16: Tandem reaction reported by Müller *et al.*.

1.4   3*H*-1,2,3,4-Triazaphospholes[170]

Triazaphospholes can be classified into two main frameworks, differing in the position of the phosphorus atom. In 1,2,4,3-triazaphospholes (Figure 10, **I**), the phosphorus atom is located between the nitrogen atoms, while in 1,2,3,4-triazaphospholes it is positioned after the triaza-chain (**II**). Both groups can further be separated in three subgroups by the position of the hydrogen atoms.[171] This work deals exclusively with the last compounds, the derivatives of 3*H*-1,2,3,4-triazaphospholes.
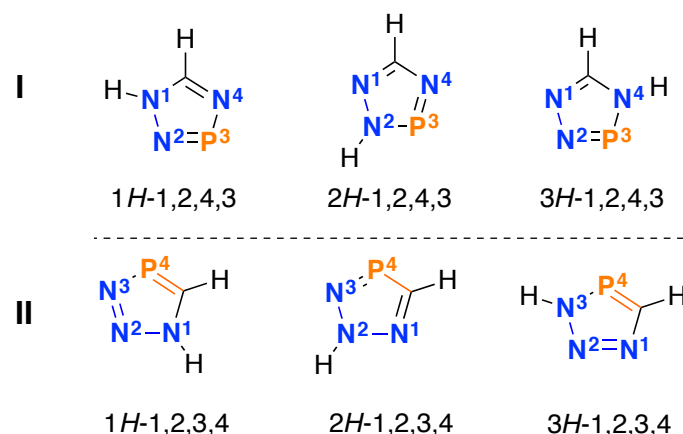
Figure 10: Triazaphosphole frameworks.

1.4.1   Properties of 3*H*-1,2,3,4-Triazaphospholes

The 3,5-disubsituted triazaphosphole derivatives are mainly colourless, crystalline stable compounds and can be handled in air for short time without any decomposition. Similar to phosphinines, the chemical shift in $^{31}P\{^1H\}$ NMR spectroscopy is found between δ = 160-220 ppm.[171] This is a good hint for the aromaticity of the system and in accordance with DFT calculations performed by Nyulászi and Regitz, from which a conjugated π-system and a high degree of aromaticity were proposed. The arrangement of the molecular orbitals in the 3*H*-1,2,3,4-triazaphospholes resemble strong to the ones of $\lambda^3\sigma^2$-phosphinines. In both molecules, the phosphorus atom shows a high contribution of the LUMO. Taking additionally the symmetry into account, a π-accepting property can be derived.[170] The HOMO orbital assembles in the same symmetry and a considerable N-C=P ↔ N+=C-P- conjugation, a rather high π-donor ability was attributed to these systems.[172,173] A further correlation between the phosphorus containing heterocycles is the location of the phosphorus atom lone pair which is found in the

energetically low-lying HOMO^{-4} for the five membered and HOMO^{-2} for the six membered heterocycle. Additionally, the nitrogen N^1 and N^2 atom lone pairs are contributing equally to this molecular orbital. However, adjacent to the frontier molecular orbitals, the nitrogen N^1 and N^2 atom lone pairs are also present with comparable large coefficients.[170]

Crystallographic characterisations of 3*H*-1,2,3,4-triazaphospholes exhibited a planar system. In context with the discussion of aromaticity, the C=P bond length 1.709 Å is comparable large and indicate a delocalisation. Localised bond length lie, as already mentioned, between 1.83 Å for single bond and 1.692 Å for double bond systems.[148,174] The carbon phosphorus double bond in 2,4,6-triarylphosphinines has an average distance of around 1.75 Å.[170] The phosphorus shapes the five-membered heterocycle as it was observed for the phosphinines. Most obvious is the N-P-C angle of around 87 °, demonstrating the low potential of the phosphorus atom to undergo hybridisation as the second period elements implemented in the ring system. Due to their *sp²*-hybridisation a trigonal planar surrounding would be preferred. In polyphosphaphospholes the planarity of the system for the σ^3-phosphorus atom was explained in a similar way.[86,175,176] The structural aspects support Regitz's suggestion of a strong aromatic compound. In phosphinines the average value of C-P-C angle is ∼100 °.[170,177]

1.4.2 Synthesis of 3*H*-1,2,3,4-Triazaphospholes

The 1,2,3,4-triazaphospholes (**3**) are the formal product of a 1,3-dipolar cycloaddition of phosphaalkynes **1** and azides **2** (Scheme 17). In contrast to the Huisgen reaction (*vide infra*), the product formation proceeds selectively without the need of any catalyst. Regitz *et al.* first reported this compound class in 1984.[178] The question of whether the selectivity of the reaction is caused by electronic or steric reasons is a matter of dispute. DFT calculations, performed by Nguyen *et al.*, of the cycloaddition reaction of phospha-alkynes forming the related diazaphospholes showed a strong steric influence on the transition state, yielding selectively the *trans* product.[179] However, Regitz *et al.* also reported the selective formation of the *trans* product (**6**) starting form methyl azide **4** and methylidynephosphane **5**, compounds with minimal steric demand. Apparently, in the synthesis of triazaphospholes an electronic effect might be crucial.[63] Consequently, the very slightly polarised carbon phosphorus triple bond, simplified by the difference in the electronegativity in both elements (*vide supra*), can be considered to be most likely

responsible.[170] As a remarkable aside, the reaction of organic azides (**1**) and are also known and classical phosphorus (**7**) compounds part of the Staudinger reaction yielding λ⁵-phosphinimine of type **8** (Scheme 17, Box). These differences in the chemical behaviour of alkynes, phosphaalkynes and classical phosphorus (III) compounds open up the capability to generate the phosphorus analogue of the widely used 1*H*-1,2,3-triazoles. Successive exchange of the substituents **R** and **R'** (Scheme 17) enables a modular approach.
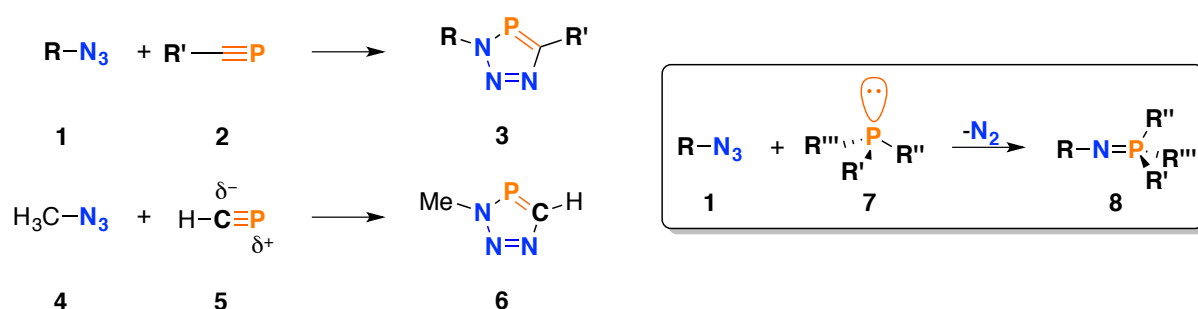
Scheme 17: (**Top, left**) Generalised reaction of an organic azide and a phosphaalkyne. (**Bottom, left**): electronic effect on the reaction. (Box): Staudinger reaction without hydrolysis.

However, this strategy struggles with the limited amount of kinetically stable phosphaalkynes (*vide supra*). The use of steric less demanding phosphaalkynes are reported[33,34,64,66,180,181] and in some cases, the *in-situ* generation was necessary.[63] Here it should be mentioned, that also some substituents causes instability by means of a rearrangement. The cycloaddition reaction of phosphaalkynes and TMS-N_3 or hydrazoic acid (H-N_3) is followed by a [1,5]-shift of the azide substituent, causing the formation of the 2*H*-triazaphosphole derivative (e.g., Figure 9).

Another approach in generating 3*H*-1,2,3,4-triazaphospholes is based on the [3+2] cycloaddition of azides and phosphaalkenes. 1-Chloro-2-trimethylsilyl-2-phospha-ethenes of type **9** (Scheme 18) form with organic azides **1** the 4,5-dihydro-3H-1,2,3,4-trazaphospholes (**10**). Aromaticity is achieved by spontaneous α-elimination of TMSCl, yielding the corresponding triazaphosphole derivative **11**.[62,64,171,180]
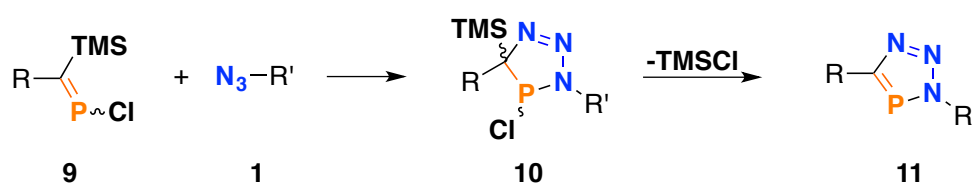
Scheme 18: Formation of triazaphospholes *via* phosphaalkenes.

A good example for demonstrating the diversity of this approach is the synthesis of 5-triphenylphosphine derivative **15** (Scheme 19). The (chlorophosphanylidene) triphenylphosphonium salt **12** undergoes a [3+2]-cycloaddition reaction with phenyl azide **13**, followed by trimethylsilyl chloride elimination.[182]
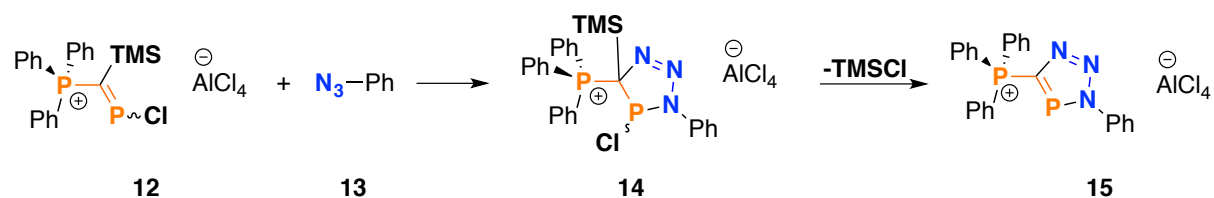
Scheme 19: Synthesis of triphenyl-(3-phenyl-3*H*-1,2,3,4-triazaphosphol-5-yl)phosphonium salt **15**.

Pyridyl-functionalised systems were developed by Regitz and co-workers (Scheme 20).[183–185] The reaction of triazido-methylnicotinonitrile **14** with the phosphaalkyne **15** yielded a product mixture of mono-, di- and tri- substituted derivatives **16**, **17** and **18**.
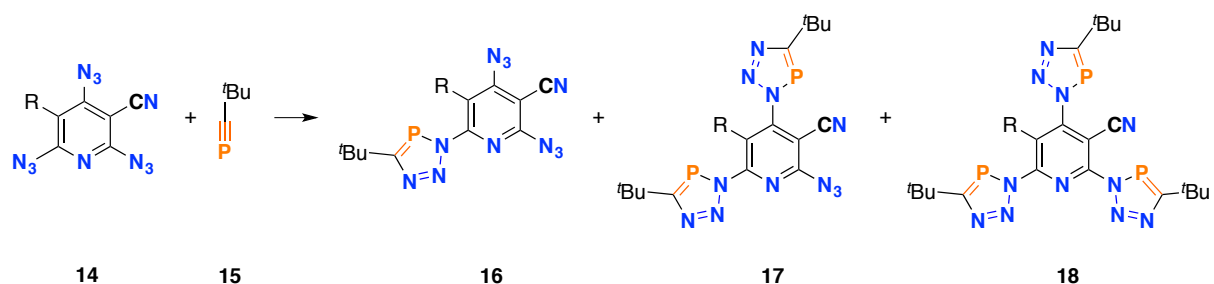
Scheme 20: Pyridyl-substituted triazaphospholes by Regitz.

These initial donor-functionalised heterocycles were not employed in metal coordination, but were a directive approach, since polydentate systems are more likely to form stable bonds to metal centres in higher oxidation states.[186] Especially the hybrid ligands, the combination of contrary donation effects, showed positive effects in catalytic reactions as they enhanced reactivity and selectivity.[187–189]

1.4.3 Coordination Chemistry of 3*H*-1,2,3,4-Triazaphospholes

The knowledge of metal complexes with 3*H*-1,2,3,4-triazaphaphosphole based ligands is rare and mainly caused by the fact that the first coordination compound was reported almost 30 years after their discovery by Regitz (*vide supra*). This is interesting, because their phosphorus-lacking analogues are an established ligand class in coordination chemistry. Previously, some coordination attempts were performed by Schmidpeter and van Koten and may have shown coordination *via* the phosphorus or one of the nitrogen lone pair towards metal centres before.[190–194] However, different coordination modes are possible and were reported. Jones *et al.* reported the mode **19** (Figure 11) in 2010.[195] Further, the authors provide the first molecular structure in the crystal of triazaphospholes and as framework in metal complexes. In the phosphorus lacking analogous heterocycles this coordination mode is most common, because the N^3 atom in triazoles is known to be the most nucleophilic one (*vide infra*). A few years later in 2013, the same group reported the σ^1-coordination mode *via* the nitrogen N^1 atom lone pair (**20**).[196] The corresponding mode of type **21** will be discussed in this work. A coordination of the N^3 lone pair cannot be expected, because it is integrated into the aromatic system of the heterocycle. Therefore, a further interesting compounds was contributed by So and co-workers.[197] This group reported the **Ge**(II)-N^3 bond situation of type **22**. However, to this point no complexes without any additional binding side had been reported.
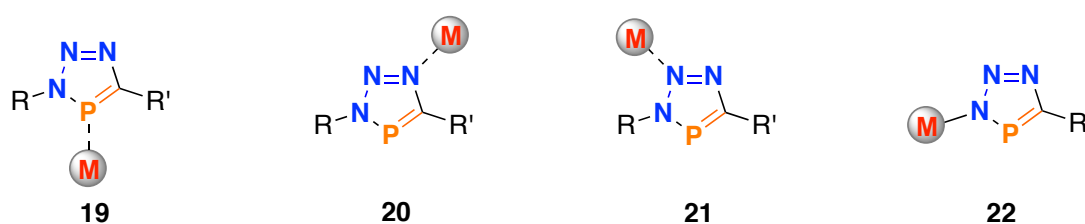
Figure 11: Overview of simplified coordination modes found in 3*H*-1,2,3,4-triazaphospholes.

The working group around Jones described the synthesis of different tripodal low-coordinated phosphorus compounds.[198] Scheme 21 shows the phosphorus containing analogue of the well-known tris[(1-benzyl-1*H*-1,2,3-triazole-4-yl)methyl]amine (tbta), established by Fokin *et al.*.[199] Like the triazole derivative, the triazaphospholes **25** are generated from the corresponding azide **23** and (phospha)alkynes **24**, 1-phospha-2-*tert*-butyl-acetylene (*t*Bu-C$\equiv$P) or 1-phospha-2-methyl-acetylene (Me-C$\equiv$P).
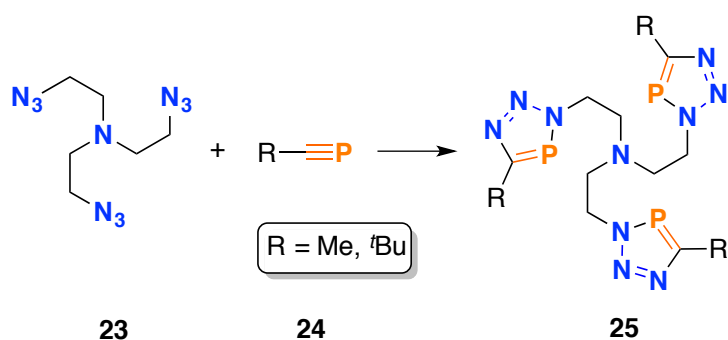
Scheme 21: Generation of the phosphorus containing analogue of tbta.

The second set of tripodal compounds (type **26**) is based on the 1,3,5-tris(azidomethyl)-2,4,6-trimethylbenzene (type **28**, Scheme 22). These molecules provide a large cavity and their molecular structures in the crystals resemble a open vessel. Most interesting, the triazaphosphole subunits are in both cases orthogonal to the benzene plane. In the methyl-substituted derivatives the binding sites are orientated as it was found for the *tert*-butyl derivatives of triazaphospholes. But due to the increased steric bulk of the substituents, one *tert*-butyl substituted triazaphosphole is positioned opposite to the others. In coordination chemistry two different **Pt**(0) complexes were identified by ^{31}P{^{1}H} NMR spectroscopy with 1:1 and 2:1 metal to ligand ratios. The authors reported for **29** the molecular structure in the crystal of the 2:1 complex of the *tert*-butyl derivative of **28**. The lone pairs of the phosphorus atoms coordinate to the metal centres. One **Pt**(0) centre was bond to all three triazaphosphole units. Two of the phosphorus atoms bridged the second **Pt**(0) which is further coordinated by a η^2-interaction to a norbornene molecule.
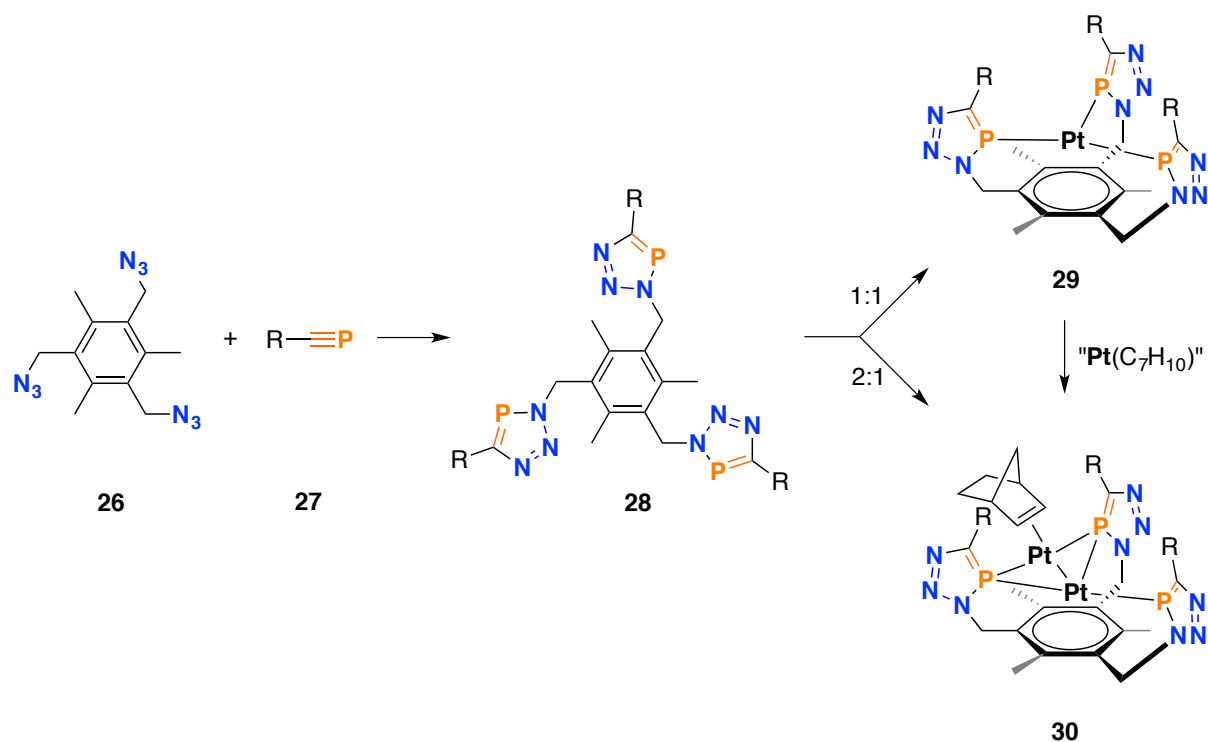
Scheme 22: Synthesis of tripodal triazaphosphole **28** and corresponding **Pt**(0) complexes **29** and **30**.

For the **Pt**(0) ligand (1:1) complex, the authors' proposal for the structure is shown in Scheme 21. The addition of one equivalent more of the metal precursor yields the same system, as starting from the 2:1 ratio, indicating a dynamic system.

More recently, the group reported a new batch of potential ligands, including ferrocene, cyclohexyl and polymeric backbones (Figure 12).[196]
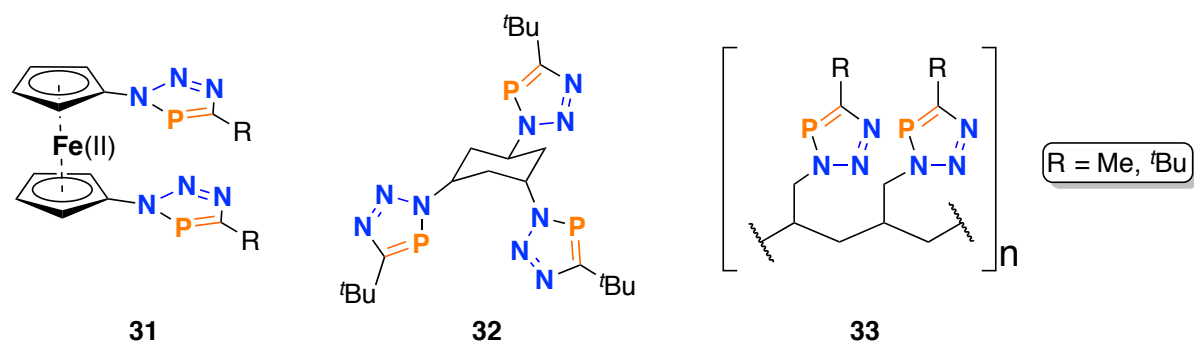
Figure 12: Bis- tris and poly triazaphosphole systems synthesised by Jones *et al.*.

The structures of the 1,1'-bis-triazaphosphole ferrocenes **31** was proven crystallographically. This compound was further investigated in electrochemical studies, revealing a one-electron oxidation process at significant higher potential than ferrocene.

In order to oxidise the ferrocene backbone chemically, the bis-triazaphosphole was treated with $\mathbf{Ag}\{\mathbf{Al}[OC(CF_3)_3]_4\}$. Much to their surprise, they were not able to obtain the oxidised ferrocenium(III) species **34**, but the corresponding tetranuclear N^1-$\mathbf{Ag}$(I) complex **35** (Scheme 23).
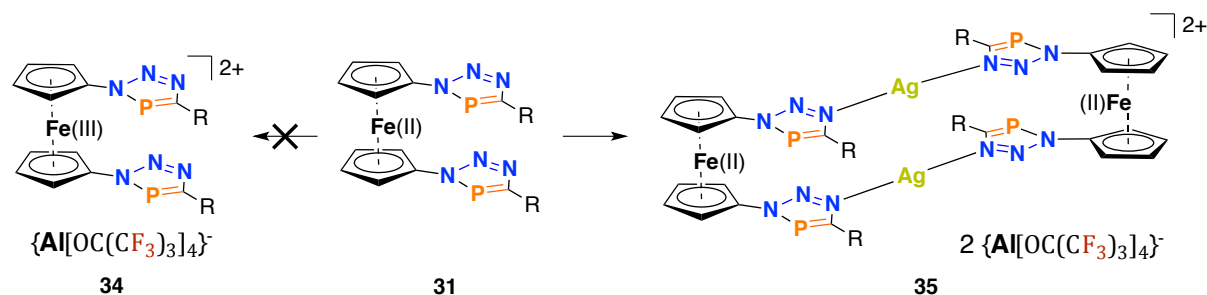
Scheme 23: Synthesis of **Ag**(I) triazaphosphole complex.

Triazaphosphole based metal complexes require not necessarily the cycloaddition product. Si *et al.* demonstrated in an elegant way the formation of a σ-bond N^3 germanium complex, starting from the **Ge**-N_3 **36** and the adamantyl phosphaalkyne **37**. The complex **38** was obtained in quantitative yield (Scheme 24).
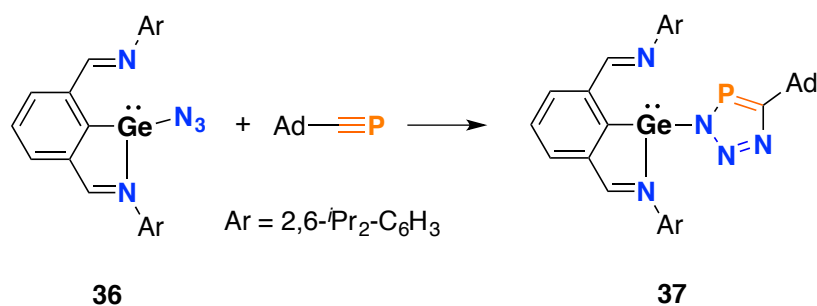
Scheme 24: Formation of the germanium(II) triazaphosphole.

1.4.4 Properties of 3*H*-1,2,3,4-Triazaphospholes

The product class of the triazaphospholes is less well investigated than for instance the phosphinines. The [1-5]-shift of the 3-subsitutent (TMS or H) yielding the 2*H*-isomer was previously mentioned (*vide supra*). However, these isomers can either be hydrolysed (**Eq. 1**) or decomposed by vacuum flash pyrolysis (**Eq. 2**) yielding the hydrogen derivative and the 1,2- and 1,3-benzazaphsopholes respectively (Scheme 25).

The hydrolysis can even be achieved by stirring a mixture in the presence of silica and moisture.[63]
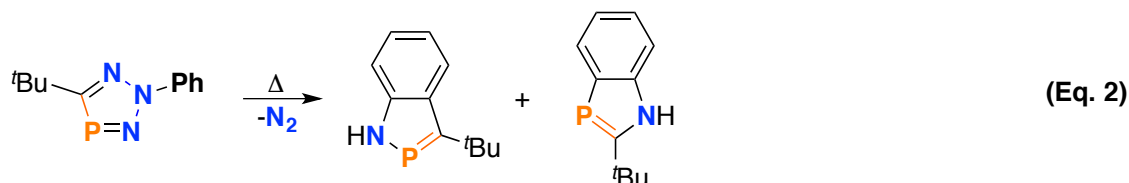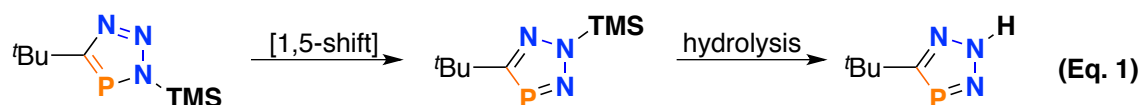
Scheme 25: Rearrangement to and reactions of 2*H*-1,2,3,4-triazaphospholes.

In contrast to phosphinines or phospholes the phosphorus atom of 3*H*-1,2,3,4-triazaphospholes cannot be oxidised. The generation of λ^5-sulfides and λ^5-spiro triazaphosphole derivatives show either decomposition or no change of the chemical shift in ^{31}P NMR spectroscopy. Also the oxidation with DDQ in the presence of water was reported to show side products (Scheme 26).[200]
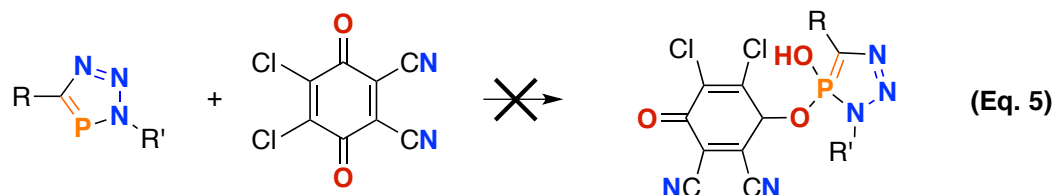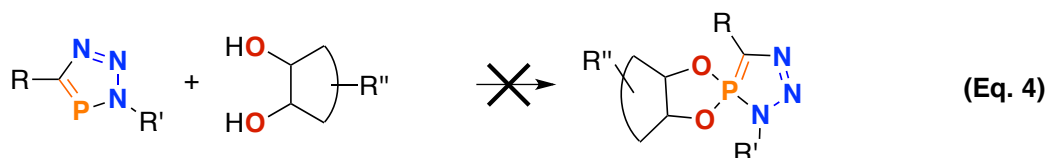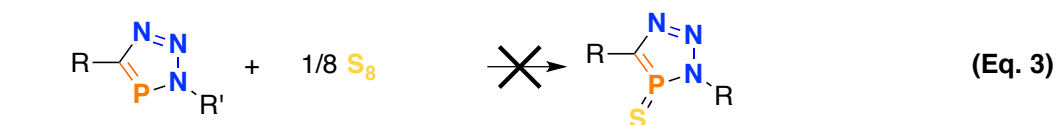
Scheme 26: Synthetic approaches in oxidising triazaphospholes.

However, triazaphosphole oxides were reported, but in contrast to their phosphinine relatives, only the dihydro-triazaphopshole oxides are known and thus no C=P double bond is present. Furthermore, they are also not generated by a phosphaalkyne but by the reaction of organo phosphites with organo azides (Scheme 27). [201,202]
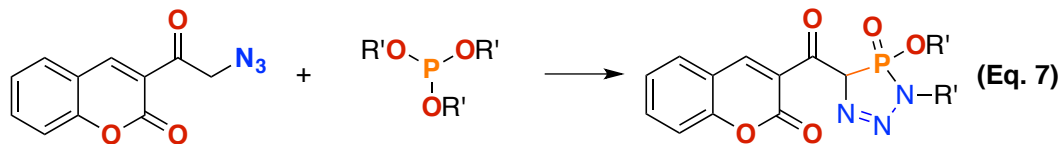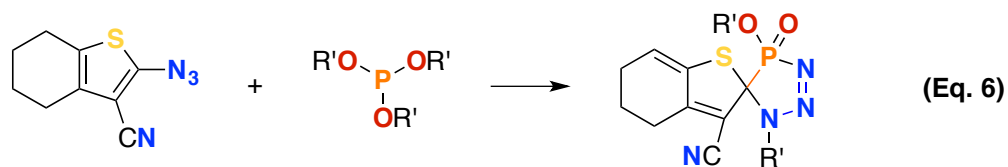
Scheme 27: Synthesis of dihydro-triazaphosphole oxides.

1.5 1*H*-1,2,3-Triazoles

The 1*H*-1,2,3-triazole derivatives are the result of the reaction between alkynes **1** and (organic) azides **2**. The reaction is named after Rolf Huisgen[203] and was extensively investigated and the reactions expand to nitril oxides, diazoalkanes and ozine.[204–207] The reaction proceeds without any discrimination of the two possible isomers, the 1,4- (**3**) and the 1,5-regioisomer (Scheme 28, **4**).
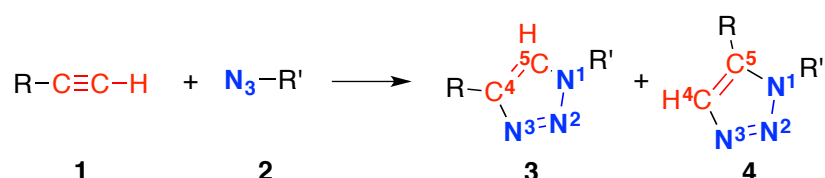
Scheme 28: The Huisgen reaction.

Further, Huisgen investigated the influence of electronic effects on the kinetics of the reactionand reported an enhancement of the reaction by electron withdrawing substituents, such as esters.[208]

1.5.1 Regular and Inverse 1*H*-1,2,3-Triazoles

First, inverse triazoles were mentioned in 1966 as a result of an inverse Diels-Alder reaction (Figure 13).[209–211]

regular 1,4-1*H*-1,2,3-triazole   **inverse** 1,4-1*H*-1,2,3-triazole
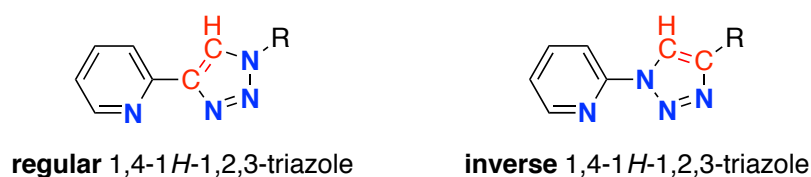
Figure 13: Regular and inverse pyridyl-triazoles.

Crowley *et al.* set up a structured study on the comparison of invers and regular 1*H*-1,2,3-triazoles. The molecular structure of these compounds was quite similar but strong differences in the reported comparable study exhibited significant differentiations in their properties, besides structural similarities. A very interesting feature was the photo activity of the ruthenium(II) complex with the invert ligands, while the complex based on the normal triazole showed no emission at all.[212] Further, in

a medical study these type of compounds showed high potential as a drug for inhibition of matrix metalloproteinases.[213]

Excursion 2: "Click" Chemistry[214]

In 2001, Sharpless defined a new class of desirable reactions and by this introduced the term "click" chemistry. Reactions with this predicate are requested to proceed without any solvent or in water and form selectively one product in high yields that can be obtained without chromatographic purification. Further, the starting material is expected to be cheap. The reaction should also provide a molecular toolbox by means of a modular system. Additionally, the product formation should be strongly thermodynamically favoured and the reaction should tolerate functional groups. A few chemical transformations show these features, like thiol-ene reactions,[215,216] selected nucleophile reaction on strained rings[217] as well as different types of cycloaddition reactions,[218,219] including the reaction of phosphaalkynes and azides.[198]

However, the Huisgens dipolar cycloaddition is in this context only in a modified form found – in Sharpless copper catalysed alkyne azide cycloaddition.

1.5.2   Mechanism of the CuAAC

Bertrand contributed the latest state of the art of the CuAAC mechanism in 2015 (Scheme 29). The reaction can proceed *via* two different pathways, involving one or two copper centres in a slow or fast reaction, respectively. Starting from N-heterocyclic carbene stabilised copper salts **5** the σ-acetylide complex is formed by addition of **6**. This σ-acetylide **7** undergoes the cycloaddition with an azide **8** showing a two magnitudes lower rate constant. After the cycloaddition, the copper triazolid **9** is formed. The catalyst is regenerated and the product **10** is released by the substitution of one equivalent of **6**. From the σ-acetylide complex **7** with a second equivalent of the copper salt **5** the π,σ-bis(copper) acetylide **11** can be formed. The cycloaddition yields the bis(copper) triazolide **12**. The catalyst regeneration is analogue to the slower process. Bertrand *et al.* were able to characterise the intermediates **11** and **12** crystallographically and their conclusions were kinetic studies and on research of other groups.
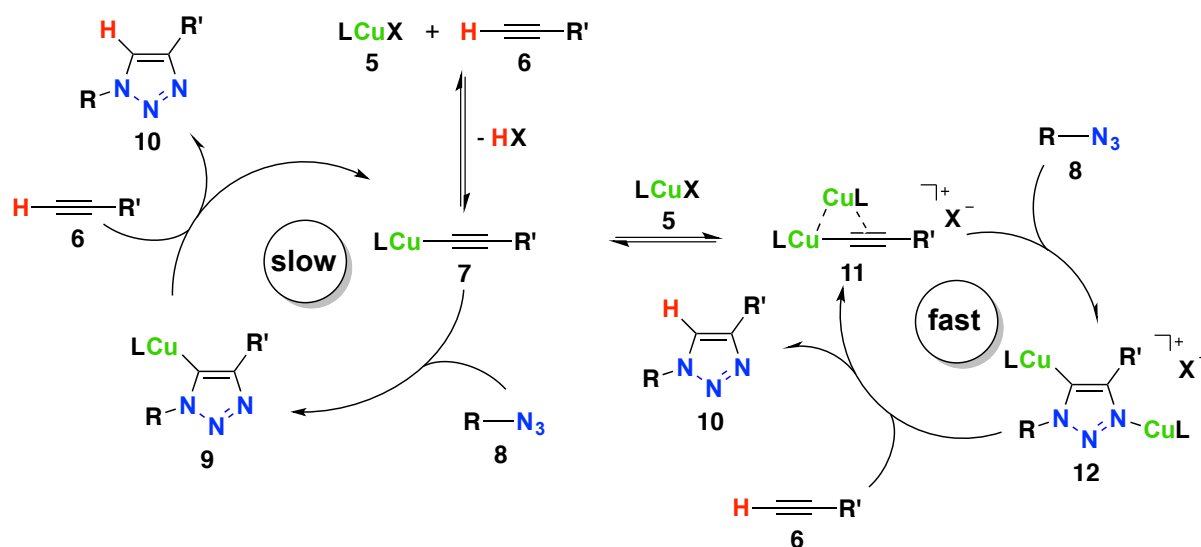
Scheme 29: Reaction mechanism proposed by Bertrand *et al.*.

However, this mechanism includes conclusions of more than ten years intense research, combining both, mono- and bis-nuclear, pathways. In 2002 Sharpless proposed a mechanism based on one **Cu**(I) ions[220] and got supported by a DFT study of Fokin in 2005.[221] Further investigation by means of a kinetic study, performed by the same group, revealed a second order dependency of the CuAAC of copper catalyst.[222] The stabilisation of the **Cu**(I) by bulky *N*-heterocyclic carbene[223–226] facilitated preparation of defined copper acetylyl species and the first isolation of an intermediate, a copper triazolide of the catalysis by Straub. Within this report the authors showed further the possibility of the mono-nuclear mediated pathway.[227] This results were not verified by DFT calculations, suggesting a binuclear mechanism.[228,229] This pathway was approved by heat-flow reaction calorimetry and mass spectrometry treating copper acetylides with enriched [63]Cu as additional external copper source. These experiments exhibited an exchange of the [63]Cu by enriching the [63]Cu/[65]Cu ratio from 69% to 85%. This was the first evidence or an interplay of binuclear copper intermediates.[230]

1.5.1 Properties and Application of 1*H*-1,2,3-Triazoles

1,2,3 triazoles are stable, aromatic heterocycles and the high tolerance towards functional groups provides an endless variation of possible substitution pattern.[231] The nitrogen N[3] is the most nucleophilic due to a higher electron density at this atom.[231,232]

Consequently, hard Lewis acids, such as protons,[233] alkylium ions[234] but also transition metals,[231] will interact with the lone pair of this nitrogen atom. The nitrogen N^2 lone pair can also interact with Lewis acids.[235] The triazole C-H is quite acidic due to a high dipole moment.[236,237] This results in a weak Lewis acid property,[238] as hydrogen bonding or deprotonating is possible, providing further applications. To give an example, the hydrogen bonding was used in supramolecular structures as a key compound for a chloride sensor.[239] Deprotonating provides another coordination side, either as triazolide *via* the carbanione or after methylation as triazolium salt *via* the carbene lone pair.[238]

1.5.4 Coordination Chemistry of 1*H*-1,2,3-Triazoles

The coordination chemistry of 1*H*-1,2,3-triazoles is manifold and strongly depends on the substituents. Most common are the mono-,[240][241] bi-[242,243] and tridentate[244,245] ligand systems. In monodentate ligands the nitrogen N^3 atom lone pair coordinates to the metal centre (type **13**, Figure 14). The coordination of metal ions *via* the N^2 atom lone pair (**14**) is only possible, if this binding side is favoured by the chelate effect[238,246–248] or if the triazole is coordinated to two different metal ions (**15**).[247] In cyclometalated compounds coordination by N^2[249] and N^3[250] lone pairs is possible. Deprotonating the triazole C-H bond enables the coordination of the carbanion in fashion **16**.[251] If the heterocycle is alkylated with methylium cation, for example, the metal centre can be coordinated though the carbene species **17**.[252]
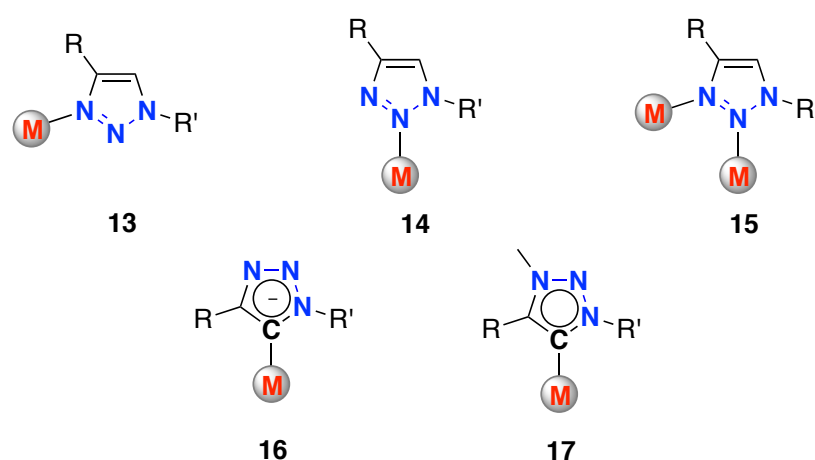
Figure 14: Coordination modes of 1*H*-1,2,3-triazoles and modified species.

Bibliography of Chapter 1

(1)   Mathey, F. *Angew. Chem. Int. Ed.* **2003**, *42* (14), 1578.

(2)   Becker, G. *Z. Anorg. Allg. Chem.* **1977**, *430* (1), 66.

(3)   Dimroth, K.; Hoffmann, P. *Angew. Chem. Int. Ed.* **1964**, *3* (5), 384.

(4)   Dimroth, K.; Hoffmann, P. *Chem. Ber.* **1966**, *99* (4), 1325.

(5)   Markl, G.; Lieb, F.; Merz, A. *Angew. Chem. Int. Ed.* **1967**, *6* (5), 458.

(6)   Ashe III, A. J. *J. Am. Chem. Soc.* **1971**, *93* (13), 3293.

(7)   Gier, E. T. *J. Am. Chem. Soc.* **1961**, *83* (7), 1769.

(8)   Schoeller, W. W. *J. Chem. Soc. Chem. Commun.* **1985**, 334.

(9)   Waluk, J.; Klein, H. P.; Ashe III, A. J.; Michl, J. *Organometallics* **1989**, *8* (12), 2804.

(10)   Le Floch, P. *Coordination Chemistry Reviews*. 2006, pp 627–681.

(11)   Lacombe, S.; Gonbeau, D.; Cabioch, J.; Pellerin, B.; Denis, J.; Pfister-Guillouzo, G. *J. Am. Chem. Soc.* **1988**, *110*, 6964.

(12)   Schmidt, M. W.; Truong, P. N.; Gordon, M. S. *J. Am. Chem. Soc.* **1987**, *109* (15), 5217.

(13)   Schleyer, P. V. R.; Kost, D. *J. Am. Chem. Soc.* **1988**, *110* (7), 2105.

(14)   Duchamp, J. C.; Pakulski, M.; Crowley, A. H.; Zlim, K. W. *J. Am. Chem. Soc.* **1990**, *112*, 6803.

(15)   Dillon, K. B.; Mathey, F.; Nixon, J. F. *Phosphorus: The Carbon Copy*; JOHN WILEY & SONS: Weinheim, 2001.

(16)   van der Knaap, T. A.; Bickelhaupt, F.; Kraaykamp, J. G.; van Koten, G.; Bernards, J. P. C.; Edzes, H. T.; Veeman, W. S.; de Boer, E.; Baerends, E. J. *Organometallics* **1984**, *3* (3), 1804.

(17)   Apfel, R.; Casser, C.; Knoch, F. *J. Organomet. Chem.* **1985**, *293* (2), 213.

(18)   Lorenz, I.-P.; Pohl, W.; Nöth, H.; Schmidt, M. *J. Organomet. Chem.* **1994**, *475* (1-2), 211.

(19)   Knoll, K.; Huttner, G.; Wasiucionek, M.; Zsolnai, L. *Angew. Chem. Int. Ed.* **1984**, *23* (9), 739.

(20)   Pellerin, B.; Denis, J. M.; Perrocheau, J.; Carrie, R. *Tetrahedron Lett.* **1986**, *27* (47), 5723.

(21)   Meriem, A.; Majoral, J.-P.; Revel, M.; Navech, J. *Tetrahedron Lett.* **1975**, *24* (19), 1975.

(22)   Bauer, S.; Marinetti, A.; Ricard, L.; Mathey, F. *Angew. Chem. Int. Ed.* **1990**, *29* (10), 1166.

(23)   de Vaumas, R.; Marinetti, A.; Mathey, F. *J. Organomet. Chem.* **1991**, *413*, 411.

(24)   Regitz, M. *Chem. Rev.* **1990**, *90* (1), 191.

(25)   Eshtiagh-Hosseini, H.; Kroto, H. W.; Nixon, J. F. *J. Chem. Soc., Chem. Commun.* **1979**, 653.

(26)   Hopkinson, M. J.; Kroto, H. W.; Nixon, J. F.; Simmons, N. P. C. *Chem. Phys. Lett.* **1976**, *42* (3), 460.

(27)   Burckett, J. C. T. R.; Laurent, S.; Cooper, T. A.; Kroto, H. W.; Nixon, J. F.; Ohashi, O.; Ohno, K. *J. Mol. Struct.* **1982**, *79*, 215.

(28)   Durrant, M. C.; Kroto, H. W.; McNaughton, D.; Nixon, J. F. *J. Mol. Spectrosc.* **1985**, *109*, 8.

(29)   Cooper, T. A.; Kroto, H. W.; Nixon, J. F.; Ohashi, O. *Chem. Commun.* **1980**, 333.

(30)   Appel, R.; Maier, G.; Reisenauer, H. P. *Angew. Chem. Int. Ed.* **1981**, *20* (2), 197.

(31)   Mansell, S. M.; Green, M.; Kilby, R. J.; Murray, M.; Russell, C. A. *C. R. Chim.* **2010**, *13* (8-9), 1073.

(32)   Becker, G.; Gresser, G.; Uhl, W. *Z. Naturforsch. B* **1981**, *36* (1), 16.

(33)   Allspach, T.; Regitz, M. *Synthesis* **1986**, *1986* ((1)), 31.

(34)   Mack, A.; Pierron, E.; Allspach, T.; Bergsträßer, U.; Regitz, M. *Synthesis* **1998**, *1998* (1), 1305.

(35)   Märkl, G.; Sejpka, H. *Angew. Chem.* **1986**, *98* (3), 286.

(36)   Veeck, W.-G. 1,2,4-Diazaphosphole mit Phosphanyl- und Arsanylsubstituenten [mit einem Anhang über ein Bis(phosphaalkin)], Universität Kaiserslautern, 1997.

(37)   Brym, M.; Jones, C. *Dalton Trans.* **2003**, *476* (22), 3665.

(38)   Carmichael, D.; Al-Resayes, S. I.; Nixon, J. F. *J. Organomet. Chem.* **1993**, *453* (2), 207.

(39)   Becker, G.; Herrmann, W. A.; Kalcher, W.; Kriechbaum, G. W.; Pahl, C.; Wagner, C. T.; Ziegler, M. L. *Angew. Chem. Int. Ed.* **1983**, *22*, 413.

(40)   James, J. C. T. R.; Hitchcock, P. B.; Kroto, H. W.; Meidine, M. F.; Nixon, J. F. *J. Organomet. Chem.* **1982**, *238* (4), C82.

(41)   Hitchcock, P. B.; Meidine, M. F.; Nixon, J. F. *J. Organomet. Chem.* **1987**, *333* (3), 337.

(42)   Meidine, F.; Meir, J.; Nixon, F. *J. Organomet. Chem.* **1985**, *297* (2), 255.

(43)   Bartsch, R.; Hitchcock, P. B.; Meidine, M. F.; Nixon, J. F. *J. Organomet. Chem.* **1984**, *266* (3), C41.

(44)   Al-Resayes, S. I.; Hitchcock, P. B.; Nixon, J. F.; Michael, D.; Mingos, P. *J. Chem. Soc., Chem. Commun.* **1985**, 365.

(45)   Appel, R.; Westerhaus, A. *Tetrahedron Lett.* **1981**, *22* (23), 2159.

(46)   Guillemin, J.-C.; Janati, T.; Denis, J.-M. *J. Chem. Soc., Chem. Commun.* **1992**, 415.

(47)   Haber, S.; Le Floch, P.; Mathey, F. *J. Chem. Soc., Chem. Commin.* **1992**, No. 24, 1799.

(48)   Berger, D. J.; Gaspar, P. P.; Grev, R. S.; Mathey, F. *Organometallics* **1994**, *13* (2), 640.

(49)   Guillemin, J.-C.; Janati, T.; Denis, J. M.; Guenot, P.; Savignac, P. *Angew. Chem. Int. Ed.* **1991**, *30* (2), 196.

(50)   Burckett-St. Laurent, J. C. T. R.; King, M. A.; Kroto, H. W.; Nixon, J. F.; Suffolk, R. J. *J. Chem. Soc., Dalt. Trans.* **1983**, 755.

(51)   Laali, K. K.; Geissler, B.; Regitz, M.; Houser, J. J. *J. Org. Chem.* **1995**, *60* (20), 6362.

(52)   Antipin, M. Y.; Chernega, A. N.; Lysenko, K. A.; Struchkova, Y. T.; Nixon, J. F. *J. Chem. Soc., Chem. Commun.* **1995**, 505.

(53)   Chernega, A. N.; Antipin, M. Y.; Struchkov, Y. T.; Meidine, M. F.; Nixon, J. F. *Heteroat. Chem.* **1992**, *2* (6), 665.

(54)   Arif, A. M.; Barron, A. R.; Cowley, A. H.; Hall, S. W. *J. Chem. Soc., Chem. Commun.* **1988**, 171.

(55)   Wagner, O.; Ehle, M.; Regitz, M. *Angew. Chem. Int. Ed.* **1989**, *28*, 225.

(56)   Weber, W.; de Meijere, A. *Angew. Chem. Int. Ed.* **1980**, *19* (2), 138.

(57)   Schafer, A.; Weidenbruch, M.; Saak, W.; Pohl, S. *Angew. Chem. Int. Ed.* **1987**, *26* (8), 776.

(58)   Cowley, A. H.; Hall, S. W.; Nunn, C. M.; Power, J. M. *J. Chem. Soc., Chem. Commun.* **1988**, 753.

(59)   Niecke, E.; Barion, D. *Tetrahedron Lett.* **1989**, *30* (4), 459.

(60)   Wettling, T.; Schneider, J.; Wagner, O.; Kreiter, C. G.; Regitz, M. *Angew. Chem. Int. Ed.* **1989**, *28* (8), 1013.

(61)   Regitz, M.; Hees, U.; Rösch, W. *Chem. Ber.* **1987**, *120*, 1645.

(62)   Ko, Y. Y. C. Y. L.; Carrié, R.; Muench, A.; Becker, G. *J. Chem. Soc., Chem. Commun.* **1984**, 1634.

(63)   Rösch, W.; Facklam, T.; Regitz, M. *Tetrahedron* **1987**, *43* (14), 3247.

(64)   Fuchs, E. P. O.; Hermesdorf, M.; Schnurr, W.; Rösch, W.; Heydt, H.; Regitz, M.; Binger, P. *J. Organomet. Chem.* **1988**, *338* (3), 329.

(65)   Allspach, T.; Regitz, M.; Becker, G.; Becker, W. *Synthesis* **1986**, 31.

(66) Rosch, W.; Vogelbacher, U.; Allspach, T.; Regitz, M. *J. Organomet. Chem.* **1986**, *306*, 39.

(67) Bergsträßer, U.; Hoffmann, A.; Regitz, M. *Tetrahedron Lett.* **1992**, *33* (8), 1049.

(68) Bergsträßer, U.; Stannek, J.; Regitz, M. *J. Chem. Soc., Chem. Commun.* **1994**, 1121.

(69) Grundmann, C. *Synthesis* **1970**, 344.

(70) Rösch, W.; Regitz, M. *Z. Naturforsch. B* **1986**, *41b*, 931.

(71) Fink, J.; Rosch, W.; Vogelbacher, U.-J.; Regitz, M. *Angew. Chem. Int. Ed.* **1986**, *25* (3), 280.

(72) Blatter, K.; Rosch, W.; Vogelbacher, U.-J.; Fink, J.; Regitz, M. *Angew. Chem. Int. Ed.* **1987**, *26* (1), 85.

(73) Maas, G.; Fink, J.; Wingert, H.; Blatter, K.; Regitz, M. *Chem. Ber.* **1987**, *120*, 819.

(74) Annen, U.; Regitz, M. *Tetrahedron Lett.* **1987**, *28* (43), 5141.

(75) Hitchcock, P. B.; Maah, M. J.; Nixon, J. F.; Zora, J. A.; Leigh, G. J.; Bakar, M. A. *Angew. Chem. Int. Ed.* **1987**, *26* (5), 474.

(76) Burckett-St. Laurent, J. C. T. R.; Hitchcock, P. B.; Kroto, H. W.; Nixon, J. F. *J. Chem. Soc. Chem. Commun.* **1981**, 1141.

(77) Al-Resayes, S. I.; Klein, S. I.; Kroto, H. W.; Meidine, M. F.; Nixon, J. F. *J. Chem. Soc., Chem. Commun.* **1983**, 930.

(78) Binger, P.; Muller, P.; Benn, R.; Rufinska, A.; Gabor, B.; Kruger, C. *Chem. Ber.* **1989**, *122* (6), 1035.

(79) Brauers, G.; Green, M.; Jones, C.; Nixon, J. F. *J. Chem. Soc., Chem. Commun.* **1995**, 1125.

(80) Binger, P.; Biedenbach, B.; Herrmann, A. T.; Langhauser, F.; Betz, P.; Goddard, R.; Krüger, C. *Chem. Ber.* **1990**, *123* (8), 1617.

(81) Al-Resayes, S. I.; Hitchcock, P. B.; Meidine, M. F.; Nixon, J. F. *J. Chem. Soc., Chem. Commin.* **1984**, 1080.

(82) Trathen, N.; Leech, M. C.; Crossley, I. R.; Greenacre, V. K.; Roe, S. M. *Dalton Trans.* **2014**, *43* (24), 8961.

(83) Cordaro, J. G.; Stein, D.; Rüegger, H.; Grützmacher, H. *Angew. Chem. Int. Ed.* **2006**, *45* (37), 6159.

(84) Müller, C.; Sklorz, J. A. W.; de Krom, I.; Loibl, A.; Habicht, M.; Bruce, M.; Pfeifer, G.; Wiecko, J. *Chem. Lett.* **2014**, *43* (9), 1390.

(85) Müller, C.; Broeckx, L. E. E.; de Krom, I.; Weemers, J. J. M. *Eur. J. Inorg. Chem.* **2013**, 187.

(86) Nyulászi, L. *Inorg. Chem.* **1996**, *35* (16), 4690.

(87) Glukhovtsev, M. N.; Dransfeld, A.; Schleyer, P. V. R. *J. Phys. Chem.* **1996**, *100* (96), 13447.

(88) Märkl, G.; Dietl, S.; Ziegler, M. L.; Nuber, B. *J. Chem. Inf. Model.* **2013**, *53* (9), 1689.

(89) Deschamps, E.; Ricard, L.; Mathey, F. *Angew. Chem. Int. Ed.* **1994**, *33* (1), 1158.

(90) Märkl, G.; Dorfmeister, G. *Tetrahedron Lett.* **1987**, *28* (10), 1093.

(91) Märkl, G.; Dörges, C.; Riedl, T.; Klärner, F. G.; Lodwig, C. *Tetrahedron Lett.* **1990**, *31* (32), 4589.

(92) Märkl, G.; Olbrich, H. *Angew. Chem. Int. Ed.* **1966**, *5* (6), 588.

(93) Märkl, G. *Angew. Chem. Int. Ed.* **1966**, *5* (9), 846.

(94) Mathey, F. *Tetrahedron* **1972**, *28* (15), 4171.

(95) Mathey, F. *Tetrahedron* **1973**, *29* (5), 707.

(96) Mathey, F.; Thavard, D.; Bartet, B. *J. Can. Chem.* **1975**, *54* (6), 855.

(97) Alcaraz, J. M.; Breque, A.; Mathey, F. *Tetrahedron Lett.* **1982**, *23* (15), 1565.

(98) Mathey, F. *Tetrahedron Lett.* **1979**, *20* (20), 1753.

(99)   Märkl, G.; Matthes, D. *Tetrahedron Lett.* **1974**, *15* (49-50), 4381.

(100)   Holand, S.; Ricard, L.; Matheys, F. *J. Org. Chem.* **1991**, *56* (12), 4031.

(101)   Keglevich, G.; Ujszaszy, K.; Kovacs, A.; Toke, L. *J. Org. Chem.* **1993**, *58* (4), 977.

(102)   Le Floch, P.; Mathey, F. *Tetrahedron Lett.* **1989**, *30* (7), 817.

(103)   Teunissen, H. T.; Bickelhaupt, F. *Tetrahedron Lett.* **1992**, *33* (24), 3537.

(104)   Le Floch, P.; Mathey, F. *J. Chem. Soc., Chem. Commun.* **1993**, No. 16, 1295.

(105)   Vogelbacher, U. J.; Ledermann, M.; Schach, T.; Micheks, G.; Hees, U.; Regitz, M. *Angew. Chem. Int. Ed.* **1988**, *27* (2), 272.

(106)   Breit, B. *J. Mol. Catal. Chem.* **1999**, *143* (1-3), 143.

(107)   Märkl, G.; Baier, H. *Liebigs Ann. Chem.* **1981**, No. 5, 919.

(108)   Märkl, G.; Kneidl, F. *Angew. Chem. Int. Ed.* **1973**, *12* (11), 931.

(109)   Le Floch, P.; Carmichael, D.; Ricard, L.; Mathey, F. *J. Am. Chem. Soc.* **1993**, *115* (23), 10665.

(110)   Kostenko, N.; Ericsson, C.; Engqvist, M.; Gonzalez, S. V.; Bayer, A. *Eur. J. Org. Chem.* **2013**, *2* (22), 4756.

(111)   Habicht, M. H.; Wossidlo, F.; Weber, M.; Müller, C. *Chem. Eur. J.* **2016**.

(112)   Müller, C.; Wasserberg, D.; Weemers, J. J. M.; Pidko, E. A.; Hoffmann, S.; Lutz, M.; Spek, A. L.; Meskers, S. C. J.; Janssen, R. A. J.; Van Santen, R. A.; Vogt, D. *Chem. Eur. J.* **2007**, *13* (16), 4548.

(113)   Loibl, A.; de Krom, I.; Pidko, E. a; Weber, M.; Wiecko, J.; Müller, C. *Chem. Commun.* **2014**, *50* (64), 8842.

(114)   De Krom, I.; Broeckx, L. E. E.; Lutz, M.; Müller, C. *Chem. Eur. J.* **2013**, *19* (11), 3676.

(115)   Müller, C.; Pidko, E. A.; Lutz, M.; Spek, A. L.; Vogt, D. *Chem. Eur. J.* **2008**, *14* (29), 8803.

(116)   Dimroth, K.; Greif, N.; Stade, W.; Steuber, F. W. *Angew. Chem. Int. Ed.* **1967**, *6* (8), 711.

(117)   Märkl, G.; Lieb, F.; Merz, A. *Angew. Chem. Int. Ed.* **1967**, *6* (11), 944.

(118)   Rigo, M.; Sklorz, J. A. W.; Hatje, N.; Noack, F.; Weber, M.; Wiecko, J.; Müller, C. *Dalton Trans.* **2015**, *3*, 2218.

(119)   Schleyer, P. V. R.; Maerker, C.; Dransfeld, A.; Jiao, H.; Van Eikema Hommes, N. J. R. *J. Am. Chem. Soc.* **1996**, *118* (26), 6317.

(120)   Fowler, P. W.; Havenith, R. W. A.; Jenneskens, L. W.; Soncini, A.; Steiner, E. *Angew. Chem. Int. Ed.* **2002**, *41* (9), 1558.

(121)   Baldridge, K. K.; Gordon, M. S. *J. Am. Chem. Soc.* **1988**, *110* (13), 4204.

(122)   Nyulászi, L.; Veszprémi, T.; Réffy, J. *J. Phys. Chem.* **1993**, *97* (16), 4011.

(123)   Jonas, V.; Frenking, G. *Chem. Phys. Lett.* **1993**, *210* (1-3), 211.

(124)   Le Floch, P.; Mathey, F. *Coord. Chem. Rev.* **1998**, *178-180*, 771.

(125)   Wong, T. C.; Bartell, L. S. *J. Chem. Phys.* **1978**, *61* (7), 2840.

(126)   Batich, C.; Heilbronner, E.; Hornung, V.; Ashe III, A. J.; Clark, D. T.; Cobley, U. T.; Kilcast, D.; Scanlan, I. *J. Am. Chem. Soc.* **1973**, *95* (3), 928.

(127)   Nyulaszi, L.; Keglevich, G. *Heteroat. Chem.* **1994**, *5* (2), 131.

(128)   Hodges, R. V.; Beauchamp, J. L.; AsheIII, A. J.; Chan, W. T. *Organometallics* **1985**, *4* (3), 457.

(129)   Dave, T. N.; Kaletsch, H.; Dimroth, K. *Angew. Chem. Int. Ed.* **1984**, *23* (12), 989.

(130)   Bene, J. E. Del; Elguero, J. *Magn. Reson. Chem.* **2006**, *44* (8), 784.

(131) Moores, A.; Ricard, L.; Le Floch, P. *Angew. Chem. Int. Ed.* **2003**, *42* (40), 4940.

(132) Ashe III, A. J.; Sharp, R. R.; Tolan, J. W. *J. Am. Chem. Soc.* **1976**, *98* (18), 5451.

(133) Dimroth, K.; Städe, W. *Angew. Chem. Int. Ed.* **1968**, *7* (11), 881.

(134) Hettche, A.; Dimroth, K. *Tetrahedron Lett.* **1972**, *13* (9), 829.

(135) Märkl, G.; Baier, H.; Liebl, R.; Stephenson, D. S. *Liebigs Ann. Chem.* **1981**, *1981* (5), 870.

(136) Märkl, G.; Merz, A. *Tetrahedron Lett.* **1969**, *10* (16), 1231.

(137) Märkl, G.; Lieb, F.; Merz, A. *Angew. Chem. Int. Ed.* **1967**, *6* (1), 87.

(138) Märkl, G.; Merz, A. *Tetrahedron Lett.* **1968**, *9* (2), 3611.

(139) Baudler, M.; Bock, M. *Angew. Chem. Int. Ed.* **1974**, *13* (2), 148.

(140) Ashe, A. J.; Smith, T. W. *Tetrahedron Lett.* **1977**, *18* (5), 407.

(141) Bruce, M.; Meissner, G.; Weber, M.; Wiecko, J.; Müller, C. *Eur. J. Inorg. Chem.* **2014**, 1719.

(142) Tolman, C. A. *J. Am. Chem. Soc.* **1970**, *92* (10), 2956.

(143) Tolman, C. A.; Seidel, W. C.; Gosser, L. W. *J. Am. Chem. Soc.* **1974**, *96* (1), 53.

(144) Tolman, C. A. *Chem. Rev.* **1977**, *77* (3), 313.

(145) Evans, D.; Osborn, J. A.; Wilkinson, G. *J. Chem. Soc. A* **1968**, 3133.

(146) DiMauro, E. F.; Kozlowski, M. C. *J. Chem. Soc., Perkin Trans. 1* **2002**, 439.

(147) Müller, C. *Phosphorus(III) Ligands Homog. Catal. Des. Synth.* **2012**, No. Iii, 287.

(148) Daly, J. J. *J. Chem. Soc. Abstr.* **1964**, No. 3799 - 3810.

(149) Bart, J. C. J. *Angew. Chem. Int. Ed.* **1968**, *7* (9), 730.

(150) Deberitz, J.; Nöth, H. *Chem. Ber.* **1970**, *103* (8), 2541.

(151) Vahrenkamp, H.; Nöth, H. *Chem. Ber.* **1972**, *105* (4), 1148.

(152) Deberitz, J.; Nöth, H. *J. Organomet. Chem.* **1973**, *49*, 453.

(153) Nainan, K. C.; Sears, C. T. *J. Organomet. Chem.* **1978**, *148*, C31.

(154) Deberitz, J.; Nöth, H. *Chem. Ber.* **1973**, *106* (7), 2222.

(155) Arce, A. J.; Deeming, A. J.; Sanctis, Y. De; Manzur, J. *J. Chem. Soc., Chem. Commun.* **1993**, 325.

(156) Rosa, P.; Le Floch, P.; Ricard, L. *J. Am. Chem. Soc.* **1997**, *119* (40), 9417.

(157) Broeckx, L. E. E.; Bucci, A.; Zuccaccia, C.; Lutz, M.; Macchioni, A.; Müller, C. *Organometallics* **2015**, *34*, 2943.

(158) Hettche, A.; Dimroth, K. *Chem. Ber.* **1973**, *106* (3), 1001.

(159) Alcaraz, J.-M.; Mathey, F. *J. Chem. Soc., Chem. Commun.* **1984**, 508.

(160) Holah, D. G.; Hughes, A. N.; Knudsen, K. L. *J. Chem. Soc., Chem. Commun.* **1988**, 493.

(161) Pfeifer, G.; Ribagnac, P.; Le Goff, X. F.; Wiecko, J.; Mézailles, N.; Müller, C. *Eur. J. Inorg. Chem.* **2015**, 240.

(162) Kanter, H.; Mach, W.; Dimroth, K. *Chem. Ber.* **1977**, *110* (2), 395.

(163) Märkl, G.; Beckh, H. J.; Ziegler, M. L.; Schmitz, A. *Angew. Chem. Int. Ed.* **1987**, *26* (11), 1134.

(164) Breit, B. *Chem. Commun.* **1996**, 2071.

(165) Baeuerlein, P. S.; Gonzalez, I. A.; Weemers, J. J. M.; Lutz, M.; Spek, A. L.; Vogt, D.; Müller, C. *Chem. Commun.* **2009**, No. 33, 4944.

(166) Müller, C.; Vogt, D. *Dalton Trans.* **2007**, 5505.

(167) Broeckx, L. E. E.; Lutz, M.; Vogt, D.; Müller, C. *Chem. Commun.* **2011**, *47* (7), 2003.

(168) Broeckx, L. E. E.; Delaunay, W.; Latouche, C.; Lutz, M.; Hissler, M.; Müller, C. **2013**, *45*, 10738.

(169) Roesch, P.; Nitsch, J.; Lutz, M.; Wiecko, J.; Steffen, A.; Müller, C. *Inorg. Chem.* **2014**, *53* (18), 9855.

(170) Sklorz, J. A. W.; Müller, C. *Eur. J. Inorg. Chem.* **2016**, 595.

(171) Bansal, R. K.; Gupta, N. *Sci. Synth.* **2004**, *13*, 743.

(172) Nyulászi, L.; Veszpremi, T.; Reffy, J.; Burkhardt, B.; Regitz, M. *J. Am. Chem. Soc.* **1992**, *114* (23), 9080.

(173) Lowe-Ma, C.; Nissan, R. A.; Wilson, W. S. *J. Org. Chem.* **1990**, *55* (12), 3755.

(174) Van Der Knaap, T. A.; Klebach, T. C.; Visser, F.; Bickelhaupt, F.; Ros, P.; Baerends, E. J.; Stam, C. H.; Konijn, M. *Tetrahedron* **1984**, *40* (4), 765.

(175) Nyulászi, L. *J. Phys. Chem.* **1996**, *100* (15), 6194.

(176) Nyulászi, L. *Tetrahedron* **2000**, *56* (1), 79.

(177) Mézailles, N.; Mathey, F.; Le Floch, P. *Prog. Inorg. Chem* **2001**, *49*, 455.

(178) Rösch, W.; Regitz, M. *Angew. Chem. Int. Ed.* **1984**, *9*, 900.

(179) Nguyen, L. T.; Proft, F. De; Dao, V. L.; Nguyen, M. T.; Geerlings, P. *J. Phys. Org. Chem.* **2003**, *16*, 615.

(180) Märkl, G.; Tretsch-Schaller, I.; Holzl, W. *Tetrahedron Lett.* **1988**, *29* (7), 785.

(181) Regitz, M.; Binger, P. *Angew. Chem. Int. Ed.* **1988**, *27*, 1484.

(182) Schrodel, H.-P.; Schmidpeter, A. *Chem. Ber./Recueil* **1997**, *130*, 89.

(183) Chapyshev, S. V.; Bergstrasser, U.; Regitz, M. *Khim. Geterotsikl. Soedin.* **1996**, No. 1, 67.

(184) Chapyshev, S. V.; Bergstrasser, U.; Regitz, M. *Russ. Chem. B.* **1996**, *45* (1), 242.

(185) Chapyshev, S. V.; Anisimov, M. V. *Chem. Heterocycl. Compd.* **1997**, *33* (5), 587.

(186) da Silva, J. J. R. F. *J. Chem. Educ.* **1983**, *60* (5), 390.

(187) Grützmacher, H. *Angew. Chem. Int. Ed.* **2008**, *47* (10), 1814.

(188) Grützmacher, H. *Angew. Chem.* **2008**, *120* (10), 1838.

(189) Wassenaar, J.; Reek, J. N. H. *Org. Biomol. Chem.* **2011**, *9* (6), 1704.

(190) Weinmaier, J. H.; Tautz, H.; Schmidpeter, A.; Pohl, S. *J. Organomet. Chem.* **1980**, *185* (1), 53.

(191) Schmidpeter, A.; Tautz, H.; Seyerl, J. von; Huttner, G. *Angew. Chem. Int. Ed.* **1981**, *20* (4), 408.

(192) Issleib, K.; Vollmer, R. *Z. Anorg. Allg. Chem.* **1981**, *481* (10), 22.

(193) Kraaijkamp, J. G.; Koten, G. van; Vrieze, K.; Grove, D. M.; Klop, E. A.; Spek, A. L.; Schmidpeter, A. *J. Organomet. Chem.* **1983**, *256* (2), 375.

(194) Kraaijkamp, J. G.; Grove, D. M.; Van, K. G.; Schmidpeter, A. *Inorg. Chem.* **1988**, *27* (15), 2612.

(195) Crassous, J.; Réau, R. *Dalton Trans.* **2008**, No. 48, 6865.

(196) Choong, S. L.; Nafady, A.; Stasch, A.; Bond, A. M.; Jones, C. *Dalton Trans.* **2013**, *42* (21), 7775.

(197) Chia, S. P.; Li, Y.; So, C. W. *Organometallics* **2013**, *32* (18), 5231.

(198) Choong, S. L.; Jones, C.; Stasch, A. *Dalton Trans.* **2010**, *39*, 5774.

(199) Chan, T. R.; Hilgraf, R.; Sharpless, K. B.; Fokin, V. V. *Org. Lett.* **2004**, *6* (27), 2853.

(200) Nowak, D. Untersuchung von Einelektronenoxidationen an λ^3-Phosphininen, Master Thesis Freie Universität Berlin, 2016.

(201) Li, Z.; Zhu, A.; Yang, J. *J. Heterocycl. Chem.* **2012**, *49* (Scheme 1), 1458.

(202) Abdou, W. M.; Ganoub, N. A.; Sabry, E. *Monatsh. Chem.* **2016**, *147* (3), 619.

(203) Huisgen, R.; Knorr, R.; Möbius, L.; Szeimies, G. *Chem. Ber.* **1965**, *98* (12), 4014.

(204) Huisgen, R. *Chem. Ber.* **1967**, *100* (8), 2494.

(205) Huisgen, R. *Proc. Chem. Soc.* **1961**, 357.

(206) Huisgen, R. *Angew. Chem.* **1963**, *13* (1938), 604.

(207) Huisgen, R. *Angew. Chem. Int. Ed.* **1963**, *2* (10), 565.

(208) Huisgen, R. *Angew. Chem. Int. Ed.* **1963**, *2* (11), 633.

(209) Seitz, G.; Kämpchen, T. *Arch. Pharm. (Weinheim).* **1972**, *310* (3), 269.

(210) Miller, J. A.; Dudley, M. W.; Kehne, J. H.; Sorensen, S. M.; Kane, J. M. *Br. J. Pharmacol.* **1992**, *107* (1), 78.

(211) Baumann, L.; Kämpchen, T.; Seitz, G. *Chem. Ber.* **1992**, *125* (1), 171.

(212) Lo, W. K. C.; Huff, G. S.; Cubanski, J. R.; Kennedy, A. D. W.; McAdam, C. J.; McMorran, D. A.; Gordon, K. C.; Crowley, J. D. *Inorg. Chem.* **2015**, *54* (4), 1572.

(213) Hugenberg, V.; Riemann, B.; Hermann, S.; Schober, O.; Scha, M.; Zhang, W.; Kopka, K.; Wagner, S. *J. Med. Chem.* **2013**, *56*, 6858.

(214) Kolb, H. C.; Finn, M. G.; Sharpless, K. B. *Angew. Chem. Int. Ed.* **2001**, *40* (11), 2004.

(215) Hoyle, C. E.; Bowman, C. N. *Angew. Chem. Int. Ed.* **2010**, *49* (9), 1540.

(216) Lowe, A. B. *Polym. Chem.* **2010**, *1* (1), 17.

(217) Kashemirov, B. A.; Bala, J. L. F.; Chen, X.; Ebetino, F. H.; Xia, Z.; Russell, R. G. G.; Coxon, F. P.; Roelofs, A. J.; Rogers, M. J.; McKenna, C. E. *Bioconjugate Chem.* **2008**, *19* (12), 2308.

(218) Stöckmann, H.; Neves, A. A.; Stairs, S.; Brindle, K. M.; Leeper, F. J. *Org. Biomol. Chem.* **2011**, *9*, 7303.

(219) Blackman, M. L.; Royzen, M.; Fox, J. M. *J. Am. Chem. Soc.* **2008**, *130* (41), 13518.

(220) Rostovtsev, V. V.; Green, L. G.; Fokin, V. V.; Sharpless, K. B. *Angew. Chem. Int. Ed.* **2002**, *41* (14), 2596.

(221) Himo, F.; Lovell, T.; Hilgraf, R.; Rostovtsev, V. V.; Noodleman, L.; Sharpless, K. B.; Fokin, V. V. *J. Am. Chem. Soc.* **2005**, *127* (1), 210.

(222) Rodionov, V. O.; Fokin, V. V.; Finn, M. G. *Angew. Chem.* **2005**, *44* (15), 2210.

(223) III, A. J. A.; Krafczyk, R.; Schmutzler, R.; Craig, H. A.; Goerlich, J. R.; Marshall, W. J.; Unverzagt, M. *Tetrahedron* **1999**, *55* (51), 14523.

(224) Goj, L. A.; Blue, E. D.; Munro-leighton, C.; Gunnoe, T. B.; Carolina, N.; Uni, S.; Carolina, N.; Bennett, C. E.; Virginia, W.; Uni, V.; Virginia, W. *Inorg. Chem.* **2005**, *44* (24), 8647.

(225) Mankad, N. P.; Gray, T. G.; Laitar, D. S.; Sadighi, J. P. *Organometallics* **2004**, *23* (6), 1191.

(226) Díez-González, S.; Correa, A.; Cavallo, L.; Nolan, S. P. *Chem. Eur. J.* **2006**, *12* (29), 7558.

(227) Nolte, C.; Mayer, P.; Straub, B. F. *Angew. Chem.* **2007**, *119* (12), 2147.

(228) Straub, B. F. *Chem. Commun.* **2007**, 3868.

(229) Cantillo, D.; Ávalos, M.; Babiano, R.; Cintas, P.; Jiménez, J. L.; Palacios, J. C. *Org. Biomol. Chem.* **2011**, *9* (8), 2952.

(230) Worrell, B. T.; Malik, J. a.; Fokin, V. V. *Science* **2013**, *340*, 457.

(231) Schulze, B.; Schubert, U. S. *Chem. Soc. Rev.* **2014**, *43* (8), 2522.

(232) Maisonial, A.; Serafin, P.; Traïkia, M.; Debiton, E.; Théry, V.; Aitken, D. J.; Lemoine, P.; Viossat, B.; Gautier, A. *Eur. J. Inorg. Chem.* **2008**, No. 2, 298.

(233) Schweinfurth, D.; Hardcastle, K. I.; Bunz, U. H. F. *Chem. Commun.* **2008**, 2203.

(234) Guisado-Barrios, G.; Bouffard, J.; Donnadieu, B.; Bertrand, G. *Angew. Chem. Int. Ed.* **2010**, *49* (28), 4759.

(235) Song, L.-C.; Wang, L.-X.; Yin, B.-S.; Li, Y.-L.; Zhang, X.-G.; Zhang, Y.-W.; Luo, X.; Hu, Q.-M. *Eur. J. Inorg. Chem.* **2008**, *2008* (2), 291.

(236) Begtrup, M.; Nielsen, C. J.; Nygaard, L.; Samdal, S.; Sjogren, C. E.; Sorensen, G. O. *Acta Chem. Scand. Ser.* **1988**, *A42*, 500.

(237) Hua, Y.; Flood, A. H. *Chem. Soc. Rev.* **2010**, *39* (4), 1262.

(238) Struthers, H.; Mindt, T. L.; Schibli, R. *Dalton Trans.* **2010**, *39* (3), 675.

(239) Gassensmith, J. J.; Matthys, S.; Lee, J. J.; Wojcik, A.; Kamat, P. V.; Smith, B. D. *Chem. Eur. J.* **2010**, *16* (9), 2916.

(240) Suijkerbuijk, B. M. J. M.; Aerts, B. N. H.; Dijkstra, H. P.; Lutz, M.; Spek, A. L.; van Koten, G.; Klein Gebbink, R. J. M. *Dalton Trans.* **2007**, 1273.

(241) Badèche, S.; Daran, J.-C.; Ruiz, J.; Astruc, D. *Inorg. Chem.* **2008**, *47* (11), 4903.

(242) Makoto Obata, Asuka Kitamura, Akemi Mori, Chiaki Kameyama, J. A. C.; Tanaka, R.; Kinoshita, I.; Kusumoto, T.; Hashimoto, H.; Harada, M.; Mikata, Y.; Funabiki, T.; Yano, S. *Dalton Trans.* **2008**, No. 25, 3292.

(243) Urankar, D.; Pinter, B.; Pevec, A.; De Proft, F.; Turel, I.; Kosmrlj, J. *Inorg. Chem.* **2010**, *49* (11), 4820.

(244) Yang, W.; Wang, L.; Zhong, Y.; Yao, J. *Organometallics* **2011**, *30*, 2236.

(245) Crowley, J. D.; Bandeen, P. H.; Hanton, L. R. *Polyhedron* **2010**, *29* (1), 70.

(246) Amadio, E.; Scrivanti, A.; Chessa, G.; Matteoli, U.; Beghetto, V.; Bertoldini, M.; Rancan, M.; Dolmella, A.; Venzo, A.; Bertani, R. *J. Organomet. Chem.* **2012**, *716*, 193.

(247) Jahromi, E. Z.; Gailer, J. *Dalton Trans.* **2010**, No. 2, 329.

(248) Ju, R.; Tessier, M.; Olliff, L.; Woods, R.; Summers, A.; Geng, Y. *Chem. Commun.* **2011**, *47* (1), 268.

(249) Beyer, B.; Ulbricht, C.; Escudero, D.; Friebe, C.; Winter, A.; González, L.; Schubert, U. S. *Organometallics* **2009**, *28* (18), 5478.

(250) Maity, R.; Hohloch, S.; Su, C. Y.; Van Der Meer, M.; Sarkar, B. *Chem. Eur. J.* **2014**, *20* (32), 9952.

(251) Schuster, E. M.; Botoshansky, M.; Gandelman, M. *Angew. Chem. Int. Ed.* **2008**, *47* (24), 4555.

(252) Mathew, P.; Neels, A.; Albrecht, M. *J. Am. Chem. Soc.* **2008**, *130*, 13534.

2 Scope of this Work

Detailed knowledge regarding the properties of 3*H*-1,2,3,4-triazaphosphole based ligand systems is basically non-existent, and only one metal complex was reported in literature described at the start of the here presented experimental work. Further, that report did not contain any analysis concerning advantages and disadvantages of the used ligand system. The aim of this work is, therefore, exploring the coordination chemistry of different substituted 3*H*-1,2,3,4-triazaphosphole based ligands towards late transition metals in low oxidation state and a detailed comparison to their well-known 1*H*-1,2,3-triazole analogues. The requirement of a supplementary binding side will reveal to be critical, with one exception and the suitability of different binding sites shown. The dichotomy of π-donor and π-acceptor properties in chelating ligands will be demonstrated on **Re**(I) carbonyl complexes. Potential applications of the phosphorus-containing compounds will be investigated with interesting results on their antagonists. One part of the thesis will consider the photophysical properties of the 1,2,3,4-triazaphospholes and 1*H*-1,2,3-triazoles and their corresponding **Re**(I) complexes as well as the nature of the participating molecular orbitals. Those **Re**(I) and additionally **Mn**(I) complexes will show the limitation of those ligands in electrochemical carbon dioxide reduction and in contrast to this, the overwhelming advantages can be demonstrated in **Cu**(I) catalysed alkyne-azide cycloaddition reactions.

In a last part, the chemical modification of 3*H*-1,2,3,4-triazaphospholes by selected examples will be shown; disadvantages of the triazaphospholium salts and advantages in cycloreversion reactions will be highlighted.

No differences in the binding mode of the two ligand systems will be observed, therefore in the last part of this work, the strong differences of 3*H*-1,2,3,4-triazaphospholes and 1*H*-1,2,3-triazoles in the chemical treatment of the ligands will be set out.

Within this study on 3*H*-1,2,3,4-triazaphospholes and 1*H*-1,2,3-triazoles, the isolobal analogy between a CH-fragment and a phosphorus atom will also be proven for these aromatic heterocycles.

3. Results and Discussion

3.1 Non-Conjugated Triazaphospholes and Triazoles

3.1.1 Monodentate Ligands

Low-coordinate $\lambda^3\sigma^2$-phosphorus compounds bearing one binding side, e.g. phosphinines, are quite established in organometallic chemistry.[1–5] For these systems, the $\sigma(\eta^1)$-binding motifs are favoured (Chapter 1). Since no systematic investigation on the coordination chemistry of triazaphospholes has been published, the question arises of how far the electronic properties and therefore the binding mode can be tuned by different substituents. As mentioned in Chapter 1, only a few phosphaalkynes are stable at room temperature. Therefore, the TMS and *tert*-butyl substitution pattern was chosen, since their steric hindrance is smaller compared to the supermesityl- or adamantyl-group. Furthermore, attached to an aromatic system, both groups are known and have opposite electronic effects (Scheme 30).
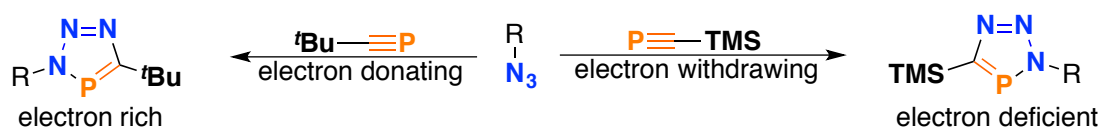
Scheme 30: Synthesis of electron rich and deficient 3*H*-1,2,3,4-triazaphospholes by positive (*tert*-Butyl) and negative (trimethylsilyl) hyperconjugation properties of the substituents.

The TMS-group, connected directly to an aromatic system, withdraws electron density by an inverse hyperconjugation and the resulting ligand was expected to have a stronger π-accepting capacity.

The synthesis of **A1** (Scheme 31) follows a protocol of S. M. Mansell *et al.*[6] starting from commercially available (chloromethyl)trimethylsilane (**1**), which was transferred to the corresponding Grignard compound (**2**) at room temperature and reacted with phosphorus trichloride at T = -78 °C, yielding dichloro((trimethylsilyl)methyl)-phosphine (**3**, 49%). Passing dry hydrogen chloride through the reaction mixture supports the precipitation of the manganese salts and increases the yield. Another suitable option is to use a HCl solution in diethylether. The TMS substituted phosphaalkyne **A1** is generated by first reacting the air and moisture-sensitive phosphane **3** with silver triflate, introducing a good leaving group, allowing the abstraction of the methylene protons by the addition of DABCO. The product cannot be

isolated from the aromatic solvent, since an azeotrope is formed. Consequently, it is impossible to determine the exact yield. Estimations (± 10%) are possible, using triphenylphosphine and relaxation agents, or contrary to the literature report[6], by determining the yield by NMR, titrating the reaction mixture with a well-defined amount of azide. An increase of the yield from 29%, the average literature value, to 52% could be achieved by stirring the reaction mixture for additional 48 h at T = -78 °C.
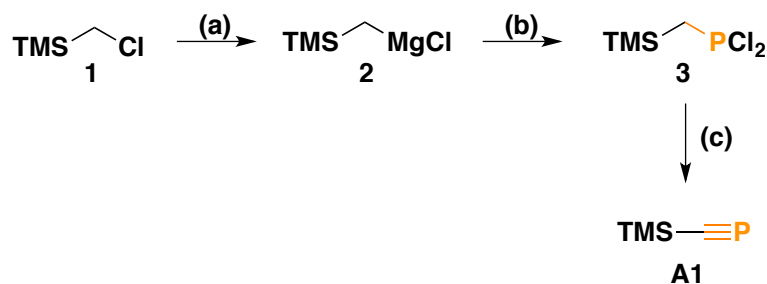
Scheme 31: Synthesis of ((trimethylsilyl)(methylidyne)phosphane **A1**; reaction conditions (a): Mg (2300 eq.) 170 mL Et$_2$O, 1 h reflux. (b): Et$_2$O, slow addition of **2** to PCl$_3$ (1 eq.), T = -78 °C -> r.t. over night, 49 %; (c): exclusion of light, AgOTf (2.2 eq) 5 min r.t., DABCO (2.2 eq.) 48 h, T = -78 °C, 52%.

The synthesis of the *tert*-butyl substituted phosphaalkyne (*vide infra,* Scheme 33) requires tris-trimethylsilylphosphine (P(TMS)$_3$) (**6**) as a different phosphorus(III) source. This phosphorus compound is obtained from a two-step reaction (Scheme 32), starting with the conversion of trichlorophosphine (**4**) with *N*-(dichlorophosphino)piperidine, yielding the phosphanyl species **5**[7] followed by the reduction to phosphine **6**.[8]
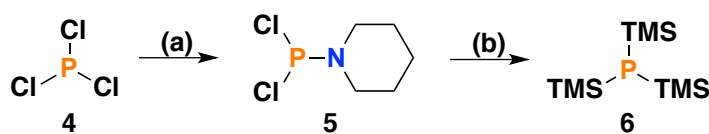
Scheme 32: Synthesis of phosphane **6**. Reaction conditions (a): Piperidine (2 eq.) Et$_2$O, T = -78 °C to r.t., 58 %; (b): Li (6 eq.), TMSCl (4 eq.), THF, 6 h, T = 80 °C, 18 h r.t., 74%.

Excursion 3: Optimization of the Synthesis of Tris(trimethylsilyl)phosphine[9]

An easy and safe way to obtain **6** has been reported by Niecke and Westermann,[8] by reducing *N*-(dichlorophosphino)piperidine in the presence of chloro-trimethylsilane with lithium in boiling THF. In contrast to the reported procedure, the reaction time is on average, seven times longer than in the literature procedure that was mentioned. Since this phosphorus(III) source combines a high reactivity, but is much more save to handle than PH_3. The reaction was thus investigated in detail. First attempts indicated a correlation between the enlarged stirring speed and an enhanced reaction time, based on a mechanical abrasion, yielding small lithium particles as well as an activated surface of the granules used. To prove this assumption, the lithium granules were first stirred before the solvent and the reaction partners were added. As a matter of fact, it turned out that the reaction time could be reduced from 7 d to 30 h (Table 1, Entries 1-3).

Table 1: Approaches towards optimization of compound **6** by using different stirring speeds and Li sources.

Entry	Li Source	Li equiv.	Stirring speed [rpm]	n(5) [mmol]	Time	Yield
0	unknown	7	unknown	100	over night[I] 7d[II]	71 %
1	granular[a]	7	750	200	7d	69 %
2	granular[a]	7	750	200	7d	70 %
3	granular[b]	7	1000	200	30 h	70 %
4	granular[b]	7	750	200	34 h	74 %
5	granular[c]	7	1000	200	2 d	72 %
6	granular[c]	7	1000	200	2 d	70 %
7	granular[c]*	7	1000	200	2 d	71 %
8	granular[c]*	7	1000	200	2 d	70 %
9	foil[c]	7	1000	200	20 h	68 %
10	foil[c]	14	1000	200	16 h	72 %
11	rod[c]**	7	1000	200	7 d	69 %
12	rod[c]***	7	1000	200	12 d	69 %

(I) Reported reaction time; (II) found reaction time; (a) Li handled under air; (b) Li handled under air, activated by stirring; (c) exclusively handled under Ar atmosphere, no activation; * Li, 99 %, trace metals basis; ** horizontal and vertically sliced; *** vertically sliced.

Further approaches with different lithium sources, purity and handling the metal under Schlenk techniques, exhibited rather the coherence of the reaction speed depending on the size of the lithium surface than towards the grade. Also, the way of handling the lithium shows an influence on the reaction time, but with minor impact (compare Entries 2, 3 and 5). This can be demonstrated nicely, by comparing the reaction time of the lithium foil with the rod, sliced in different ways (Entries 9-12) and the 99 % trace metals basis lithium in contrast to the one without specific grade (Entries 5-8). Handling the lithium exclusively under argon atmosphere also contributes to an acceleration of the reaction time (Entries 5-8), but in contrast to the mechanical abrasion, the synthesis requires twice of the reaction time (Entries 3 and 4). To prove the reproducibility, the reactions were performed twice, except Entries 3,4 and 9,10, where small changes in the reaction conditions showed almost the same results in comparison to the other attempts.

In order to obtain **A2**, the **P**(TMS)$_3$ is first transformed by the addition of pivaloyl chloride into the phosphanylpropan-1-one **7**, which undergoes 1,3-TMS shift above T = 0 °C forming the stable phosphanylidene **8**.[10] The *tert*-butyl substituted phosphaalkyne **A2** is finally obtained by dropping **8** under reduced pressure on hot sodium hydroxide and collecting the volatile products at T = -78 °C (Scheme 33).[11,12]
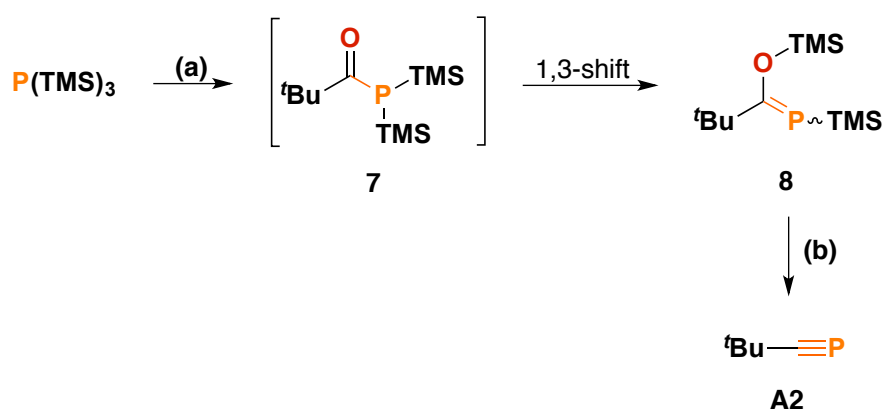
Scheme 33: Synthesis of (2,2-dimethylpropylidyne)phosphane (**A2**). Reaction conditions (a): **6** (1eq.), pivaloyl chloride (1.1 eq.) pentane, 24h r.t., 96 %; (b): NaOH (cat., 10 eq.), T = 160 °C, 20 mbar, 91%.

The alkynes **A1** (δ(^{31}P{^{1}H}) = 99.2 ppm, toluene) and **A2** (δ(^{31}P{^{1}H}) = -69.6 ppm, benzene-d$_6$) are sensitive towards moisture and air and decompose slowly under argon

atmosphere at room temperature. The differences in their chemical shifts indicate the electron withdrawing (**A1**) and donating (**A2**) effect of the substitution pattern.

At first, the formation of the corresponding triazaphospholes were studied with benzyl azide, because it is easily accessible and a proton splitting of the resonance assigned to the methylene protons due to $^3J_{\text{H-P}}$ coupling was expected. Besides the chemical shift in the ^{31}P{^{1}H} NMR spectrum, this is further evidence for product formation, based on the second starting material (Scheme 34).
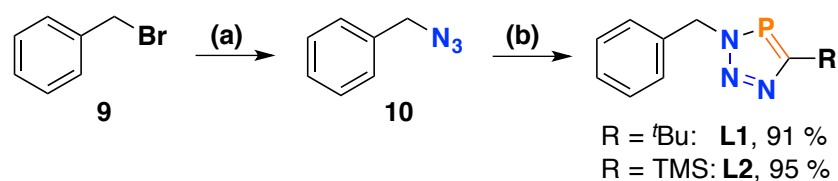
Scheme 34: Synthesis of benzylazide **10** and triazaphospholes **L1** and **L2**. Reaction conditions (a): sodium azide (1.1 eq.), DMSO, over night, r.t. 96 % yield; (b): **A1** (1.1 eq.) toluene, 2h r.t. or **A2** (1.1 eq.) DCM, T = -196 °C -> r.t..

The benzyl azide (**10**) is obtained from commercially available benzyl bromide (**9**), and sodium azide in DMSO.[13] The solvent must be removed completely, because traces of DMSO have already lead to notable decomposition of the phosphaalkyne **A1** in the second reaction. The synthesis of the TMS substituted triazaphospholes (**L1**) is straightforward. The solution of alkyne **A1** in toluene is added stepwise under argon atmosphere to the azide and the reaction progress can immediately be monitored *via* ^{31}P{^{1}H} NMR spectroscopy. The titration is continued until a slight excess of the alkyne **A1** is found. The solvent is removed under vacuum and **L1** is recrystallized from pentane, yielding single crystals suitable for X-ray analysis (Figure 15).
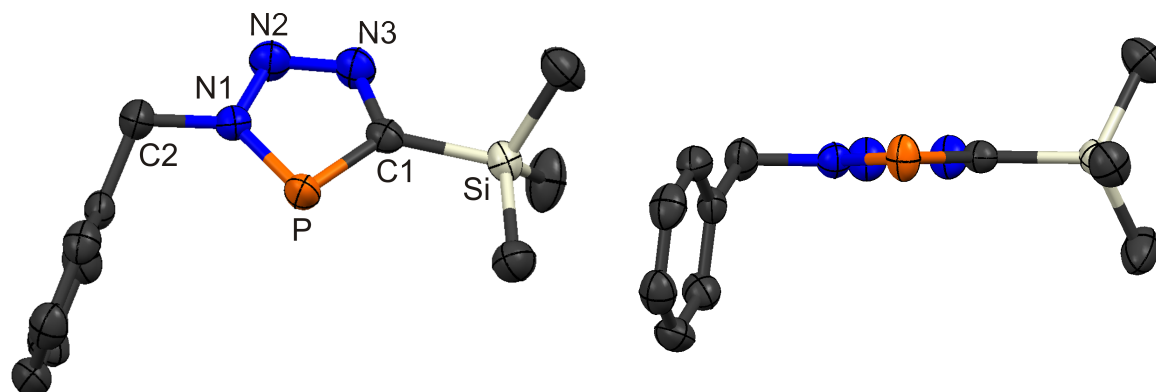
Figure 15: Molecular structure of **L1** in the crystal. Displacement ellipsoids are shown at the 50% probability level. Hydrogen atoms are omitted for clarity. Selected bond length (Å) and angles (deg): C(1)-P(1): 1.709(2), P(1)-N(1): 1.679(2), N(1)-N(2): 1.345(3), N(2)-N(3): 1.314(2), N(3)-C(1): 1.369(3), C(1)-Si(1): 1.877(2), N(1)-C(2): 1.485(3). C(1)-P(1)-N(1): 87.5(1).

Excursion 4: Attempts and Limitations of TMS-Substitution Reactions on L1

To overcome the drawback of the limited stability found in phosphaalkynes, the question arose of whether standard protocols for chemical transformations, either of the alkyne or of the corresponding 'click'-product, could be developed. This would comply with an essential element in investigating the 3H-1,2,3,4-triazaphosphole chemistry. With the trimethylsilyl-substituent in **L1**, a useful leaving group was expected to be found, since the carbon-silicon bond dissociation energy (BDE = 451 kJ mol^{-1}) differs around 156 kJ mol^{-1} from the carbon-carbon bond (BDE = 607 kJ mol^{-1}). Moreover, the C-Si bond is already considerably polarized (EN$_C$=2.55 and EN$_{Si}$ = 1.90).[14] 'Free' fluoride anions, such as in NR$_4^+$F$^-$ are particularly useful reaction agents in breaking the carbon silicon bond. This behaviour is also utilised in the palladium catalysed cross-coupling reaction, for instance in the Hiyama[15] or the Sila-Sonogashira-Hagihara reaction.[16] Hence, different approaches to modify triazaphosphole **L1** have been developed (Scheme 35).
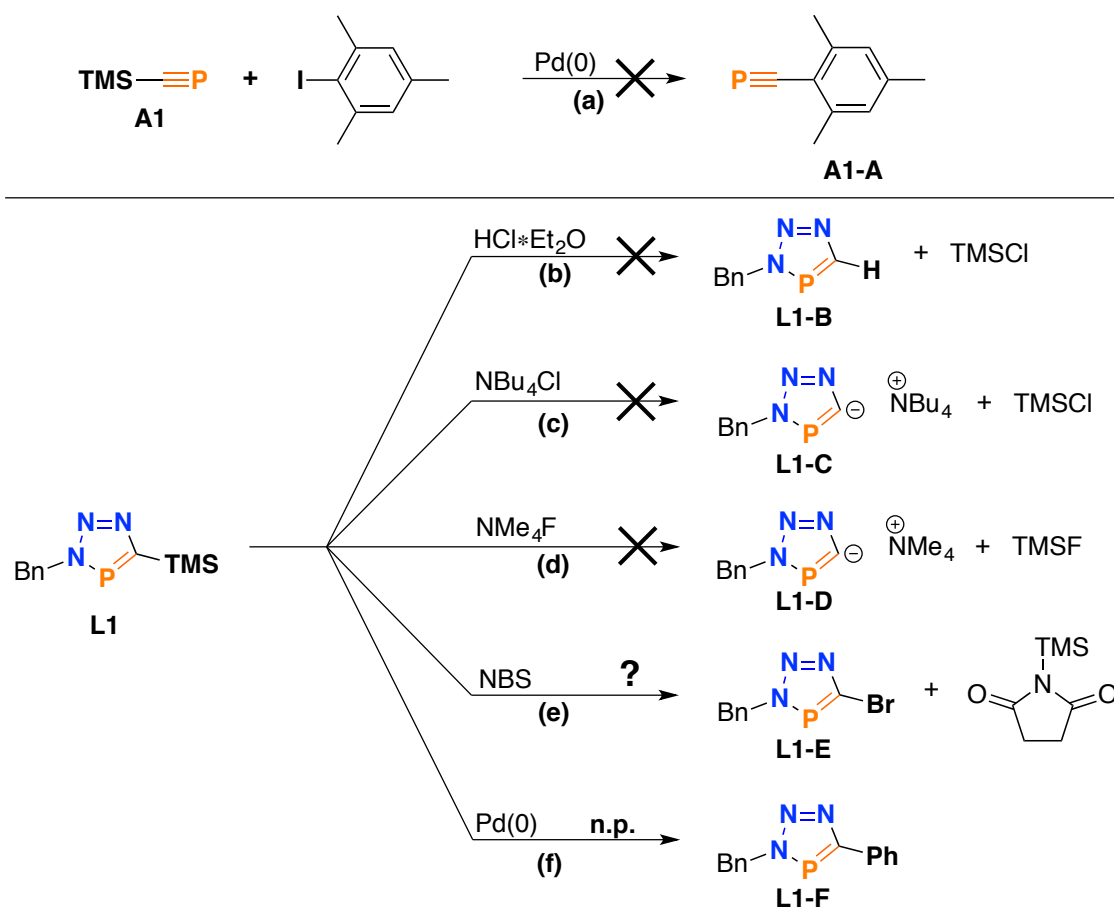
Scheme 35: Strategies for substituting the TMS-group in compound **L1**. Reaction conditions (a): Pd(PPh$_3$)$_4$ (0.05 eq.), CuCl (1.5 eq), Mes-I (1 eq.); (b): Excess of HCl•Et$_2$O, DCM, r.t.; (c) NBu$_4$Cl (1.1 eq), DCM, 48h, T = 50 °C; (d) NMe$_4$F (1.1 eq.) DCM, T = 65°C, over night; (e) NBS (1.1 eq.), drop wise, T = 0 °C, DCM.

As a suitable way for a unified transformation, the direct conversion of phosphaalkyne **A1** was considered. As a suitable target molecule for a test reaction, the mesityl phosphaalkyne **A1-A** was selected. The compound has a good balance between the steric bulk needed to provide adequate stability and the challenge towards steric demanding phosphaalkynes. This is interesting, because the phosphaalkynes bearing larger groups need more reaction steps in general (Chapter 1).

The reaction (**a**) in Scheme 35 followed a protocol by Takagi *et al.*[16] for TMS-cleaving alkynes, but no product could be observed by means of $^{31}P\{^1H\}$ NMR spectroscopy. Therefore, splitting the C-Si bond using hydrogen chloride solution in diethyl ether (**b**) to obtain a P=C-H subunit in the heterocycle and trimethylsilyl chloride as a by-product has been carried out, but no selective reaction was observed (multiple products). In the best-case scenario, the reaction mixture showed two signals in the $^{31}P\{^1H\}$ NMR spectrum. This observation might be caused by the protonation of the nitrogen atoms N^1 or N^2, followed by decomposition of the heterocycle and as a different chloride source tetrabutylammonium chloride was used (**c**). Again the electrophilic substitution of the silyl-group on the aromatic system was not successful.

TMS (protecting) groups can be cleaved off selectively by 'free' fluoride anions, present in e.g. tetramethylammonium fluoride. An addition of this fluoride source did not caused a shift of the resonance in the $^{31}P\{^1H\}$ NMR spectrum (**d**). Following a protocol of Choi *et al.* for triazoles,[17] the reaction mixture was heated over night at a T = 65 °C bath temperature. Again, no change of the signal in the $^{31}P\{^1H\}$ NMR spectrum was observed.

Another strategy for modifying triazoles has been shown by Harrity *et al.*[18], yielding the brominated derivative. Transferring this approach to **L1**, a selective reaction could be observed (**e**). In the $^{31}P\{^1H\}$ NMR spectrum (DCM-D_2) besides the major (product) signal at δ = 171 ppm and a second at δ = -2.9 ppm. The signal in $^{31}P\{^1H\}$ NMR spectroscopy (DCM-D_2) shifts from δ = 214.7 ppm of the TMS substituted triazaphospholes to δ = 170.7 ppm for the (expected) derivative **L1E**. The difference in chemical shift is in line with the replacement of the electron-withdrawing group by a π-donating substituent, such as the *tert*-butyl group (*vide infra*). Compared to phosphinines, the difference in the chemical shift in $^{31}P\{^1H\}$ NMR spectra of the trimethylsilyl- and bromine-substituted phosphinines accounts Δδ = 22 ppm (TMS-phosphinine: δ(DCM-D_2) = 232 ppm Br-phosphinine: δ(DCM-D_2) = 210 ppm)[19,20] and therefore is minor compared to the observed shift in the case of the triazaphospholes. This might be attributed to the higher π-donor character of triazaphospholes, due to the inclusion of

nitrogen atoms into the conjugated system (*vide supra*). This property is also found in 1,3-azaphospholes.[21–24] The higher electron density in triazaphospholes was derived from electrochemistry and the π-donation property was found in the shape of the frontier orbitals (*vide infra*). The modification of the triazaphospholes with NBS was stopped, because the molecular structure was not determined (Figure 16).
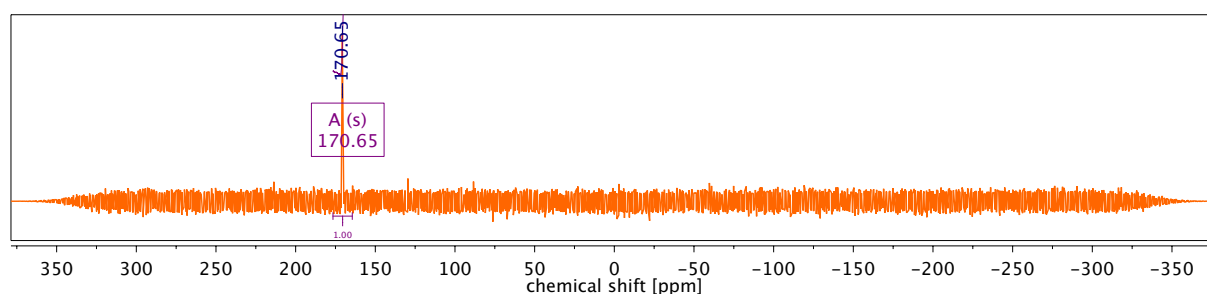
Figure 16: $^{31}P\{^1H\}$ NMR spectrum of **L1e** in DCM-d_2.

For cross coupling reactions **(f)**, two different approaches for the related 1*H*-1,2,3-triazoles are known. Both require TMS substitutions, such as **(d)** and **(e)**, leading to the conclusion that only the pathway from Harrity *et al.*[18] can be considered, because **(d)** did not work. However, since no clear evidence for the successful conversion of **L1** into **L1-E** was given, this attempt was discontinued. In contrast to **A1**, the *tert*-Bu-substituted phosphaalkyne **A2** was obtained in a pure form. Although it can be transferred to the azide by trap-to-trap condensation, the reaction is extremely exothermic and therefore requires a non-oxidative as well as aprotic solvent. The product formation proceeded similar to **L1**. The pure product was obtained after removal of the solvent and an excess of **A2**. Recrystallization of **L2** by slowly cooling down a hot saturated solution in pentane to T = -20 °C yielded single crystals suitable for X-ray analysis (Figure 17).
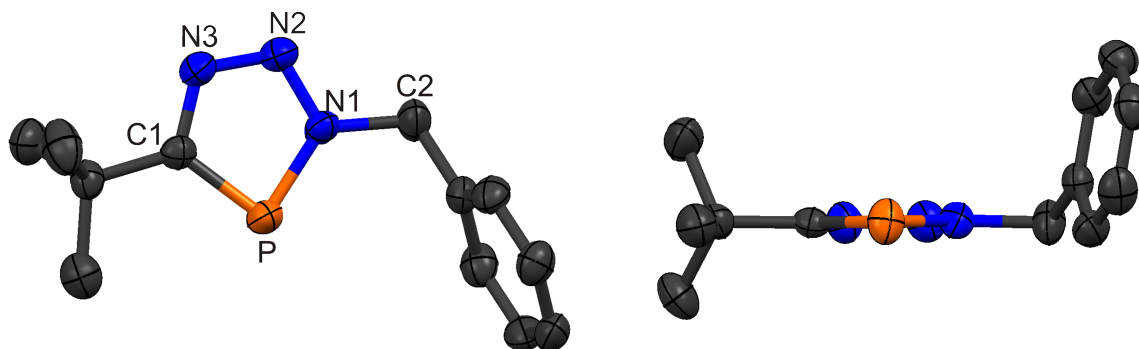
Figure 17: Molecular structure of ligand **L2** in the crystal. Displacement ellipsoids are shown at the 50% probability level. Hydrogen atoms are omitted for clarity. Selected bond length (Å) and angles (deg): P(1)-C(1): 1.713(2), P(1)-N(1): 1.683(2), N(1)-N(2): 1.340(2), N(2)-N(3): 1.314(2), N(3)-C(1): 1.314(2); C(1)-P(1)-N(1): 86.39(9).

The influence of the different substituents on the phosphorus atom is not only visible in ^{31}P{^{1}H} spectra the phosphaalkyne, but also in the synthesized ligands **L1** and **L2** (Figure 18).
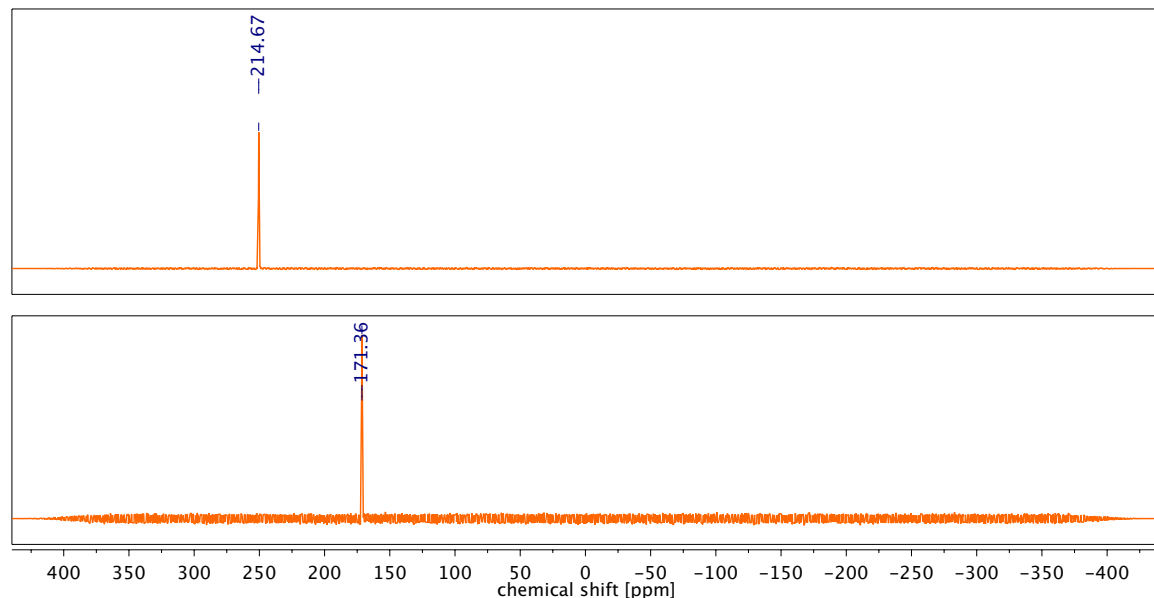
Figure 18: ^{31}P{^{1}H} NMR spectra (DCM-D$_2$) of compounds **L1** and **L2**. The difference of the shifts depending on the nature of the substituent is around $\Delta\delta$ = 43 ppm.

Another compound was obtained from the conversion of phosphaalkyne **A2** with tosyl azide **12**. This azide is synthesized by nucleophilic substitution of the chloride by sodium azide[25] (Scheme 36). The proposed compound was not meant to become a ligand in the first place, since the tosyl azide is known to be an azide transfer reagent, able to exchange the metal atom from an organolithium compound by an electrophilic substitution.[26] As previously mentioned, the formation of 3H-1,2,3,4-triazaphospholes, starting from phosphaalkynes and organic azides, exclusively forms the 1,3-regioisomer due to the polarized carbon phosphorus triple bond (Chapter 1). Therefore the question arises of whether the 1,3-dipolar cycloaddition occur in the known 1,4 fashion caused by the steric bulk or contrary charge of the azide is yielding the 1,5-regioisomer.
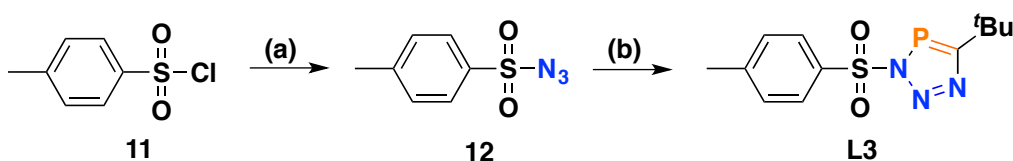
Scheme 36: Preparation of 4-methylbenzenesulfonyl azide **12** and 5-(*tert*-butyl)-3-torsyl-3H-1,2,3,4-triazaphosphole **L3**. Reaction conditions (a): NaN$_3$ (1.11 eq.) acetone/EtOH/H$_2$O 100:57:3, r.t. overnight, 78 %; (b): **A2** (1.1 eq.) DCM, T = -196 °C -> r.t., 84%.

Cooling down a saturated solution of **L4** in pentane yielded single crystals, insufficient for a detailed X-ray analysis (Figure 19). Nevertheless, the connectivity can be clearly determined. Contrary to the expectations, the 1,4-substituted regioisomer was formed. Further investigations by force field geometry optimisation (MMFF94s, implemented in Avogadro program) revealed an energy difference of $\Delta E = 13.2$ kJ mol^{-1} in favour of the 1,4-regioisomer. Although this result is only a rough approximation, it is still a good demonstration for the steric demand of the *tert*-Bu-substituent and the resulting repulsive interactions. The exchange of this bulky substituent by a methyl group in the optimised structures, followed by an additional geometry optimisation (MMFF94s, implemented in Avogadro program) showed that the 1,5-regioisomer is by $\Delta E = 29.5$ kJ mol^{-1} the most stable compound.
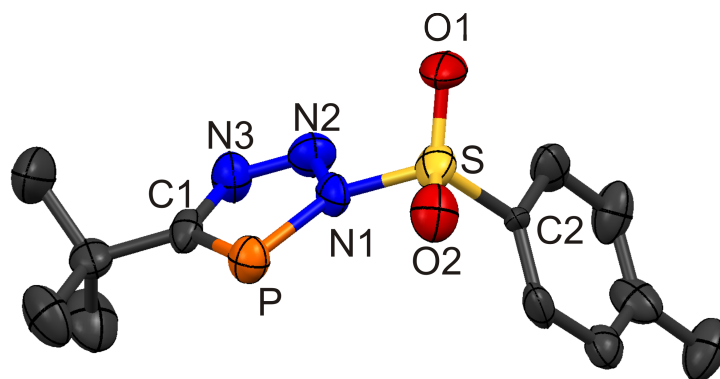
Figure 19: Molecular structure in the crystal of compound **L3**. Displacement ellipsoids are shown at the 50% probability level. Hydrogen atoms are omitted for clarity.

Although the tosyl substituent is supposed to be an electron withdrawing substituent, the chemical shift in ^{31}P{^{1}H} NMR of **L3** ($\delta = 177.2$ ppm, DCM-d$_2$) is only shifted slightly more downfield, compared to the benzyl substituent ($\delta = 171.4$ ppm, DCM-d$_2$).

Crowley and colleagues observed a similar behaviour in the related 1*H*-1,2,3-triazoles.[27] The **Re**(I) metal complexes of chelating triazoles with different substituents in 4-position varying in their electron donation or withdrawing strength, no significant change in the absorption and emission spectra as well as their electrochemical behaviour had been observed, expect for the nitrobenzene substituent. Therefore, the authors concluded, that triazoles act as electronic insulators.[27] Transferring this concept to the 3*H*-1,2,3,4-triazaphospholes with respect to the CH-P analogy, a comparable low downfield shift in ^{31}P NMR spectroscopy by the variation of the substituent in 5-position becomes plausible. These compounds might be an interesting ligand, if the tosyl

substituent is able to withdraw electron density from the N_3 subunit and thus might lead to a preferential metal coordination *via* the phosphorus lone pair.

3.1.2 Coordination Chemistry of Monodentate Triazaphospholes:

As already explained in Chapter 1, low-coordinate phosphorus compounds coordinate preferentially to late transition metals in low oxidation states due to the strong π-accepting character of the phosphorus atom. As suitable metal source, the noble metals in a low oxidation state were chosen to investigate the coordination chemistry respective to the substitution pattern of the obtained monodentate ligands **L1** to **L3**. The results by means of the chemical shifts are displayed in Table 2.

Table 2: Chemical shifts in $^{31}P\{^1H\}$ NMR spectra (DCM-d$_2$) of the reaction mixtures containing compounds **L1** to **L3** and the metal precursors.

Entry	Coin Metal **M(I)**	δ [ppm] of **M(I)@L1** (**L1**: 215 ppm)	δ [ppm] of **M(I)@L2** (**L2**: 171 ppm)	δ [ppm] of **M(I)@L3** (**L3**: 177 ppm)
1	CuBr•SMe$_2$	215	170	176.6
2	AgOTf	215	n.p.	124.4
3	Au(CO)Cl	n. p.	170 ***	91.09 (d, J = 113.9 Hz) 92.03 (d, J = 151.7 Hz)
4	AuCl•SMe$_2$	215 **	170 ***	11.5

*: no signal observed; **: broadening observed; ***: Au(0) formation observed .

From the reaction mixture of ligand **L3** with gold chloride dimethyl sulfide single crystals suitable for X-ray analysis could be obtained. Much to our surprise, it turned out that a 1,3,2,4-diazaphosphetidine was formed, rather than a simple Au(I)-triazaphosphole complex. This could be verified by means of X-ray crystallography (Figure 20). Furthermore, it should be noticed that the *tert*-butyl group were converted into the *iso*-pentenyl substituents obviously by methyl-migration.
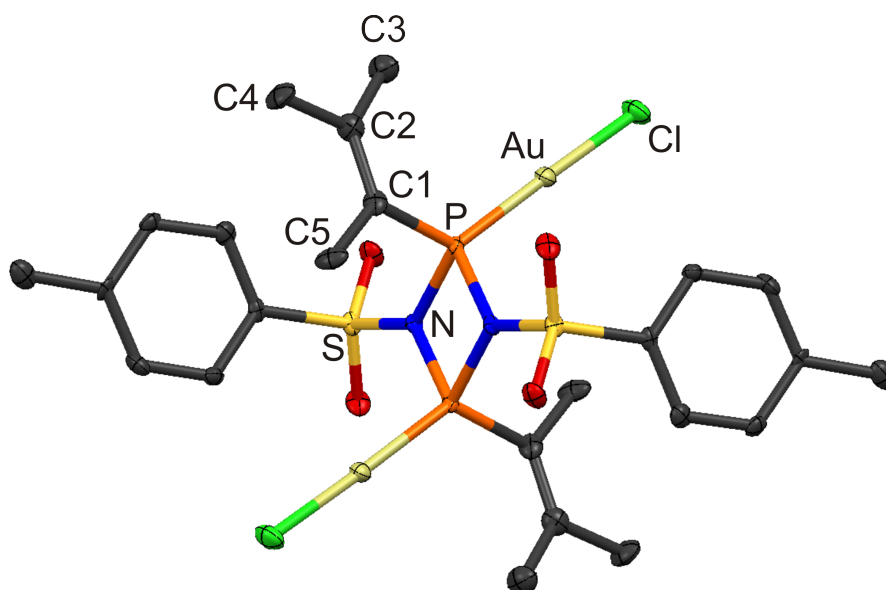
Figure 20: Molecular structure in the crystal of coordination compound **C1**. Displacement ellipsoids are shown at 50 % probability level. Hydrogen atoms are omitted for clarity. Selected bond length (Å) and angles (deg): P(1)-N(1): 1.720(5), N(1)-P(1b): 1.732(5), P(1)-Au(1): 2.203(1), P(1)-(C1): 1.796(7), C(1)-C(2): 1.337(9), C(2)-C(3): 1.497(9), C(2)-C(4):1.51(1), C(1)-C(5): 1.54(1), N(1)-S(1): 1.657(5); N(1)-P(1)-N(1b): 79.9(2), P(1)-N(1)-P(1b): 100.1(3).

Excursion 5: 1,3,2,4-Diazaphosphetidines

1,3,2,4-Diazadiphosphetidines, first reported by W. Flick *et al.*,[28,29] are four-membered heterocycles and can be obtained from the reaction of phosphorus dichloride derivatives and primary amines. The formed isomer depends on the substituents and result mainly in *cis*-isomers or isomeric mixtures. Furthermore, the thermal transformation of a *cis*-into a *cis*-/*trans*- mixture is reported.[30] Metal complexes[31,32], Lewis adducts[33] and diradical species[34] based on 1,3,2,4-diazaphosphetidines are also known.

The obtained nitrogen elimination reaction has so far been unknown for 3*H*-1,2,3,4-triazaphospholes and the observed *trans* arrangement was rarely observed for 1,3,2,4-diazaphosphetidines.[30] Nevertheless, in 2000, Maas *et al.* reported on the substituent-dependent formation of 1,3,2,4-diazaphosphosphetidines (Scheme 37, **E**) or 1*H*-1,2,4-λ^5-diazaphospholes (**F**). Starting from diazoalkan-2-one (**B**), which is the major product of the equilibrium with the more reactive diazoalke-1-enes (**A**), and a triazaphosphole, an unstable diazaphosphole[4,3-*d*][1,2,3,4]triazaphospholes bicycle (**C**) was formed. N_2 elimination of the N^1 and N^2 atoms in the triazaphosphole subunit generated the 4-imino-1,2,4-(λ^5)-diazaphosphole (**D**)-based intermediate. The substitution pattern within this heterocycle determines the product of the reaction.

While a phenyl-substituent in 3-position allows the formation of the diazaphosphetidines (**E**), this reaction is prevented by an ester substituent *via* 1,3-OR-shift, yielding diazaphospholes of type **F**. [35]
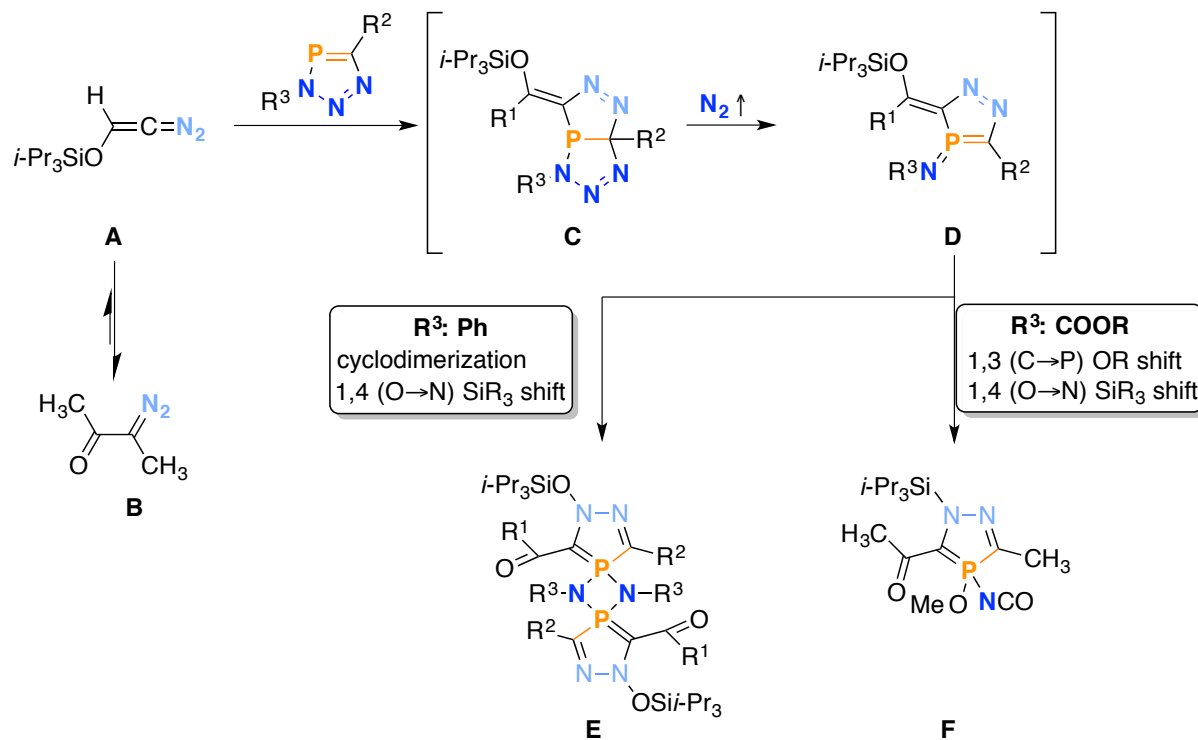
Scheme 37: Synthesis and reaction mechanism of 1,3,2,4-diazaphosphetidines and 1*H*-1,2,4-λ^5-diazaphosphol starting from 4-imino-1,2,4-(λ^5)-diazaphospholes.[35]

The here observed behaviour of triazaphospholes has never been described before. In comparison, the only nitrogen containing structurally related 5-membered heterocycles, 1,2,3-triazoles and 2*H*-tetrazoles show some similarities. In a theoretical study by Bozzelli *et al.*, retro-[3+2]-cycloaddition reactions of these and other molecules, were investigated by means of the reaction pathway as well as their reaction enthalpies and free energies. For both structurally related compounds, the ring opening and nitrogen evolution is favoured over the azide and alkyne or nitrile formation.[36] Besides this theoretical investigation, transition metal catalysed ring-opening-ring-closing metathesis reactions are also described. This type of reaction is based on the thermal isomerization of 1,2,3-triazoles (Scheme 38, top) and are therefore carried out at T = 70 to 130 °C. The plausible mechanism depends on the transition metal (**Pd**[0] or **Rh**[II]) [37–39] as well as on the directing groups in cooperation with additives (**Cu**[II])[40], but mainly the metal centre insert by oxidative addition into the diazonium C-N_2^+, followed by N_2-elimination. Most interestingly, Foklin *et al.* reported an azavinyl carbene-based

migration of a hydrogen atom as well as of a methyl group, starting from 1,2,3-triazoles. Within these examples the reaction of the triazole derivative of **L3** was included (Scheme 38, bottom).[41]
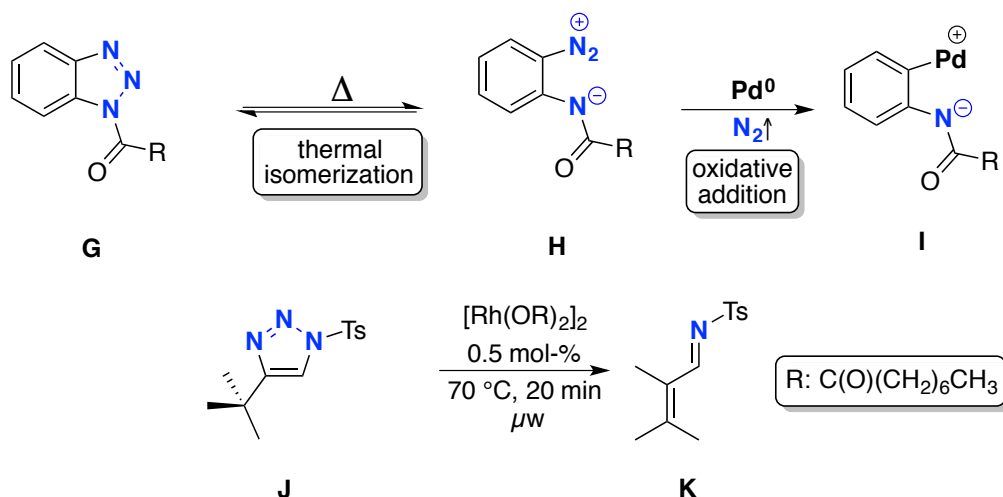
Scheme 38: (Top) Thermal isomerization of 1*H*-1,2,3-triazoles and oxidative addition of Pd(0) metal centre and 1,2 methyl shift in structural relevant triazole (**Bottom**).

Taking the literature review in account, a reaction mechanism for the synthesis of **C1** can be proposed. Since the reaction was performed at room temperature and due to the use of Au(I) in the absence of light, a thermal isomerization and a light induced N_2 elimination can be excluded. Furthermore, triazaphosphole **L3** existing in the open form, demonstrated by the molecular structure in the crystal can also be excluded. As the X-ray diffraction measurements were performed at T = 100 K, the assumption of the open-form analogue to **XY** at room temperature might be taken into account. This can easily be ruled out by the small difference compared to **L2** in the $^{31}P\{^1H\}$ NMR spectrum ($\Delta\delta = 6$ ppm), while a cation attached in α-position would cause a stronger shift. Additionally, the absences of a diazonium N-N triple-bond stretching vibration (2135-2316 cm^{-1})[42] in the IR spectrum substantiate this assumption. According to the HASB concept, the gold ion favours the phosphorus atom lone pair (Scheme 39, **L**), yielding the diazonium species (**M**). From this resonance stabilised zwitterionic compound (**M**, **M-b**), nitrogen eliminates (**N**, **N-b**) and by charge equalisation, the carbine compound **O** is formed. Subsequently, an 1,2 methylshift is yielding the more stable phosphanylidene aminde gold(I) complex **P**. The P=N double bond is more reactive than the analogue C=N bond and undergoes subsequently a cyclodimerization, yielding **C1**.
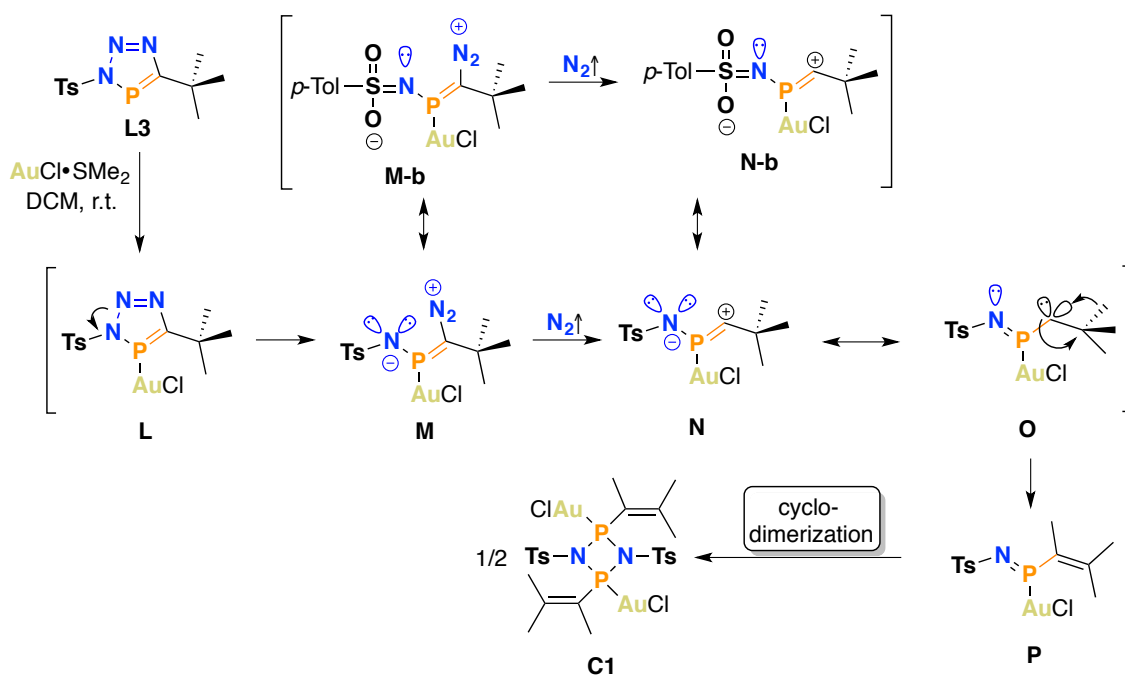
Scheme 39: Proposed mechanism for the rearrangement of **L3** caused by **Au**(I) coordination.

Due to the transition-metal-induced nitrogen elimination, the question arises of whether this behaviour is caused only by the gold ion, or if this finding is a matter of a strong π-back bonding from the metal to the ligand. Therefore, the reaction was performed with a **Rh**(I) precursor, another representative of a late transition metal in a low oxidation state, whereby a coordination mode *via* the phosphorus atom lone pair is expected. Just as in the synthesis of the gold complex, gas evolution was noticed as soon as the solvent was added. Additionally, the ^{103}Rh NMR-active nucleus provides structural information in addition to the molecular structure in the crystal. ^{31}P{^{1}H} NMR spectrum (Figure 21) of the crude product shows only one resonance at δ (DCM-d$_2$) = 91.9 ppm (d), with a coupling constant of $^1J_{\text{P-Rh}}$ = 132.3 Hz in contrast to the gold complex. The strong upfield shift might indicate a similar product to **C1**, which was obtained with the gold precursor. Furthermore, a strong gas evolution was noticed as the solvent was added. Mass spectrometry confirmed the decomposition of the heterocycle and different fragments were obtained. Unfortunately, a structural characterization of the product still remains elusive at this point.
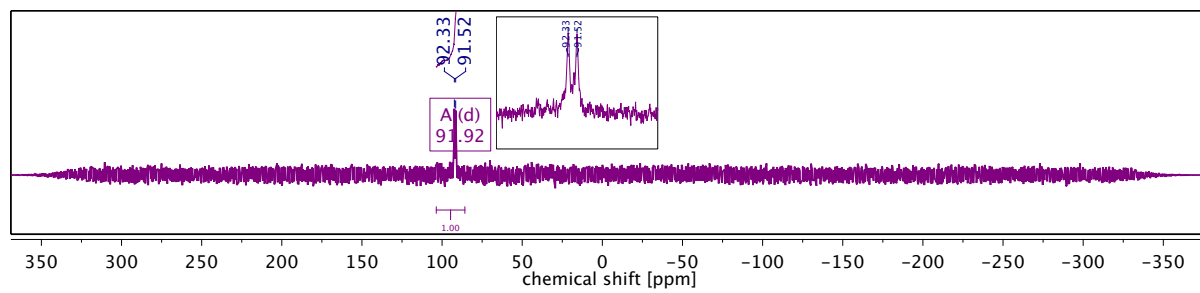
Figure 21: $^{31}P\{^1H\}$ NMR spectrum of Rh(I) based complex **C2**.

3.1.3 Chelating Ligands

3.1.3.1: Picolyl-substituted Triazaphospholes and Triazoles[43]

The attempts in coordination chemistry of monodentate triazaphosphole ligands did not yield the expected metal complexes and so an additional binding side was introduced. All-nitrogen containing chelates, such as bipyridines (**A**), phenantrolines (**B**), picolyl triazoles (**C**) and pyridine triazoles (**E**) as well as their inverse click products (**D**) and (**F**) (Figure 22), are well-established ligands in coordination chemistry.
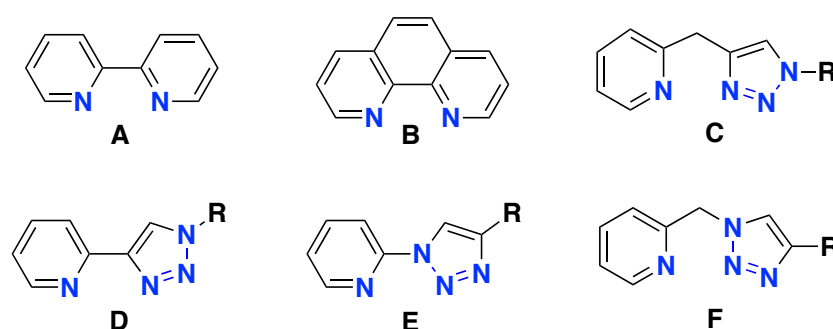
Figure 22: Selected nitrogen-based bidentate ligands. **A**: 2,2'-bipyridine; **B**: 1,10-phenanthroline; **C**: 2-(1*H*-1,2,3-triazol-4-yl)pyridine; **D**: 2-(1*H*-1,2,3-triazol-1-yl)pyridine; **E**: 2-((1*H*-1,2,3-triazol-4-yl)methyl)pyridine; **F**: 2-((1*H*-1,2,3-triazol-1-yl)methyl)pyridine.

The combination of 'hard' and 'soft' binding sides in terms of Lewis, the so-called P,N-hybrid ligands, a phosphinine and a pyridine imbedded in one chelating ligand, was first developed by François Mathey *et al*. by the NIPHOS ligand (Figure 23),[44] but due to the lack of stability, his system did not find its way towards application. In the corresponding triaryl phosphinine system, the P,N-ligand gains stability in addition to the ability to coordinate transition metals with high oxidation state[45] and can be electronically tuned further by the variation of the **R** substituent, as shown in detail by the Müller group.[46]
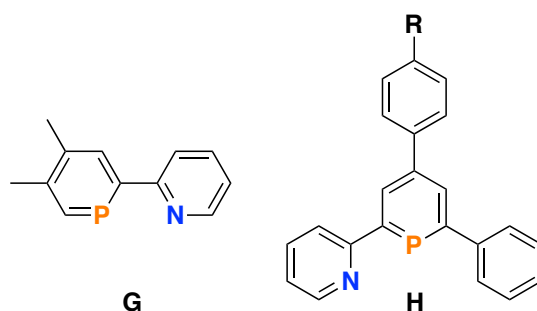
Figure 23: P,N-Ligands NIPHOS (**G**) and pyridyl-functionalized phosphinine (**H**).

Synthesis of Compounds L4 to L7

Adopting this strategy made by the introduction of the pyridyl-substituent in triaryl phosphinines and transferring it to triazaphospholes in the most easily accessible fashion by reaction of a 2-picolyl azide with phosphorus alkynes, this type of ligand should be able to bind metal centres in two different binding modes, **I** and **J**, due to the chelate effect (Scheme 38).
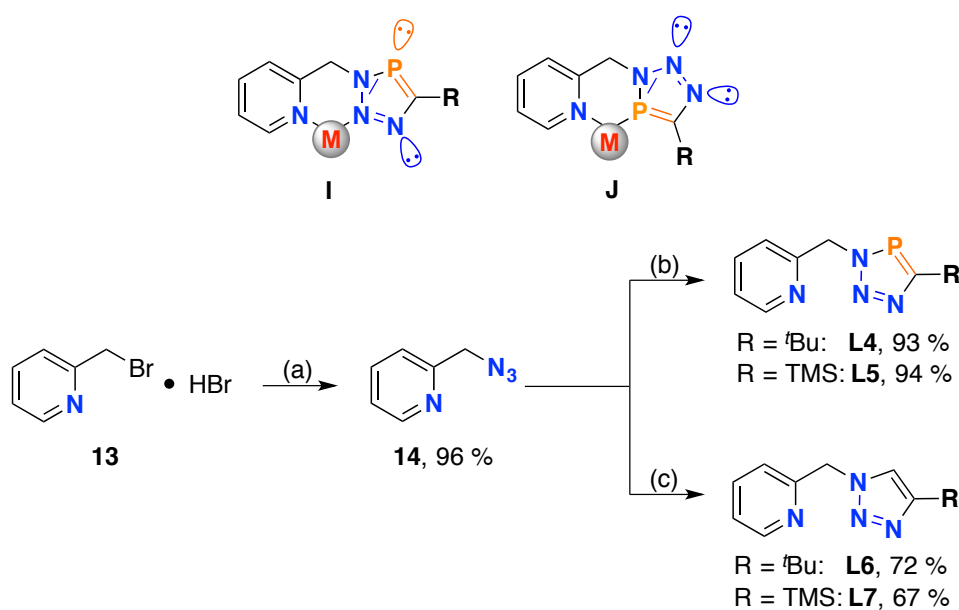
Scheme 40: (Top) Possible binding modes to metal centre of the picolyl-substituted triazaphosphole; (Bottom) Synthesis of picolyl substituted triazaphosphole and triazoles. Reaction conditions: (a) 1. NaHCO$_3$ (1.1 eq.), 5 min stirring; 2. NaN$_3$ (1.1 eq.) over night; DMSO, r.t.; (b) R= ^{t}Bu: THF/^{t}BuCP, R=TMS: toluene. (c) 2-(azidomethyl)pyridine (1 eq.), Alkyne (1 eq.), sodium ascorbate (0.1 eq.) CuSO$_4$•5H$_2$O (0.05 eq.) in H$_2$O/^{t}BuOH (*v:v* 1:1) r.t., Ar atm., over night.

Starting from commercially available 2-(bromomethyl) pyridine hydrobromide, the 2-picolyl azide can be obtained after abstraction of the hydrobromic acid with sodium hydrogen carbonate followed by a nucleophilic substitution with sodium azide in DMSO. The isolated azide was than dissolved in dry toluene and phosphaalkyne **A2** was added, yielding the picolyl-triazaphosphole **L4**. The 5-TMS substituted compound **L5** is obtained from the direct addition of the phosphaalkyne **A1** toluene solution to the azide. Both products are colourless solids and their chemical shift in the ^{31}P{^{1}H} NMR spectra (DCM-d$_2$) are similar to those of the benzyl-substituted triazaphospholes (5-^{t}Bu: benzyl: 171.4 ppm; 2-picolyl: 173.1 ppm and 5-TMS: benzyl: 214.7 ppm; 2-picolyl: 216.5 ppm).

In ¹H NMR spectrum of **L4** shows a doublet resonance for the methylene bridge (Figure 15).
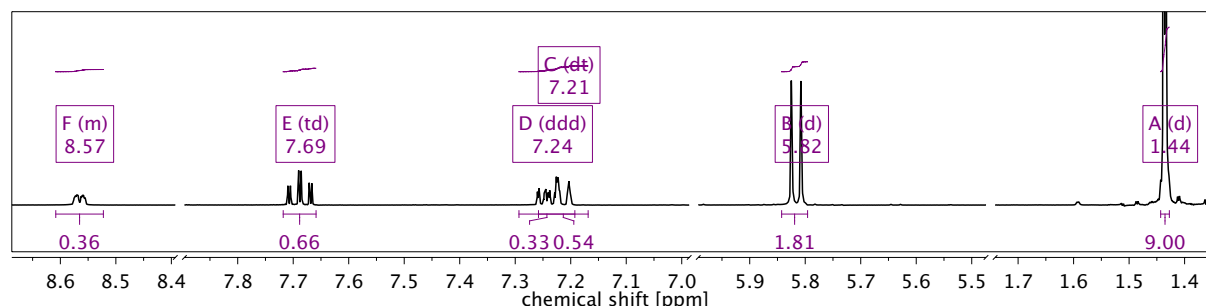
Figure 24: ¹H NMR spectrum of the compound **L4**. Aromatic region enlarged.

The corresponding triazoles were obtained by using a slightly modified protocol by Zhu *et al.*[47] yielding the products **L6** and **L7** as colourless solids in 72 and 67% yield, respectively. Subsequently, the ligands **L4** to **L7** were used in metal coordination, using rhenium pentacarbonyl bromide as a metal precursor. The electronic properties of the ligand can be investigated by using the Tolman electronic parameter (Excursion 6), as Crowley *et al.* demonstrated in 2014 for a series of *fac*-**Re**(I) carbonyl complexes based on 2-picolyl triazoles, bearing different substitutes in 4-position of triazole subunit (phenyl, 4-nitrophenyl, 4-methoxyphenyl and benzyl).[27]

Excursion 6: Tolman Electronic Parameter

The connection between the electron donating or withdrawing ability of ligands and the relative shift of the C-O stretching vibrations in the IR-Spectrum, first published by Walter Strohmeier,[48] and closer investigated by Chadwick A. Tolman,[49] is based on the ability of carbonyl metal fragments to develop in addition to the M-C σ-bond a π-backbonding by pushing electron density into the π* C-O orbitals. This donation leads to a stronger M-C bond, but also reduces the bond order of the carbon-oxygen bond. This effect thereby depends on the nature of the co-ligands; an increasing (or decreasing) of the π-electron density on the metal centre by a π-donating (or withdrawing) ligand system, results in a weakening (or strengthening) of the C-O bond. The strength of the C-O bond can be determined by IR spectroscopy, whereas a weakened C-O bond absorbs infrared radiation at lower wave numbers while stronger C-O bonds act reciprocal.[49]

Synthesis of Re(I) Carbonyl Complexes Based on Non-Conjugated Ligands

The synthesis of metal complexes **C3** and **C4** (Scheme 41) had been followed by means of $^{31}P\{^{1}H\}$ NMR spectroscopy measurements and quantitative consumption of the ligands was achieved within 8 h. The same had been found for the synthesis of complexes **C5** and **C6**, while the reaction was monitored by means of ^{1}H NMR spectroscopy in DCM-d$_2$.

R = ^{t}Bu: **C3**, 72 %   R = ^{t}Bu: **C5**, 89 %
R = TMS: **C4**, 43 %   R = TMS: **C6**, 57 %
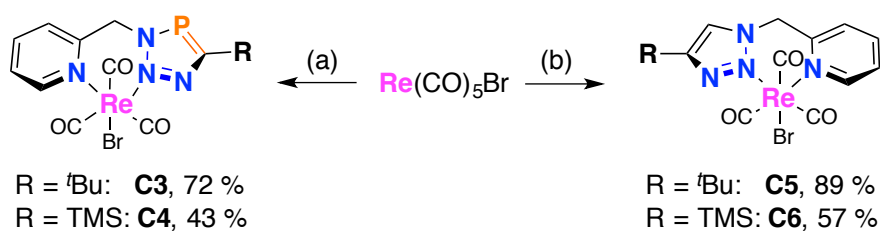
Scheme 41: Synthesis of Re(I) carbonyl complexes **C3** to **C5**. Reaction conditions (a): 1 eq. **L4/L5**, DCM, T = 80 °C, 8h; (b): 1 eq. **L6/L7**, DCM-d$_2$, T = 80 °C, 8h. The product is a racemic mixture.

While the reaction with the *tert*-butyl substituted ligands (**L4** and **L6**) proceeded in a straightforward manner, the reaction solution of the TMS (**L5** and **L7**) substituted compounds turned black, indicating side reactions, for instance by cleavage of the carbon silicon bond. Characterisation of the complexes by means of ^{1}H NMR spectroscopy revealed the splitting of the prochiral hydrogen atoms of the methylene bridge in all compounds, e.g. in complex **C3**, the signals split and shift from δ = 5.79 to 5.74 and 6.20 ppm (DCM-d$_2$). In $^{31}P\{^{1}H\}$ NMR spectra, the signal of the phosphorus containing complexes shifts relative to the free ligands about Δδ = 18.2 ppm (**C3**, δ = 191.3 ppm) and Δδ = 14.7 ppm (**C4**, δ = 231.1 ppm) to low field, providing no information about the coordination mode of the triazaphospholes due to the absence of NMR active Re cores. Therefore, X-ray analyses were performed on single crystals of all complexes. Suitable crystals of compounds **C3** (Figure 25) and **C4** (Figure 26) were obtained by slowly cooling down a hot saturated solution in DCM to T = -21 °C, whereas suitable crystals of **C5** (Figure 27) and **C6** (Figure 28) were obtained by S. Hoof during her Master Thesis by slow diffusion of diethyl ether into a DCM solution of the complex.
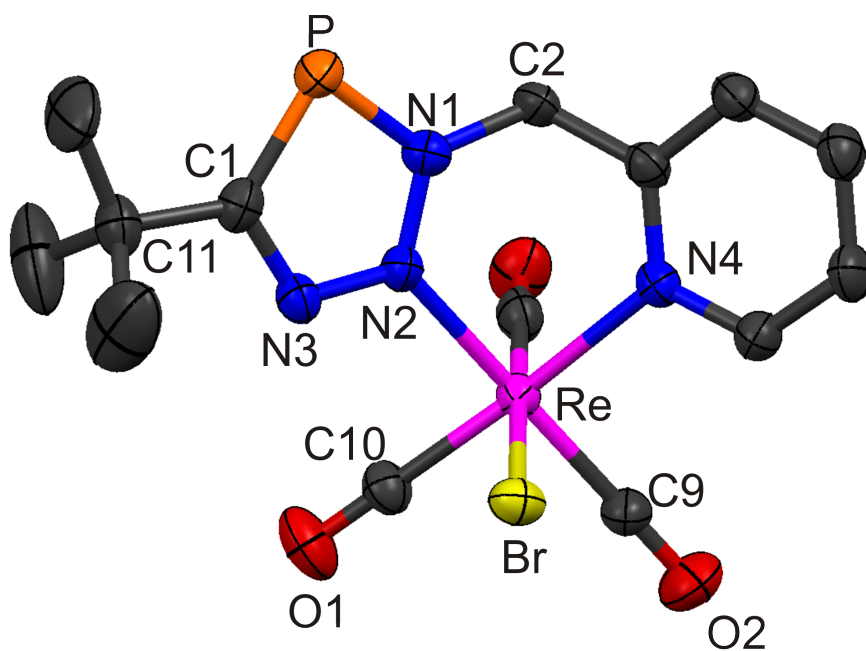
Figure 25: Molecular structure in the crystal of *fac*-Re(I) carbonyl bromide complexe **C3**. Displacement ellipsoids are shown at the 50% probability level. Hydrogen atoms are omitted for clarity. Selected bond lengths (Å) and angles (°): P(1)-C(1): 1.731(7); C(1)-N(3): 1.363(8); N(3)-N(2): 1.302(6); N(2)-N(1): 1.341(7); N(1)-P(1): 1.699(5); N(1)-C(2): 1.481(7); C(2)-C(3): 1.515(8); N(2)-Re(1): 2.163(5); N(4)-Re(1): 2.205(5); Re(1)-Br(1): 2.6258(7). N(1)-P(1)-C(1): 86.2(3) ; N(2)-Re(1)-N(4): 83.31(18).
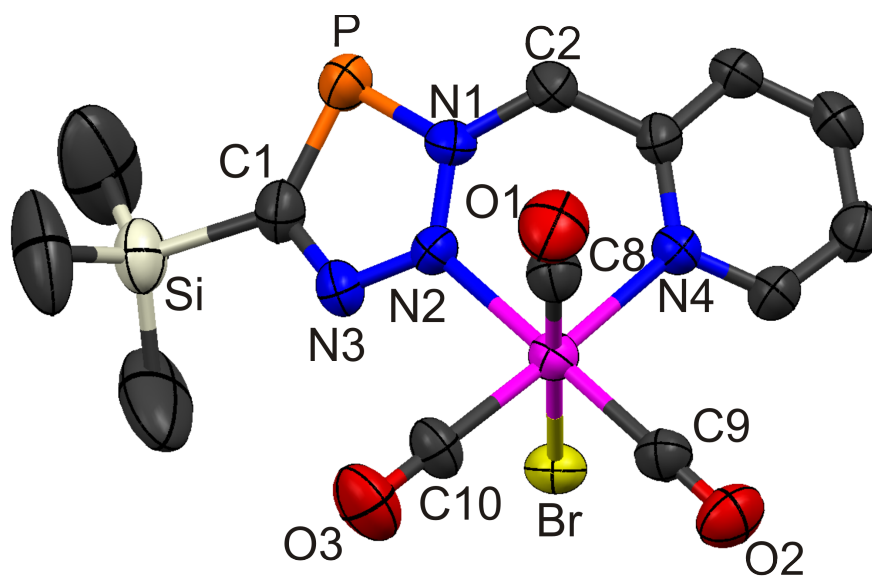
Figure 26: Molecular structure in the crystal of *fac*-Re(I) carbonyl bromide complexe **C4**. Displacement ellipsoids are shown at the 50% probability level. Hydrogen atoms are omitted for clarity. Selected bond lengths (Å) and angles (°): P(1)-C(1): 1.730(8); C(1)-N(3): 1.348(10); N(3)-N(2): 1.306(8); N(2)-N(1): 1.336(7); N(1)-P(1): 1.702(6); N(1)-C(2): 1.481(8); C(2)-C(3): 1.509(9); N(2)-Re(1): 2.163(5); N(4)-Re(1): 2.192(5); Re(1)-Br(1): 2.6248(8); C(1)-Si(1): 1.892(8). N(1)-P(1)-C(1): 86.7(3); N(2)-Re(1)-N(4): 83.7(2).
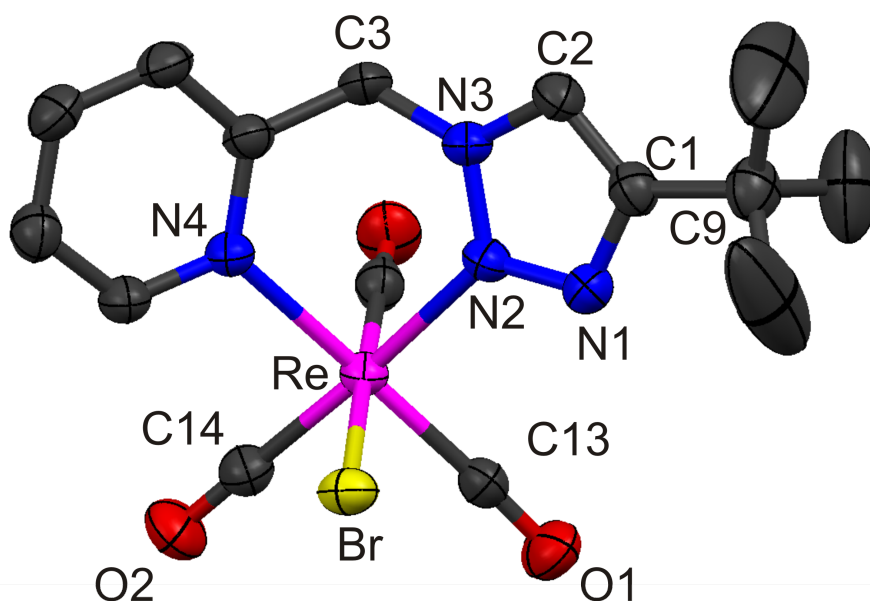
Figure 27: Molecular structure in the crystal of *fac*-Re(I) carbonyl bromide complex **C5**. Displacement ellipsoids are shown at the 50% probability level. Hydrogen atoms are omitted for clarity. Selected bond lengths (Å) and angles (°): C(2)-C(1): 1.366(7); C(1)-N(1): 1.352(6); N(1)-N(2): 1.321(5); N(2)-N(3): 1.337(5); N(3)-C(3): 1.460(6); C(3)-C(4): 1.512(7); C(4)-N(4): 1.351(5); N(2)-Re(1): 2.175(3); N(4)-Re(1): 2.218(3) ; Re(1)-Br(1): 2.6278(6). N(3)-C(2)-C(1): 105.4(4); N(2)-Re(1)-N(4): 82.78(13).
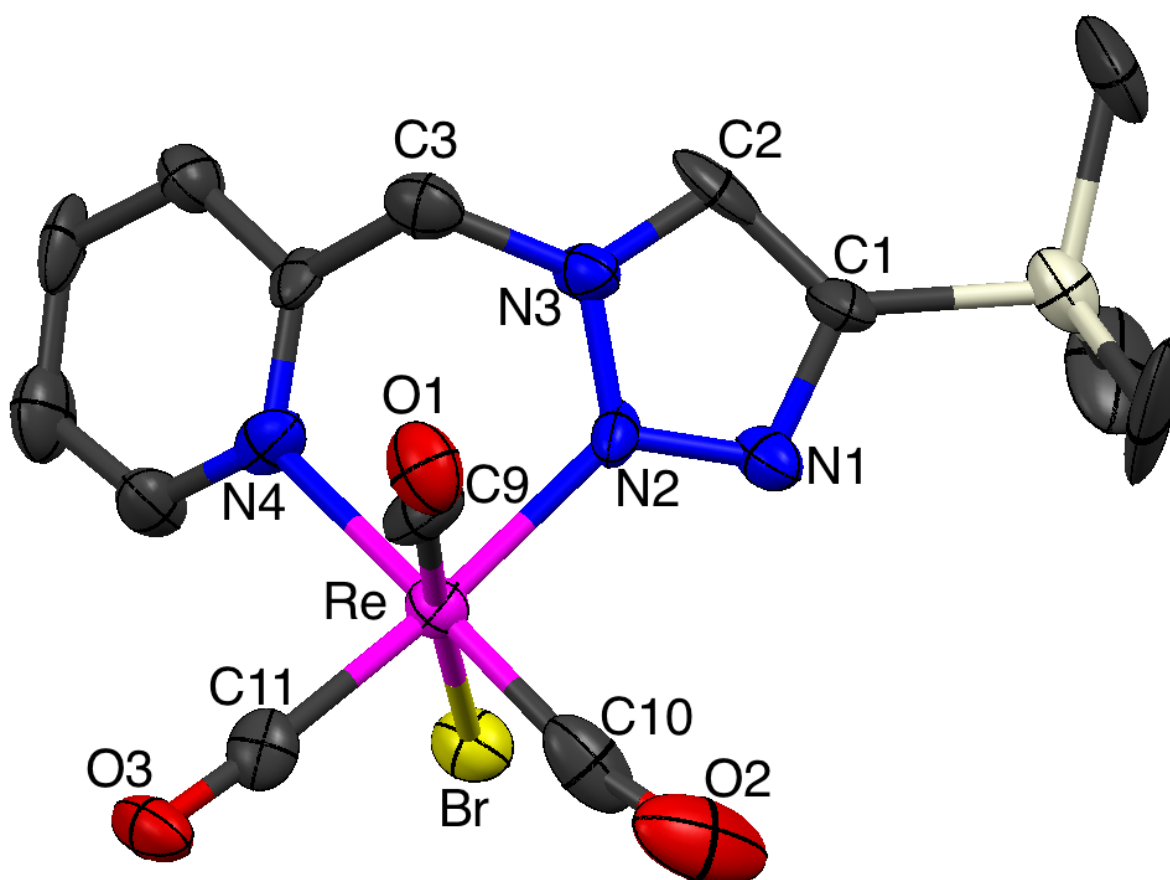
Figure 28: Molecular structure in the crystal of *fac*-Re(I) carbonyl bromide complex **C6**. Displacement ellipsoids are shown at the 50% probability level. Hydrogen atoms are omitted for clarity. Selected bond lengths (Å) and angles (°): C(2)-C(1): 1.43(3); C(1)-N(3): 1.42(2); N(3)-N(2): 1.32(2); N(2)-N(1): 1.36(2); N(1)-C(2): 1.34(3); N(1)-C(3): 1.51(3); C(3)-C(4): 1.44(3); C(4)-N(4): 1.37(2); N(2)-Re(1): 2.163(16); N(4)-Re(1): 2.233(18); Re(1)-Br(1): 2.598(3); N(3)-C(2)-C(1): 107.0(17); N(2)-Re(1)-N(4): 82.5(6).

Characterization of the Coordination Compounds

The crystallographic characterisation (Figure 25 to Figure 28) shows that the coordination of the triazaphosphole to the metal occurs in a facial fashion *via* the N^2 atom, which for triazoles, has been found to be the least nucleophilic one (Chapter 1), but this arrangement is also found in the nitrogen analogue complexes, due to the chelate effect. Next, the electronic structure of the ligand was explored by means of analysing the relative shifts of the CO stretching vibrations by IR spectroscopy (Table 3). In the triazole-based complexes **C4** and **C6**, the carbonyl stretching vibrations are slightly shifted to higher wave numbers, compared to their phosphorus analogues, (**C3** and **C4**) exhibiting a higher π-electron density due to the inclusion of the phosphorus atom in the aromatic heterocyclic system. Neither in the triazoles nor in the triazaphospholes, an influence of the substituent pattern of the starting (phosphorus) alkyne was found. This is in line with the observations that were previously made (*vide supra*) and the results shown by Crowley and colleagues[27]. Further investigations on the electronic structure of the *fac*-Re(I) carbonyl complexes **C3-C6** as well as their ligands **L4-L7** were performed by means of cyclic voltammetry measurements.

Table 3: Carbonyl stretching vibrations of the Re(I) complexes **C3** to **C6**.

Compound	$\tilde{v}_1$ (CO) [cm^{-1}]	$\tilde{v}_2$ (CO) [cm^{-1}]	$\tilde{v}_3$ (CO) [cm^{-1}]
C3	2023	1919	1885
C4	2021	n.d.	1879
C5	2032	1952	1891
C6	2026	1949	1898

For compounds **C3** and **C5**, irreversible oxidation processes were found in DCM at E_p^{ox} = +1.022 V and E_p^{ox} = +0.952 V *vs* Fc/Fc$^+$, while the non-phosphorus compounds **C4** and **C6** undergo quasi-reversible oxidation at E^{ox} = +0.909 and E^{ox} = +0.917 V (Figure 29). All compounds show irreversible reduction waves in THF: E_P^{red} = -2.56 V (**C3**), E_P^{red} = -2.61 V (**C4**), E_P^{red} = -2.36 V (**C5**), E_P^{red} = -2.14 V (**C6**) vs Fc/Fc$^+$. Similar to the results derived from the IR spectroscopy values of the CO stretch vibrations, the Re(I) complexes containing the triazole based ligands, are easier to reduce than the triazaphosphole-based coordination compounds. However, in contrast to the situation described above, an influence of the (phospha)alkene subunit on the heterocycle was

found. According to the electron-withdrawing nature of the TMS-group, these compounds are obviously easier to reduce.
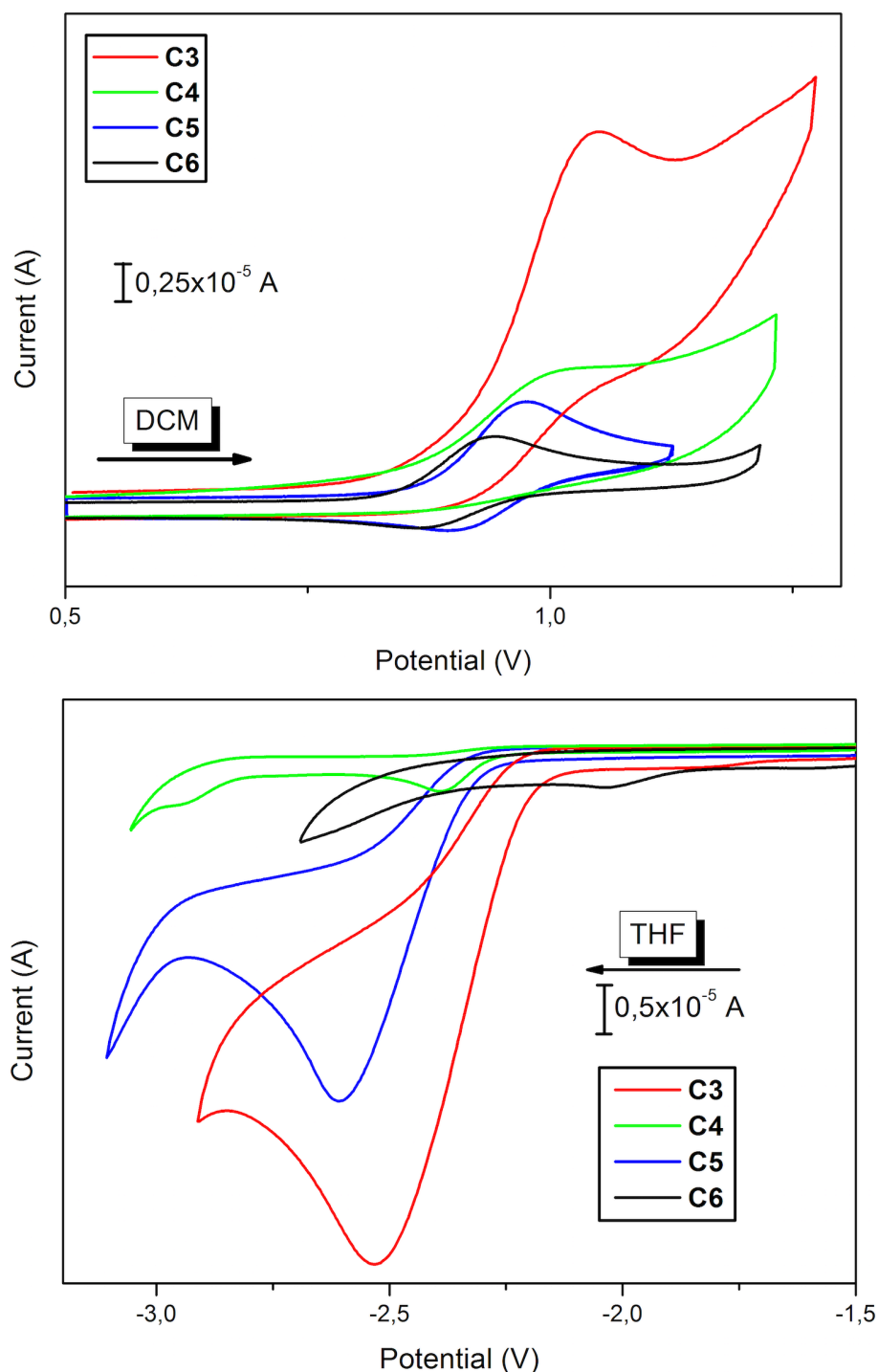
Figure 29: Cyclic voltammograms of Re(I) coordination compounds **C3** to **C6**. (**Top**) Oxidation in DCM; (**Bottom**): Reduction in THF. Referenced to Fc/Fc⁺, 0.1 M Bu₄PF₆, v = 100 mV/s.

For the cyclic voltammetry measurements of the ligands, both *tert*-Bu-substituted compounds, **L4** and **L6** undergo only one irreversible process during oxidation, E_p^{ox} = +1.438 V (**L4**) and E_p^{ox} = +1.451 V (**L6**), while the TMS substituted compounds

97

could not be oxidised within the solvent range of DCM, conforming the electron-withdrawing effect of this substituent. In comparison, the phosphorus-containing heterocycle is slightly easier to oxidise. The reduction performed in THF showed irreversible processes at E_p^{red} = -2.957 V (**L4**), E_p^{red} = -2.691 V (**L5**), E_p^{red} = -29.11 V (**L6**) and E_p^{red} = -2.636 V (**L7**) (Figure 30).
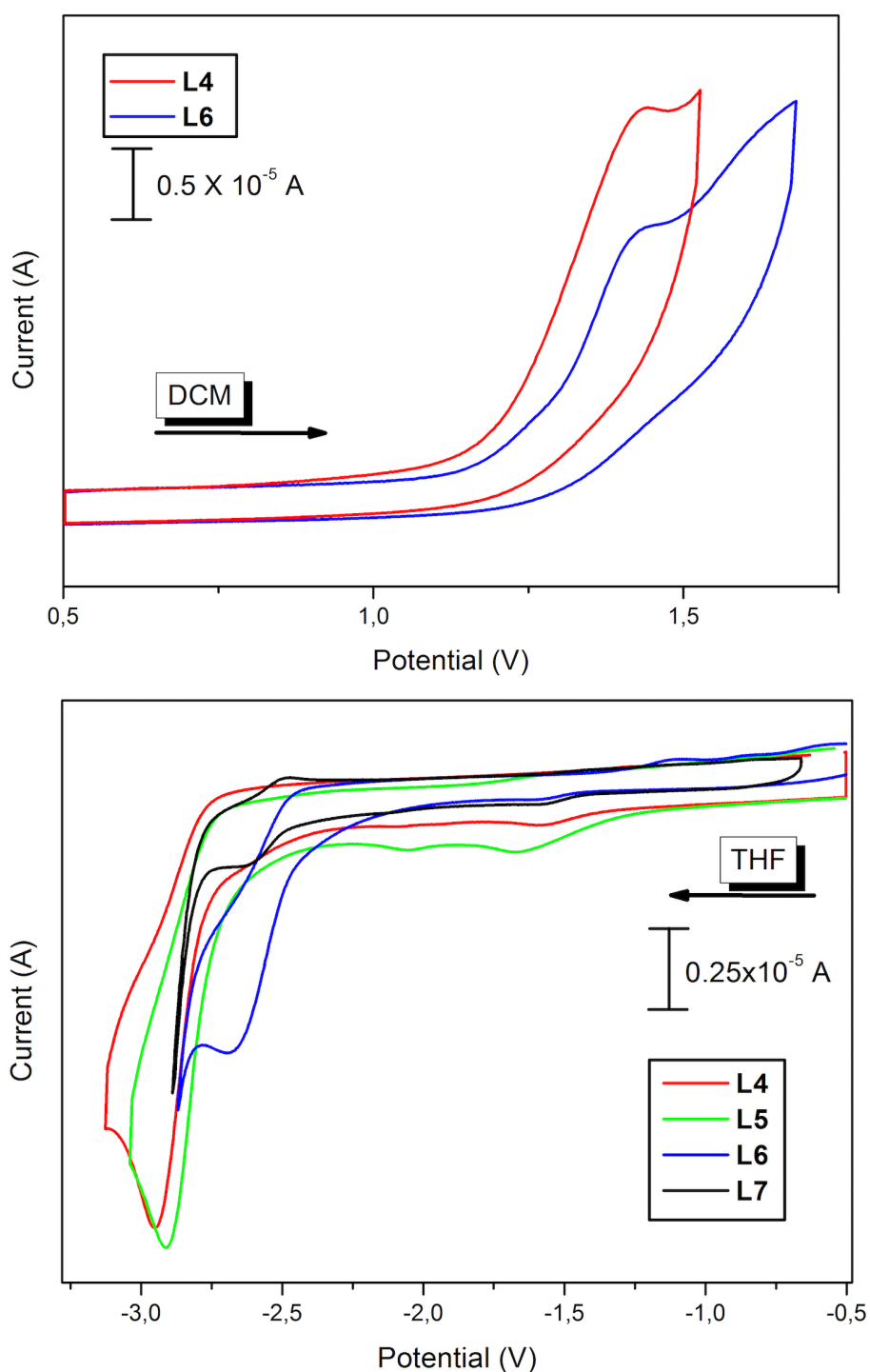
Figure 30: Cyclic voltammograms of compounds **L4** to **L6**. (**Top**): Oxidation in DCM; (**Bottom**): Reduction in THF. Referenced to Fc/Fc+, 0.1 M Bu$_4$PF$_6$, v = 100 mv/s.

As already observed for the **Re**(I) complexes, the ligands show similar trends in their electrochemical behaviour. The phosphorus-bearing compounds **L4** and **L6** are slightly more difficult to reduce in comparison to the triazoles, while the TMS group slightly lowers the necessary voltage for the reduction process. The exchange of the triazole CH-unit by the phosphorus atom results in a heterocycle that is obviously more electron-rich.

In a corporation with the group of B. Sarkar, DFT calculations were performed using the B3LYP functional.[50] As a starting point the molecular structure in the crystal of the **Re**(I) carbonyl complexes of the triazaphospholes (**C3**) and triazoles (**C5**) were chosen and geometry optimisations were performed, without the **Re**(CO)$_3$Br-fragment. The comparison between the molecular orbital plots (Figure 31) indicates a great similarity between both compounds, demonstrated by the shapes of HOMO and HOMO^{-1}, which are nearly the same. The HOMO of **L4** is formed by the contributions of the C=P double bond and the N^2 atom, all with π-symmetry. In **L6** coefficients of the C=C as well as N^2, N^1 and N^3 are contributing to the π-shaped MO, in sequence decreasing by their magnitude.

Distinctions are found in the shapes of the LUMO; while the triazaphosphole-based ligand shows that the coefficients are mainly found in the five-membered ring, the pyridyl substituent dominates the coefficient in the triazole-based heterocycle. For unsubstituted phosphinines a similar linear combination of the atomic orbitals is found in the LUMO. Nevertheless, the HOMO-LUMO gaps exhibit almost the same value with ΔE = 0.03 eV as well as the molecular orbitals being close in their energy level, e.g. LUMO (ΔE = 0.045 eV), HOMO (ΔE = 0.017 eV) and HOMO^{-1} (ΔE = 0.037 eV). This behaviour accounts for low-coordinate phosphorus compounds to be uncommon [51–53] and compared to aza- and diaza-phosphinines, where the replacement of a CH unit by a nitrogen atom diminishes the HOMO-LUMO gaps.[54] It is obvious that the inclusion of the C=P subunit into the triaza-based framework leads to an enlarged HOMO-LUMO gap with almost the same energy values, due to an electron-rich heterocycle and a possible N-C=P <–> $^+$N=C-P$^-$ conjugation, which is also found in 1,3-azaphospholes.[55] An enhancement of the π-back bonding can therefore not be expected. This is in line with the observations made in the IR analysis, where the phosphorus containing heterocycle appears to be the stronger π-donor, due to the large coefficients on the N^2 and the C=P double bond of π-symmetry found in frontier orbitals of the HOMO. For both molecules, the first molecular orbitals with σ-symmetry are found in the HOMO^{-1} with a similar large coefficient at the N^3 (triazole) and N^1 (triazaphosphole) nitrogen atoms followed

by the contributions of the nitrogen N^2 atoms with minor influence. In the HOMO^{-5}, a larger coefficient can be attributed to the phosphorus lone pair. The molecular orbital plots of HOMO^{-2} to HOMO^{-4} are less relevant and not included in Figure 31, because they consist mainly of coefficients in π-symmetry (HOMO^{-2}) or are located at the pyridyl substituent indicating σ-donating properties of the N^{Py} nitrogen lone pair (HOMO^{-3} & HOMO^{-4}) and show a high degree of resemblance.
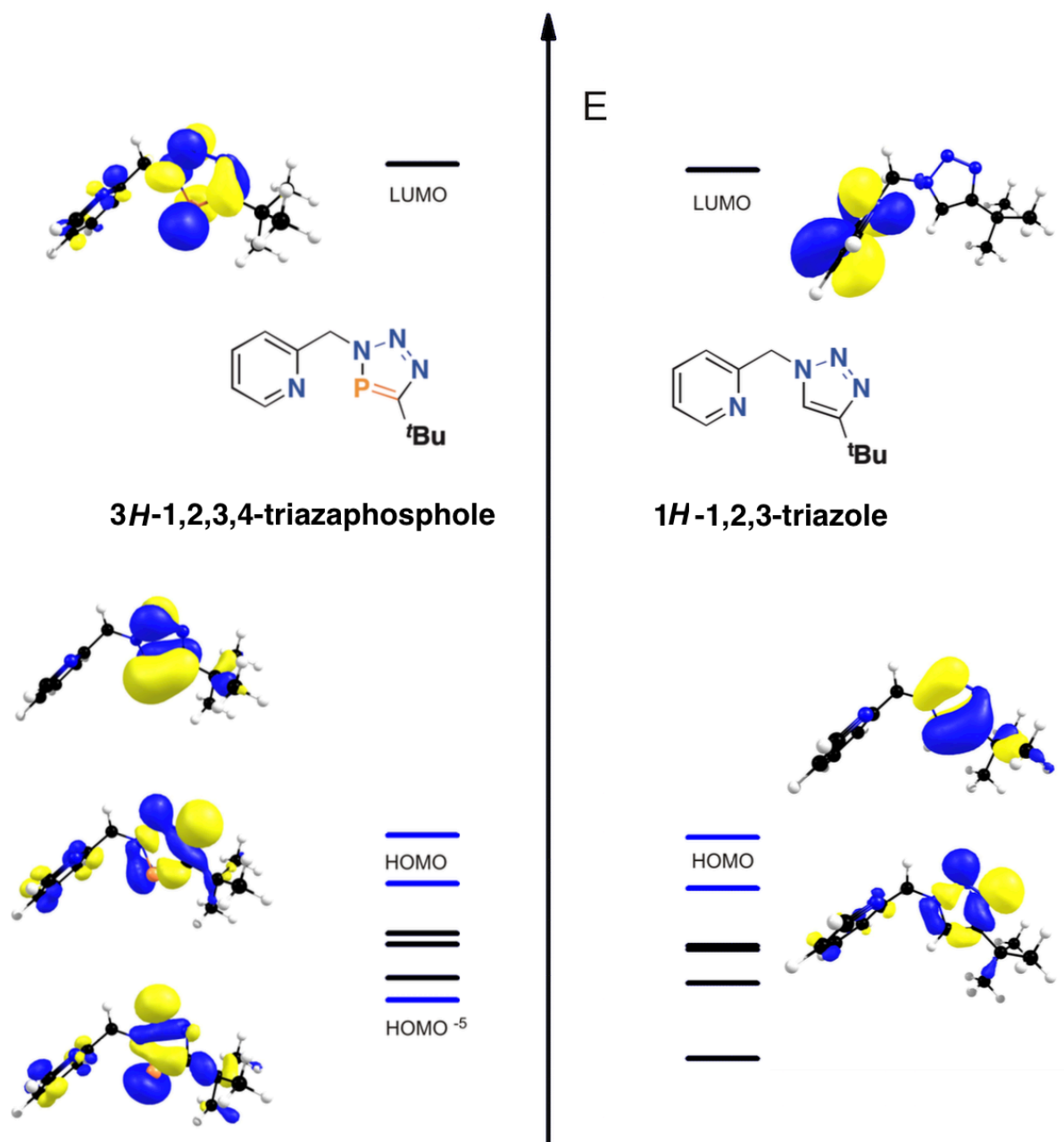
Figure 31: Molecular orbital plots of triazaphosphole (left) and **L4** triazole **L6** (right): Displayed occupied MOs are marked in blue.

Excursion 7: Attempts towards 3*H*-1,2,3,4-Triazaphospholes based Bimetallic Complexes

The picolyl-substituted triazaphospholes coordinates to the **Re**(I) metal centre, shown by the molecular structure in the crystal, in N^{Py}^^{m}N^{2TAP} fashion. By this, the phosphorus lone pair still provides an additional binding side. The question arises of whether this lone pair is available for coordination towards a second metal centre (Scheme 42) or not.
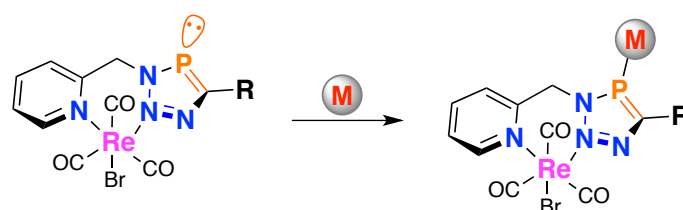
Scheme 42: Coordination chemistry of coordination compounds **C3** and **C4** towards bimetallic complexes.

Coordination with electron-rich metal centres should be favoured with respect to the HASB concept and the coin metals were chosen for the attempts towards achieving the synthesis ofbimetallic complexes. First reactions proceeded with (**Cu**(MeCN)$_4$BF$_4$) and the reaction progress, monitored by means of ^{31}P{^{1}H} NMR spectroscopy, showed conversion of the starting material within 72 h at room temperature (Figure 32).
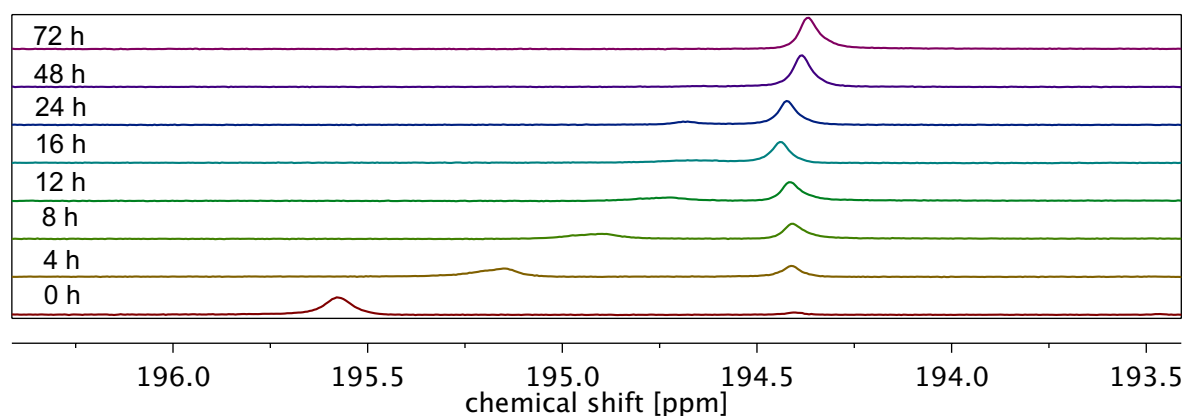
Figure 32: Time-depended conversion of coordination complex **C3** using [**Cu**(MeCN)$_4$BF$_4$]in DCM, monitored by means of ^{31}P NMR spectroscopy.

No suitable crystals for X-ray analysis could be obtained, since the complex reacted back to the starting material during crystallization consequently the reaction was carried out with other precursors: copper bromide dimethyl sulphide (**Cu**Br•SMe$_2$), silver triflate

(**Ag**OTf) and gold(I) chloride dimethyl sulphide (**Au**Cl•SMe$_2$). The results are summarised in Table 4.

Entry	Coin metal M(I)	Ratio M(I) : CX	Solvent	δ [ppm] of M(I)@C3	δ [ppm] of M(I)@C4
1	**Cu**Br•SMe$_2$	1:1	DCM	190.0	224.4
2	**Cu**(MeCN)$_4$BF$_4$	1:1	DCM	194.4	226.2
3	**Ag**OTf	1:1	DCM	*	230.3
4	**Ag**OTf	1:1	MeCN	194.4 192.6** 173.1***	n. p.
5	**Ag**OTf	2:1	MeCN	194.4 173.1***	n. p.
6	**Au**Cl•SMe$_2$	1:1	DCM	*	230.7

Chemical shifts of **C3** δ = 191.3 ppm and **C4** δ = 191.3 ppm. * Decomposition, ** unidentified, expected to be starting material, *** resonance of free ligand.

From the chemical shifts in Table 4, it is obvious that some results indicate the formation of different bimetallic complexes, especially in Entry 1. But in contrast, comparing the signals in the ^{31}P{^{1}H} NMR spectra obtained from the reaction mixtures in Entries 2, 4 and 5, quite a similar chemical shift is found, although different metals and ratios were used. This indicates that a substitution reaction as shown in Scheme 43 is obviously preferred over the formation of bimetallic complexes.
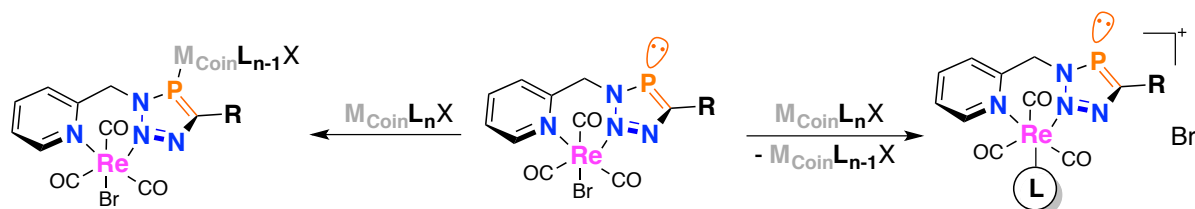
Scheme 43: Beside the formation of bimetallic complexes (**left**) also the substitution of the counter ion (**right**) must be taken into account.

To prove ligand substitution reactions by means of a halogen-solvent exchange, in a control experiment compound **C3** was treated with different coordinating solvents,

contained in the used metal precursors. To accelerate the solvent adduct formation, different amounts of silver triflate were used and the results are summarised in Table 5.

Table 5: Chemical shifts in $^{31}P\{^1H\}$ NMR spectra (DCM-d$_2$) obtained from the control experiments for the formation of bimetallic coordination compounds.

Entry	Coin metal	Ratio M(I) : C3	Solvent	δ [ppm] of M(I)@C3 (C3: 191.3 ppm)
1	-	-	MeCN	194.2
2	AgOTf	1:1	MeCN	194.3
3	AgOTf	2:1	MeCN	194.3
4	-	-	SMe$_2$	189.7
5	AgOTf	1:1	SMe$_2$	189.6

The control experiments clearly demonstrate the substitution of the bromide ligand by solvent molecule, despite the fact that identical chemical shifts were obtained for assumed bimetallic complexes. Therefore, the formation of these complexes can be excluded.

Excursion 8: Attempts towards Copper(I)-Picolyl-Triazaphosphole Complexes

Besides the coordination of the tricarbonyl-**Re**(I) fragment, the reaction behaviour of the ligands **L4** and **L5** towards **Cu**(I) sources were investigated. In contrast to the **Re**-subunit, no other π-accepting ligands such as CO are present in this complex. Furthermore, **Cu**(I)-halogen complexes are known to form clusters.[56–59] In this context, the dependency of the binding strength of the counter ion was also of interest (Figure 33).
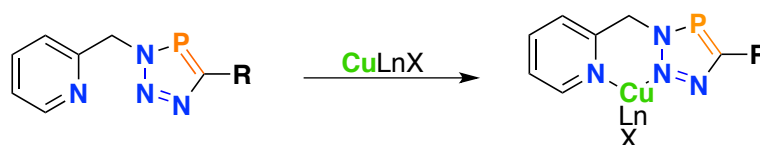
Figure 33: Synthesis of Cu(I) complexes on basis of **L4** and **L5**. Reaction conditions: DCM, room temperature.

For the reactions performed (precursors, conditions and results are summarised in Table 6) $^{31}P\{^1H\}$ NMR spectra show only one resonance of the formed product in all

cases. The chemical shifts of the triazaphosphole-based coordination compounds **C7** to **C11** show an interesting behaviour. For the coordinative counter ion, independent of the substituent in 5-position, an upfield shift is observed. While the more electron deficient metal complexes show a downfield shift due to the weaker coordinative counter ions. No single crystals could be obtained to determine the molecular structure by means of X-ray diffraction and these complexes were therefore not investigated any further.

Table 6: Chemical shifts in $^{31}P\{^1H\}$ NMR spectra (DCM-d$_2$) of the Cu(I) PicTAP-^{t}Bu/TMS coordination compounds.

Entry	Metal Precursor	Ligand	Complex-Nr	Chemical Shift δ [ppm]
1	**Cu**Br•SMe$_2$	**L4**	**C7**	159.4
2	**Cu**(MeCN)$_4$BF$_4$	**L4**	**C8**	180.7
3	**Cu**OTf)$_2$•C$_6$H$_6$	**L4**	**C9**	182.7
4	**Cu**Br•SMe$_2$	**L5**	**C10**	193.8
5	**Cu**(MeCN)$_4$BF$_4$	**L5**	**C11**	216.5*

* Chemical shift correspond to the free ligand

3.1.3.2: Alkoxy-Substituted 3H-1,2,3,4-Triazaphospholes[60]

Inspired from the interesting results shown in Section 3.1.3.1, especially with the N$^{Py\wedge m}$N$^{2\text{-TAP}}$ metal coordination of the chelating ligand system, the triazaphosphole subunit was modified with a less π-accepting but stronger σ-donating binding side to increase the electron density of metal ion. This might lead to a strong π-back bonding ability and would force the phosphorus atom into metal coordination. Several coordination compounds with hybrid donor-combinations, such as N^O, N^P and P^O are already quite established and also found application as precursors in homogeneous catalysis, as well as electronic and luminescent materials.[61–63] As a suitable compound an azide containing alcohol (**17**) synthesised by a procedure of K. Raman Rao *et al.*[64] had been chosen. This two-step synthesis not only provides simple access to the P^O-ligand, but is also an approach towards chiral triazaphosphole-based ligands. Starting with a nucleophilic substitution from 2-bromo-1-(*p*-tolyl)ethan-1-one (**15**) to the corresponding azide in the presence of *β*-cyclodextrin, followed by a reduction of **16** with sodium borohydride, gave the racemic alcohol **17**. Since the phosphaalkynes are sensitive towards protic solvents, a protection group was inserted (Scheme 44).
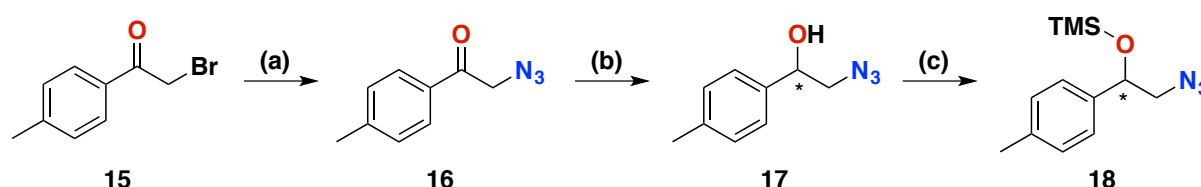
Scheme 44: Synthesis of azide **18** following the Raman Raos protocol for chiral alcohols. Reaction conditions (a): *β*-CD (1 eq.) H_2O, NaN_3 (1.5 eq.) 2d, 90 %; (b):$NaBH_4$ (2 eq.), EtOH, T = 0 °C, Ar-Atm, over night, 89%; (c): DABCO (1.3 eq.), TMSCl (1.6 eq), pentane, r.t., over night, 84%.

Azide **18** was than treated with phosphaalkyne **A2** to give the desired ligand **L8** (Figure 34) and, in another attempt, with **A1** to yield **L9** (Figure 35). Both ligands could be crystallised from cooling down a hot saturated solution to T = -21 °C.
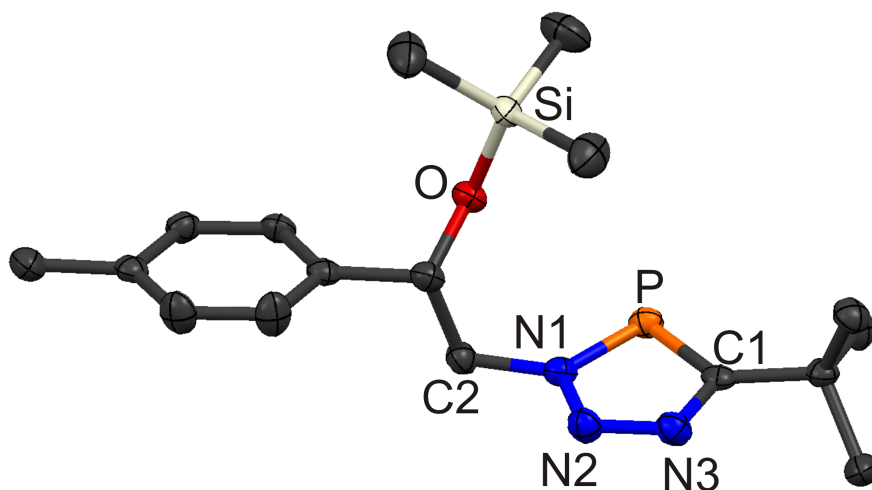
Figure 34: Molecular structure in the crystal of **L8**. Displacement ellipsoids are shown at the 50% probability level. Hydrogen atoms were omitted for clarity. Selected bond lengths (Å) and angles (°). *s*-Enantiomer displayed: P(1)-C(1): 1.723(2), P(1)-N(1): 1.680(2), N(1)-N(2): 1.345(3), N(2)-N(3): 1.305(3), C(1)-C(11): 1.512(4), N(1)-C(2): 1.464(3) , C(3)-O(1): 1.426(3), O(1)-Si(1): 1.655(2). N(1)-P(1)-C(1): 86.21(11).

The molecular structures in the crystal confirmed the formation of the desired ligands **L8** and **L9**. Both compounds were used as starting materials for deprotection reaction to obtain the corresponding anionic ligands **L10** and **L11** (Scheme 45). Unfortunately, neither the *tert*-Bu- nor the TMS-substituted compounds could be isolated. From the reaction mixture, an insoluble solid was obtained, preventing further investigations by means of ^{1}H and ^{13}C{^{1}H} NMR spectroscopy.
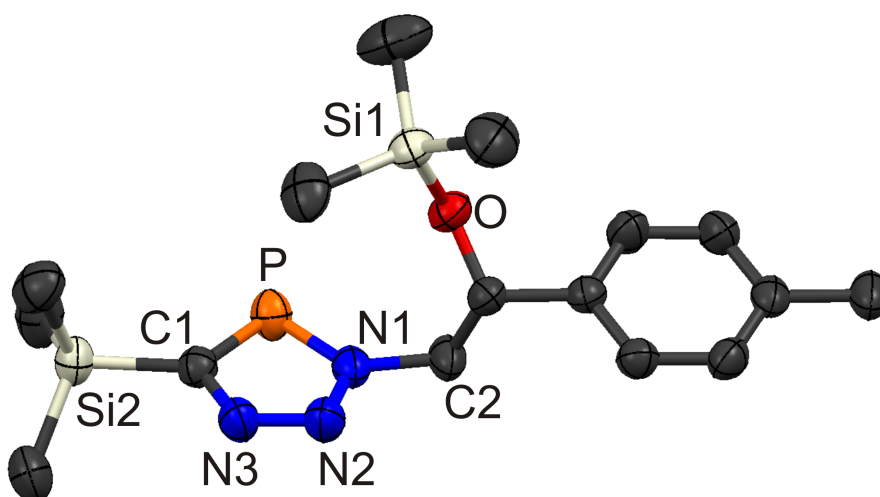
Figure 35: Molecular structure in the crystal of **L8**. Displacement ellipsoids are shown at the 50% probability level. Hydrogen atoms were omitted for clarity. Selected bond lengths (Å) and angles (°). *s*-Enantiomer displayed: P(1)-C(1): 1.713(2), P(1)-N(1): 1.673(2), N(1)-N(2): 1.343(3), N(2)-N(3): 1.309(3), C(1)-Si(2): 1.873(2), N(1)-C(2): 1.475(3), C(3)-O(1): 1.412(3), O(1)-Si(1): 1.656 (2). N(1)-P(1)-C(1): 87.48(11).
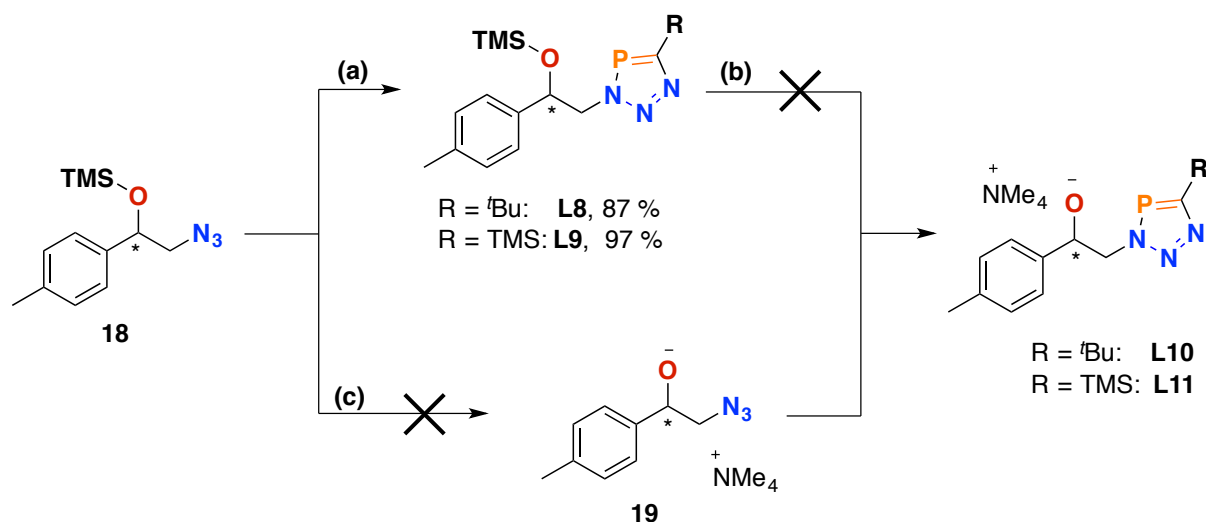
Scheme 45: Synthetic route towards the anionic compounds **L10** and **L11**. Reaction conditions: all reactions performed under Ar atm. Dry reagents and solvents were used. (a): R-CP (3 eq.) 1 h r.t., R=^{t}Bu THF; R=TMS toluene; (b): NMe$_4$F (1.1 eq.) DCM, r.t., 24 h; (c): NMe$_4$F (1.1 eq.) DCM, r.t., 24 h.

The synthesis of the isolated compounds **L10** and **L11** failed, wherefore a one-pot synthesis was developed. Firstly, the ligand was supposed to coordinate with, either the nitrogen or the phosphorus atom to the metal centre. The resulting, prearranged complex was than treated with tetramethylammonium fluoride (Scheme 46).
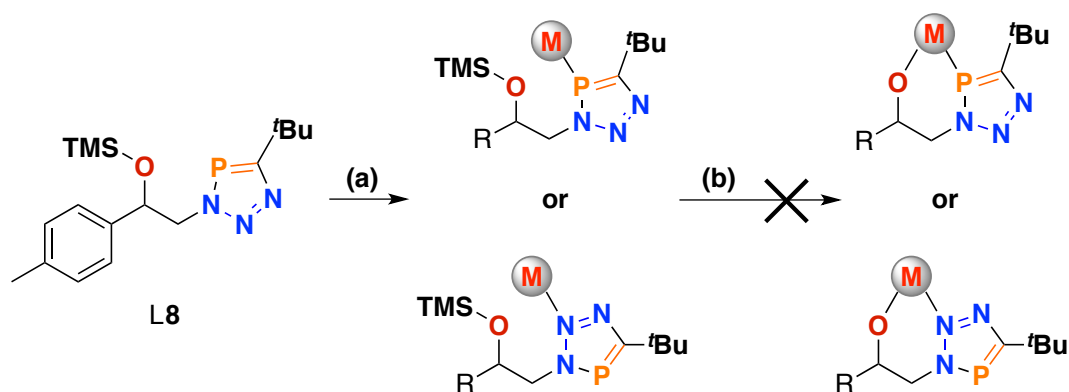
Scheme 46: Desired pathway for alcoxy-functionalized triazaphosphole based metal complexes. Reaction conditions (a): Pt(COD)Cl$_2$ (1 eq.), AgOTf (2.2 eq), DCM, r.t. 10 min; (b) NMe$_4$F (1.5 eq.) DCM, r.t., 24 h.

The obtained coordination compounds could not be reproduced using **Pt**(II) as metal precursor. Further coordination attempts towards **Rh**(I) failed, hence the metal coordination experiments with these ligands were discontinued.

Experimental Details of Non-Conjugated Triazaphospholes and Triazoles

Synthesis of Dichloro((trimethylsilyl)methyl)phosphane (3)

$$TMS \diagup PCl_2$$

In a 1L-Schlenk flask, equipped with reflux condenser and dropping funnel, 20.6 g (611 mmol, 1.5 eq.) magnesium was first activated with iodine and than top layered with 500 mL Et$_2$O and treated afterwards with 50 g (408 mmol, 1 eq.) (chloromethyl)trimethylsilane, dissolved in 200 mL diethyl ether. The reaction was started with local heating of the flask and after the exothermic reaction eased, the mixture was allowed to stir for 1 h at r.t.. Subsequently the filtrate was added drop-wise to a solution of 84.8 g (618 mmol 1.5 eq.) phosphorus trichloride in 300 mL Et$_2$O, cooled down to T = -78 °C. The reaction mixture was cooled over night at this temperature and after reaching r.t. 120 mL of a 2M hydrochloric acid diethyl ether solution was added and the mixture was stirred for 4 h. The suspension was filtered and the solvent was removed in vacuum. Compound **3** was obtained in 49% yield (56.7 g, 300 mmol) as slightly orange oil.

^{1}H NMR (400 MHz, CDCl$_3$): δ = 0.18 (s, 9 H, Me$_3$Si), 2.05 (d, J = 15.5 Hz, 2 H, CH$_2$) ppm.
^{31}P{^{1}H} NMR (162 MHz, CDCl$_3$): δ = 207.3 ppm.
^{31}P NMR (162 MHz, CDCl$_3$): δ = 207.3 (t, $^2J_{P\text{-}H}$ = 14.9 Hz) ppm.

Spectroscopic data are consistent with literature data.[6,65]

Synthesis of ((trimethylsilyl)methylidyne)phosphane (A1)

$$TMS \!\!-\!\!\!\equiv\!\! P$$
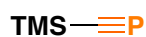
In a 500 mL Schlenk-flask 4.8 g (25.4 mmol) dichloro((trimethylsilyl)methyl)phosphane (**3**) were dissolved in 300 mL dry toluene. The reaction was done under the exclusion of light, 14.4 g (56 mmol, 2.2 eq.) silver triflate was added and than stirred for 1 h at r.t. After treatment with 6.26 g (55.8 mmol, 2.2 eq.) the mixture was stirred again for 1 h at light exclusion. The azeotropic mixture of the and toluene was obtained by trap-to-trap condensation. The yield (52%, 44 mmol) was estimated by a [3+2] cycloaddition with benzyl azide.

¹H NMR (400 MHz, CDCl₃): δ = 0.05 ppm.

³¹P{¹H} NMR (162 MHz, CDCl₃): δ = 99.3 ppm.

Spectroscopic data are consistent with literature data.[66]

Synthesis of 1-(dichlorophosphanyl)piperidine (*5*)
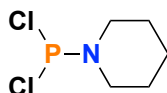
To solution consisting of 123 g (900 mmol, 1 eq.) phosphorus trichloride in 200 mL dry diethyl ether, cooled to T = -78 °C, was drop-wise treated with 153 g (1.79 mol, 2 eq.) piperidine. The reaction was allowed to warm up over night and the resulting suspension was diluted with 200 mL dry Et₂O. The solid was removed by filtration and washed 5x with 250 mL diethyl ether. The solvent was removed by vacuum and the crude product was purified by vacuum distillation (50-53 °C, 1.9*10⁻² mbar). The product was obtained as colourless liquid in 58% yield (96.7 g, 0.52 mol).

¹H NMR (400 MHz, CDCl₃): δ = 1.60 (6H, m, CH₂) 3.23-3. 31 (4H, m, CH₂) ppm.

³¹P{¹H} NMR (162 MHz, CDCl₃): δ = 157.8 ppm.

Spectroscopic data are consistant with literature data.[7,67]

Synthesis of 1,1,1,3,3,3-hexamethyl-2-(trimethylsilyl)disilaphosphane (*6*)
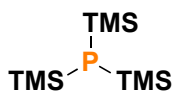
General procedure of the tris(trimethylsilyl)phosphine synthesis: Lithium (9.6 g, 1.38 mol) was top layered with 350 mL dry THF as well as 85.4 g (197 mmol) chlorotrimethyl-silane. The mixture was refluxed and **5** (36.6 g, 786 mmol), dissolved in 220 mL dry THF, was added drop-wise to the reaction flask. The mixture was heated for 8 h and was than allow to cool down to r.t. and stirred until the reaction was complete. The solvent was removed in vacuum, redissolved in 400 mL dry pentane and filtrated. The solid was washed 3x with 200 ml pentane and the combined organic phased were dried in vacuum and the crude product purified by vacuum distillation (b.p. 48-50 °C, 10⁻³ mbar).

¹H NMR (400 MHz, C_6D_6): δ = 0.19 (9H, s, CH_3) ppm.
³¹P{¹H} NMR (162 MHz, C_6D_6): -251.9 (s, 1P) ppm.

Spectroscopic data are consisted with literature data.[8]

Synthesis of (2,2-dimethyl-1-((trimethylsilyl)oxy)propylidene)(trimethylsilyl)phosphane (*8*)
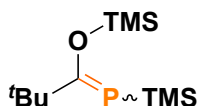
A solution of 10 g (40.0 mmol, 1 eq.) **6** in 20 mL dry pentane was treated with a solution of pivaloyl chloride (4.05 g, 33.6 mmol) in 20 mL pentane and stirred for 6 d at room temperature. The solvent is removed in vacuum and the crude product distilled in reduced pressure (62-64 °C, 0.36 mbar), yielding 7.59 g (86%) of a yellow liquid.

¹H NMR (500 MHz, C_6D_6): δ = 0.23 (s, 9H, O-Si$(CH_3)_3$), 0.36 (d, $^3J_{H-P}$ = 3.9 Hz, 9H, s, P-Si$(CH_3)_3$), 1.27 (d, $^5J_{H-P}$ = 1.5 Hz, 9H, C$(CH_3)_3$) ppm.
³¹P{¹H} NMR (162 MHz, C_6D_6): -121.6 (s, 1P) ppm.

Spectroscopic data consist with literature.[10,11]

Synthesis of (2,2-dimethylpropylidyne)phosphane (*A2*)
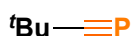
Into a 2-necked flask, equipped with dropping funnel containing 7.57 g (28.85 mmol) **8**, 13.33 g (333 mmol) of dry NaOH were placed and the flask was heated up to T = 160 °C. Under reduced pressure (1 mbar) **8** is slowly dropped on the hot NaOH and the produced gases were collected in a cooling trap (CO_2(s), EtOH). The crude product was purified by trap-to-trap condensation, yielding 2.77 g (27.7 mmol, 96%) of a colourless liquid.

¹H NMR (400 MHz, C_6D_6): δ = 1.02 (s, $^4J_{H-P}$ = 1.5 Hz, 9H) ppm.
¹³C{¹H} NMR (101 MHz, C_6D_6): δ = 31.0 (d, $^3J_{C-P}$ = 6.1 Hz, $(CH_3)_3$), 36.09 0 (d, $^2J_{C-P}$ = 18.1 Hz, C_{quart.}), 184.5 (d $^1J_{C-P}$ = 38.1 Hz, CP) ppm.
³¹P{¹H} NMR (162 MHz, C_6D_6): - 68.0 (s, 1P) ppm.

Spectroscopic data are consistent with literature data.[11]
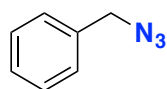
In a 100 mL flask 2.85 g (43.9 mmol, 1.5 eq.) NaN_3 were dissolved in 60 mL DMSO and treated afterwards with 5 g (29.2 mmol, 1 eq.) benzyl bromide. The reaction mixture was stirred at r.t. over night, diluted with 100 mL water. The crude product was extracted with Et_2O (5x 100 ml) and the combined organic phases were first washed with H_2O (3x 50 mL) followed by Brine-solution and than dried over $MgSO_4$ and filtered. The solvent was removed in vacuum, yielding 3,77 g (28.3 mmol, 97%) of the title compound as yellow oil.

¹H NMR (400 MHz, $CDCl_3$): δ = 4.33 (s, 2H, CH_2) 7.25-7.55 (m, 5H, Ar-H) ppm.

¹³C{¹H} NMR (101 MHz, $CDCl_3$): δ = 54.8 (s, $C-CH_2$), 128.2 (Ar-C), 128.3 (Ar-C), 128.9 (Ar-C), 135.4 (Ar-C) ppm.

Spectroscopic data are consistent with literature data.[13]

*Synthesis of 3-benzyl-5-(trimethylsilyl)-3H-1,2,3,4-triazaphosphole (**L1**)*
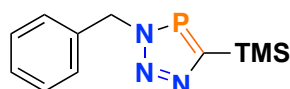
Benzyl azides **10** (3.75 mmol) were propounded with a stirring bar in a 250 mL flask, the azide was frozen and the flask evacuated, followed by the addition of around 100 mL dry ((trimethylsilyl)methylidyne)phosphine in toluene (large excess). The reaction solution was allowed to warm to r.t. and stirred for 24 h. The solvent and the excess of alkyne were removed in vacuum and the crude product recrystallized from cooling down a hot saturated pentane solution. **L1** was obtained as white crystalline solid (93% yield, 3,48 mmol).

¹H NMR (400 MHz, methylene chloride-d₂): δ = 0.38 (d, $^4J_{H-P}$ = 0.5 Hz, 9H, Me-H9, Me-H10, Me-H11), 5.81 (d, $^3J_{H-P}$ = 6.0 Hz, 2H),7.37 (m, 1H).ppm.

¹³C{¹H} NMR (101 MHz, Methylene Chloride-d₂): δ = -0.1 (d, $^3J_{C-P}$ = 3.5 Hz, $Si(CH_3)_3$), 56.1 (d, $^2J_{C-P}$ = 12.1 Hz, CH_2-C2), 128.9 (d, $^4J_{C-P}$ = 1.2 Hz, Ar-C4, Ar-C5), 129.0 (s, Ar-C6), 129.4 (s, Ar-C5, Ar-C7), 137.9 (d, $^3J_{C-P}$ = 2.0 Hz, Ar-C3), 185.5 (d, $^1J_{C-P}$ = 74.8 Hz, Ar-C1) ppm.

³¹P{¹H} NMR (162 MHz, methylene chloride-d₂): δ = 214.7 (s) ppm.

ESI-TOF-MS (+, 200 V)**:** [M+H]$^+$ = 250.0909 m/z (calc.: 250.09239 m/z).

EA(NCH): N: 15.78%, C: 51.85%, H: 6.59%; calc.: N: 16.85%, C: 52.99%, H: 6.47%.

*Synthesis of 3-benzyl-5-(tert-butyl)-3H-1,2,3,4-triazaphosphole (**L2**)*
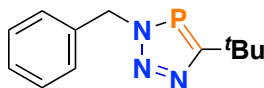
Benzyl azide **10** (3.75 mmol) was propounded with a stirring bar in a 100 mL flask, the azide was frozen and the flask evacuated, followed by the addition of around 50 mL dry toluene as well as (dimethyllidyne)phosphine (412.9 mg, 4.13 mmol, 1.5 eq.). The reaction solution was allowed to warm to r.t. and stirred for 24 h. The solvent and the excess of alkyne were removed in vacuum. The resulting solid was recrystallized from a hot saturated *n*-pentane solution. **L2** was obtained as white crystalline solid (88% yield, 3.3 mmol).

^{1}H NMR (500 MHz, methylene chloride-d$_2$): δ = 1.43 (d, $^4J_{H-P}$ = 1.6 Hz, 9H, Me-H), 5.69 (d, $^3J_{H-P}$ = 6.8 Hz, 2H, CH$_2$), 7.36 (m, 5H, Ar-H) ppm.

^{13}C{^{1}H} NMR (176 MHz, methylene chloride-d$_2$): δ = 31.9 (d, $^3J_{C-P}$ = 8.0 Hz, Me-C10, Me-C11, Me-C12), 35.7 (d, $^2J_{C-P}$ = 16.2 Hz, ^{t}Bu-C9), 56.6 (d, $^2J_{C-P}$ = 13.0 Hz, CH$_2$-C2), 128.9(s, Ar-C5, Ar-C7), 129.0 (s, Ar-C6), 129.4 (s, Ar-C4, Ar-C8), 137.9 (d, $^4J_{C-P}$ = 1.9 Hz, Ar-C3), 198.2 - 199.3 (d, $^1J_{C-P}$ = 56.3 Hz, Ar-C1) ppm.

^{31}P{^{1}H} NMR (162 MHz, methylene chloride-d$_2$): δ = 171.4 (s) ppm.

ESI-TOF-MS (+, 200 V)**:** [M+H]$^+$ = 234.1151 m/z (calc.: 234.11546).

EA(NCH): N: 17.79%, C: 61.79%, H: 6.905%; calc.: N: 18.02%, C: 61.79%, H: 6.91%.

*Synthesis of 4-methylbenzenesulfonyl azide (**12**)*
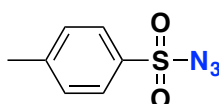
In a 500 mL flask 1.421 g (22 mmol, 1.1 eq.) sodium azide were dissolved in H$_2$O/EtOH mixture (57/3 mL) and within 10 min 3.8 g (19.9 mmol, 1 eq.) of *p*-toluenesulfonyl chloride dissolved in 100 mL acetone were added drop-wise. The reaction mixture was stirred over night, diluted with 100 mL H$_2$O and the crude product was extracted with Et$_2$O (3x 100 mL). The combined organic phased were dried over MgSO$_4$ and filtered off,

the solvent removed in vacuum and the compound dried over night at T = 30 °C at high vacuum. 89% yield (17.7 mmol).

^{1}**H NMR** (400 MHz, CDCl$_3$): δ = 2.48 (s, 3 H, CH$_3$) 7.37 - 7.44 (m, 2H, 2C$_{Ar}$H), 7.83 (dd, $^3J_{H-H}$ = 8.4 Hz, 1.3 Hz, 2H, C$_{Ar}$H) ppm.

^{13}**C{^{1}H} NMR** (101 MHz, CDCl$_3$): δ = 21.7 (C-Me), 127.5 (Ar-C), 130.3 (Ar-C), 135.5 (Ar-C), 146.3 (Ar-C) ppm.

Spectroscopic data consist with literature.[25]

*Synthesis of 5-(tert-butyl)-3-tosyl-3H-1,2,3,4-triazaphosphole (**L3**)*
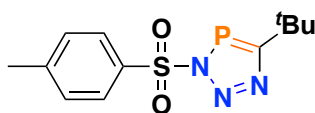
Tosyl azide **12** (3.75 mmol) was propounded with a stirring bar in a 100 mL flask, the azide was frozen and the flask evacuated, followed by trap-to-trap condensation of ca. 50 mL dry toluene and **A2** (412.9 mg, 4.13 mmol, 1.5 eq.). The reaction solution was allowed to warm to r.t. and stirred for 24 h. The solvent and the excess of alkyne were removed in vacuum. The resulting solid was recrystallized from a hot saturated *n*-pentane solution. **L3** was obtained as white crystalline solid (85% yield, 3.19 mmol).

^{1}**H NMR** (700 MHz, methylene chloride-d$_2$): δ = 1.47 (d, $^4J_{H-P}$ = 3.2 Hz, 9H, Me-H), 2.47 (s, 3H, CH$_{3-toysl}$), 7.44 (d, $^3J_{H-H}$ = 8.3 Hz, 2H, 2CH), 8.06 (d, $^3J_{H-H}$ = 8.5 Hz, 2H, 2CH) ppm.

^{13}**C{^{1}H} NMR** (176 MHz, methylene chloride-d$_2$): δ = 22.1 (C-Me$_{tosyl}$), 31.5 (d, $^3J_{C-P}$ = 8.2 Hz, 3C-Me$_{tert-Butyl}$), 36.2 (d, $^2J_{C-P}$ = 14.1 Hz, C-^{t}Bu), 56.6 (d, $^2J_{C-P}$ = 13.0 Hz, CH$_2$-C2), 128.9(s, Ar-C5, Ar-C7), 129.0 (s, Ar-C6), 129.4 (s, Ar-C4, Ar-C8), 137.9 (d, $^4J_{C-P}$ = 1.9 Hz, Ar-C3), 198.2 – 199.3 (d, $^1J_{C-P}$ = 56.3 Hz, Ar-C1) ppm.

^{31}**P{^{1}H} NMR** (162 MHz, methylene chloride-d$_2$): δ = 171.4 (s) ppm.

EI-MS(+): 297.078 m/z (calc.: 297.0701).

In a J. R. Young-NMR tube, 50 mg (0.17 mmol, 1 eq.) **L3** were propounded, followed by 48.5 mg (0.17 mmol, 1 eq.) of **Au**Cl•SMe$_2$ and DCM-d$_2$ (0.4 mL), leading immediately to a gas evolution.

^{31}P{^{1}H} NMR (162 MHz, CD$_2$Cl$_2$): δ = 117 or 122 or 140 (s) ppm.

Synthesis of tetracarbonyl dirhodium(I) 2,4-bis(3-methylbut-2-en-2-yl)-1,3-ditosyl-1,3,2,4-diazadi-phosphetidine dichloride (C2)
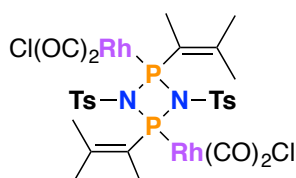
In a J. R. Young-NMR tube, 50 mg (0.17 mmol, 1 eq.) **L3** were propounded, followed by 32.7 mg (0.08 mmol, 0.5 eq.) of [**Rh**(CO)$_2$Cl]$_2$ and DCM-d$_2$ (0.4 mL), leading immediately to a gas evolution.

^{31}P{^{1}H} NMR (162 MHz, CD$_2$Cl$_2$): δ = 91.9 (d, $^{1}J_{\text{P-Rh}}$ = 140.2 Hz) ppm.

ESI-TOF-MS (MeCN, 250V): [M-{(CO)$_2$Cl}+MeCN]$^+$= 922.13554 m/z (calc.: 922.1403 m/z).

Synthesis of 2-(azidomethyl)pyridine (14)
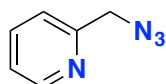
In a 100-mL Schlenk-flask 1.93 g (29.7 mmol) NaN$_3$ were dissolved in 60 mL degassed DMSO. Than 5 g (19.8 mmol) of 2-(bromomethyl) pyridine hydrobromide (**13**) and 3.15 g (29.7 mmol) NaHCO$_3$ were added. After the reaction mixture was stirred for 1 h at r.t. it was slowly diluted in 450 mL H$_2$O and the crude product was extracted with Et$_2$O (5x 75 mL). The combined organic phases were dried over Na$_2$SO$_4$, filtrated and the

solvent removed in vacuum, yielding 2.19 g (83%, 24.7 mmol) of a yellow oil. No further purification was necessary.

¹H NMR (400 MHz, CDCl₃): δ = 4.44 (s, 2H, CH₂), 7.25 - 7.34 (m, 1H, Ar-H), 7.67 (td, $^3J_{H\text{-}H}$ = 7.7, 1.8 Hz, ArH), 8.56 (ddd, $^3J_{H\text{-}H}$ = 4.8, 1.7, 0.9 Hz, Ar-H) ppm.

Spectroscopic data are consistent with literature data.[68]

Synthesis of 2-((5-(tert-butyl)-3H-1,2,3,4-triazaphosphol-3-yl)methyl)pyridine (L4)
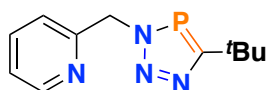
2-(Azidomethyl)pyridine (387.8 mg, 2.89 mmol, 1 eq.) dissolved in 20 mL of dry diethylether and (2,2-dimethylpropylidyne)phosphine (318,3 mg, 3.18 mmol) was added to the reaction mixture and allowed to warm to r.t. and stirred for overnight. The solvent was removed under vacuum, yielding a white solid (629,6 mg, 2.69 mmol, 93% isolated yield).

¹H NMR (400 MHz, CD₂Cl₂): δ = 1.41 (d, $^4J_{P\text{-}H}$ = 1.4 Hz, 9H, CH₃), 5.79 (d, $^3J_{P\text{-}H}$ = 6.8 Hz, 2H, CH₂), 7.20 (s, 1H, H$_{Ar}$), 7.20 - 7.24 (m, 1H, H$_{Ar}$), 7.60 - 7.69 (m, 2H, H$_{Ar}$), 8.54 (ddd, J = 4.8, 1.8, 1.0 Hz, 1H, H$_{Ar}$) ppm.

¹³C{¹H} NMR (101 MHz, CD₂Cl₂): δ = 31.3 (d, $^3J_{P\text{-}C}$ = 7.7 Hz, CH₃), 35.2 (d, $^2J_{P\text{-}C}$ = 15.8 Hz, C$_{tBu}$), 57.5 (d, $^2J_{P\text{-}C}$ = 12.2 Hz, CH₂), 122.3 (d, $^4J_{P\text{-}C}$ = 1.4 Hz, C$_{3,\,Ar}$) 123.1 (C$_{Ar}$), 137.1, 149.7, 156.4 (d, $^3J_{P\text{-}C}$ = 1.6 Hz, C$_{2,\,Ar}$), 198.3 (d, $^1J_{P\text{-}C}$ = 56.4 Hz, C=P) ppm.

³¹P{¹H} NMR (162 MHz, CD₂Cl₂): δ = 173.1 ppm.

ESI-TOF-MS (MeCN, 250V): [M+H]⁺= 235.1118 m/z (calc.: 235.1113 m/z), [M+Na]⁺= 257.0939 m/z (calc.: 257.0932 m/z).

Synthesis of 2-((5-(trimethylsilyl)-3H-1,2,3,4-triazaphosphol-3-yl)methyl)pyridine (L5)
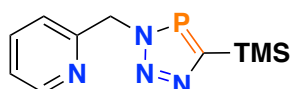
2-(Azidomethyl)pyridine (228 mg, 1.70 mmol, 1 eq.) was added to a solution of **A1** in toluene. After stirring for 1 h at room temperature, the solvent was removed in vacuum giving the title compound as white solid (399 mg, 1.59 mmol, 94%).

¹H NMR (400 MHz, CD$_2$Cl$_2$): δ = 0.35 (s, 9H, CH$_3$), 5.9 (d, $^3J_{\text{P-H}}$ = 6.1 Hz, 2H, CH$_2$), 7.21 (m, 2H, H$_{\text{Ar}}$), 7.66 (td, J = 7.8, 1.8 Hz, 1H, H$_{\text{Ar}}$), 8.53 (m, 1H, H$_{\text{Ar}}$) ppm.

¹³C{¹H} NMR (101 MHz, CD$_2$Cl$_2$): δ = -0.2 (d, $^3J_{\text{P-C}}$ = 3.5, Si(CH$_3$)$_3$), 57.5 (d, $^2J_{\text{P-C}}$ = 11.1 Hz, CH$_2$), 122.9 (d, $^4J_{\text{P-C}}$ = 1.4 Hz, C$_{3,\,\text{Ar}}$), 123.6 (C$_{\text{Ar}}$), 137.6, 150.2, 156.8 (d, $^3J_{\text{P-C}}$ = 1.6 Hz, C$_{2,\,\text{Ar}}$), 185.5 (d, $^1J_{\text{P-C}}$ = 74.7, C=P) ppm.

³¹P{¹H} NMR (162 MHz, CD$_2$Cl$_2$): δ = 216.5 (s) ppm.

Synthesis of 2-((4-(tert-butyl)-1H-1,2,3-triazol-1-yl)methyl)pyridine (*L6*)
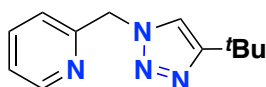
2-(Azidomethyl)-pyridine (268 mg, 2 mmol, 1 eq.) was added to a mixture of sodium ascorbate (20 mg, 0.2 mmol, 0.1 eq.), copper(II) sulfate pentahydrate (20 mg, 0.1 mmol, 0.05 eq.) and 3,3-dimethylbut-1-yl (164 mg, 2 mmol, 1eq.) in 4 mL of a H$_2$O/^{t}BuOH mixture (*v:v* 1:1) and stirred at r.t. overnight. The solvent was removed and the crude product was purified by column chromatography (Alox, DCM; 311 mg, 72%, 1.44 mmol).

¹H NMR (400 MHz, CDCl$_3$): δ = 1.34 (s, 9H, CH$_3$), 5.61 (s, 2H, CH$_2$), 7.16 (m, 1H, H$_{\text{Ar}}$), 7,26 (m, 1H, H$_{\text{Ar}}$), 7,39 (s, 1H, H$_{\text{Triazole}}$), 7.68 (td, ^1J = 7.7, 1.8 Hz, 1H, H$_{\text{Ar}}$), 8.60 (d, ^1J = 4.1 Hz, 1H) ppm.

¹³C{¹H} NMR (101 MHz, CD$_2$Cl$_2$): δ = 30.6 (s, CH$_3$), 31.2 (s, C$_{\text{tBu}}$), 56.0 (s, CH$_2$), 119.7 (s, C$_{\text{Triazole}}$), 122.7 (s, C$_{\text{Ar}}$), 123.7 (s, C$_{\text{Ar}}$), 137.7 (s, C$_{\text{Ar}}$), 150.2 (s, C$_{\text{Ar}}$), 155.7 (S, C$_{\text{Ar}}$), 158.4 (s, C$_{\text{Triazole}}$) ppm.

ESI-TOF-MS(DCM/MeOH, 200V): [M+Na]$^+$= 239.1270 m/z (calc.: 239.1267 m/z).

Synthesis of 2-((4-(trimethylsilyl)-1H-1,2,3-triazol-1-yl)methyl)pyridine (*L7*)
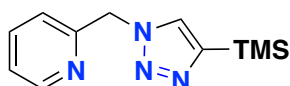
Trimethylsilylacetylene (540 mg, 5.50 mmol, 1.1 eq.) was dissolved in 10 mL of DMF/Water (*v:v* 4:1). Sodium azide (390 mg, 6.00 mmol, 1.2 eq.), sodium carbonate (1.58 g, 14.9 mmol, 2.98 eq.), copper(II) sulfate pentahydrate (245 mg, 1 mmol, 0.2 eq.), sodium ascorbate (991 mg, 5 mmol, 1 eq.) and 2-(bromomethyl)pyridine hydrobromide (1.26 g, 5.00 mmol, 1 eq.) were added. After stirring for 24 h at r.t., the reaction mixture was added to a EDTA/NH$_{3,\text{aq}}$ solution (1M, 30 mL) and the crude product was extracted

with DCM (30 mL), washed with Brine solution (3x 30 mL) and dried with sodium sulfate and filtered. The product was obtained as colourless oil (534 mg, 57%, 4.35 mmol) without further purification by removing the solvent in vacuum.

^{1}H NMR (400 MHz, CD$_2$Cl$_2$): δ = 0.29 (s, 9H, CH$_3$), 5.66 (s, 2H, CH$_2$), 7.17 (d, J = 7.8 Hz, 1H, H$_{Ar}$), 7,25 (ddd, J = 7.6, 4.9, 1.1 Hz, 1H, H$_{Ar}$), 7,68 (td, J = 7.7, 1.8 Hz, 1H, H$_{Ar}$), 7.72 (s, 1H, H$_{Triazole}$), 8.57 (d, J = 4.1 Hz, 1H, H$_{Ar}$) ppm.

^{13}C{^{1}H} NMR (101 MHz, CD$_2$Cl$_2$): δ = -0.9 (s, Si(CH$_3$)$_3$), 55.4 (s, CH$_2$), 122.8 (s, C$_{Ar}$), 123.7 (s, C$_{Ar}$), 130.3 (s, C$_{Triazole}$), 137.7 (s, C$_{Ar}$) 147.1 (s, C$_{Ar}$), 150.2 (s, C$_{Triazole}$), 155.5 (S, C$_{Ar}$) ppm.

*Synthesis of Tris(carbonyl)-2-((5-(tert-butyl)-1H-1,2,3,4-triazaphosphole-1-yl) methyl) pyridine rhenium bromide (**C3**)*
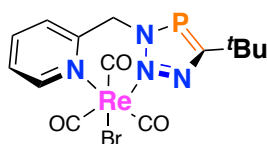
Rhenium(I)-pentacarbonyl bromide (69.4 mg, 0.17 mmol, 1 eq.) and 2-((5-(*tert*-butyl)-3*H*-1,2,3,4-triazaphosphol-3-yl)methyl)pyridine (**1**, 40 mg, 0.17 mmol, 1 eq.) were suspended in dry DCM (0.6 mL) in a Young-NMR-Tube and heated for 8 h at T = 85°C in an oil bath. Recrystallization from hot saturated DCM solution yielded **C3** (72% yield, 0.12 mmol).

^{1}H NMR (400 MHz, CD$_2$Cl$_2$): δ = 1.46 (d, $^{4}J_{P-H}$ = 1.4 Hz, 9H, CH$_3$), 5.74 (dd, $^{3}J_{P-H}$ = 15.4, 6.3 Hz, 1H, CH$_2$), 6.20 (dd, $^{3}J_{P-H}$ = 15.3, 4.5 Hz, 1H, CH$_2$), 7.48 (ddd, J = 7.4, 5.7, 1.4 Hz, 1H, H$_{Ar}$), 7.64 (d, J = 7.6 Hz, 1H, H$_{Ar}$), 7.99 (td, J = 7.7, 1.6 Hz, 1H, H$_{Ar}$), 9.22 (dd, J = 5.5, 1.2 Hz, 1H, H$_{Ar}$) ppm.

^{13}C{^{1}H} NMR (101 MHz, CD$_2$Cl$_2$): δ = 31.4 (d, $^{3}J_{P-C}$ = 7.6 Hz, CH$_3$), 36.4 (d, $^{2}J_{P-C}$ = 14.4 Hz, C$_{tert\text{-}butyl}$), 58.4 (d, $^{2}J_{P-C}$ = 15.6 Hz, CH$_2$), 126.4 (d, $^{4}J_{P-C}$ = 58.8 Hz, C$_{3, Ar}$), 140.6 (s, C$_{Ar}$), 153.8 (d, $^{3}J_{P-C}$ = 3.4 Hz, C$_{2, Ar}$), 159.0 (s, C$_{Ar}$), 198.8 (d, $^{1}J_{P-C}$ = 60.9 Hz, C$_{C=P}$) ppm.

^{31}P{^{1}H} NMR (162 MHz, CD$_2$Cl$_2$): δ = 191.3 (s) ppm.

ESI-TOF-MS(MeCN, 250V): [M-Br]$^{+}$= 505.0424 m/z (calc.: 505.0439 m/z), 662.9219 m/z (calc.: 662.9260) m/z.

Synthesis of Tris(carbonyl)-2-((5-(trimethylsilyl)-1H-1,2,3,4-triazaphosphole-1-yl)methyl)pyridine rhenium bromide (C4)
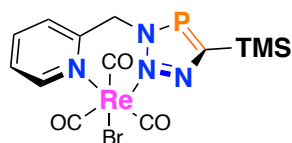
Rhenium(I)-pentacarbonyl bromide (69.4 mg, 0.17 mmol, 1 eq.) and 2-((5-(trimethylsilyl)-3*H*-1,2,3,4-triazaphosphol-3-yl)-methyl)pyridine (**2**, 42.8 mg, 0.17 mmol, 1 eq.) were suspended in dry DCM (0.6 mL) in a Young-NMR-Tube and heated for 8 h at T = 85°C in an oil bath. Recrystallization from hot saturated DCM solution yielded the **C4** (43% yield, 0.07 mmol).

^{1}H NMR (400 MHz, CD$_2$Cl$_2$): δ = 0.42 (s, 9H, CH$_3$), 5.81 (dd, $^3J_{P\text{-}H}$ = 15.4, 5.9 Hz, 1H, CH$_2$), 6.39 (dd, $^3J_{P\text{-}H}$ = 15.3, 3.8 Hz, 1H, CH$_2$), 7.47 (m, 1H, H$_{Ar}$), 7.70 (dd, J = 7.7, 0.6 Hz, 1H, H$_{Ar}$), 8.00 (td, J = 7.7, 1.6 Hz, 1H, H$_{Ar}$), 9.22 (ddd, J = 5.7, 1.6, 0.6 Hz, 1H, H$_{Ar}$) ppm.

^{13}C{^{1}H} NMR (101 MHz, CD$_2$Cl$_2$): δ = -0.6 (d, $^3J_{P\text{-}C}$ = 3.4 Hz, Si(CH$_3$)$_3$), 58.1 (d, $^2J_{P\text{-}C}$ = 13.9 Hz, CH$_2$), 126.3 (s, C$_{Ar}$), 126.7 (s, C$_{Ar}$) 140.6 (s, C$_{Ar}$), 153.9 (d, $^3J_{P\text{-}C}$ = 3.2 Hz, C$_{2,\,Ar}$), 158.9 (s, C$_{Ar}$), 187.4 (d, $^1J_{P\text{-}C}$ = 80.2 Hz, C$_{C=P}$) ppm.

^{31}P{^{1}H} NMR (162 MHz, CD$_2$Cl$_2$): δ = 231.1 (s) ppm.

Synthesis of Tris(carbonyl)-2-((4-(tert-butyl)-1H-1,2,3-triazol-1-yl)methyl) pyridine rhenium bromide (C5)
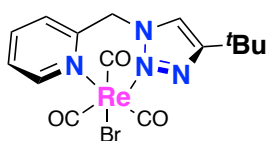
Rhenium(I)-pentacarbonyl bromide (69.4 mg, 0.17 mmol, 1 eq.) and 2-((5-(*tert*-butyl)-3*H*-1,2,3-triazol-3-yl)methyl)pyridine (**3**, 36.8 mg, 0.17 mmol, 1 eq.) were suspended in dry DCM (0.6 mL) in a Young-NMR-Tube and heated for 8 h at T = 85°C in an oil bath. Recrystallization from hot saturated DCM solution yielded the **C5** (89% yield, 0.15 mml).

^{1}H NMR (400 MHz, CD$_2$Cl$_2$): δ = 1.37 (s, 9H, CH$_3$), 5.58 (d, J = 15.5 Hz, 1H, CH$_2$), 6.11 (d, J = 15.5 Hz, 1H, CH$_2$), 7.49 (ddd, J = 7.4, 5.7, 1.5 Hz, 1H, H$_{Ar}$), 7.58 (m, 1H, H$_{Ar}$), 7.64 (s, 1H, H$_{Triazole}$), 7.98 (td, J = 7.7, 1.7 Hz, 1H, H$_{Ar}$), 9.25 (ddd, J = 5.7, 1.6, 0.7 Hz, 1H, H$_{Ar}$) ppm.

¹³C{¹H} NMR (101 MHz, CD$_2$Cl$_2$): δ = 30.2 (s, CH$_3$), 31.7 (s, C$_{tert\text{-butyl}}$), 56.6 (s, CH$_2$), 123.2 (s, C$_{Triazole}$), 126.3 (s, C$_{Ar}$), 126.7 (s, C$_{Ar}$), 140.5 (s, C$_{Ar}$), 152.7 (s, C$_{Ar}$), 159.1 (s, C$_{Ar}$), 159.99 (s, C$_{Triazole}$) ppm.

ESI-TOF-MS (DCM/MeOH, 200V): [M+Na]$^+$= 588.9834 m/z (calc.: 588.9837 m/z).

*Synthesis of Tris(carbonyl)-2-((5-(trimethylsilyl)-1H-1,2,3-triazole-1-yl) methyl)pyridine rhenium bromide (**C6**)*
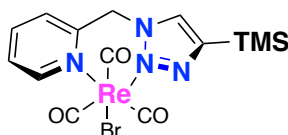
Rhenium(I)-pentacarbonyl bromide (69.4 mg, 0.17 mmol, 1 eq.) and 2-((5-(trimethylsilyl)-3*H*-1,2,3-triazol-3-yl)methyl)pyridine (**4**, 39.5 mg, 0.17 mmol, 1 eq.) were suspended in dry DCM (0.6 mL) in a Young-NMR-Tube and heated for 8 h at T = 85°C in an oil bath. Recrystallization from hot saturated DCM solution yielded the **C5** (57% yield, 0.10 mml).

¹H NMR (400 MHz, CD$_2$Cl$_2$): δ = 0.35 (s, 9H, CH$_3$), 5.64 (d, *J* = 15.5 Hz, 1H, CH$_2$), 6.18 (d, *J* = 15.5 Hz, 1H, CH$_2$), 7.48 (ddd, *J* = 7.5, 5.7, 1.4 Hz, 1H, H$_{Ar}$), 7.90 (s, 1H, H$_{Triazole}$), 7.62 (d, *J* = 7.6 Hz, 1H, H$_{Ar}$), 7.98 (td, *J* = 7.7, 1.6 Hz, 1H, H$_{Ar}$), 9.26 (m, 1H, H$_{Ar}$) ppm.

¹³C{¹H} NMR (101 MHz, CD$_2$Cl$_2$): δ = -1.2 (s, Si(CH$_3$)$_3$), 56.3 (s, CH$_2$), 126.4 (s, C$_{Ar}$), 126.7, 132.7 (s, C$_{Ar}$), 140.6 (s, C$_{Ar}$), 150.4 (s, C$_{Ar}$), 152.8 (s, C$_{Ar}$), 159.1 (s, C$_{Triazole}$) ppm.

*Synthesis of copper (I) 2-((5-(tert-butyl)-3H-1,2,3,4-triazaphosphol-3-yl)methyl)pyridine bromide (dimer) (**C7**)*
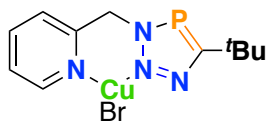
In a J. R. Young-NMR tube 37.8 mg (0.12 mmol, 1 eq.) copper bromide dimethyl sulfide and 28.1 mg (0.12 mmol, 1 eq.) **L7** were suspended in 0.5 mL dry CD$_2$Cl$_2$. The chemical shift was obtained after 24 h aggregation time.

³¹P{¹H} NMR (162 MHz, CD$_2$Cl$_2$): δ = 159.4 (s) ppm.
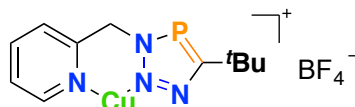
In a J. R. Young-NMR tube 37.7 mg (0.12 mmol, 1 eq.) tetrakis(acetonitrile) copper(I) tetrafluoroborate dimethyl sulfide and 28.1 mg (0.12 mmol, 1 eq.) **L7** were suspended in 0.5 mL dry CD_2Cl_2. The chemical shift was obtained after 24 h aggregation time.

$^{31}P\{^1H\}$ NMR (162 MHz, CD_2Cl_2): δ = 180.7 (s) ppm.
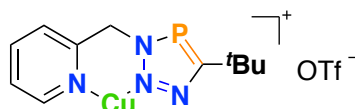
In a J. R. Young-NMR tube 30.2 mg (0.12 mmol, 1 eq.) copper(I) triflate benzene complex ([(CuOTf)$_2$•C$_6$H$_6$]) and 28.1 mg (0.12 mmol, 1 eq.) **L7** were suspended in 0.5 mL dry CD_2Cl_2. The chemical shift was obtained after 24 h aggregation time.

$^{31}P\{^1H\}$ NMR (162 MHz, CD_2Cl_2): δ = 182.7 (s) ppm.

In a J. R. Young-NMR tube 37.8 mg (0.12 mmol, 1 eq.) copper(I) bromide dimethyl sulfide and 30 mg (0.12 mmol, 1 eq.) **L7** were suspended in 0.5 mL dry CD_2Cl_2. The chemical shift was obtained after 24 h aggregation time.

$^{31}P\{^1H\}$ NMR (162 MHz, CD_2Cl_2): δ = 193.8 (s) ppm.

Synthesis of 2-azido-1-(p-tolyl)ethan-1-one (16)
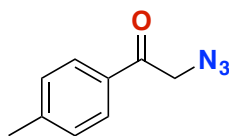
In a 100 mL flask 5.04 g (23.65 mmol, 1eq.) **15** was dissolved in 60 mL DMSO and slowly 3.06 g (47.06 mmol, 2 eq.) sodium azide were added. The reaction mixture was stirred for 1 h at r.t., than diluted with 30 mL water and extracted with toluene (3x 20 mL). The combined organic phases were washed with Brine-solution, dried over Na_2SO_4 and filtered. The solvent was removed in vacuum, yielding 3.89 g of a brown solid (92%, 21.76 mmol).

^{1}H NMR (400 MHz, CDCl$_3$): δ = 2.42 (s, 3H, Me), 4.53 (s, 2H, CH$_2$N), 7,28 (dd, $^3J_{H\text{-}H}$ = 8.0, 0.6 Hz, 2H, Ar-H), 7.77-7.82 (m, 2H, Ar-H) ppm.

^{13}C{^{1}H} NMR (101 MHz, CDCl$_3$): δ = 21.9 (C-Me), 54.8 (C-N$_3$), 128.0 (Ar-C), 129.8 (Ar-C), 132.1 (Ar-C), 145.3 (Ar-C), 192.8 (C=O) ppm.

FT-IR (ATR, neat): ṽ = 2990 (N$_3$), 1690 (C=O), 1610, 1270, 1200, 1160, 1000, 900, 790 cm^{-1}.

EI-MS (80 eV) m/z: 147.0687 [M-N$_2$]$^{+\bullet}$ (calc.: 147.0684).

Spectroscopic data are consistent with literature data.[69]

Synthesis of 2-azido-1-(p-tolyl)ethan-1-ol (17)
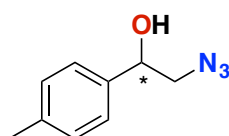
In a 250 mL Schlenk-flask 3.02 g (17.3 mmol, 1 eq.) **16** were dissolved in 55 mL dry EtOH and treated at T = 0 °C with 1.53 g (40.4 mmol, 2 eq.) NaBH$_4$. The reaction mixture was allowed to warm up over night and the reaction progress was monitored by TLC (SiO$_2$, DCM R$_f$(**16**) = 0.875; R$_f$(**17**) = 0.75). Afterwards, 35 mL (1 M) hydrochloric acid solution was added. The crude product was extracted by Et$_2$O (3x 50 mL) and the combined organic phases were dried over MgSO$_4$, filtered and the solvent removed in vacuum and purified by column chromatography (SiO$_2$, DCM). The solvent was removed in vacuum, yielding 2.69 g (88%, 15,22 mmol) of a colourless oil.

¹H NMR (400 MHz, C$_6$D$_6$): δ = 1.78 (d, $^3J_{H-H}$ = 3.5 Hz, 1H,), 2.09 (s, 3H, CH$_3$), 2.80 (dd, 1H, $^3J_{H-H}$=12.6, 3.6 Hz, CH$_2$N), 2.96 (dd, 1H, $^3J_{H-H}$ = 12.6, 8,4 Hz), 4.32-4.37 (m, 1H, CHO), 6.92 – 7.01 (m, 4H, Ar-H) ppm.

¹³C{¹H} NMR (101 MHz, C$_6$D$_6$): δ = 20.8 (C-Me), 57.8 (C-N$_3$), 73.3 (C-OH), 125.9 (Ar-C), 129.0 (Ar-C), 137.4 (Ar-C), 138.3 (Ar-C) ppm.

FT-IR (ATR, neat): ṽ = 3407(OH), 2927, 2090 (N$_3$), 1515, 1433, 814 cm^{-1}.

ESI-TOF-MS (m/z): [M+Na]+ = 200.0801 found (calc.: 200.0794), [M$_2$+Na]$^+$ = 377.1674 found (calc. 377.1695).

Spectroscopic data are consistent with literature data.[6,64]

*Synthesis of (2-azido-1-(p-tolyl)ethoxy)trimethylsilane (**18**)*
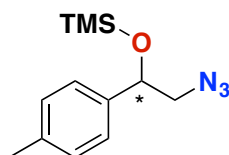
Compound **17** was dissolved in penante (65 mL) and 1,4-diazabicyclo[2.2.2]octane (1.47 g, 13 mmol, 1.3 eq.) were added under stirring. Subsequently, trimethylsilylchloride (1.73 g, 16 mmol, 1.6 eq.) was added and the reaction mixture was stirred overnight at room temperature. Diluted hydrochloric acid (1 N, 35 mL) was added and the mixture was neutralized with NaHCO$_3$. The organic phase was extracted three times with diethylether and the collected solutions were washed with water, brine and dried over MgSO$_4$ and filtered. The solvent was removed in vacuum, yielding a yellow oil (2.1 g, 84%, 8.4 mmol).

¹H NMR (400 MHz, CDCl$_3$): δ = 0.03 - 0.11 (m, 9H, Si(CH$_3$)$_3$), 2.34 (s, 3H, CH3), 3.05 - 3.12 (m, 1H, CH$_2$N), 3.32 - 3.41 (m, 1H, CH$_2$N), 4.81 (dd, 1H, *J* = 8.5; 3.0 Hz, CHO(Si(CH$_3$)$_3$), 7.11 - 7.23 (m, 4H, Ar-H) ppm.

¹³C{¹H} NMR (101 MHz, CDCl$_3$): δ = 0.00 (Si(CH$_3$)$_3$), 21.3 (CH$_3$), 58.7 (C-N^3), 74.8 (C-OSi(CH3)3), 126.0 (Ar), 129.2 (Ar), 137.7 (Ar), 138.6 (Ar) ppm.

FT-IR (ATR, neat): ṽ = 2958 (N$_3$); 2095 (N$_3$); 1509; 1436; 1251; 812 cm^{-1}.

EI-MS (80 eV) m/z: 221.1 [M-N2]+• (calc.: 221.1230).
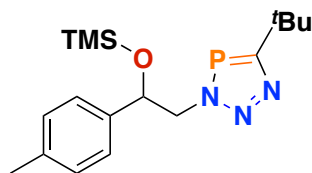
Azide **18** (0.895 g, 3.59 mmol, 1.0 eq.) was dissolved in toluene and an excess of **A2** in toluene was added. Stirring was continued at room temperature for 5 h. Subsequently, the solvent and the residual phosphaalkyne were removed in vacuum and the crude product was recrystallized from cooling down a saturated pentane solution. The product could be obtained as white crystals (1.0 g, 2.9 mmol, 87%).

¹H-NMR (400 MHz, C_6D_6): δ = -0.13 - -0.16 (m, 9H, $Si(CH_3)_3$), 1.50 (d, J = 1.4 Hz, 9H, ^tBu), 2.07 (s, 3H, CH_3), 4.28 - 4.39 (m, 1H, CH_2N), 4.46 - 4.55 (m, 1H, CH_2N), 5.04 (dd, 1H, J = 9.1; 3.4 Hz, 1H, $CHO(Si(CH_3)_3)$), 6.94 (d, J = 7.8 Hz, 2H, Ar-H), 7.10 (d, J = 8.1 Hz, 2H, Ar-H) ppm.

¹³C{¹H} NMR (101 MHz, C_6D_6): δ = 0.3 ($Si(CH_3)_3$), 21.1 (CH_3), 31.8 (^tBu), 35.3 (^tBu), 60.1 ($C-N_3$), 75.2 ($C-OSi(CH_3)_3$), 126.1 (Ar), 129.5 (Ar), 137.7 (Ar), 138.8 (C=P) ppm.

³¹P{¹H} NMR (162 MHz, C_6D_6): δ = 174.0 ppm.

FT-IR (ATR, neat): ṽ = 2956; 1252; 1088; 939; 841 cm^{-1}.

EA(NCH): C: 57.23%, N: 11.72%, H: 8.089; calc.: C: 57.29%, N: 11.88%, H: 7.81%.
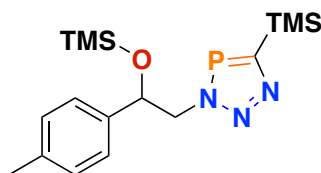
Prior to use, the concentration of **A2** in toluene was determined by means of ³¹P{¹H} NMR spectroscopy (105.7 mmol/L). This solution (25 mL, 1.0 eq.) was added to azide **10** (0.344 g, 1.38 mmol, 1.0 eq.) and stirring was continued for 1 h at room temperature, while the course of the reaction was monitored by means of ³¹P{¹H} NMR spectroscopy. The solvent and all volatiles were removed in vacuum and the product could be obtained as a white solid (479.8 mg, 1,31 mmol, 97%).

¹H NMR (400 MHz, CD$_2$Cl$_2$): δ = -0.18 - -0.28 (m, 9H, Si(CH$_3$)$_3$), 0.35 - 0.41 (m, 9H, O-Si(CH$_3$)$_3$), 2.32 (s, 3H, CH$_3$), 4.56 - 4.64 (m, 1H, CH$_2$N), 4.72 - 4.81 (m, 1H, CH$_2$N), 4.97 (dd, 1H, *J* = 9.0; 3.4 Hz, 1H, CHO(Si(CH$_3$)$_3$), 7.15 (d, *J* = 7.8 Hz, 2H, Ar-H), 7.25 (d, *J* = 7.9 Hz, 2H, Ar-H) ppm.

¹³C{¹H} NMR (101 MHz, CD$_2$Cl$_2$): δ = 0.8 (O-Si(CH$_3$)$_3$), 0.80 (Si(CH$_3$)$_3$), 20.9 (CH$_3$), 59.7 (C-N3), 74.6 (C-OSi(CH$_3$)$_3$), 126.0 (Ar), 129.1 (Ar), 137.9 (Ar), 138.3 (C=P) ppm.

³¹P{¹H} NMR (162 MHz C$_6$D$_6$): δ = 218.3 ppm.

FT-IR (ATR, neat): ṽ = 2962; 1259; 1091; 1016; 943 cm^{-1}.

Bibliography of Chapter 3.1

(1)   Mezailles, N.; Le Floch, P. *Curr. Org. Chem.* **2006**, *10* (1), 3.

(2)   Mathey, F. *Coord. Chem. Rev.* **1994**, *137*, 1.

(3)   Le Floch, P.; Mathey, F. *Coord. Chem. Rev.* **1998**, *178-180*, 771.

(4)   Müller, C.; Vogt, D. *Dalton Trans.* **2007**, 5505.

(5)   Müller, C.; Broeckx, L. E. E.; de Krom, I.; Weemers, J. J. M. *Eur. J. Inorg. Chem.* **2013**, 187.

(6)   Mansell, S. M.; Green, M.; Kilby, R. J.; Murray, M.; Russell, C. A. *C. R. Chim.* **2010**, *13* (8-9), 1073.

(7)   King, R. B.; Sadanani, N. D. *Synth. React. Inorg. Met. Chem.* **1985**, *15* (2), 149.

(8)   Niecke, P. D. E.; Westermann, H. *Synthesis* **1988**, *1988* (4), 330.

(9)   Rigo, M.; Sklorz, J. A. W.; Hatje, N.; Noack, F.; Weber, M.; Wiecko, J.; Müller, C. *Dalton Trans.* **2015**, *3*, 2218.

(10)   Becker, G. *Z. Anorg. Allg. Chem.* **1977**, *430* (1), 66.

(11)   Becker, G.; Gresser, G.; Uhl, W. *Z. Naturforsch. B* **1981**, *36* (1), 16.

(12)   Regitz, M.; Hees, U.; Rösch, W. *Chem. Ber.* **1987**, *120*, 1645.

(13)   Pardin, C.; Roy, I.; Lubell, W. D.; Keillor, J. W. *Chem. Biol. Drug Des.* **2008**, *72* (3), 189.

(14)   Luo, Y.; Kerr, J. *CRC Handb. Chem. Phys.* **2007**, 65.

(15)   Hatanaka, Y.; Hiyama, T. *J. Org. Chem.* **1988**, *53* (4), 918.

(16)   Nishihara, Y.; Inoue, E.; Noyori, S.; Ogawa, D.; Okada, Y.; Iwasaki, M.; Takagi, K. *Tetrahedron* **2012**, *68* (24), 4869.

(17)   Denmark, S. E.; Wehrli, D.; Choi, J. Y. *Org. Lett.* **2000**, *2* (16), 2491.

(18)   Huang, J.; Macdonald, S. J. F.; Harrity, J. P. a. *Chem. Commun.* **2009**, No. 4, 436.

(19)   Habicht, M. „ Neue Syntheserouten zu funktionalisierten Phosphabenzolen ", Freie Universität Berlin: Berlin, 2013.

(20)   Le Floch, P.; Carmichael, D.; Ricard, L.; Mathey, F. *J. Am. Chem. Soc.* **1993**, *115* (23), 10665.

(21)   Aluri, B. R.; Niaz, B.; Kindermann, M. K.; Jones, P. G.; Heinicke, J. W. *Dalton Trans.* **2011**, *40* (1), 211.

(22)   Niaz, B.; Iftikhar, F.; Kindermann, M. K.; Jones, P. G.; Heinicke, J. W. *Eur. J. Inorg. Chem.* **2013**, 4220.

(23)   Ghalib, M.; Jones, P. G.; Palm, G. J.; Heinicke, J. W. *RSC Adv.* **2013**, *3* (39), 17726.

(24)   Ghalib, M.; Könczöl, L.; Nyulászi, L.; Jones, P. G.; Palm, G. J.; Heinicke, J. W. *Dalton Trans.* **2014**, *43* (1), 51.

(25)   Wang, J.; Mei, J.; Zhao, E.; Song, Z.; Qin, A.; Sun, J. Z.; Tang, B. Z. *Macromolecules* **2012**, *45*, 7692.

(26)   Smith, P. A. S.; Rowe, C. D.; Bruner, L. B. *J. Org. Chem.* **1969**, *34* (11), 3430.

(27)   Anderson, C. B.; Elliott, A. B. S.; McAdam, C. J.; Gordon, K. C.; Crowley, J. D. *Organometallics* **2013**, *32* (3), 788.

(28)   Niecke, E.; Flick, W. *Angew. Chem.* **1973**, *85* (13), 586.

(29)   Niecke, E.; Flick, W. *Angew. Chem. Int. Ed.* **1973**, *12* (7), 585.

(30)   Zeiß, W.; Feldt, C.; Weis, J.; Gudrun, D. *Chem. Ber.* **1987**, *111*, 1180.

(31)   Siddiqui, M. M.; Mague, J. T.; Balakrishna, M. S. *J. Organomet. Chem.* **2015**, *794*, 81.

(32)   Siddiqui, M. M.; Mague, J. T.; Balakrishna, M. S. *Inorg. Chem.* **2015**, *54* (13), 6063.

(33)   Bendle, M.; Kuzora, R.; Manners, I.; Rupar, P.; Schulz, A.; Villinger, A. *Eur. J. Inorg. Chem.* **2014**, 1735.

(34)   Beweries, T.; Kuzora, R.; Rosenthal, U.; Schulz, A.; Villinger, A. *Angew. Chem.* **2011**, *123* (38), 9136.

(35)   Kerth, J.; Werz, U.; Maas, G. *Tetrahedron* **2000**, *56*, 35.

(36)   Heterocycles, F. N.; Silva, G.; Bozzelli, J. W. **2008**, 1343.

(37)   Nakamura, I.; Nemoto, T.; Shiraiwa, N.; Terada, M. *Org. Lett.* **2009**, *11* (5), 1055.

(38)   Medina, F.; Besnard, C.; Lacour, J. *Org. Lett.* **2014**, *16* (12), 3232.

(39)   Aggarwal, V. K.; Sheldon, C. G.; Macdonald, G. J.; Martin, W. P. *J. Am. Chem. Soc.* **2002**, *124* (35), 10300.

(40)   Battula, S.; Kumar, A.; Gupta, A. P.; Ahmed, Q. N. *Org. Lett.* **2015**, *17* (22), 5562.

(41)   Selander, N.; Worrell, B. T.; Fokin, V. V. *Angew. Chem. Int. Ed.* **2012**, *51* (52), 13054.

(42)   Piao, Y.; Meany, B.; Powell, L. R.; Valley, N.; Kwon, H.; Schatz, G. C.; Wang, Y. *Nat. Chem.* **2013**, *5* (10), 840.

(43)   Sklorz, J. A. W.; Hoof, S.; Sommer, M. G.; Weißer, F.; Weber, M.; Wiecko, J.; Sarkar, B.; Müller, C. *Organometallics* **2014**, *33* (2), 511.

(44)   Alcaraz, J. M.; Breque, A.; Mathey, F. *Tetrahedron Lett.* **1982**, *23* (15), 1565.

(45)   De Krom, I.; Pidko, E. A.; Lutz, M.; Müller, C. *Chem. Eur. J.* **2013**, *19* (23), 7523.

(46)   Loibl, A.; de Krom, I.; Pidko, E. a; Weber, M.; Wiecko, J.; Müller, C. *Chem. Commun.* **2014**, *50* (64), 8842.

(47)   Michaels, H. A.; Zhu, L. *Chem. Asian J.* **2011**, *6* (10), 2825.

(48)   Strohmeier, W.; Müller, F. J. *Chem. Ber.* **1967**, *100* (9), 2812.

(49)   Tolman, C. A. *Chem. Rev.* **1977**, *77* (3), 313.

(50)   Becke, A. D. *J. Chem. Phys.* **1993**, *98* (7), 5648.

(51)   Rozhenko, A. B.; Schoeller, W. W.; Povolotskii, M. I. *Magn. Reson. Chem.* **1999**, *563*, 551.

(52)   Le Floch, P. *Coord. Chem. Rev.* **2006**, *250* (5-6), 627.

(53)   Mathey, F. *Angew. Chem. Int. Ed.* **2003**, *42* (14), 1578.

(54)   Frison, G.; Sevin, A.; Avarvari, N.; Mathey, F.; Le Floch, P. *J. Org. Chem.* **1999**, *64* (15), 5524.

(55)   Nyulászi, L.; Csonka, G.; Réffy, J.; Veszprhmi, T.; Heinicke, J. W. *J. Organomet. Chem.* **1989**, *373*, 49.

(56)   Roesch, P.; Nitsch, J.; Lutz, M.; Wiecko, J.; Steffen, A.; Müller, C. *Inorg. Chem.* **2014**, *53* (18), 9855.

(57)   Mézailles, N.; Le, P.; Waschbijsch, K.; Ricard, L.; Mathey, F.; Kubiak, C. P. *J. Organomet. Chem.* **1997**, *541*, 277.

(58)   Shiotsuka, M.; Tanamachi, T.; Urakawa, T.; Munakata, M.; Matsuda, Y. *J. Supramol. Chem.* **2002**, *2* (1-3), 211.

(59)   Mao, Y.; Lim, K. M. H.; Li, Y.; Ganguly, R.; Mathey, F. *Organometallics* **2013**, *32* (12), 3562.

(60)   Sklorz, J. A. W.; Schnucklake, M.; Kirste, M.; Weber, M.; Wiecko, J.; Müller, C. *Phosphorus. Sulfur. Silicon Relat. Elem.* **2016**, *191* (3), 558.

(61)   Concepcion, J. J.; Tsai, M.-K.; Muckerman, J. T.; Meyer, T. J. *J. Am. Chem. Soc.* **2010**, *132* (14), 1545.

(62)   In *Topics in Organometallic Chemistry*; Lees, A. J., Ed.; 2010; Vol. 29.

(63)   Takeda, H.; Ishitani, O. *Coord. Chem. Rev.* **2010**, *254* (3-4), 346.

(64)   Reddy, M. S.; Narender, M.; Rao, K. R. *Tetrahedron* **2007**, *63* (2), 331.

(65)   Averre, C. E.; Coles, M. P.; Crossley, I. R.; Day, I. J. *Dalton Trans.* **2012**, *41* (1), 278.

(66)   Mack, A.; Pierron, E.; Allspach, T.; Bergsträßer, U.; Regitz, M. *Synthesis* **1998**, *1998* (1), 1305.

(67)   Hobuß, D.; Baro, A.; Axenov, K. V.; Laschat, S.; Frey, W. *Eur. J. Inorg. Chem.* **2011**, 384.

(68)   Alvarez, S. G.; T., A. M. *Synthesis* **1997**, *1997* (4), 413.

(69)   Narender, T.; Rajendar, K.; Sarkar, S.; Singh, V. K.; Chaturvedi, U.; Khanna, A. K.; Bhatia, G. *Bioorganic Med. Chem. Lett.* **2011**, *21* (21), 6393.

3.2 Conjugated 3*H*-1,2,3,4-Triazaphospholes and 1*H*-1,2,3-Triazoles

3.2.1 Photophysical Properties of Conjugated 3*H*-1,2,3,4-Triazaphospholes and their Phosphorus-Lacking Analogues[1]

Inspired by the interesting results presented in the previous chapter, the question emerges to which extent the coordination properties, such as coordination mode and π-donating or accepting abilities, change by using a chelate, in which the biding sides are connected by means of a conjugated system. π-Conjugated systems are fundamental additives in organic light-emitting diodes (OLEDs) and different approaches for the molecular design have been developed.[2–9] Nitrogen-based ligand systems, such as (poly-) pyridines,[10] cyclometalated 2-phenyl pyridines as well as pyridine azaole derivatives, including inverse and regular triazoles[10–12] with coordinating different metal centres, e.g. **Ru**(II),[13,14] **Rh**(III), **Re**(I)(CO)₃,[7,11,15] **Os**(II)[16], **Ir**(III)[10,12] and **Pt**(II),[11,17] including homobimetallic and heterobimetallic coordination modes,[18,19] and more [16,20–23] have been described in detail.

In this context, phosphorus compounds have proven to be a suitable compound class to contribute to this field of chemistry,[24,25] due to their unique electronic properties (see Chapter 1). Thereby, different colours of the emitted light (e.g. a green light emitter, Figure 36, **A**) have been reported and even examples of white organic light-emitting devices (WOLEDs, **B**) are known.[26,27]
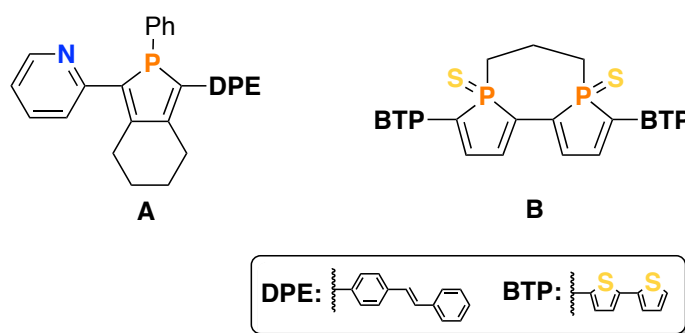
Figure 36: Examples of phosphorus containing dopants in OLEDS.

Since this field of chemistry is quite young, only a few metal complexes including triaryl-phospinine-based complexes were reported by Müller *et al.*. In these compounds, the low-coordinate P(III)-ligands coordinate to e.g. **Ir**(III) **C**, **Cu**(I) **D** and **Ru**(II) **E** metal centres and their photophysical properties were investigated (Figure 37).[28–30]
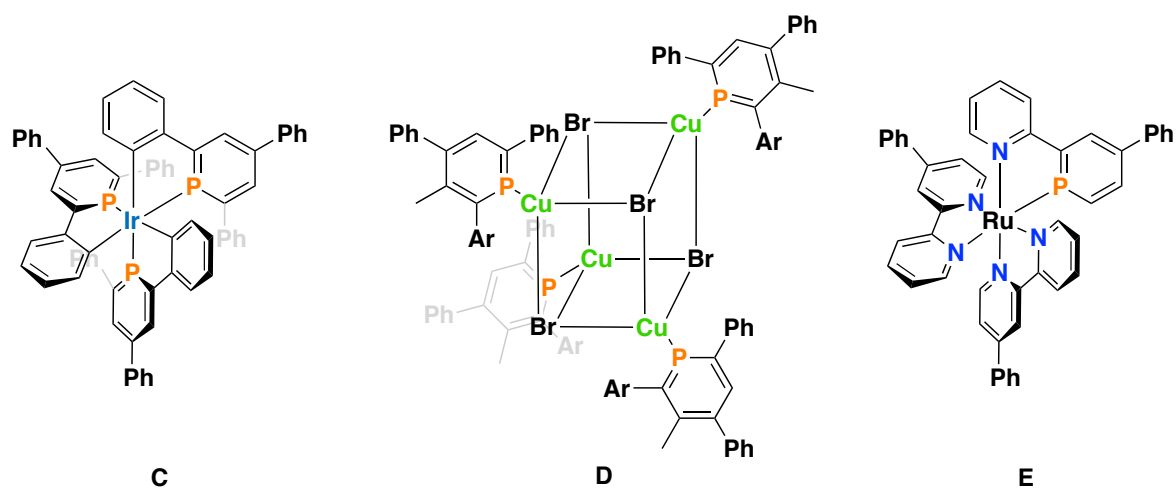
Figure 37: Aryl phosphinine-based metal complexes with luminescent properties. Ar: 2,3-dimethylbenzene.

Synthesis and Characterisation of conjugated 3H-1,2,3,4-Triazaphospholes and 1H-1,2,3-Triazoles

The photophysical properties of 3*H*-1,2,3,4-triazaphospholes have not been investigated to date. Several low-substituted biaryls were designed for the investigation and compared to a selection of triazoles. Using the protocol from Liang *et al.*[31] for the conversion of aryl bromides **20-23**, the azides **24-27** were obtained in good yields, and transformed into the corresponding triazaphospholes **28-33** (Scheme 47). The 5-TMS substituted compounds were synthesised by Santina Hoof during her Master Thesis.

In contrast to azides **24-26**, the 2-pyridyl azide **27** is found in an equilibrium (Scheme 47, box), which is strongly shifted to the tetrazole side **27b**[32] but can be forced by higher temperatures towards the open azide form.[33] Cycloaddition reactions based upon tetrazoles and yielding inverse 1*H*-1,2,3-triazoles are not straightforward and have only been described by the group of Gevorgyan,[34] who showed that the CuAAC proceeds under harsh conditions. Analogous to this procedure, the reactions with the phosphaalkynes were carried out in toluene at T = 120 °C, albeit without the addition of a catalyst. Besides the signal of the main product at δ = 167.5 ppm, the ^{31}P{^{1}H} NMR spectrum revealed the formation of several by-products, which could not be separated from the product.
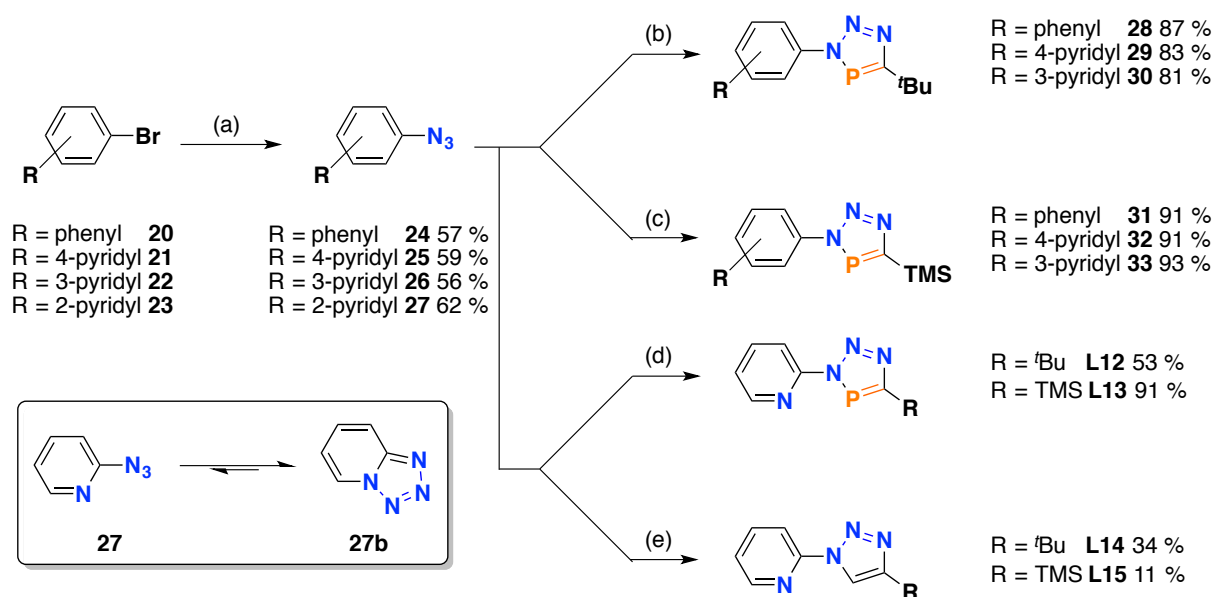
Scheme 47: (Top) Synthesis of aryl azides **24-27**. Reaction conditions (a) NaN$_3$ (2 eq.), CuI (0.1 eq.), DMEDA (0.15 eq), Na ascorbate (0.05 eq), EtOH/H$_2$O 7:3 (*v:v*), reflux, Ar. **(Box)** Azid-tetrazole equilibrium. **(Bottom)** Reaction conditions (a): 1.5 eq. **A1**, toluene, 1 h, r.t. (b): 1.5 eq. **A2**, toluene, 1 h r.t. (d): 1.5 eq. **A1** or **A2**, toluene, 7d, T = 60 °C, Ar; (e)1.1 eq. TMS/^{t}Bu-CCH, 0.1 eq. (CuOTf)$_2$•C$_6$H$_6$, 4 h, T = 140 °C, μW.

Therefore, the reaction temperature was successively reduced until a selective formation of the product could be observed at T = 60 °C. The compounds **24-26** could be crystallised by cooling down a hot saturated pentane solution. In the molecular structure, the aromatic sub-units of compounds **28** (Figure 38) and **30** (Figure 39) are strongly twisted along the N^2-N^1-C^2-C^3 torsion angle, with 46.5° and 37.7°, respectively (Table 7).
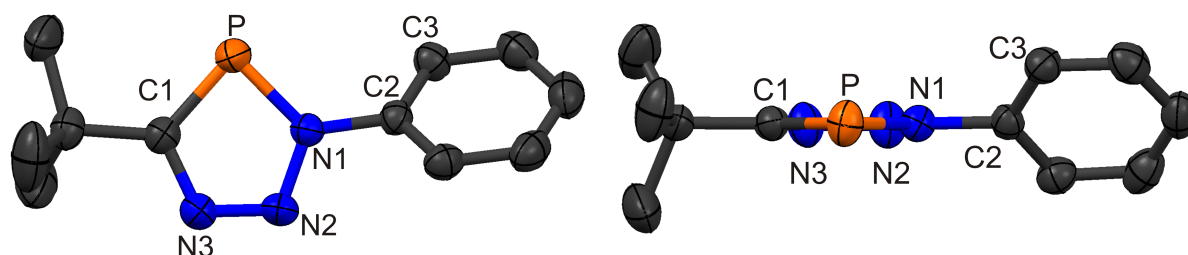
Figure 38: Molecular structure in the crystal of compound **28 (left)** side views **(right)**. Hydrogen atoms are omitted for clarity. Displacement ellipsoids are shown at 50% probability level. Selected bond lengths (Å) and angles (°) are available in **Table 7**and **Table 8**.
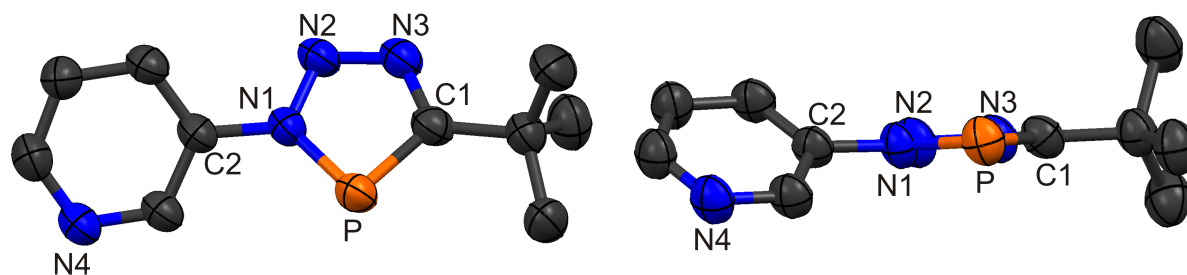
Figure 39: Molecular structure in the crystal of compound **30 (left)** side views **(right)**. Hydrogen atoms are omitted for clarity. Displacement ellipsoids are shown at 50% probability level. Selected bond lengths (Å) and angles (°) are available in **Table 7** and **Table 8**.

In contrast, compounds **29** (Figure 40) and **L12** (Figure 41) are coplanar (Table 7). Besides the phosphorus containing heterocycles, the ligand **L14** was also crystallised and analysed by means of X-ray diffraction. The obtained solid-state structure proved slightly twisted with -19.4° (see Figure 42, page 133). Single crystals suitable for X-ray diffraction measurements could not be obtained from the TMS substituted molecules, as they showed high light sensitivity and/or instability of the triazaphospholes.
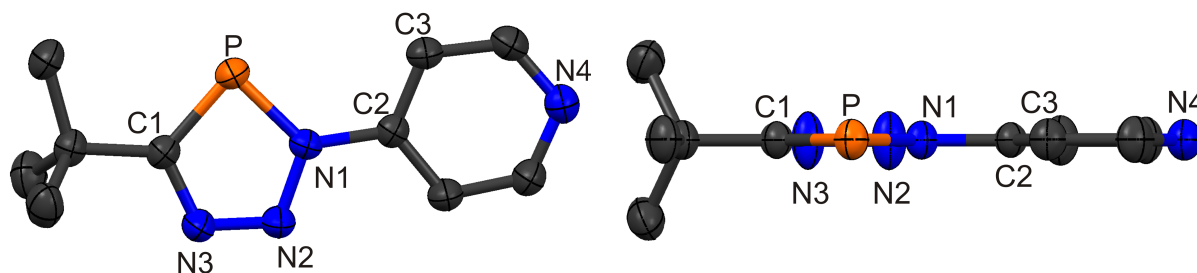
Figure 40: Molecular structure in the crystal of compound **29 (left)** side views **(right)**. Hydrogen atoms are omitted for clarity. Displacement ellipsoids are shown at 50% probability level. Selected bond lengths (Å) and angles (°) are available in Tables in **Table 7** and **Table 8**.
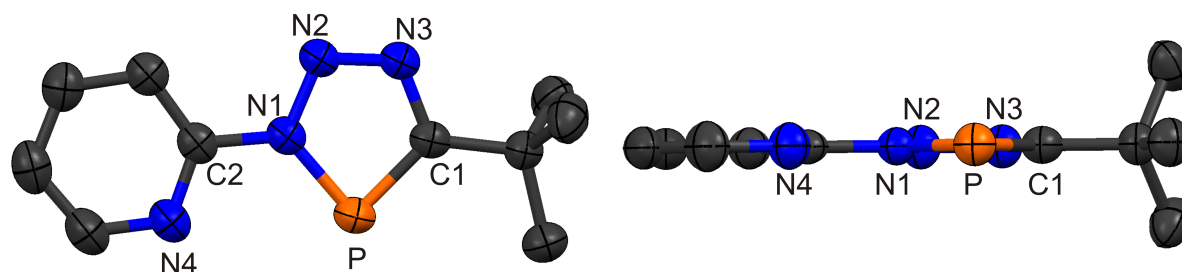
Figure 41: Molecular structure in the crystal of compound **L12 (left)** side views **(right)**. Hydrogen atoms are omitted for clarity. Displacement ellipsoids are shown at 50% probability level. Selected bond lengths (Å) and angles (°) are available in Tables in **Table 7** and **Table 8**.

Selected inter-ring parameters.

Compound	N^1-C^2 [Å] (N^1-C^3)	C^1-P^1-N^1 [°]	N^2-N^1-C^2-C^3 [°]
28	1.436(5)	86.5(2)	-133.5(4)
29	1.435(2)	86.51(9)	180.0(2)
30	1.444(7)	86.6(3)	-38.6(7)
L12	1.436(2)	85.77(8)	0.0(2)
L2	1.484(3)	86.39(9)	153.1(2)
L14	1.4273(16)	-	-19.42(17)

While the N^1-C^2 distances in the aryl-substituted triazaphospholes are quite similar, the benzyl substituted N^1-C^2 (**L2**) is about 0.03 Å longer. In all cases, the C^1-P^1-N^1 angle is around 86° and characteristic for this type of low-coordinate phosphorus compounds (Chapter 1). The inter-ring distance in **L14** is slightly shorter than in **L12**, indicating the strong conjugation in the biarylic system of **L14**.

Table 8: Structural parameters of the triazaphosphole sub-unit.

Compound	P^1-C^1 [Å]	C^1-N^3 [Å]	N^3-N^2 [Å]	N^2-N^1 [Å]	N^1-P^1 [Å]
28	1.711(4)	1.351(5)	1.309(5)	1.350(4)	1.689(3)
29	1.704(2)	1.353(3)	1.303(2)	1.352(3)	1.694(2)
30	1.717(6)	1.370(8)	1.320(7)	1.358(6)	1.696(4)
L12	1.7133(19)	1.368(2)	1.300(2)	1.353(2)	1.7012(16)
L2	1.713(2)	1.351(3)	1.314(2)	1.340(2)	1.683(2)

Independent from the substitution pattern and dihedral angle of the aromatic units (in the conjugated systems), the triazaphosphole sub-unit does not change its steric parameters with respect to the experimental error. A small deviation is notable with the

slightly shorter P^1-N^1 and N^2-N^1 single bond distances, suggesting a slightly stronger delocalisation of the N^1-lone pair.

The dihedral angle is an important factor for light-emitting compounds, since it contributes to the HOMO-LUMO energy gap (E_g). Other parameters influencing the E_g in an isolated system are the bond-length alternation, the aromatic character of the sub-units and the electronic nature of the substituents participating in the π-system.[27,35,36] An appropriate approach to adjusting the dihedral angle in aromatic systems for chelating ligands involves using metal ions.[27,37,38] Hence, the coordination chemistry of compounds **L12** to **L14** was investigated regarding **Re**(I) carbonyl bromide, given that these complexes are good light emitters (*vide supra*). Due to the multidentate nature of the triazaphosphole-based ligand systems as well as the π-conjugation of those compounds, the coordination mode was not predictable (Figure 43). Considering DFT calculations performed with the B3LYP (cc-pVTZ) functional, and starting from the atomic coordinates of the crystal structure determinations, do not indicate a preferred coordination mode. The molecular orbital plots of compounds **L12** and **L14** (Figure 44) strongly differ from those of compounds **L4** and **L6** (e.g. Chapter 3.1).
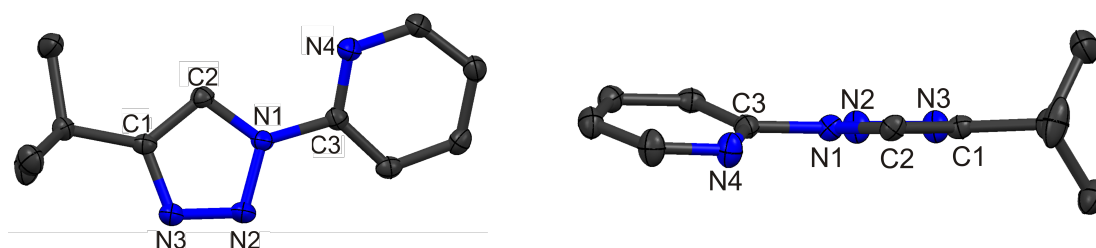
Figure 42: (Left) Molecular structure in the crystal of compound **L14**. **(right)** side view. Hydrogen atoms are omitted for clarity. Displacement ellipsoids are shown at 50% probability level. Selected bond lengths (Å) and angles (°):C(2)-C(1): 1.3639(17), C(1)-N(3): 1.3704(16), N(3)-N(2): 1.3136(15), N(2)-N(1): 1.3537(15), N(1)-C(2): 1.3541(16), N(1)-C(3): 1.4273(16), C(3)-N(4): 1.3281(16). C(1)-C(2)-N(1): 105.02(11), N(1)-N(2)-N(3): 106.71(10).
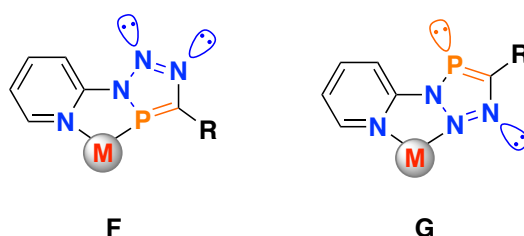
Figure 43: Possible coordination modes of 2-pyridyl-subsituted triazaphospholes.

Most notable are the contributions from the triazole nitrogen atoms N^2 and N^3 as well as the phosphorus lone pair, which are found in HOMO^{-2} to HOMO^{-4}. This becomes even

more interesting with the coefficients belonging to the pyridyl nitrogen lone pair. In **L4**, coefficients from the phosphorus lone pair are also found in HOMO[-5]. Moreover, the shapes of the HOMO and LUMO are quite similar and their main coefficients are found in the C=P bond (HOMO, not displayed in Figure 44) and at the phosphorus atom (LUMO).
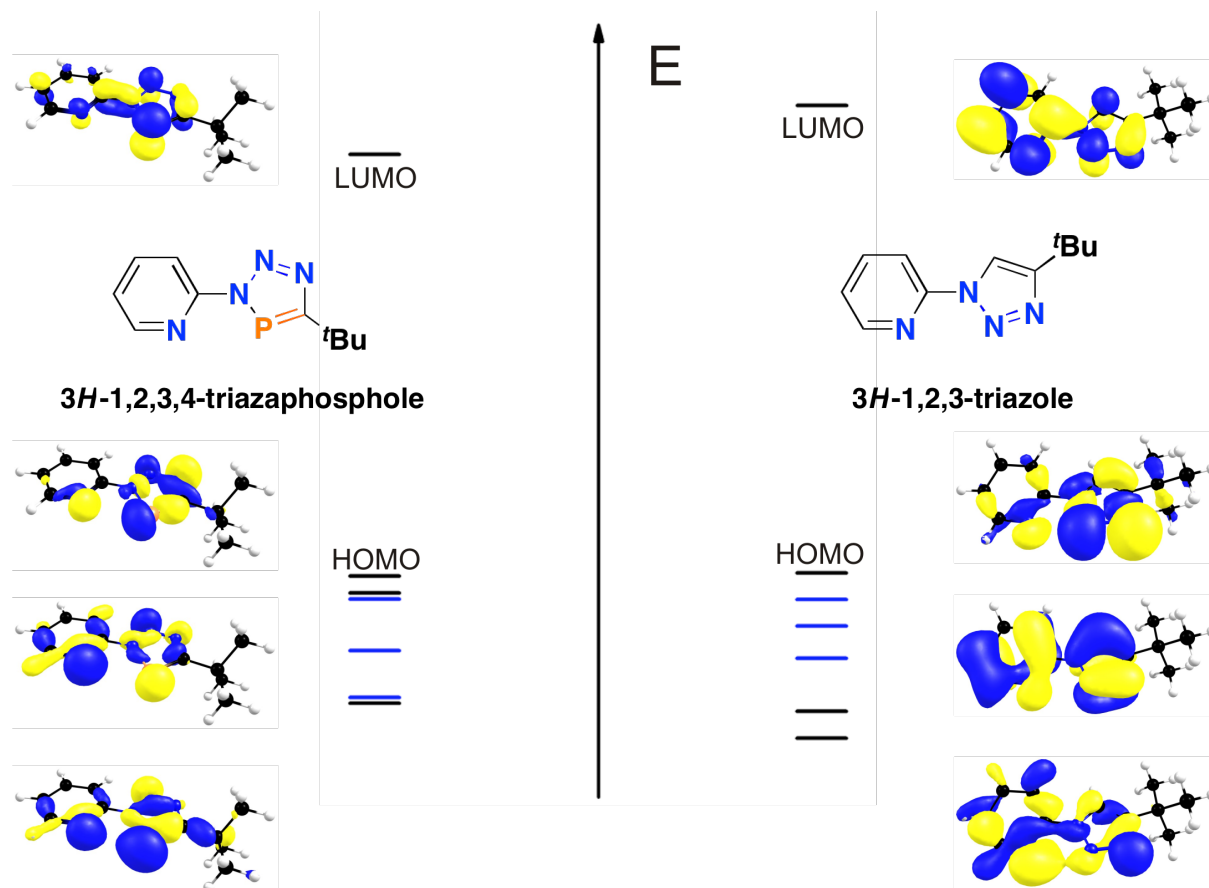
Figure 44: Selected molecular orbital plots of ligands **L12** and **L14**. HOMOs and MOs without contribution of lone pairs are omitted for clarity. Blue lines representing the HOMO; red lines representing MOs with lone pair contribution.

Interestingly, coefficients are also found at the N^1-C^3 in the LUMO. From single electron reduction of bis(phosphinines) and bis(pyridines) with a similar LUMO shape, a contraction of the inter-ring distance was observed, due to population of the LUMO.[39–43] Comparing both biarylic, chelating ligands, the influence of the phosphorus atom on the aromatic compound with a lower lying LUMO becomes obvious. Therefore, the HOMO-LUMO gap is smaller in **L12** than in the analogous triazole component. In contrast to the five-membered aromatic heterocycles, the influence of the heteroatom in phosphinines is remarkably larger compared to pyridines, due to a relatively higher energy level of the HOMO in C_5H_5P.[44]

Coordination Chemistry towards Re(I) Carbonyl Fragment

The coordination towards the **Re**(I) metal centre provides information about the electronic properties of the ligands (Chapter 3.1), although the coordination mode is not predictable at present, as derived from the DFT calculations on **L12**. The compounds **L12**-**L15** were reacted with equimolar amounts of **Re**(CO)$_5$Br. The reactions for the phosphorus containing heterocycles was monitored by means of ^{31}P{^{1}H} NMR spectroscopy, while the reactions of the triazole-based compounds were carried out in deuterated dichloromethane, whereby the reaction progress could be monitored by means of ^{1}H NMR spectroscopy. Within eight hours, the ligands were transformed quantitatively into the corresponding complexes.

R = ^{t}Bu: **C12**, 63 %
R = TMS: **C13**, n.o.*

R = ^{t}Bu: **C14**, 57 %
R = TMS: **C15**, 11 %
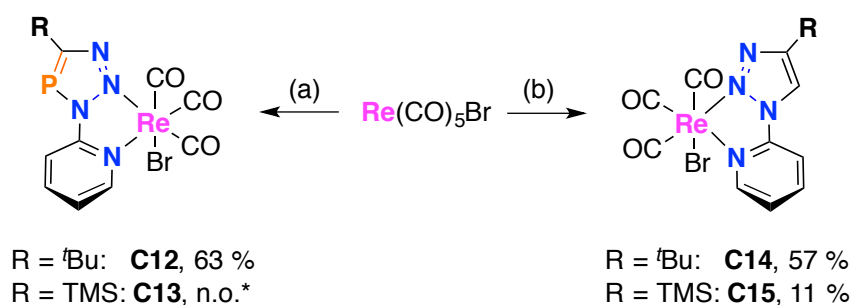
Scheme 48: Synthesis of Re(I) carbonyl complexes starting from 2-pyridyl subsituted triazaphospholes and triazoles. Reaction conditions (a): 1 eq. **L12**/ **L13**, DCM, T = 80 °C, 8 h; (b): 1 eq. **L14**/ **L15**, 80 °C, 8 h. Yields refer to the isolated crystalline product. * Compound was observed by means of ^{31}P{^{1}H} NMR spectroscopy, ^{1}H NMR spectroscopy revealed several by-products.

The reaction of ligands **L12**–**L15** towards the corresponding *fac*-Re(I) triscarbonyl complexes (Scheme 48) is straightforward for the *tert*-butyl substituted ligands, whereas during the reaction with the 5-TMS substituted compounds the formation of side-products was observed. Crowley *et al.* recently investigated rhenium complexes based upon inverse triazoles like **C14** and **C15**.[11] The product in ^{31}P{^{1}H} NMR resonance of **C12** is shifted around $\Delta\delta$ = 23.8 ppm and in the same area compared to the methylene-bridged compound (see Chapter 3.1). Single crystals suitable for X-ray crystal structure determination could be obtained for **C12** (Figure 45) and **C14** (Figure 46) by slowly cooling down the reaction solutions, while single crystals of **C15** (Figure 47) were obtained from slow diffusion of diethyl ether into a DCM solution.

The X-ray crystal structure determination analysis proved the N^2^N^4 coordination mode for complex **C12**. Like in the picolyl-substituted triazaphospholes, the metal is chelated *via* the least nucleophilic nitrogen atom in the triazole. In order to investigate this

surprising finding, Nyulászi *et al.* performed additional DFT calculations (ωB97xD/6-31+G*, with def2-TZVP basis at **Re**) of the complex, showing that the chelating phosphorus nitrogen coordination mode (Figure 43, **F**) is less stable than the $N^2{^\wedge}N^4$ coordination mode by 9.9 kcal/mol (Figure 43, **G**). This can be attributed the preference of rhenium to bind to the nitrogen rather than the phosphorus atom, as demonstrated by calculating the binding energy of the mono-coordinated **N-** and **P-** mode, revealing that the nitrogen bound structure is 12.4 kcal/mol more stable. For the dihedral angles, the solid-state structures show an almost coplanar arrangement. The largest deviation is found in complex **C15** (5°), while the two aromatic sub-units in the 5-*tert*-butyl triazole-based compound and the 2-pyridyl triazaphosphole are twisted about 2° and 0°, respectively.
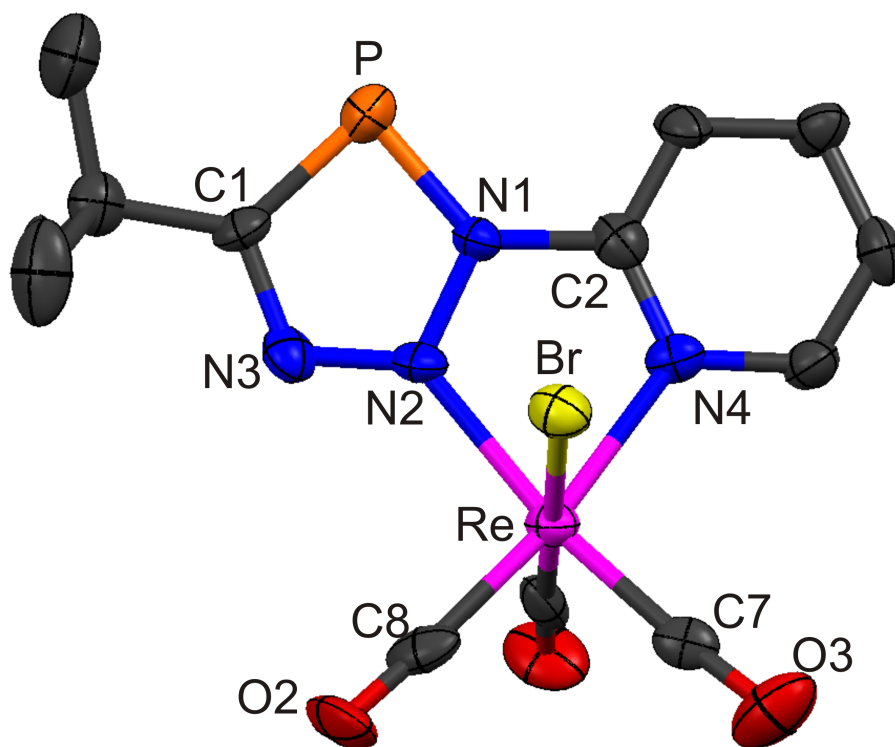
Figure 45: Molecular structure in the crystal of *fac*-Re(I) complexes **C12**, presentation of only one independent molecule; non-coordinated CH_2Cl_2 molecules and hydrogen atoms are omitted for clarity. Displacement ellipsoids are shown at 50% probability level. Selected bond lengths (Å) and angles (°): P(1)-C(1): 1.706(11), P(1)-N(1): 1.714(8), N(1)-N(2): 1.349(12), N(2)-N(3): 1.302(13), N(3)-C(1): 1.336(13), N(1)-C(2): 1.413(12), N(2)-Re(1): 2.147(9), N(4)-Re(1): 2.179(11). N(1)-P(1)-C(1): 85.4(5), N(4)-Re(1)-N(2): 73.6(4), N(2)-N(1)-C(2)-N(4): -0 (1).
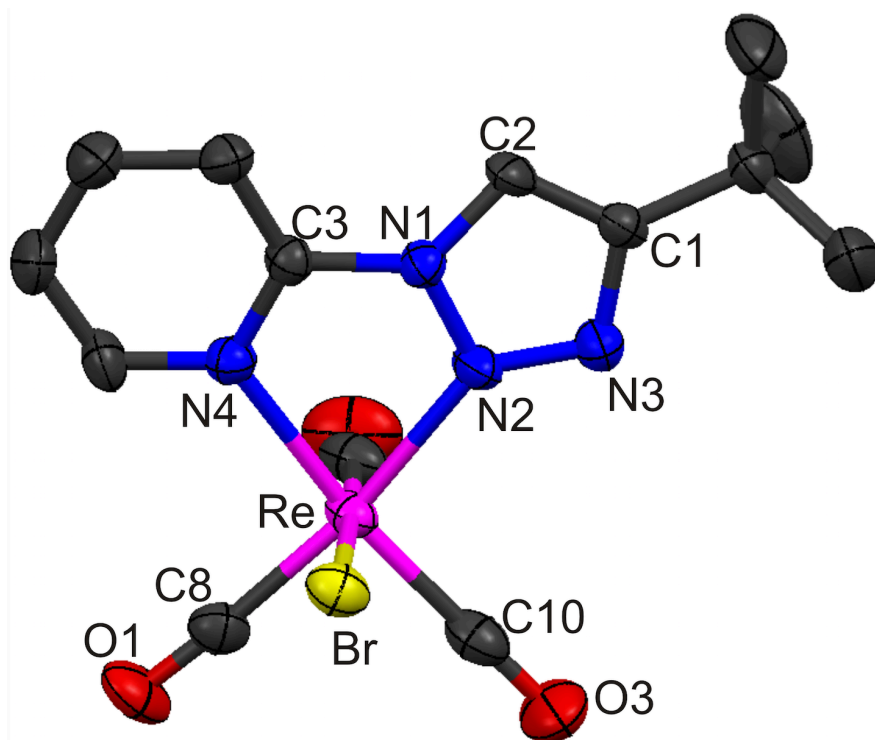
Figure 46: Molecular structures in the crystal of *fac*-Re(I) complexes **C14**, non-coordinated CH_2Cl_2 molecule and hydrogen atoms are omitted for clarity. Displacement ellipsoids are shown at 50% probability level. Selected bond lengths (Å) and angles (°):C(1)-C(2): 1.365(7), C(2)-N(1): 1.356(6), N(1)-N(2): 1.352(6), N(2)-N(3): 1.313(5), N(3)-C(1): 1.367(6), N(1)-C(3): 1.417(6), N(2)-Re(1): 2.146(4), N(4)-Re(1): 2.189(4). N(4)-Re(1)-N(2): 73.93(15). N(2)-N(1)-C(3)-N(4): -2.0(6).
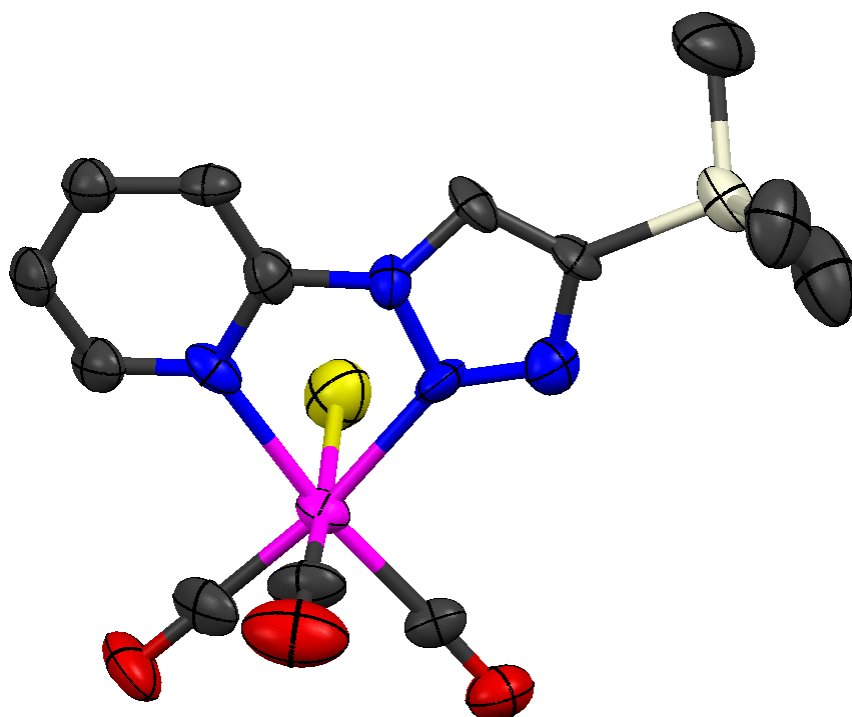
Figure 47: Molecular structures in the crystal of *fac*-Re(I) complexes **C15**. Displacement ellipsoids are shown at the 50% probability level. Hydrogen atoms are omitted for clarity. Displacement ellipsoids are shown at 50% probability level. Selected bond lengths (Å) and angles (°):C(1)-C(2): 1.36(2), C(2)-N(1): 1.36(2), N(1)-N(2): 1.39(2), N(2)-N(3): 1.30(2), C(1)-N(3): 1.39(2), N(2)-Re(1): 2.15(1), N(4)-Re(1): 2.18(1). N(2)-Re(1)-N(4): 74.9(4). N(2)-N(1)-C(3)-N(4): -5(2).

Furthermore, in **C12** the N^1-C^2 bond length is shortened by 0.032 Å (1.436(2) in the free ligand and 1.413(12) in the complex), while the same is true for the C^1-N^3 distance (free ligand: 1.368(2); complex: 1.336(13)). This effect is less obvious in the triazole-based complex **C13**, where the inter-ring distance is 0.01 Å shorter. These findings are in line with the shapes and the relative energy levels of the frontier molecular orbitals of the free ligands and result from the increased bond order due to π-back bonding.

For additional verification, infrared spectroscopy measurements were performed on the **Re**(I) complexes (Table 9).

Table 9: Carbonyl stretching values in complexes **C12**, **C14** and **C15** obtained by IR-spectroscopic analysis

Compound	$\tilde{v}_1(CO)$ [cm^{-1}]	$\tilde{v}_2(CO)$ [cm^{-1}]	$\tilde{v}_3(CO)$ [cm^{-1}]
C12	2023	1992	1900
C14	2026	1913	1870
C15	2023	1919	1885

The values of the $\tilde{v}2$ and $\tilde{v}3$ stretching vibrations are significantly shifted to higher wave numbers in **C12** compared to **C14**. This supports the observations made by DFT and X-ray structure determination analysis and can be attributed to the higher π-accepting properties in the triazaphosphole ligand **L12** causing a stronger back bond. While this finding is contrary to the picolyl-substituted triazaphospholes, the influence of the substituent effect demonstrated by the relative CO band shift of the triazole compounds **C14** and **C15** is in line with the previously-made observations (Chapter 3.1). The effect of the conjugation on chelating triazaphospholes containing ligand systems obviously inverts the π-donating/accepting properties if steric restrictions are neglected.

Excursion 9: Attempts to Cyclometalation of 3*H*,1,2,3,4-Triazaphospholes

The phenyl-substituted triazaphosphole **28** was investigated towards cyclometalation, first described by Dubeck *et al.*[45] This was expected to be a second pathway to adjust the dihedral angle in this type of low-coordinate phosphorus compounds, while the value of such compounds in light-emitting diodes has also been proven several times.[8,16,46–53] The photophysical properties of cyclometalated phosphinines were also explored.[44,54,55]

While iridium (III)-based aryl-triazole compounds show quite interesting emission properties,[56,57] the triazaphosphole-based systems have not been investigated to date.

The attempts in cyclometalation were performed with commercially available [Cp*RhCl$_2$]$_2$ and [Cp*IrCl$_2$]$_2$ metal precursors, which were reacted in a 1:2:2 ratio with **28** and sodium acetate. The reaction progress was monitored by means of ^{31}P{^{1}H} NMR spectroscopy. The obtained spectra indicated an almost quantitative formation of new species after 33 h at T = 80 °C bath temperature (Figure 48), although these do not comply with the cyclometalated species, as the ^{1}H NMR spectrum indicated. The integrals and the splitting of the resonances in the aromatic region do not undergo any change. Therefore, the observed signal can be assigned to the [(**28**)RhCp*Cl$_2$] complex, a preliminary stage in the cyclometalation. The observation is in line with results from Müller *et al.*, obtained during the cyclometalation process of phosphinines. Furthermore, this species could not be isolated, although it could be verified by mass spectrometry.[44,54] However, limited structural aspects can be derived from the ^{31}P{^{1}H} NMR spectrum. The comparably low value of the coupling constant ($J_{\text{P-Rh}}$ = 12.2 Hz) excludes a coordination mode *via* the phosphorus lone pair, which is fortified by the results of the coordination mode found in [**L12**Re(CO)$_3$Br]. Whether the Rh(III) coordination proceeds by the N^3 (Scheme 50, **J**) or the N^2 cannot be deduced from the spectrum, as both coordination modes lead to a $^3J_{\text{P-Rh}}$ coupling in the ^{31}P{^{1}H} NMR spectrum. The reaction of **28** towards the Ir(III) precursor shows similar results. In the phosphorus-lacking systems, the cyclometalation proceeds *via* N^2, although the N^1 (triazaphosphole N^3) is shown to be the most nucleophilic one (Chapter 1).
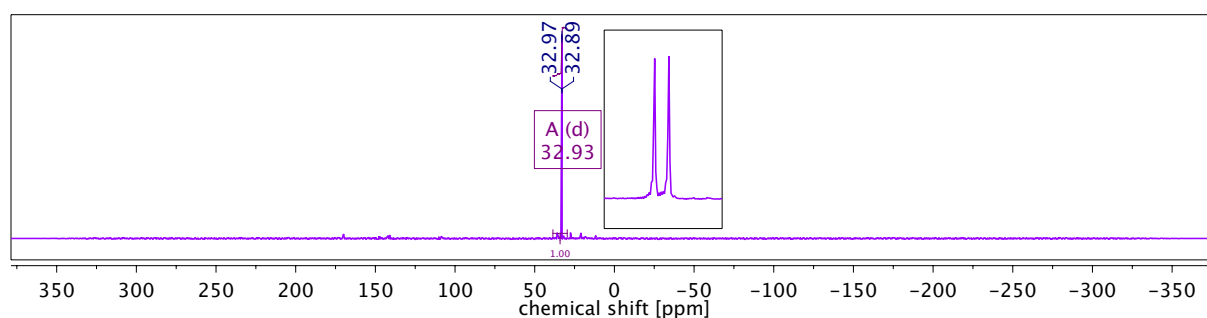
Figure 48: ^{31}P{^{1}H} NMR spectrum of the cyclometalation reaction mixture with Rh(III) after 33 h in at T = 80 °C. Box: Enlargement of the observed signal.

After a total reaction time of 60 d, the amount of side products predominating the ^{31}P{^{1}H} NMR spectrum and the consumption of the starting material **28** was observed.

Since no resonance was detected that could be assigned to the product, the reaction was discontinued (Scheme 49).
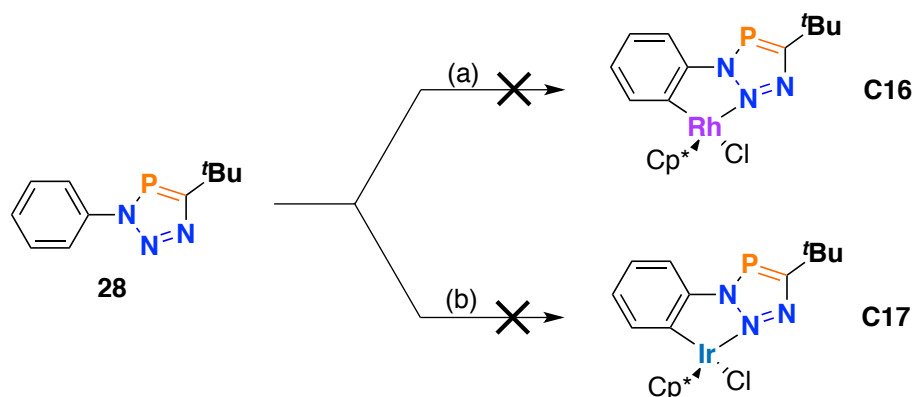
Scheme 49: Attempts to cyclometalate **28**. Reaction conditions (a): [Cp***Rh**Cl$_2$]$_2$/**28**/NaOAc 1:2:2 eq., DCM, 47 h T = 80 °C. (b): [Cp***Ir**Cl$_2$]$_2$/**28**/NaOAc 1:2:2 eq., DCM, 60 h, T = 80 °C.

In the attempts towards **Ir**(III) cyclometalation, the preliminary stage was already obtained at room temperature, without any further reaction. Heating the mixture, after 4 h several by-products were already observed by means of ^{31}P{^{1}H} NMR spectroscopy and thus the reaction was stopped after 60 h of heating. For both metals, neither lowering the temperature nor using a different solvent yielded the desired products. In 2015, Jones *et al.* reported the synthesis and characterisation of a ferrocene-based bis(triazaphosphole) of type **H** and the corresponding **Ag**$^+$ dimer **I** (Scheme 50, box).[58] Although the obtained single crystals were of poor quality, the authors could show a coordination mode *via* the N^1. Therefore, the assumption was made that similar to triazoles (N^3) N^1 is the most nucleophilic one, although in contrast to triazoles the cyclometalation does not occur for the triazaphospholes, due to metal coordination *via* the N^1 rather than the N^2 (**J**) and the resulting sterical shielding in the preliminary stage.
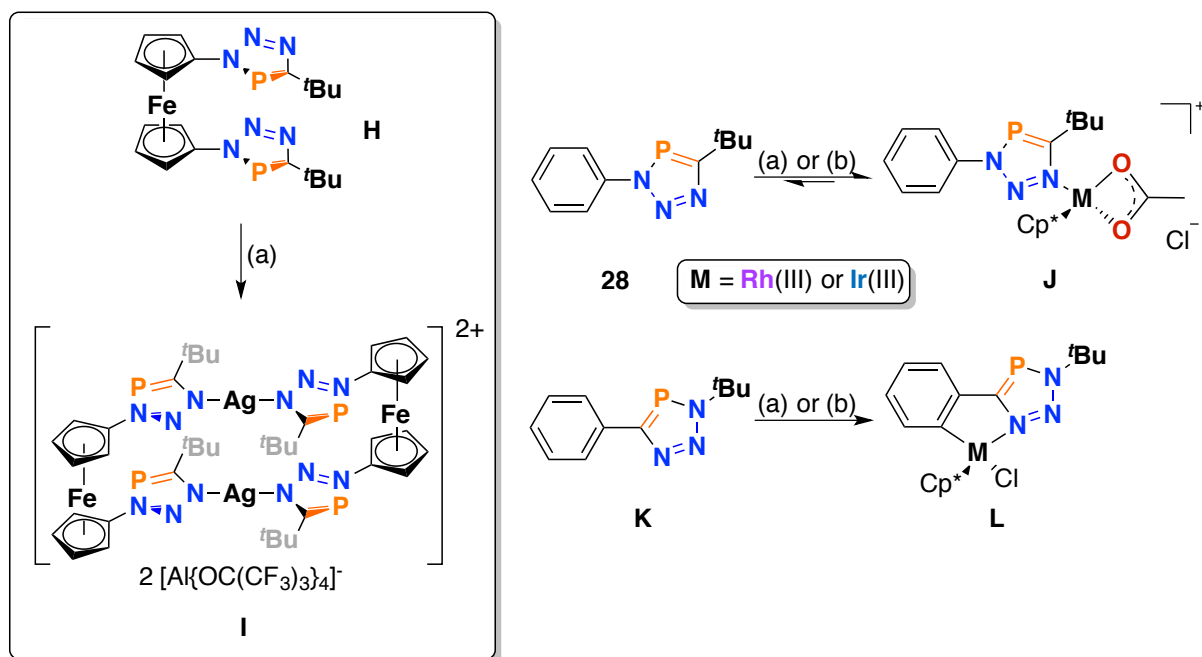
Scheme 50: (Box) First **Ag⁺** complex with triazaphospholes. **(right side, top):** Proposed structure of the preliminary stage **J**. **(right side, bottom):** regular triazaphosphole **K** and the corresponding cyclometalated species **L**.

In the case of phosphinines, the mono-coordination of the metals (corresponding structure to **J**) was reported to be reversible. Triazaphospholes might behave similarly since only the metal precursors could be crystallised from the reaction mixture, indicating that the splitting of the metal precursor dimer and its formation is a reversible process.[44,54] Notably, Müller *et al.* recently investigated the coordination behaviour of a adamantyl-bis(triazaphosphole) towards **Rh**(I), verifying the preferred coordination of metal complexes *via* the N[1] in this type of low coordinate phosphorus compounds.[59] These findings lead to the assumption that the formation of a cyclometalated compound of type **L** (Scheme 50) could only be achieved by the use of a "regular" triazaphosphole of type **K**.

The photophysical measurements for compounds **28**-**31**, **33**, **L12**-**L15**, the **Re**(I) complexes **C12,** and **C14** were performed in the group of Muriel Hissler in Rennes. Compound **C15** was not used, due to the lack of the corresponding triazaphosphole analogue. Additionally, the non-conjugated ligands **L1** and **L2** were used as reference compounds. All measurements were performed at room temperature and methylene chloride was used as a solvent. Table 10 (page 144) summarises the results.

UV-Vis spectroscopy revealed broad, medium intense absorption bands for the aryl-substituted triazaphospholes in the UV range (see Table 10 for λ_{max}). Time-dependent DFT calculations (ωB97xD/aug-ccPVDZ, group of Lászlo Nyulászi *et al.*) were performed to assign the observed transitions. Starting with the highest wavenumbers, 270 – 280 nm for *tert*-Bu- and 280 – 290 nm for TMS-substituted compounds the band is caused by the π^*-n (HOMO^{-3}–LUMO) transition. The low oscillator strength (f = 0.002 – 0.02) yields very low band intensity. Further, the three other transitions are quite close to each other and found in-between 240-260 nm. According to their f-values, the HOMO-LUMO contribution is the most mentionable (f = 0.2–0.3) and about one order of magnitude higher than the other two. These calculations are in line with the absorption spectra and contribute strongly to their composition. There is also a slight bathochromic shift ($\Delta\lambda$ = 8 nm) of **L12** towards **29** and **30**, which can be attributed to the coplanarity of **L12**.

Excursion 10: Fluorescence Spectroscopy

Fluorescence spectroscopy is an analytic technique determining the luminescence properties of molecules. The emission of "cold" light is caused by the relaxation of an excited stated. The excitation takes place because the energy of a photon is absorbed and exhibits a Stokes shift. In the simplest experimental setup, monochromatic light excites the sample, and the re-emissive light is measured orthogonal to the injective beam.[60]

Photon absorption obtains a (vibronic) excited state S1. Relaxation from an electronically excited state is possible by non-emissive energy transfer, e.g. by impacts with solvent molecules but can also proceed by the emission of a photon. As the decay

proceeds from e.g. **S1** (higher excited states are possible), the phenomena are called fluorescence is shortly (nanoseconds scale) observed after light absorption.
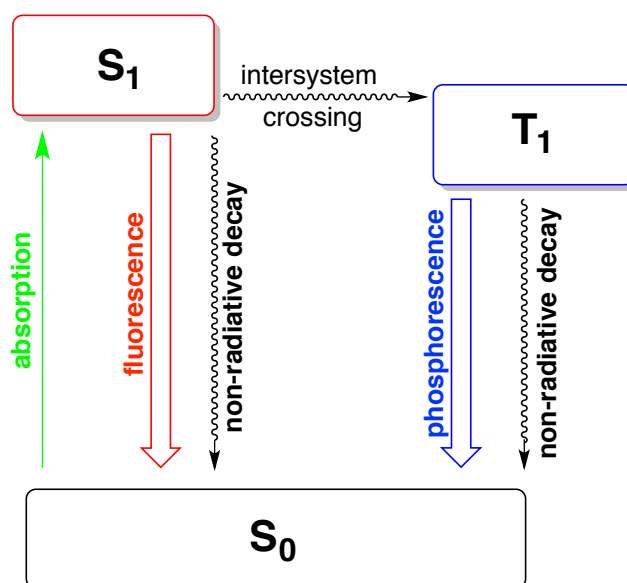
Figure 49: Perrin-Jablonski diagram in a simplified version, illustrating the differences of fluorescence and phosphorescence by intersystem crossing.

Besides the fluorescence, phosphorescence can also cause the relaxation. In case of an intersystem crossing during the vibrational relaxation process, a triplet excited state **T1** occurs. In contrast to the fluorescence from the **S1** state, re-emission from the **T1** state is a "forbidden" transition. Nevertheless, the transition still takes place, increasing the decay time significantly. Phosphorescence is observed from millisecond to long-time scales, and therefore multiple orders of magnitude slower than emission from allowed transitions. [60]

Interesting, the pyridyl-subsituted triazaphospholes **L12** and **L13** show significant fluorescence with rather good quantum yields. Consequently, these compounds resemble a new class of phosphorus-containing emitters. More striking, the corresponding pyridyl-triazoles show no fluorescence at all. The substitution pattern in 5-position leads to a red shift for the electron-rich compounds on the TMS compounds. In contrast to the absorption band maxima, the change in the emission is noticeably smaller. This might be attributed to the negative hyper conjugation effect of the TMS-substituent. Further, the results on the TMS-substituted triazaphospholes indicated decomposition of **33** during the measurements. This result might also be attributed to the lack of robustness of that compound. The quantum yields of **28-30** are ambiguous

regarding the dihedral angles in the solid-state structure. The intensity of the twisted compound **28** shows to be slightly higher than double of the value the coplanar compound **40**. The non-conjugated references **L1** and **L2** did not show any emission.

Table 10: Photophysical properties of selected 3*H*-1,2,3,4-triazaphospholes and 3*H*-1,2,3-triazoles.

Compound	N-substituent	C[1]-subsitutent	λ_{max}[a] [nm]	ε [L•mol^{-1}• cm^{-1}]	λ_{em} [nm]	ϕ [%][b]
28 (TAP)	Ph	*tert*-Bu	270	9300	371	8
31 (TAP)	Ph	TMS	268	6800	-	-[c]
29 (TAP)	4-Py	*tert*-Bu	271	5900	360	0.4
30 (TAP)	3-Py	*tert*-Bu	275	9400	370	
33 (TAP)	3-Py	TMS	278	6700	338	-[d]
L12 (TAP)	2-Py	*tert*-Bu	285	3800	370	12
L13 (TAP)	2-Py	TMS	290	1900	334	11
L14 (TA)	2-Py	*tert*-Bu	276	21400	-	-[c]
L15 (TA)	2-Py	TMS	275	11300	-	-[e]
C12 (TAP)	2-Py	*tert*-Bu	295	12200	365	1.4[f]
			420	3100		
C14 (TA)	2-Py	*tert*-Bu	266	14900	591	15
			379	4700		
L1 (TAP)	Bn	TMS	261	3900	-	-
L2 (TAP)	Bn	*tert*-Bu	258	5400	-	-
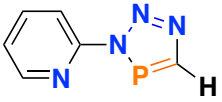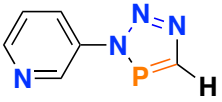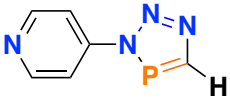
[a] measured in CH_2Cl_2. [b] Fluorescent quantum yields measured relative to quinine sulphate (H_2SO_4, 0.1 M), ± 15%. [c] Compound might be decomposed. [d] Compound is not stable and underwent decomposition. [e] Not determined, emission it too low. [f] Quantum yields measured relative to [**Ru**(bpy)$_3$]$^{2+}$ in H_2O, ϕ[**Ru**(bpy)$_3$]$^{2+}$ = 4.2%.

DFT Analysis of the Compounds

The rotational barrier of the dihedral angle was examined in the gas-phase to investigate the influence of packing effects. Therefore, the relative stabilities of the 5-H substituted analogues of compounds **29**, **30,** and **L12** were determined with different functionals and are exhibiting that **J** is approximately 5 kcal/mol stable in the optimized structures, independent of the used functional (Table 11). Also the functional with dispersion correction yields similar results, indicating an independence from steric repulsion. Further, pnictogen interactions were ruled out by the absence of bond critical points and stabilizing interactions in the second order perturbations of Natural Bond Orbital

analysis. Obviously, the N-P repulsive interactions in these compounds are smaller than N-N or H-N/P interactions. This data is supported by determining the relative energy value of the coplanar *trans*-arrangement of **J**, which is 1.6 kcal/mol less stable and frequency analysis indicate a saddle point.

Table 11: Relative stability of compounds H-J obtained from by different functionals and basis sets.

	Basis set; E_{rel} [kcal/mol]		
	ωB97xD/ aug-cc-pVTZ	ωB97xD/ aug-cc-pVTZ	ωB97xD/ aug-cc-pVTZ
cis-2-pyridyl-triazaphosphole (**J**)	0.0	0.0	0.0
cis-3-pyridyl-triazaphosphole (**K**)	5.5	5.5	5.6
4-pyridyl-triazaphosphole (**L**)	4.9	4.9	5.0

The findings for **J** and **K** are in line with the obtained data from the X-ray diffraction analysis as well as the photophysical properties, whereas **L** lost its planarity during the optimization steps. For further information, the rotation barrier around the N^1-C^2 bond of compounds **29**, **30** and **L12** was calculated using ωB97xD/aug-cc-pVDZ. The largest rotational barrier is received for the 2-pyridyl-sustituted triazaphosphole. Additionally, the energy minimum corresponds to the molecular structure of the crystal with a coplanar arrangement of the heterocycles. A second minimum is found (torsion angle of 140°), but it is 5 kcal/mol less stable. The 3-pyridyl-substituted structure has only a small energy barrier of 0.4 kcal/mol between the twisted form (energy minimum) and the planar structure. Similar, but more pronounced is the rotation barrier for **29**. Between 0-30°, the energy difference is smaller than 0.1 kcal/mol and, therefore, the results are energetically close to the solid-state structure. For **29** and **30**, the coplanar structure is a first-order saddle point (Figure 50).
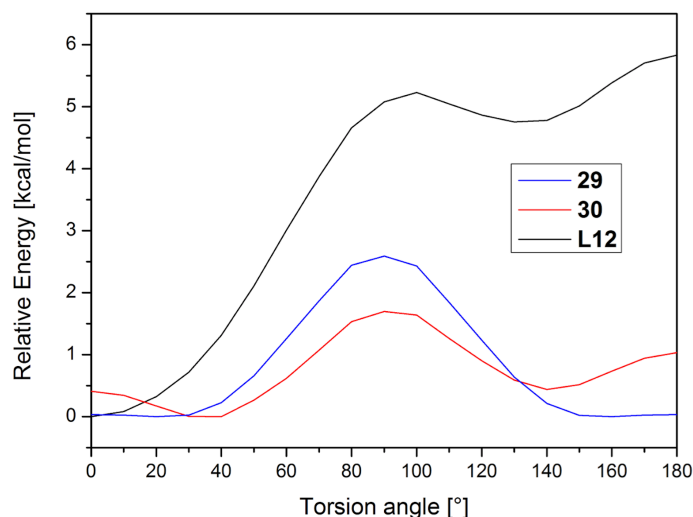
Figure 50: Rotation Barriers in 10° steps for pyridyl-substituted triazaphospholes **29**, **30,** and **L12** obtained from DFT calculations (ωB97xD/aug-cc-pVDZ).

The low relative energy in the rotation profile of **30** might indicate that packing effects cause the coplanar arrangement in the solid-state (Figure 51). The molecules arrange in the crystal lattice in oppositely directed layers. The phosphorus atom of each molecule lies above or below the centre of a pyridyl subunit. The distance between the phosphorus atom and the centroid is 3.58 Å. A similar stacking is not observed in **L12**.
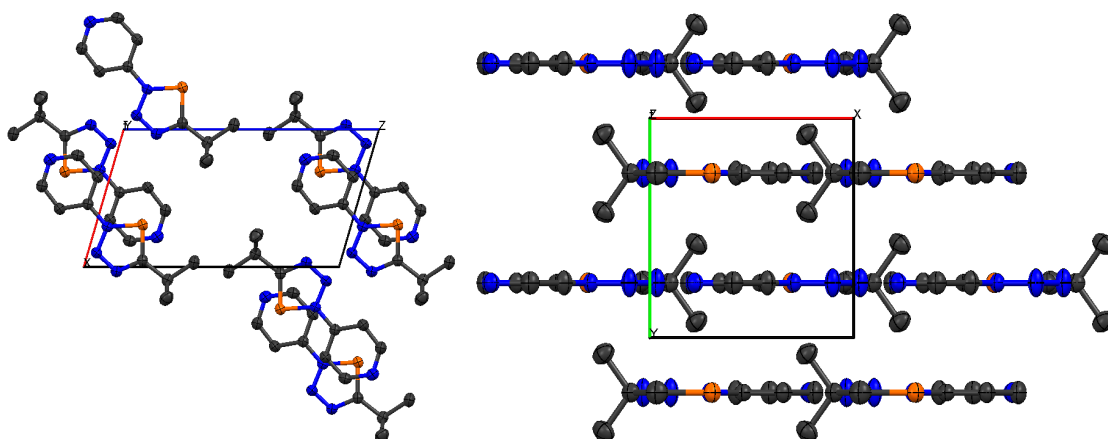
Figure 51: Packing in the crystal found for **29**. View along the *b*-axis (left) and along the *c*-axis (right).

The effect of this packing was also investigated using DFT calculations at the ωB97xD/6-311+G** level. The optimised geometry is not completely planar anymore, but still, an interaction energy of 14 kcal/mol was obtained. This significant interaction might

contribute to the observed molecular structure in the crystal. Additionally, AIM analysis was performed but observed no bond critical points.

The calculations were also completed on **L13** with the same results for its calculated structure as well as its rotation energy surface. These findings demonstrate the relation between the planarity of a system and the quantum yield nicely. The 2-pyridyl-triazole does not show any fluorescence contrasting that data, although the molecular structure in the crystal is planar and the optimized structure in the gas phase, as well as its rotation barrier is close to the observations made for the phosphorus-containing analogue.

The obtained information is based on the ground state of the molecules and did not provide any explanation of the photophysical properties. Hence, the first excited state of both 2-pyridyl-substitued compounds was investigated using time-dependent DFT (B3LYP/cc-PVTZ) geometry optimization. In dependency of the starting point, the calculations converged in the *cis*- or *trans*-arranged, planar structures for both molecules. Further, the calculations indicate, that in the case of **L12** the *cis* arrangement, like in the ground state, is more stable, while **L14** the *trans* structure is favoured (Figure 52). The differences in the calculated structures in the ground state and first excited state indicate a low overlap integral for the Franck-Condon factor and, by these differences, the probability of transitions is reduced.
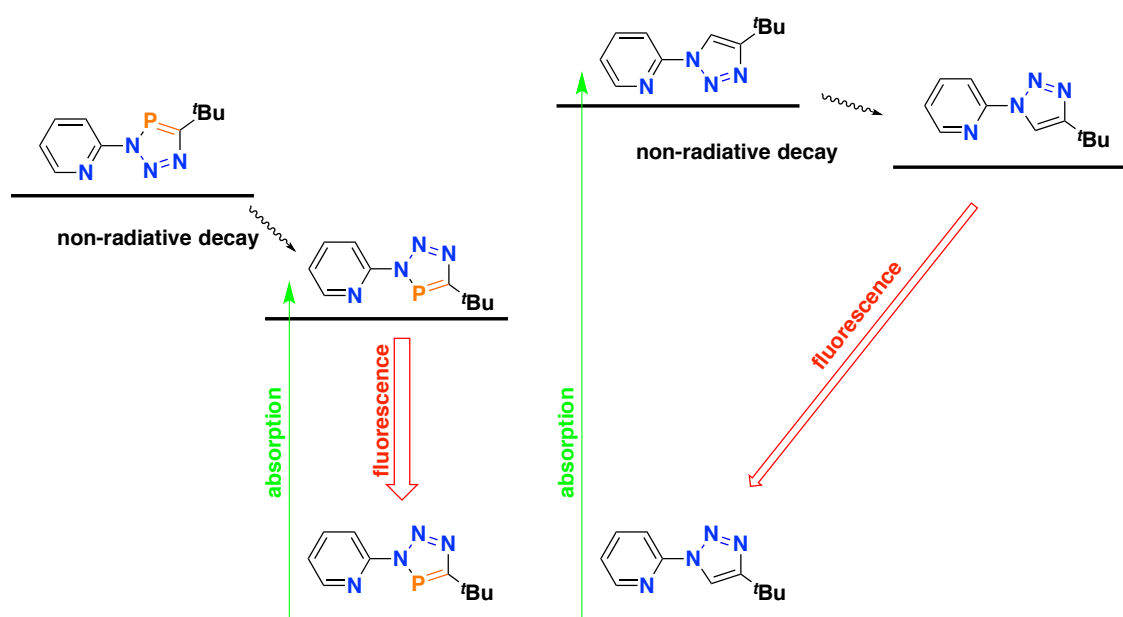
Figure 52: TD-DFT optimized structures of **L12** and **L14** in their excited states and the ground state. The emission probability is indicated by the thickness of the arrow.

The absorption and emission properties of the **Re**(I) complexes **C12** and **C14** are quite similar, as the spectra show (Figure 53). The observations made for the adsorption of the phosphorus lacking compound **C14** are close to the bands in previous reports,[11] except that the presented compound shows a red shift in the spectrum.
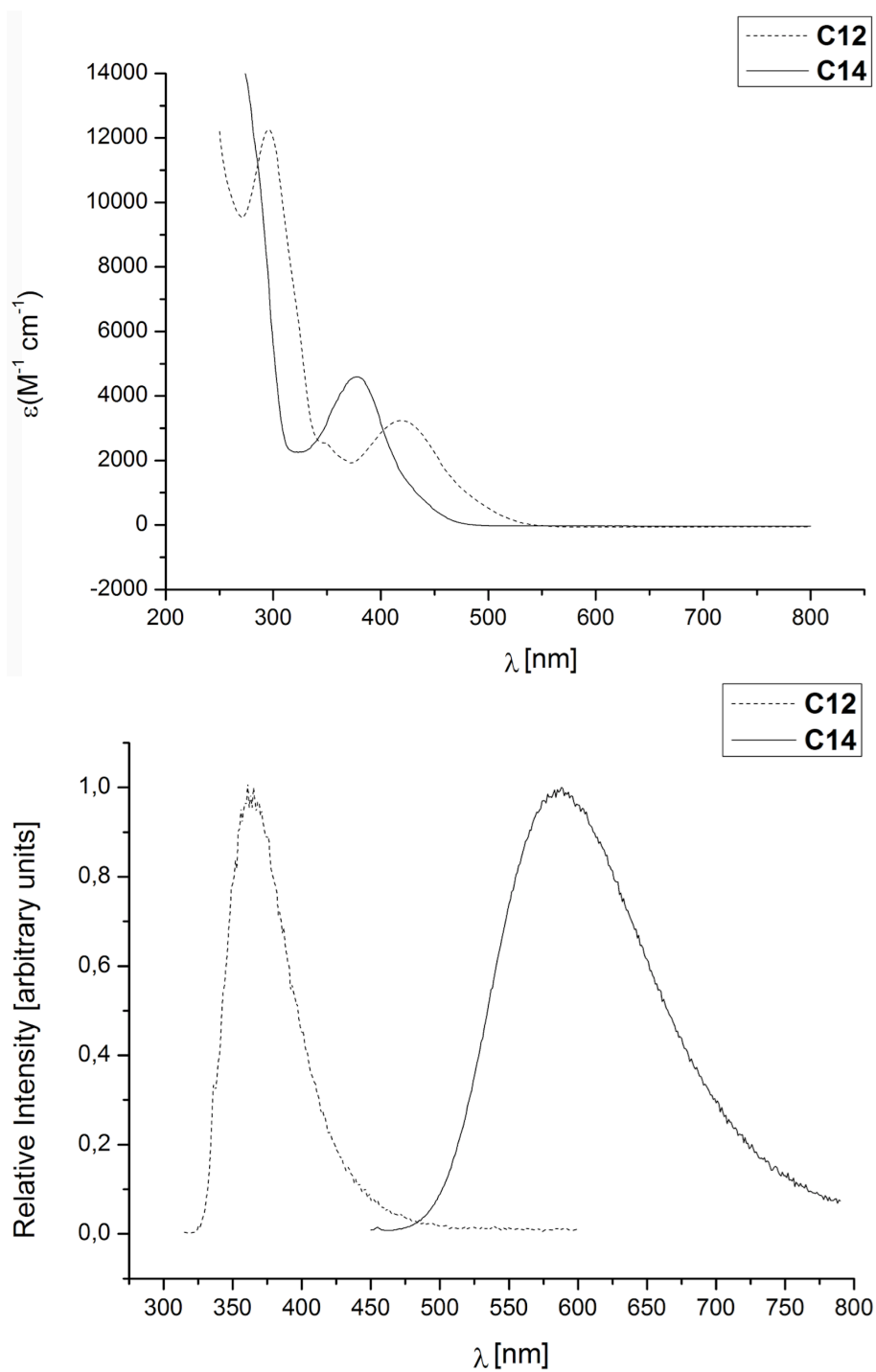
Figure 53: Electronic absorption (**Top**) and emission spectra (**Bottom**) for **Re**(I)-carbonyl complexes **C12 (dashed lines)** and **C14 (solid lines)** obtained from DCM solutions at room temperature.

An intense band attributed to an ILCT located at λ = 266 nm and further at λ = 379 nm band with band tailing down to λ = 450 nm assigned to a MLCT were found. Due to the independence of the MLCT on the triazole substituent, the band is similarly located as for the corresponding complex **C12**.[11,61]

The red shift of the absorption band maxima found in the triazaphosphole based **Re**(I) complex **C12** can be attributed to the introduction of the phosphorus atom into the five-membered heterocycle, indicated by an intense band centred at λ = 295 nm, tails and a further red shifted shoulder as well as the red shift of the MLCT band. The maximum of that band is located at λ = 420 nm and shows a strong tailing up to λ = 525 nm.

The complexes were investigated using DFT and TD-DFT calculations (Figure 54). The obtained frontier molecular orbitals of **C12** and **C14** are mainly located at the **Re**(CO)$_3$Br subunit (HOMO to HOMO^{-5}) and are shaped similarly.

LUMO **C12**   HOMO **C12**   HOMO^{-1} **C12**

LUMO **C14**   HOMO **C14**   HOMO^{-1} **C14**
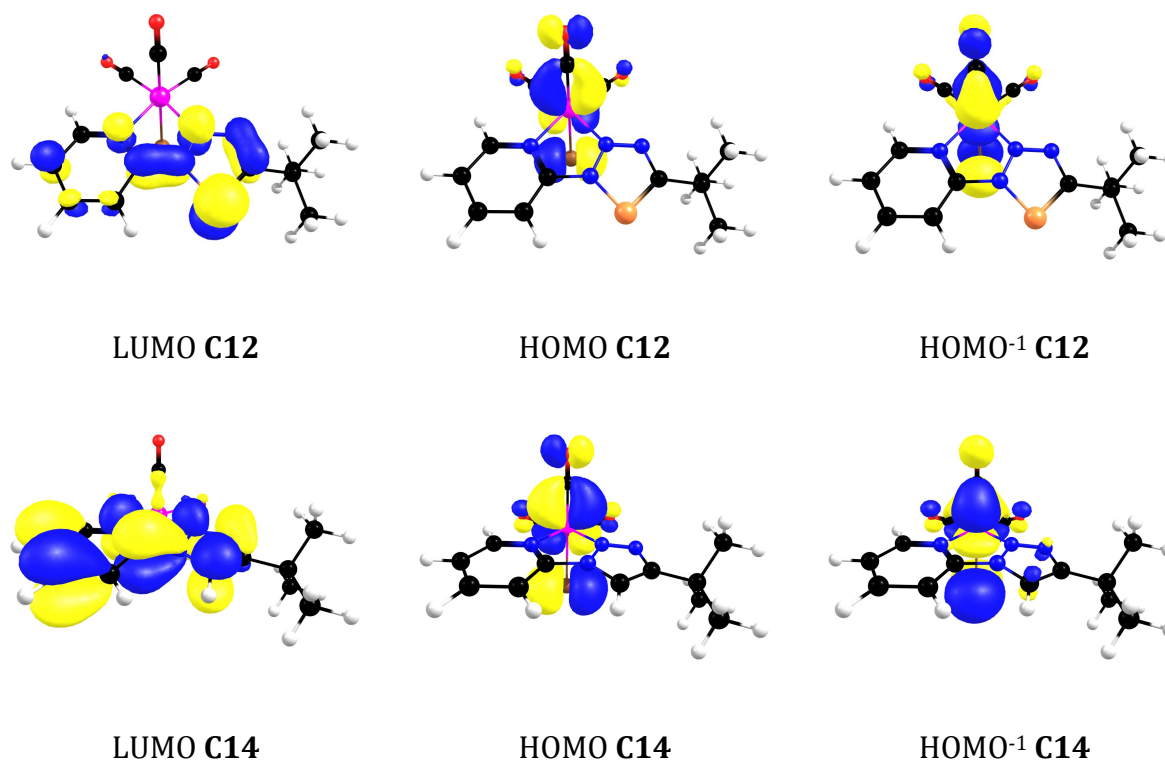
Figure 54: Selected frontier orbitals of the complexes **C12** and **C14**.

The orbitals contributing to the LUMO are localized on the ligands and the relative energy level differ in both compounds about 0.5 eV, exhibiting the LUMO in **C14** to be

149

less stable and an enlarged character on the pyridyl ring, while the triazaphosphole fragment in **C12** provides the coefficients to the LUMO (Figure 54). The stabilization of the $\pi^*_{C=P}$ orbital can be attributed to the implementation of the phosphorus atom since the observations are in line with results obtained for a series of corresponding phosphorus lacking and containing derivatives, showing an enhancement of the LUMO stability with increasing number of phosphorus atoms.[62]

The results from the TD-DFT calculations indicate 15 predicted transitions for both metal complexes. All have in common that $\lambda > 250$ nm and they are low intensity (f = 0.0001 – 0.02). With their small contribution to the spectra, they are negligible, besides three transitions. These have been assigned to the observed band maxima. The calculated transitions found at $\lambda = 444$ nm (f = 0.0607, **C12**) and $\lambda = 394$ nm (f = 0.053, **C14**), both a LUMO←HOMO-1 transition is suggested to be the MLCT bands at $\lambda = 420$ and $\lambda = 379$ nm in the spectra, respectively. The observed shoulders at $\lambda = 350$ nm in the spectrum of **C12** might be found in the $\lambda = 310$ nm (f = 0.0762) calculated band and can be assigned a metal d-π(CO) - LUMO transition. The corresponding transition for **C14** is at $\lambda = 285$ nm (f = 0.0645). The last noteworthy transition is a π^* - π one, and calculated to occur at $\lambda = 263$ nm (f = 0.2147) and $\lambda = 250$ nm (f = 0.0668) for **C12** and **C14**, respectively. The relative shifts of these bands, which influence the shape of the spectrum the most can be attributed to the relatively shifted stabilization energy of the LUMOs since the transitions are excitations to the LUMO.

Triplet emission was investigated in deoxygenated CH_2Cl_2 and only detected in **C14** at the maximum of the MLCT band. The emission maximum was centred at $\lambda = 591$ nm. However, no emission was detected at low temperatures.

The obtained photophysical data point out a radiationless deactivation, which is assumed to be the deactivation of the MLCT excited states, observed in **C12**. Due to the excitation with the maximum on the ILCT band in compound **C14**, a triplet emission is found at $\lambda = 591$ nm indicating an efficient relaxation to ^{3}MLCT excited state. The complex **C12** acts differently when the ILCT band is excited. For this transition at $\lambda = 295$ nm, relaxation occurs by fluorescent emission at $\lambda = 365$ nm equalling the observed fluoresce of the free ligand **L12**. This behaviour might be caused by the differences in the distribution of the electron density in the LUMO, as demonstrated by the TD-DFT calculations. The strong coefficients located at the triazaphosphole, especially at the phosphorus atom, might cause radiationless relaxation of the ^{3}MLCT.

3.2.2 Photoelectron Spectroscopy on Conjugated Heterocycles: A Preliminary Comparison Study between 1*H*-1,2,3-Triazoles and 3*H*-1,2,3,4-Triazaphospholes

The electronic structure of the aryl-substituted compounds **28-30** and **L12,** as well as **L14,** was explored in more detail using ultraviolet photoelectron spectroscopy (UPS). Additionally, the phosphorus lacking analogue of phenyl triazaphosphole was included (Scheme 51).
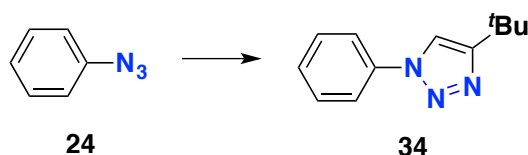
Scheme 51: Synthesis of 4-(*tert*-butyl)-1-phenyl-1,2,3-triazole **34**. Reaction conditions: 1 eq. **24**, 1,2 eq. 3,3-dimethylbut-1-yne, 0.1 eq. sodium ascorbate, 0.05 eq. CuSO₄*5H₂O, H₂O/ᵗBuOH (*v:v* 1:1) r.t., overnight, 68 % yield.

Single crystals suitable for X-ray analysis were obtained by slow evaporation of a pentane solution at room temperature (Figure 55). The obtained molecular structure in the solid state shows a twisted arrangement (-160.4°), which is around 30 ° less than the phosphorus-containing analogue **28** and might be attributed to higher H-N/P interactions due to the enlarged N^2-N^3-P angle (115.9 (3) *vs.* 110.2(1) in **34**.

Figure 55: Ellipsoid plot of the phenyl-substituted 1*H*-1,2,3-triazole **34**. Displacement ellipsoids are shown at the 50% probability level. Hydrogen atoms are omitted for clarity. Selected bond lengths (Å) and angles (°): N(1)-N(2) 1.3531 (1), N(2)-N(3): 1.3154(1), N(3)-C(1): 1.3627(1), C(1)-C(2): 1.3675(1), C(2)-N(1) 1.3498(3), N(1)-C(3): 1.4282(1); N(2)-N(1)-C(2): 110.17(1), N(2)-N(1)-C(3): 120.38(1), C(2)-N(1)-C(3): 129.40(1), N(1)-N(2)-C(3): 107.16(3), N(2)-N(3)-C(1): 109.26(3), N(3)-C(1)-C(2): 107.83(1), N(2)-N(1)-C(3)-C(4): -160.40(2).

With this additional compound, two pairs of triazaphospholes and their corresponding triazoles can be examined on their conjugative stabilization. Further, these pairs provide the possibility to cross-check with literature-known spectra.

In photoelectron spectroscopy, the kinetic energy of electrons is measured, that were previously released from the outer electron shells (UV rays) or the inner electron shells (X-rays), depending on the used irradiation.

Based on the photoelectric effect - that light energy upon a certain energy threshold can eject electrons from a molecule- the kinetic energy of those electrons can be used to determine the (molecular) orbital energies of a compound by using the law of conservation of energy (Eq. 1) and Koopmans approximation (Eq. 2).

In UPS, a molecule is ionized by UV irradiation and the kinetic energy of the released electrons is measured. From that energy, the (molecular) orbital energy can be determined, using Koopmans approximation.

$$E_{Kin} = h\nu - E_{Ion}$$

Equation 1: Einstein relation, where E_{Kin} corresponds to the kinetic energy of the electron, h Planck constant, v frequency and E_{Ion} as ionisation energy.

$$E_{Ion} = -\varepsilon$$

Equation 2: Koopmans' approximation, with E_{Ion} as ionisation energy and ε as molecular orbital energy.

The bands in the observed spectra can be assigned to molecular orbitals by using known molecules or fragments, or DFT calculations.[63–65]

This analysis of the chosen molecules also benefits from previous investigations made by Pfister-Guillouzo *et al.*,[66] which exposed a high correlation of the P=C and C=C π-bond ionization. The Lichtenberger and co-workers determined the molecular orbital structure of triazoles (Figure 56). To achieve a better comparison of UPS spectra between the selected molecules **L12** and **L14,** as well as **28** and **34,** and the investigations from Pfister-Guillouzo, Regitz and Lichtenberger, the ionisation energies and molecular orbital plots for the lower substituted compounds **A**, **B**, **C** and **D** were determined using DFT calculations (*vide infra*).
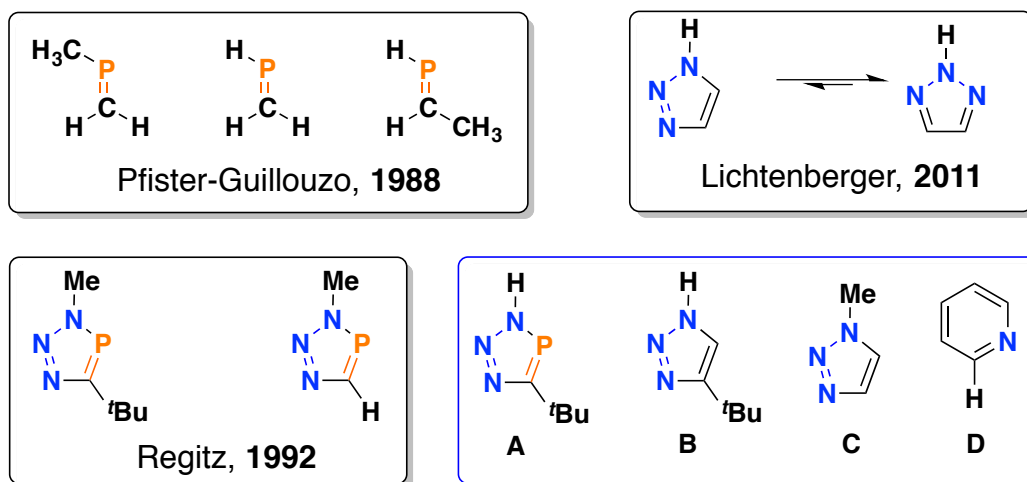
Figure 56: Reported investigations from Pfister-Guillouzo Regitz and Lichtenberger and assistant molecules **A** and **B**.

The band located in the spectra at around 11 eV was assigned to ionisations of the *tert*butyl substituent, using SAC-CI/cc-pVDZ//wb97xd/aug-cc-pVDZ and OVGF/cc-pVDZ// ωB97-xD/aug-ccpVDZ calculations and verifying these values with literature reports.[67] The intensities in the obtained photoelectron spectra of compounds **L12** and **L14** (Figure 57) approximately showed the lowest energy display. A ratio of 1:2:1:2 and 1:2:1:1 ratio for **L12** and **L14**. This data might indicate multiple (five to six) ionisation processes in this section of the spectra. Although the two different approaches in the DFT calculations gave similar results, the predicted energy values for the ionisation processes are slightly below the experimental findings. The calculated π-ionization energies for **L12** and **L14** are very alike to both types of calculation, except the second π-ionization. Here, the value is about $\Delta E = 0.4$ eV smaller for the phosphorus-containing compound, yielding nearly degenerated ionisation energy values for the first two IEs. From this calculated finding, the observed doubled intensity of the first band in the experimental spectrum might be explained. However, the second π-ionisation process in **L12** is assigned to the band centred at IE = 9.2 eV and for the triazole based compound **L14** at IE = 9.4 eV. This assignment provides a valid correlation of the second π-ionisation energy values.

153
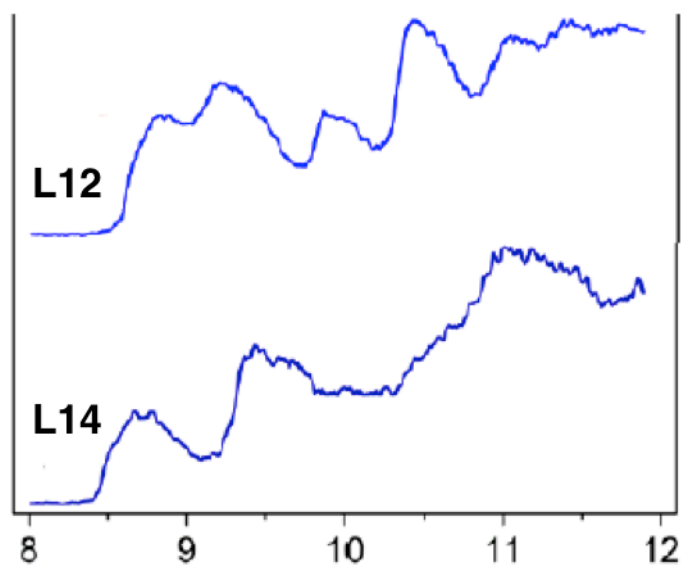
Figure 57: UPS spectra of pyridyl triazaphosphole **L12** and its phosphorus-lacking analogue **L14** of the low ionisation energy region.

Further calculations were done to examine the consistency of the DFT level, comparing the selected functionals and basis sets with previously recorded He-I photoelectron spectra.[68] The ωB97-xD/aug-cc-PVTZ calculations gave for the geometry optimization of the most stable tautomer as the same result as the previous calculations using Hartree-Fock level (HF/4-31G*). The π-IEs form the calculations using OVGF functional proved to be 0.3 eV below the experimental values, but for the first nitrogen lone pair IE, the predicted value differs only about $\Delta E = 0.1$ eV.

The nearly degenerated state of the third and fourth ionisation process causing a double intensity in the experimental spectrum could be reproduced by the calculations. The observed IEs in **L12** can correlate to the results from the UPS spectrum of pyridine.[69] By this, the previous assignment, based on Koopmans theorem, differs from the present case.

However, Lichtenberger *et al.* performed UPS measurements of (*vide supra*) and the ionisation energy values obtained from the OVGF calculations are slightly smaller than the reported ones.[70] Comparing the two triazole compounds **B** and **C**, the same assignment of the ionisation processes are found. Using the observed different IE values as an error value, the differences between the experiment and calculations found in **C** become adequate estimates.

154

Using the assignments of compounds **A** and **B** together with the one reported for pyridine, a correlation diagram of the IEs for **L12** and **L14** can be derived (Figure 58). The π-system of the pyridine heterocycle does not affect the nodal plane containing the π-orbital. It can thus be assumed, that the orbital is only localized in the five-membered ring. This data becomes evident by consistent ionisation energy values of **L12** and **L14** compared to the ones in **A** and **B**, just as the orbital in pyridine, where the IE value of E = 9.5 eV does not significantly change when embedding it into a conjugated system. In the triazole based ligand, no interaction of the lone pairs with the pyridyl lone pair can be detected, while a small splitting is observed in the phosphorus-containing compound. In both coupled systems, the largest interaction between the aromatic rings detected for the highest π-molecular orbital, located in the pyridine subunit. Further, the second π-ionisation process is found in the five-membered heterocycle. Both result in a significant splitting, yielding the HOMO in **L12** and **L14**.
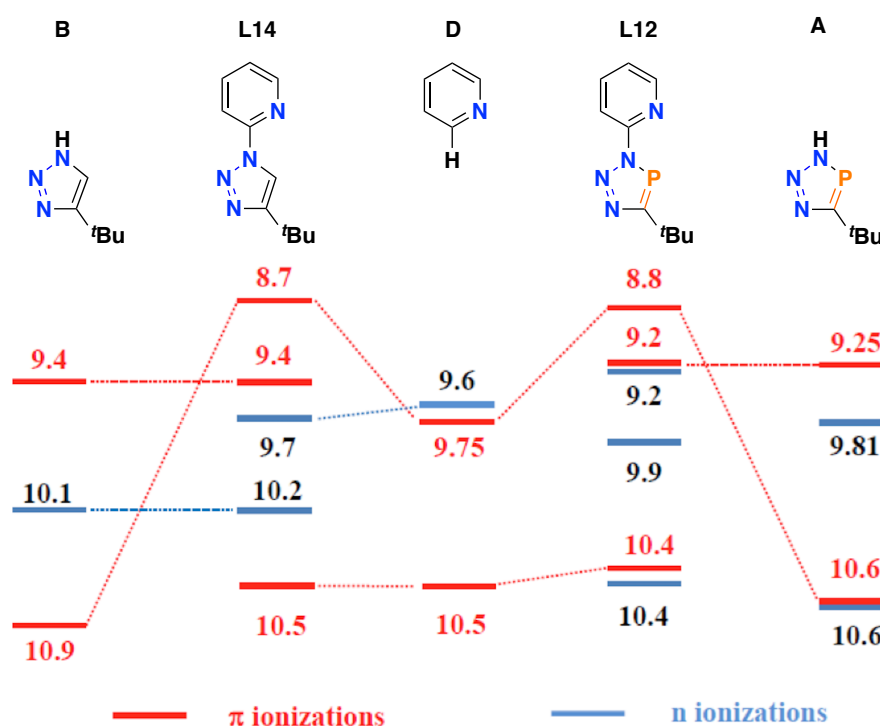
Figure 58: Molecular orbital energies of selected triazaphospholes and triazoles. Energies are given in eV.

It should be pointed out that the here-described results are preliminary investigations for the shown compounds. Both, the experiments, as well as the assignments, were not finished when this work was authored.

3.2.3 Investigations Towards Mn(I) and Re(I) Promoted Electrochemical Carbon Dioxide Reduction with Inverse 2-Pyridyl Substituted Triazaphospholes and Triazoles.

Transition metal complexes of the type [(N^N)**Re**(CO)$_3$X] with N^N as biaryl and X as halides were investigated not only towards their light emitting properties, but also towards catalytic CO_2 reduction,[71–75] a rising field in chemistry since the discovery of CO_2's major impact on the anthropogenic greenhouse effect. The IR bands located between λ = 2280 to 2400 cm^{-1} are important because electromagnetic irradiation from the sun in this area is absorbed by the carbon dioxide and not by the earth.[76,77] However, the reduction of CO_2 as part of a large-scale technology to remove the greenhouse gas caused by humanity from the atmosphere is described to be "*ridiculous*",[78] but the catalytic transformation of CO_2 would provide a cheap source of C_1 fragments.[78] **Re**(I) carbonyl complexes provide the possibility to reduce carbon dioxide photochemical catalytically.[79–81] This subsection is not part of this thesis, and only the electrochemical pathways will be described.

Pioneering work in the field of electro catalysed reduction of carbon dioxide was done by Lehn and co-workers using 2,2'-bipyridine (**bpy**) as a ligand. The most striking point in these results was the high Faradaic efficiency of 98 %.[82] Sullivan *et al*.[81] proposed the mechanism and intermediates be verified by different groups using infrared spectroelectrochemistry (SCE)[83] and EPR techniques[84]. Besides the unsubstituted **bpy** ligand, substituted derivatives were also investigated, but the substitution pattern is neglected for clarity. Most of the intermediates (Scheme 52 page 158, M = **Re**, **X** = Cl) were first observed and then chemically synthesized, isolated, and characterized. Starting from the triscarbonyl complex **A,** Kubiak *et al*. characterized the first reduced species [*fac*-**Re**(**bpy**)(CO)$_3$Cl]$^{-1}$ (**B**), [**Re**(**bpy**)(CO)$_3$] (**C**), and [**Re**(**bpy**)(CO)$_3$]$^{-1}$ (**F**).[85] The electrochemical synthesis of the dimer [**Re**(**bpy**)(CO)$_3$]$_2$ (**E**) was reported,[86] but could not be verified by Extended X-ray Absorption Fine Structure (EXAFS) experiments[87] and was recently determined to be endergonic due to the necessity of an LMCT, since the first two reductions take place at the **bpy**.[87,88] In the solid state structure of the [**Re**(**bpy**)(CO)$_3$]$^{-1}$ the chelating ligand shows high structural accordance with **bpy**$^{2-}$. This anion was determined to be the reactive species.[89] The loss of the Cl$^-$ anion occurs due to σ-π* interactions.[90,91] Adduct formation with solvent (**D**) is favoured over the five coordinated complex **C**. With CO_2 adduct (**H**), the reduction cycle starts (Scheme 52, green box). The bonding results from σ- as well as a π-interaction between the **Re**(I) and

the carbon atom, as DFT calculations showed.[89] The protonated form (**I**) was verified in the presence of an acid during infrared spectroelectrochemistry (IR-SEC).[74] However due to its instability, only the methyl ester was analysed by X-ray diffraction analysis.[92–94] An additional proton source is not needed for the carbon dioxide reduction with **Re**(I) complexes, since the solvent (MeCN) or supporting electrolyte provides them by Hofmann degradation.[86,95] Nonetheless, the presence of Brønsted acids favours the catalysis and protonation involved in the rate-determining step.[89] Independent from the pKa value of the acids, no formation of [**Re**(**bpy**)(CO)$_3$H] (**G**) was observed.[96] The protonation of **I** is thermodynamically favoured over its reduction.[88]

In contrast to rhenium, manganese is more frequently represented in in the earth crust and was assumed not to catalyse the carbon dioxide reduction.[72,83,97] This assumption was caused by the lack of current enhancement during cyclic voltammetry measurements in a CO_2-saturated solution in the absence of water.[83] In contrast to the **Re**(I) complexes, the water addition is critical for the carbon dioxide reduction with **Mn**(I) carbonyl complexes, as Deronzier *et al.* recently showed.[98] In this context, the enhancement of the catalytic activity by the presence of acids was found for the **Mn**(I).[99] However, in contrast to [**Re**(**bpy**)(CO)$_3$], the manganese analogue of **C** dimerizes rapidly and thereby, the turnover frequency (TOF) decreases. This result could be demonstrated nicely by Kubiak *et al.* using steric demanding groups to prevent the dimer formation and enhance the TOF significantly.[100] The dimer can be cleaved by a two electron reduction, yielding the active catalytic anion **F**.[98] However, the over potential for the electrochemical formation of the reactive species is lower than for [**Re**(**bpy**)(CO)$_3$Cl], making **Mn**(I) carbonyl complexes an attractive alternative.[101] From the protonated CO_2 adduct **I**, manganese accesses at a potential of E = -1.4 V (vs. SCE), the protonation-first pathway *via* intermediate **K**. At a higher potential of E = -1.8 V (vs. SCE), both metals are forming **J**. Using the reduction first pathway for the CO_2 reduction. The C-O bond cleavage yields **L** and the catalyst is regenerated by a 1 e$^-$ reduction.[88]
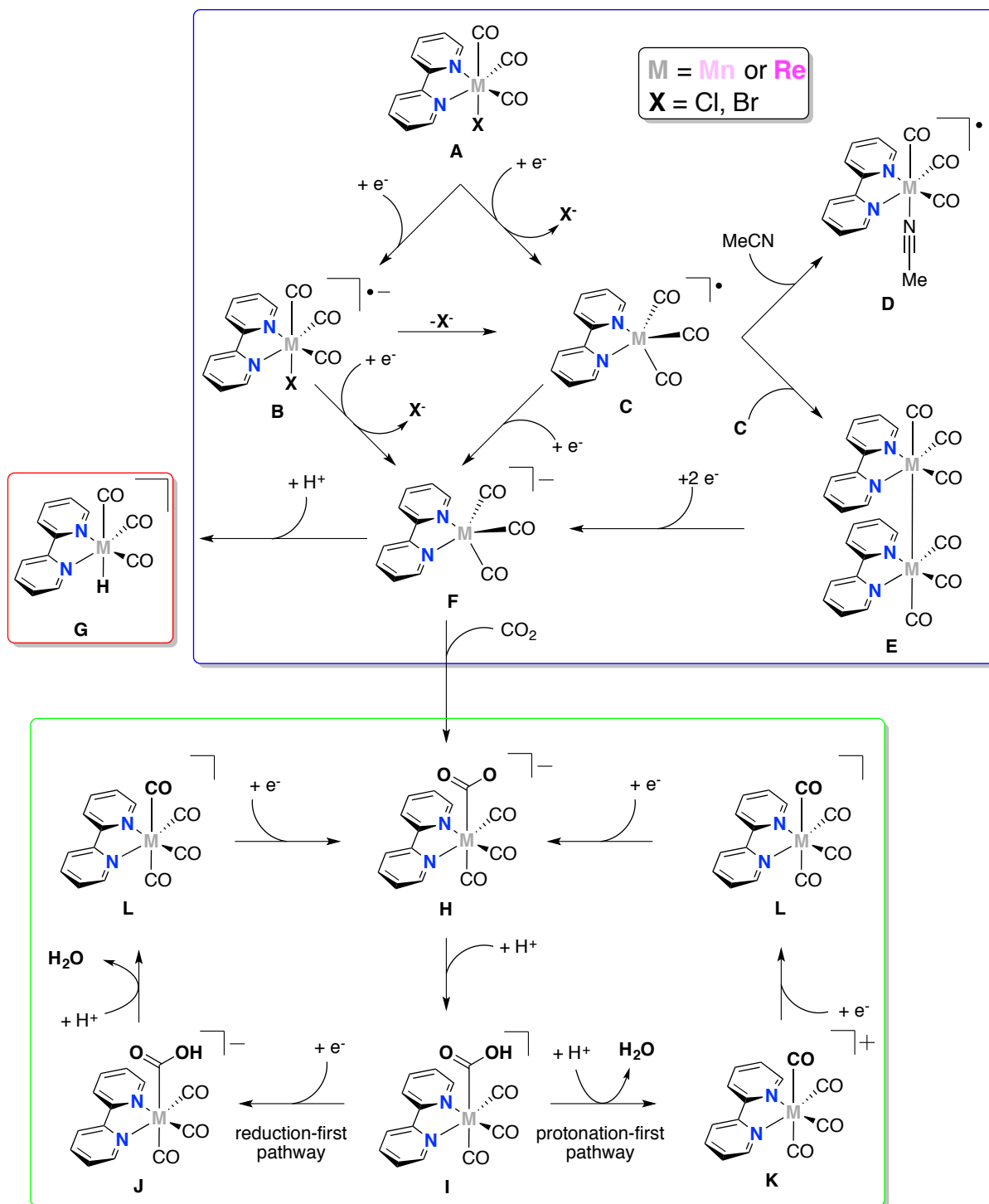
Scheme 52: Carbon dioxide reduction with Mn(I) and Re(I) bpy complexes. Blue box: activation pathways. Red box: Proton reduction. Green box: Catalysis pathways for CO2 reduction. Mechanisms proposed by Cater *et al.*.[88]

Synthesis of Triazaphosphole and Triazole-based Mn(I) Carbonyl Complexes

The synthesis of the **Re**(I) compounds **C12** and **C14** was described above. The compounds bearing TMS groups in 5-position are not included in the investigations. The corresponding **Mn**(I) complexes were obtained by slightly modified reaction conditions

as used for the **Re**(I) complexes (Scheme 53). The reaction was performed with a higher concentration of the ligands and metal precursor. The second change in parameters was the reduced reaction temperature to T = 45 °C. Using these parameters, single crystals suitable for X-ray diffraction could be obtained directly from the reaction mixture.
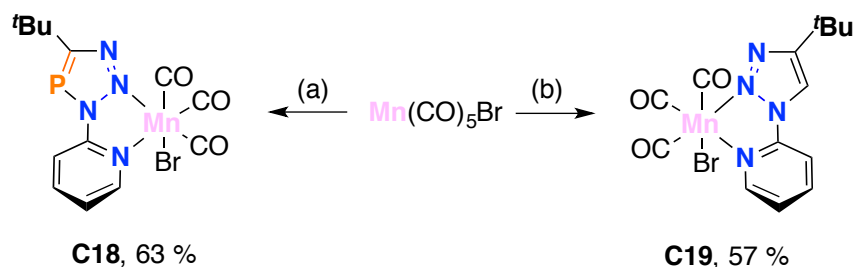
Scheme 53: Synthesis of the complexes **C18** and **C19**. Racemic mixtures obtained, only one enantiomer displayed. Reaction conditions (a): 1.1 eq. **L12**, 1 eq. Mn(CO)$_5$Br, DCM, 8 h 45 °C. (b): 1.1 eq. **L14**, 1 eq. Mn(CO)$_5$Br, DCM, 8 h, T = 45 °C. Yields refer to the crystalline material.

The molecular structure of the **Mn**(I) complexes obtained from the reaction solution exhibit also *facial* geometry as in the **Re**(I). Within in investigations of the triazaphosphole based metal complexes **C12** and **C18** (Figure 59), some interesting observations were made. The inter-ring distance in the homologous metal complexes is with 1.414(2) Å the same as in the corresponding **Re**(I) complex, taking the measurement errors into account. Small differences are discovered in the P-C^1 distance, as the bond in the **Mn**(I) is 0.03 Å shorter. Also, the inter-pnictogen distance P-N^1 is with 0.015 Å slightly longer in the manganese complex **C18**. The distances between the nitrogen bonds do not change significantly within the measurement errors.

For the triazole based complexes, the most striking difference between the **Mn**(I) and **Re**(I) complexes is the 0.01 Å shortened inter-ring distance and compared to the free ligand, a difference of 0.02 Å is notable. The other bond lengths in the two triazole based complexes remain the same concerning measurement errors.

The comparison of both **Mn**(I) complexes reveals a high similarity. The distances from the metal centre towards the N^2 and N^4 nitrogen atoms are almost identical as are the bite angles with 77.9° (**C18**) and 78.1° (**C19**, Figure 60), respectively. A small exception is found at the carbonyl carbon atom in transposition to the N^2. In the case of the triazaphosphole-based ligand, the distance is marginally larger, while the carbon-oxygen bond is not influenced.
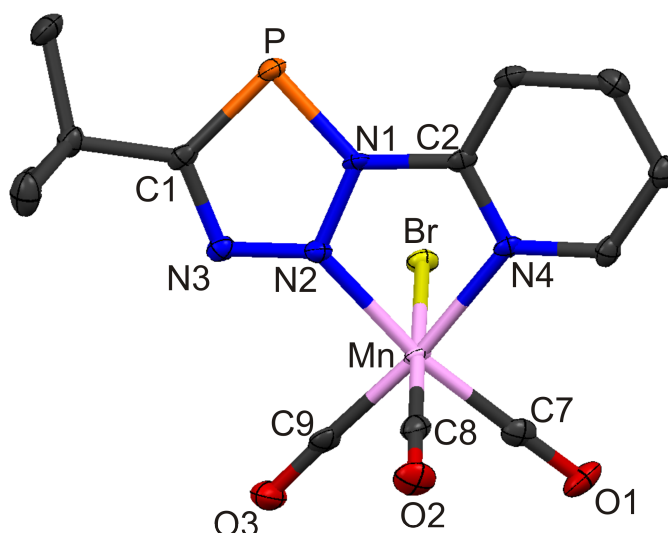
Figure 59: ORTEP plot of the metal complex **C18**. Displacement ellipsoids are shown at the 50% probability level. Hydrogen atoms are omitted for clarity. Presentation of only one independent molecule; non-coordinated CH_2Cl_2 molecules are omitted for clarity. Selected bond lengths (Å) and angles (°): P(1)-C(1): 1.724(3), P(1)-N(1): 1.699(2), N(1)-N(2): 1.358(3), N(2)-N(3): 1.299(3), N(3)-C(1): 1.360(3), N(1)-C(2): 1.414(3), N(2)-Mn(1): 2.006(2), N(4)-Mn(1): 2.045(2). N(1)-P(1)-C(1): 85.8(1), N(4)-Mn(1)-N(2): 77.93(8), N(2)-N(1)-C(2)-N(4): 3.7 (3).
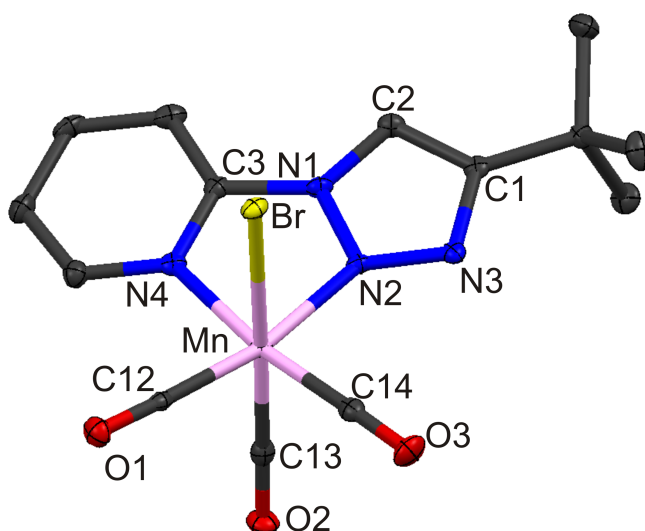
Figure 60: ORTEP plot of the complex metal **C19**. Displacement ellipsoids are shown at the 50% probability level. Hydrogen atoms and non-coordinated CH_2Cl_2 molecule are omitted for clarity. Selected bond lengths (Å) and angles (°): C(1)-C(2): 1.371(4), C(2)-N(1): 1.361(3), N(1)-N(2): 1.355(3), N(2)-N(3): 1.300(3), C(1)-N(3): 1.374(4), N(2)-Mn(1): 1.999(2), N(4)-Mn(1): 2.055(1). N(2)-Mn(1)-N(4): 78.09(9). N(2)-N(1)-C(3)-N(4): -0.4(2).

These findings are in line with with the wave numbers of the carbonyl stretches obtained by infrared spectroscopy (Table 12). Obviously, no influence of the phosphorus atom on the π-back bonding is found in the metal complexes **C18** and **C19**. These findings contrast the results obtained for the **Re**(I) complexes **C12** and **C14**. Supporting this assumption, the signal in the $^{31}P\{^{1}H\}$ NMR spectrum of **C18** is with δ(DCM-d$_2$) = 195.5 ppm around $\Delta\delta$ = 10 ppm more downfield shifted than in the

160

corresponding **Re**(I) complexes (δ(DCM-d$_2$) = 184.1 ppm), indicating a less shielded phosphorus atom.

Compound	$\tilde{v}_1(CO)$ [cm^{-1}]	$\tilde{v}_2(CO)$ [cm^{-1}]	$\tilde{v}_3(CO)$ [cm^{-1}]
C18	2032	1952	1925*
			1916*
C19	2029	1968	1913

*Two different molecules in the solid-state structure were detected.

Excursion 12: Attempts for Preparing Heterobimetallic Complexes

Besides the carbon dioxide reduction, the catalytic water oxidation is also investigated within the topic of greenhouse gas reduction and environment-friendly fuels.[102–106] In this context, the cyclometalation of the complex rhenium **C12** was investigated since the metal centre blocks the N^2 and N^3 nitrogen atoms. This data provides the possibility of an exclusive binding *via* the phosphorus atom and avoids the observed problems in the attempts to cyclometalate compound **28**. The reactions were again performed with **Rh**(III) and **Ir**(III) metal precursors (Scheme 54). While iridium complexes are known for their water oxidizing ability,[107] rhodium is used in the first place as a tool for structural investigations due to its NMR active [103]Rh core.
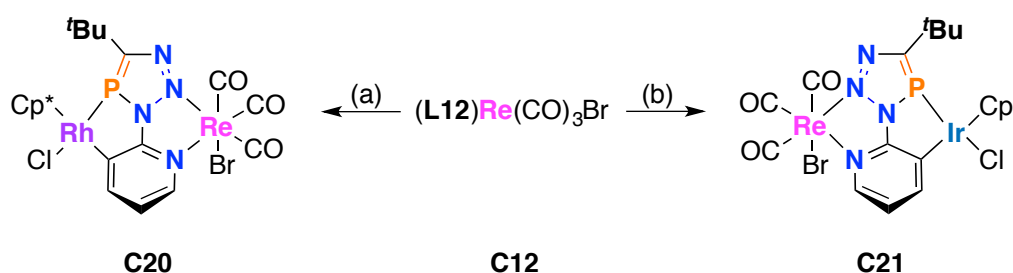
Scheme 54: Attempts in synthesis of heterobimetallic complexes **C20** and **C21**. Reaction conditions (a): [Cp***Rh**Cl$_2$]$_2$/**C12**/NaOAc 1:2:2 eq., THF, 60 d 80 °C. (b): [Cp***Ir**Cl$_2$]$_2$/**C12**/NaOAc 1:2:2 eq., THF, 31 d, T = 80 °C.

The reactions were performed under slightly modified conditions for the cyclometalation of phosphinines by using THF instead of DCM.[54] The reaction progress was monitored by means of ^{31}P{^{1}H} NMR spectroscopy. Contrary to the cyclometalation

of **28**, the reaction using the **Rh**(III) dimer resulted in a quite clean conversion to a new compound indicated by the resonance located at δ(DCM-d$_2$) = 133.1 ppm (Figure 61). This doublet has a coupling constant of $^1J_{\text{P-Rh}}$ = 137.1 Hz and is attributed to the **P**-**Rh** bond. The coupling constant is similar to the one observed in complex **C2**, where nitrogen elimination was expected to occur. However, the difference in the chemical shifts is still about $\Delta\delta$ = 20 ppm, which might be due to the higher oxidative state of the metal centre, but the loss of nitrogen would require the previous splitting of the rhenium nitrogen bonds (Chapter 3.1). Attempts of purification failed and only lead to decomposition of the product. Also, different crystallisation approaches were made, but no crystalline material could be obtained up to this point.
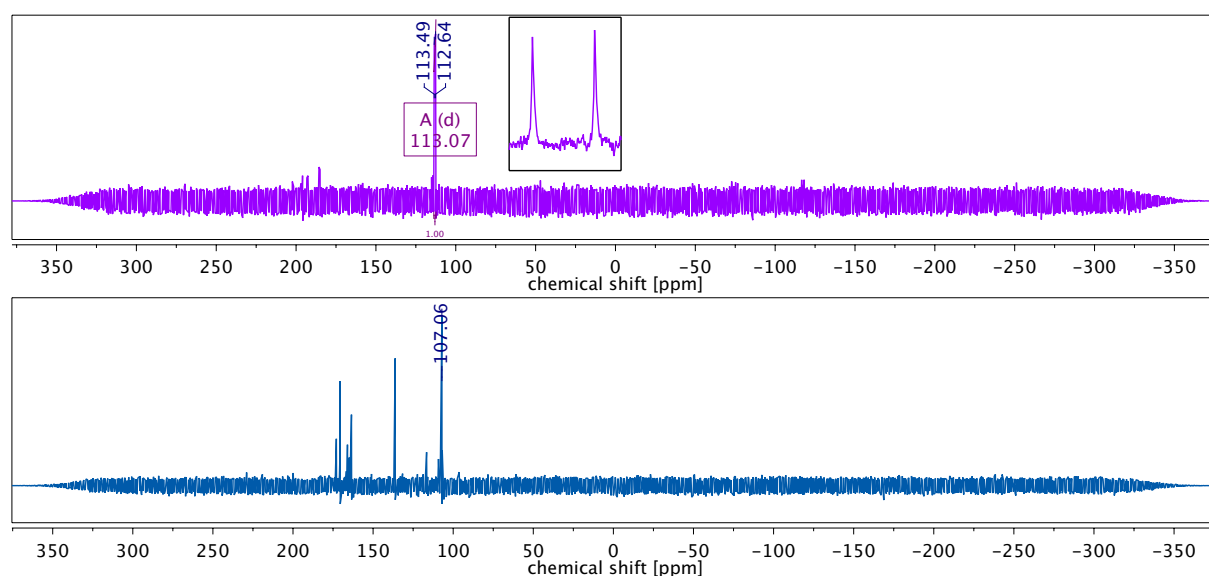
Figure 61: (**Top**) ^{31}P{^{1}H} NMR spectrum of the reaction mixture of **C20**. (**Bottom**) ^{31}P NMR spectrum of the reaction mixture of **C21**.

In cyclometalation reaction using **Ir**(III) dimer as metal precursor a different reaction behaviour was observed. The reaction was stopped after 31 days. The ^{31}P{^{1}H} NMR spectrum shows multiple side products and a major resonance at δ(DCM-d$_2$) = 107.1 ppm. As several attempts with lower temperature did not lead to a significant change in the ^{31}P{^{1}H} NMR spectra, the cyclometalation reaction with **Ir**(III) dimer was discontinued and the cyclic voltammetry measurements were only performed with the **Mn**(I) and **Re**(I) complexes.

Cyclic Voltammetry Measurements with Re(I) and Mn(I) Complexes

To investigate whether the Mn(I), as well as the Re(I) complexes, are catalysts for electrochemical carbon dioxide reduction, cyclic voltammetry measurements were performed, starting under an argon atmosphere (Figure 62, green lines). The measurements exhibited three irreversible reductions for compound **C12** at E_P^{Red} = -1.036 V, E_P^{Red} = -1.196 V, and E_P^{Red} = -1.702 V. A rerun of the experiment with a saturated carbon dioxide solution did not show any current enhancement and by this no CO_2 reduction under the given conditions, but the single redox events shifted slightly (E_P^{Red} = -1.049 V, E_P^{Red} = -1.147 V and E_P^{Red} = -1.688 V). Further measurements were performed with 5% water in the solvent. The importance of Lewis acids has been shown for both transition metals[99,108] and might be substantial for the triazaphosphole based complex as well. With the addition of water, a current enhancement was detected. However, the observed current enhancement does not resemble any other Re(I) based carbon dioxide reduction. Questionable is also the current improvement in the area around the maximum of E = -2.340 V, as an additional reduction event is found.
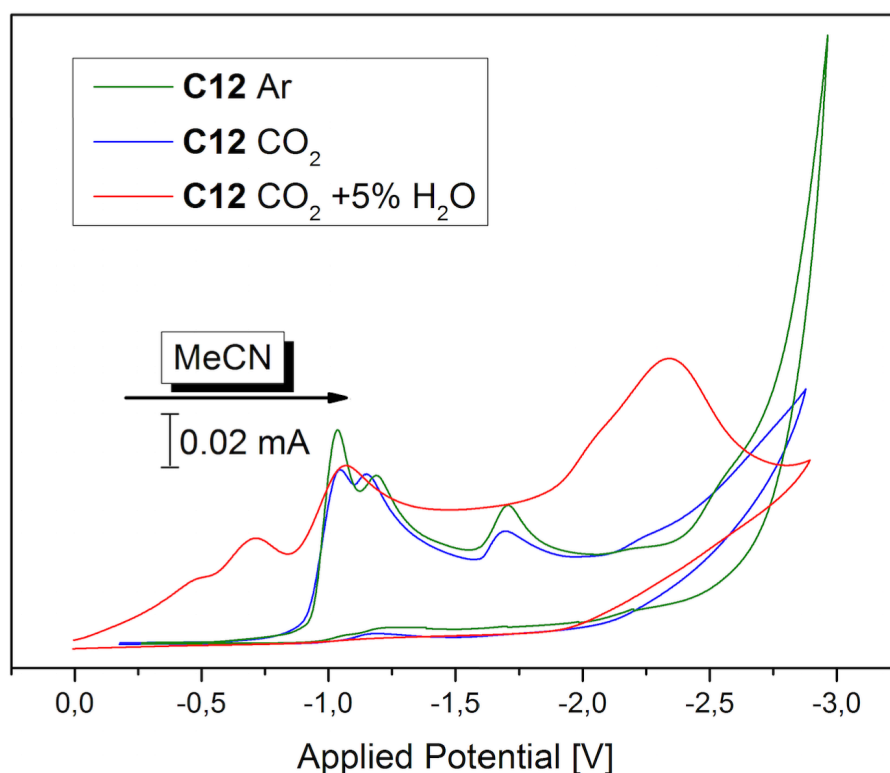
Figure 62: Cyclic voltammogram of rhenium based complexes **C12**. Conditions: 1 mM complex in MeCN with 0.1 M NBu$_4^+$PF$_6^-$ supporting electrolyte. Referenced to Fc/Fc*, v = 100 mV/s. Argon atmosphere (green), saturated CO_2 solution (red) and saturated CO_2 solution with 5 % H_2O.

The triazole based **Re**(I) complex **C14** (Figure 63) showed under argon atmosphere only two reductions at E_P^{Red} = -1.55 V and E^{Red} = -2.40 V, that might be quasi-reversible. Using a saturated carbon dioxide atmosphere, in the area of the previously first reduction two electron transfers take place (E_P^{Red} = -1.53 V and E_P^{Red} = -1.68 V). Further, the reduction at E_P^{Red} = -2.10 V vanished and a small current enhancement is found above E = -2.55 V. Rather than the results obtained for **C12**, these results point in the direction of CO_2 reduction. At last the solution was treated with 5 % water to investigate if the presence of an oxygen acceptor influences the reaction. From the cyclic voltammogram a current enhancement is evident, and two irreversible reductions are found at E_P^{Red} = -1.55 V and E_P^{Red} = -1.71 V. The current has a noticeable high value in the area from E = -1.36 V to E = -2.39 V and then drops again. Again, conclusions about catalytic carbon dioxide reduction based only on the CV data are difficult to make. The comparison to the cyclic voltammogram of [**Re**(I)(**bpy**)(CO)$_3$Br][109] evinces a lower first and second reduction in **C12**, while **C14** is in the same area. An exact determination is not possible since the exact potentials were not reported.
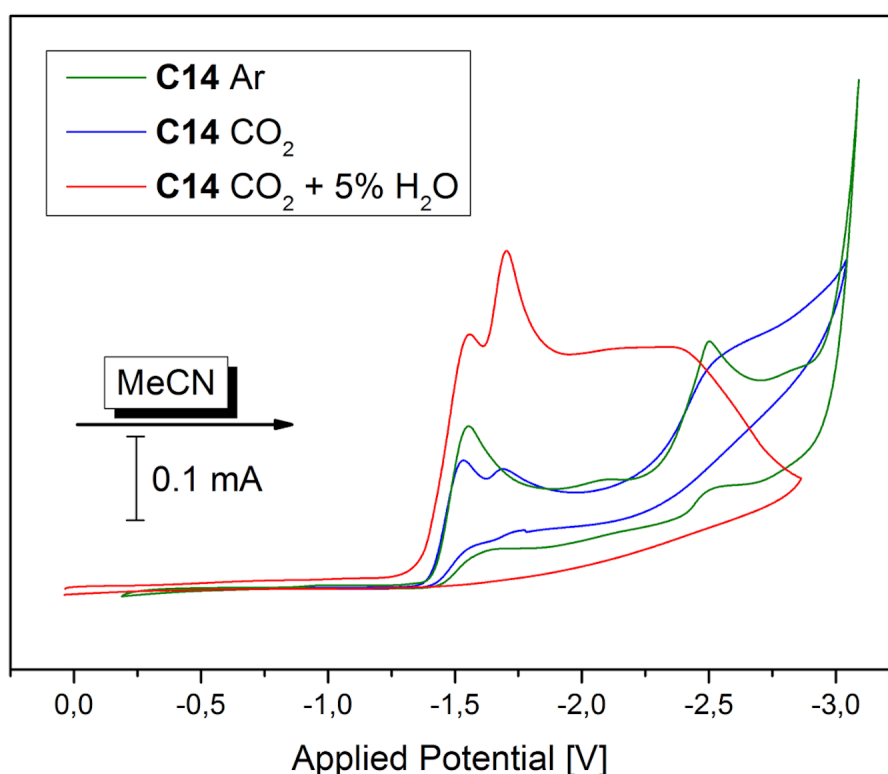
Figure 63: Cyclic voltammogram of rhenium based complexes **C14**. Conditions: 1 mM complex in MeCN with 0.1 M NBu$_4^+$PF$_6^-$ supporting electrolyte. Referenced to Fc/Fc*, v = 100 mV/s. Argon atmosphere (green), saturated CO_2 solution (red) and saturated CO_2 solution with 5 % H_2O.

Measurements using the manganese complexes **C18** (Figure 64) and **C19** (Figure 65) as catalysts were performed under the exclusion of light since light-sensitivity of theses complexes had been reported.[110,111] Both complexes show four reductions under argon at $E_P{}^{Red}$ = -1.06 V, $E_P{}^{Red}$ = -1.30 V, as well as $E_P{}^{Red}$ = -1.87 V, and $E_P{}^{Red}$ = -2.45 V. In the triazole based manganese complex **C19,** the values shift to $E_P{}^{Red}$ = -1.47 V, $E_P{}^{Red}$ = -1.73 V, as well as $E_P{}^{Red}$ = -2.52 V, and $E_P{}^{Red}$ = -2.95 V, with the third reduction being possibly quasi-reversible. For both complexes, a lower reduction potential is found than for the [Mn(I)(**bpy**)(CO)$_3$Br] reported. The first reduction occurs at E^{Red} = -0.86 V and is quasi-reversible using a CO_2 saturated anhydrous acetonitrile solution. The previously observed reduction process at E^{Red} = -1.56 V showed current enhancement in the case of the triazaphosphole-based complex **C18**. The peak potential of the first two reductions does not change, while the third one is not detected anymore. The last reduction is found at $E_P{}^{Red}$ = -2.90 V. The addition of water leads to a decrease of the last reduction wave. For **C18,** three redox processes are detected, at $E_P{}^{Red}$ = -1.27 V, $E_P{}^{Red}$ = -1.38 V, and a broad wave is located at $E_P{}^{Red}$ = -2.45 V. Current enhancement using Mn(I) carbonyl complexes is unlikely but had been observed before in a hydroxyl functionalized bipyridine complex of type [Mn(**bpy**(OH)$_2$)(CO)$_3$Br].[111]
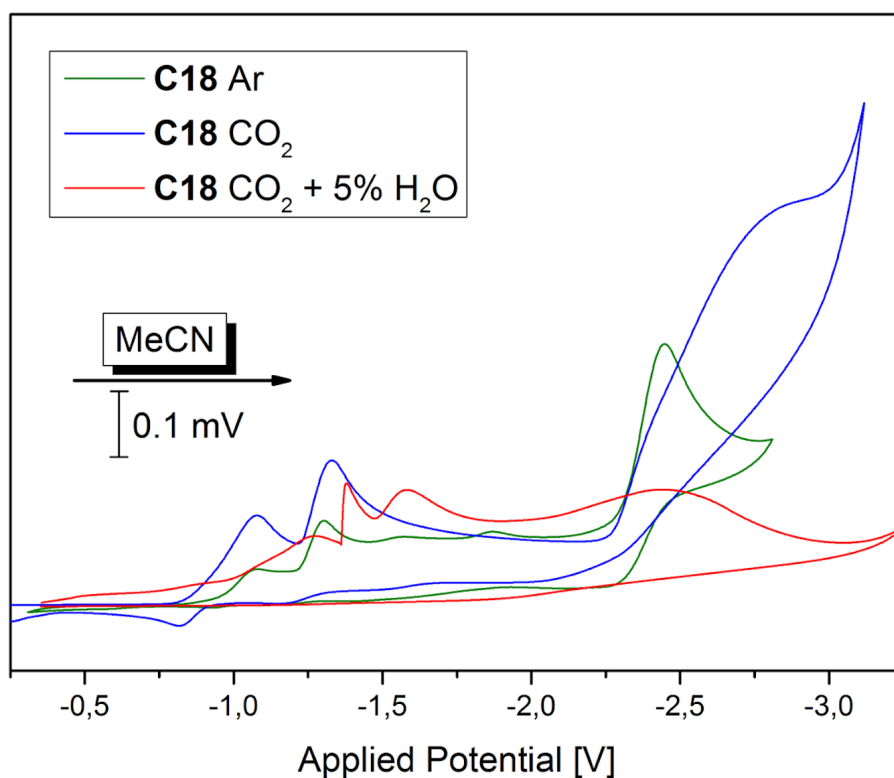
Figure 64: Cyclic voltammogram of manganese based complexes **C18**. Conditions: 1 mM complex in MeCN with 0.1 M NBu$_4{}^+$PF$_6{}^-$ supporting electrolyte. Referenced to Fc/Fc*, v = 100 mV/s. Argon atmosphere (green), saturated CO_2 solution (red) and saturated CO_2 solution with 5 % H_2O.

The same authors also describe a deterioration of current during the catalysis with 5 % water addition. The attempts at the electrochemical CO_2 reduction with the triazole based manganese complex **C19** pointed out a high instability. In a saturated, CO_2 solution, the compound decomposed completely within the cyclic voltammetric investigations. A second approach had to be made to obtain a complete electrochemical picture of the compound. However, for the catalysis in anhydrous acetonitrile solution, saturated with CO_2, no satisfying cyclic voltammogram could be obtained, the most promising is displayed in Figure 65 (blue line). The first and second reductions are located at lower potentials (E^{Red} = -1.32 V, E_P^{Red} = -1.58 V) compared to the measurements in argon. Contrary, the measurements with 5 % water in the solvent exhibits a shift to higher potentials (E_P^{Red} = -1.54 V, E_P^{Red} = -1.88 V). Further, like in the other cases, an enhancement of the current after the second reduction is noticeable. For carbon dioxide reduction, an important requirement was determined by the need of the right reduction potential, demonstrated by the variation of the substitution pattern of the **bpy** ligand with electron withdrawing and donating groups. For manganese, it was found that the catalysis already proceeds at E = -1.4 V (vs. SCE), while a minimal potential of E = -1.76 V (vs. SCE) is required for the rhenium complexes.[82,88,112]
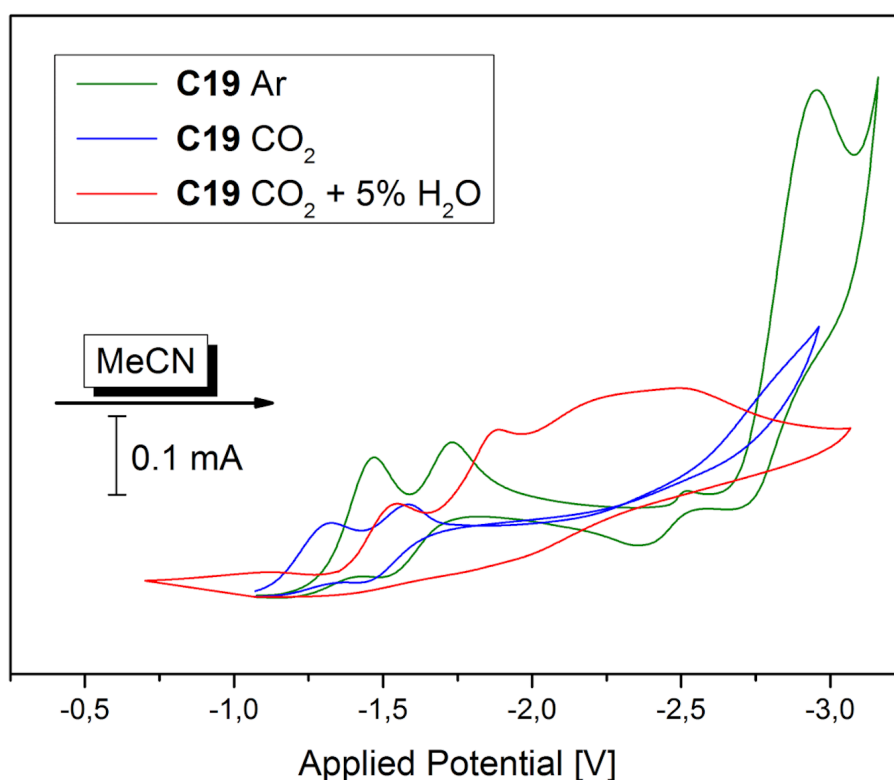
Figure 65: Cyclic voltammogram of manganese-based complexes **C19**. Conditions: 1 mM complex in MeCN with 0.1 M NBu4+PF6- supporting electrolyte. Referenced to Fc/Fc*, v = 100 mV/s. Argon atmosphere (green), saturated CO_2 solution (red) and saturated, CO_2 solution with 5 % H_2O.

As a consequence, the possibility for efficient CO_2 reduction using the presented complexes can be excluded. Only **C19** fulfils this requirement but rapidly undergoes decomposition. Furthermore, from the performed electrochemical experiments, it can be derived that the triazaphosphole-based complexes are easier to reduce than their phosphorus lacking analogues. Although the free ligands were not investigated by means of cyclic voltammetry, the phosphorus atom, due to the more stabilized LUMO in triazaphosphole containing ligand **L12**, might cause the easier reduction in **C12**. Triazaphosphole and triazole based **Re**(I) carbonyl complexes show a proportional redox activity compared to their free ligands (Chapter 3.1).[113] Taking this into account, and the fact that neither the carbonyl stretching vibrations nor the molecular structures of the **Mn**(I) complexes **C18** and **C19** show strong evidence for an influence of the ligand, it might be possible to locate the first reduction on the ligands. This assumption is substantiated by the literature reports, as the first reductions are assigned to the ligands. This property was attributed to the shorter interring distances of the bipyridine ligands in the chemically reduced **Re**(I) carbonyl complexes. Theses distances are similar to the ones observed in the **bpy**$^{2-}$.[86] Contrary, for manganese complexes, the single electron reduction yields a rapid dimerization, and the molecular structure of the crystal does not attest to reduction at the ligand in the dimer.[110] However, DFT calculations revealed a conjugated system for the HOMO over the whole complex, including ligand and metal centre.[84,86]

However, for a detailed analysis, infrared spectroelectrochemistry experiments are necessary to determine whether carbon dioxide reduction takes place at all or if other side reactions occur. Further, the products of the catalysis should be analysed using gas chromatography for supporting the IR-SCE measurements. For these investigations, chemical 1 e$^-$, as well as 2 e$^-$, reductions are necessary for the assignment of the carbonyl stretches during the spectroelectrochemistry experiments.

3.2.4 Case-study of an Autocatalytic Variant of the Copper-Catalysed Alkyne Azide Cycloaddition (CuAAC)

Synthesis and Characterisation of Triazaphosphole and Triazole Based Copper(I) Complexes

The coordination chemistry of 3H-1,2,3,4-triazaphospholes is flexible and strongly depends on the nature of the metal, while, in the bidentate triazaphospholes, additionally on the nature of the binding side (Chapter 1, Chapter 3). Although late transition metals in low oxidation states were used, the nitrogen lone pairs of the N^1 and N^2 predominantly coordinate the metal ions in a chelate fashion, leaving the phosphorus atom lone pair for further coordination (Chapter 3.1 or 3.2.1), including the electron rich noble coin metal Ag^+.[58] These observations lead to the assumption that the coordination of a **Cu** (I) ion proceeds also in the $N^{Py}\wedge N^2$ fashion (Scheme 55).
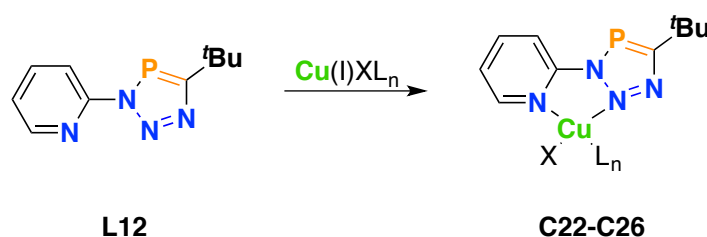
Scheme 55: Generalised reaction equation of Cu(I) complex synthesis. Reaction conditions: 1 eq. Cu(I)XL$_n$, DCM, 1 h, r.t..

Surprisingly, the synthesis of **Cu**(I) complexes **C22-C26** (metal precursors see Table 13) were unsuccessful in DCM or MeCN at room temperature, besides the formation of **C24**. Varying the reaction temperature or using an ultrasonic bath failed as well, leading to decomposition, as observed in the ^{31}P{^{1}H} NMR spectra. THF was not used, since polymerisation was observed, as known for the phosphinine based **Cu**$^+$ complex.[114]

Table 13: Chemical shifts in ^{31}P{^{1}H} NMR spectra obtained from the reaction mixtures of **C22-C26** in DCM.

	C22	**C23**	**C24**	**C25**	**C26**
Cu(I)XL$_n$	**Cu**Br•SMe$_2$	**Cu**I•SMe$_2$	[**Cu** OTf]•C$_6$H$_6$	[**Cu**(MeCN)$_4$]BF$_4$	[**Cu**(MeCN)$_4$]PF$_6$
δ[ppm]	164.2*	165.6*	178.3	174.7*	170.4*

*assigned starting material.

In contrast to the methylene bridged chelating ligands **L4** and **L5**, the chemical shifts in ^{1}H and ^{31}P{^{1}H} NMR spectroscopy did not sufficiently change to conclude metal complex

formation. Obviously, the higher π-donating properties in the non-conjugated ligands systems are imported in the coordination chemistry, as shown in Chapter 3.1.

Single crystals suitable for X-ray diffraction analysis of **C24** were obtained directly from the reaction solution (Figure 66, page 170), while **C27** precipitated as yellow powder (Scheme 56). Recrystallisation was not successful due to the poor solubility of the complex. Neither single crystals nor any participate was obtained from crystallisation attempts from a solution in MeCN, which might be attributed to a high solubility. Further, the solvent could not be removed in high vacuum form the complex. Heating led to decompositions of the complex.

Different solvents were screened to investigate the solubility of the complexes for characterising by means of ^{1}H and ^{13}C NMR spectroscopy, including THF. In case of **C24**, the sample gelated over night, indicating the polymerisation of the solvent, which did not occur in case of **C27**. The polymerisation was not investigated further.

Single crystals of **C27** suitable for X-ray diffraction analysis were finally obtained successfully by top-layering a frozen solution of **L14** with a copper(I) triflate benzene complex (1:0.5 ratio) in THF and slowly allowing the solid to warm up over night (Figure 67 page 171). Also in this case, no polymerisation was observed.
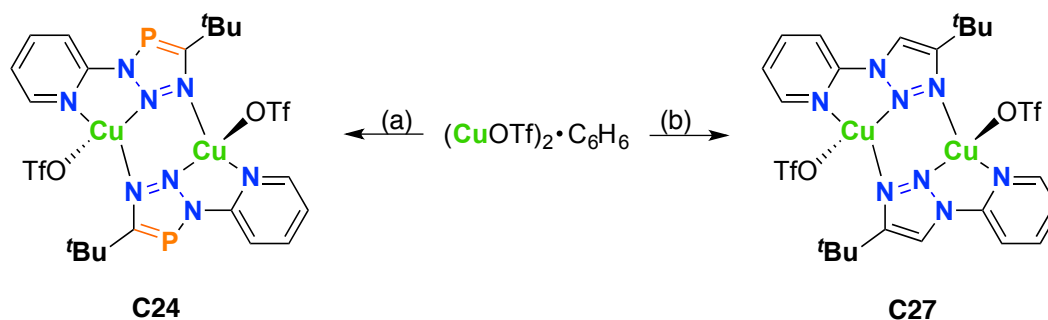
Scheme 56: Reaction equation for the synthesis of **C24** and **C27**. Dimer formation is confirmed by XRD measurements (*vide infra*). Reaction conditions (a): 1 eq. **L12**, 0.5 eq. (**Cu**OTf)$_2$•C$_6$H$_6$, DCM, 5 min, r.t. (b) 1 eq. **L14**, 0.5 eq. (**Cu**OTf)$_2$•C$_6$H$_6$, DCM, 5 min, r.t..

Interestingly, C24 and C27 turned out to be binuclear **Cu**(I) species, which are extremely rare. The metal ion is chelated by the pyridyl and the triaz(aphosph)ole N^2 nitrogen atoms, while the N^1 lone pair provides an additional binding site for the second copper atom. The coordination sphere is completed by coordination of the counter ion of each metal centre, as generally observed for triazole based **Cu**(I), **Ag**(I) as well as **Cu**(II) chelate complexes.[115–119]

Due to this unusual strained geometry, the copper shows neither a clear square planar nor a clear tetrahedral arrangement (Figure 66). While the counter ion protrude the plane of the nitrogen atoms, the $O(1)$-Cu^1-$N(X)$ angles values ($N(X)$ = N^2: 96.48, N^3: 100.76, N^4: 95.83) are less than in the ideal tetrahedral, but almost close to a rectangular, the $N(X)$-Cu^1-$N(Y)$ ($N(Y)$ = N^{2-b}, N^{3-b} and N^{4b}) angles values are contrary any prediction. The angle between the chelating nitrogen atoms of the ligand and the metal ion is with 77.4° smaller than expected, while the N^3-Cu-N^2 angle is 107.7 with close to the ideal tetrahedral angle, but the one between N^2-Cu-N^4 is almost 159° and way larger than expected. The distances between the metal centre and the nitrogen atoms are also quite different. The most nucleophilic N^3 nitrogen atom binds the **Cu**(I) with the lowest distance (1.94 Å), while the N^2–Cu bond is longer (2.21 Å).

However, the torsion angle of the biaryl compound is slightly twisted (-12.55 °) and in contrast to the corresponding **Re**(I) complex, the inter-ring distance is minimal longer, compared to the free ligand. The similarities between both structures are quite obvious, and can be proven by comparing the structural details.
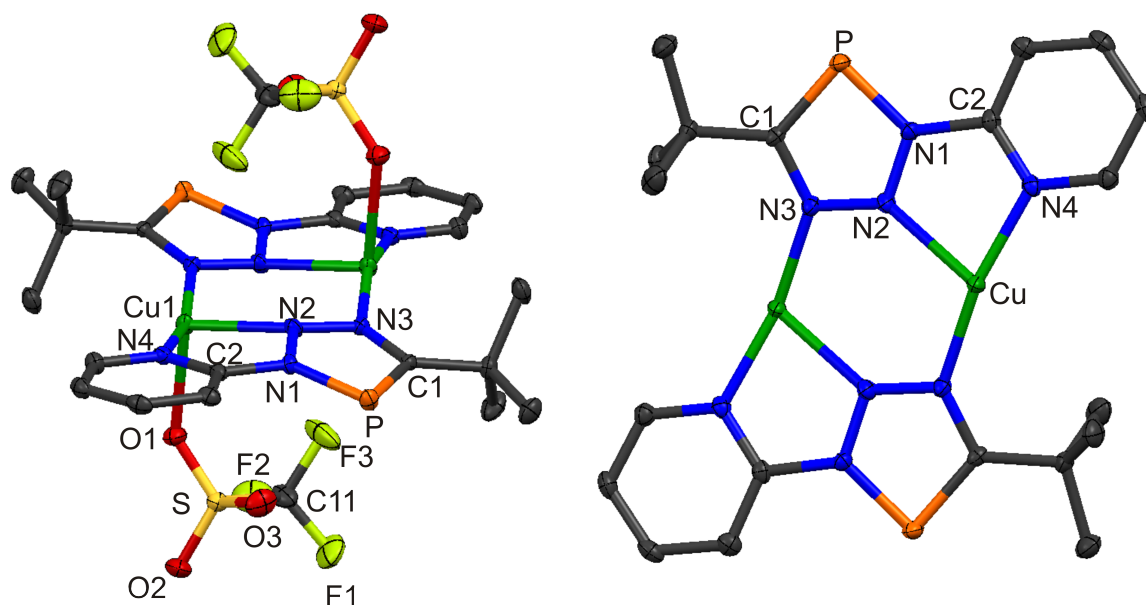
Figure 66: Molecular structure in the crystal of **C24**. Left: total structure. Right: top view, counter ions omitted for clarity. Displacement ellipsoids are shown at the 50% probability level. Hydrogen atoms are omitted for clarity. Selected bond lengths (Å) and angles (°). P(1)-C(1): 1.722, P(1)-N(1): 1.705, N(1)-N(2): 1.334, N(2)-N(3): 1.315, N(3)-C(1): 1.361, N(1)-C(2): 1.438. N(2)-Cu(1)-N(4): 77.36, N(3)-Cu(1)-N(2): 107.66, N(2)-Cu(1)-N(4): 77.36. N(2)-N(1)-C(2)-N(4): -12.55.

The geometry around the copper atom is similar, which might be attributed the slightly enlarged torsion angle of the two ring systems (-18.7° in **C27**, Figure 67). Furthermore, the distances between the metal ion and the nitrogen donor atoms are very similar

(Cu-N^3: 1.925 Å, Δ = 0.013 Å, Cu-N^4: 1.969 Å, Δ = 0.002 Å) with Cu-N^2: 2.239 Å (Δ = 0.032 Å) showing longer bonds for **C27** compared to **C24**. The bite angle inside is with 78.2 ° somewhat larger than in **C24** (77.36 °). A similar situation is found at the N^3-Cu-N^4, that is with 166.8° larger than in **C24** (160.9 °). In contrast, the N^2-Cu-N^3 angle is with 101.0 ° smaller than in the corresponding triazaphosphole complex (107.7°). In addition to this, the inter-ring distance in the triazole based **Cu**(I) complex increases (Δ = 0.01 Å). Comparing the Cu-O1 distances, it turned out that the bond in **C24** is slightly shorter than in **C27** (2.256 Å vs. 2.261 Å). Considering the frontier molecular orbital plots of both ligands, it can be assumed, that the coordination occurs only by σ- and/or π-bonding, without any significant contribution of π-back boning.
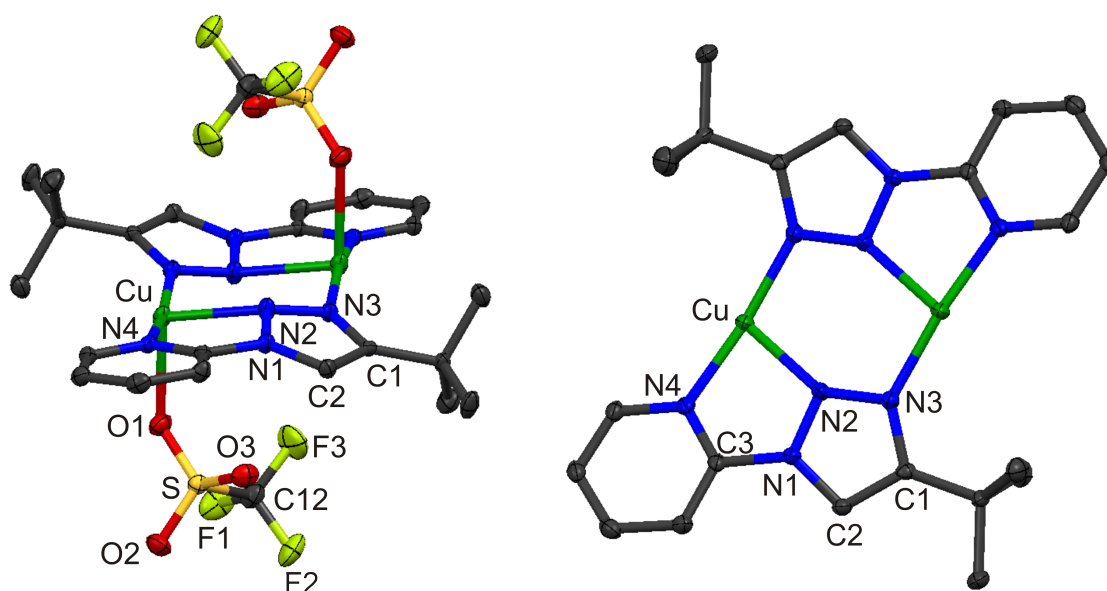
Figure 67: Ellipsoids plot **C27**. Left: Molecular structure in the crystal. Right: top view, counter ions omitted for clarity. Displacement ellipsoids are shown at the 50% probability level. Hydrogen atoms are omitted for clarity. Selected bond lengths (Å) and angles (°). P(1)-C(1): 1.722, P(1)-N(1): 1.705, N(1)-N(2): 1.334, N(2)-N(3): 1.315, N(3)-C(1): 1.361, N(1)-C(2): 1.438. N(2)-Cu(1)-N(4): 77.36, N(3)-Cu(1)-N(2): 107.66, N(2)-Cu(1)-N(4): 77.36. N(2)-N(1)-C(2)-N(4): -12.55.

Alkyne Azide Cycloaddition Reactions Catalysed by the Cu(I) Complexes

The use of carbene ligands in copper catalysed alkyne azide cycloaddition (CuAAC) was established during the last years, because of the high stability and reactivity of the deriving copper complexes. In this process, different mechanisms were discussed. The latest state of the art is a mechanism involving two copper centres, as demonstrated by Fokin *et al.*, while the group of Bertrand recently reported the solid-state structures of

the proposed intermediated. In this context, the cooperative effect of carbene copper dimers had been investigated. [120]

Further, in order to investigate catalytic competition of the triazaphospholes and triazoles based ligand systems, the complexes **C24** and **C27** were tested in the CuAAC. The reactions were carried out solvent-free and under inert conditions (Scheme 57).
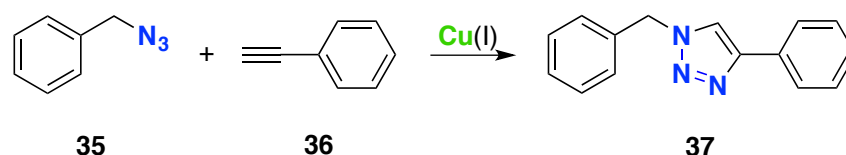
Scheme 57: Model example for the copper catalysed alkin azide cycloaddition. Reaction conditions: 1 mmol **35**, 1mmol **36**, 5 mol-% catalyst, solvent free, r.t..

From the initial results of the catalysis, a possible complexation of the catalyst with phenylacetylene was assumed. In order to investigate this finding, **C24** was treated with two equivalents of the acetylene in DCM-d$_2$ and the resulting product (Scheme 58) was investigated by means of ^{1}H as well as ^{31}P{^{1}H} NMR spectroscopy. Indeed, the formation of another complex was observed, as the shift of the acetylene proton from δ = 3.1 ppm to δ = 5.0 ppm and the resonance in the ^{31}P{^{1}H} NMR spectrum was shifted about $\Delta\delta$ = 4 ppm downfield. Further, the complex showed a higher solubility. Several crystallisation attempts were performed and the complex showed to be unstable upon vacuum drying.
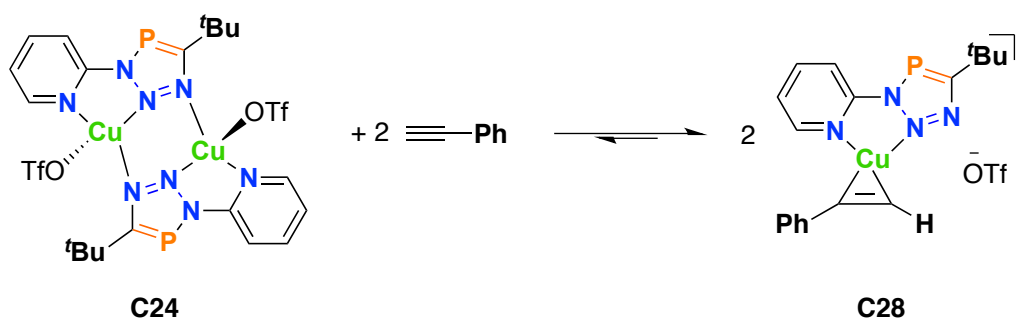
Scheme 58: Formation of **C28**. Reaction conditions: 1 eq. **C24**, 2 eq. phenyl acetylene, DCM, 5 min r.t..

This finding points out that the acetylene **Cu**(I) bond is weaker than the hydrophobic interactions between the pentane and the phenylacetylene. Single crystals suitable for X-ray diffraction analysis were obtained by cooling down the reaction mixture of **C28** to

T = -80 °C. The solid-state structure shows a square planar arrangement with η^2-coordination of the acetylyl unit to the metal centre (Figure 68).
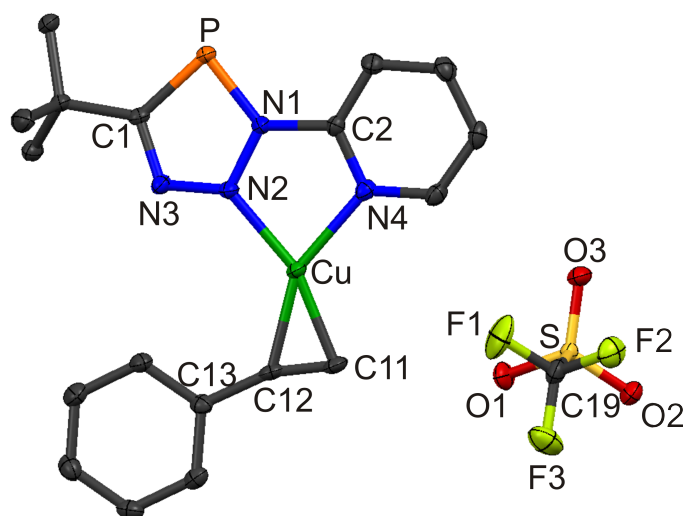
Figure 68: ORTEP plot of structure of **C28** in the crystal. Displacement ellipsoids are shown at the 50% probability level. Hydrogen atoms are omitted for clarity. Selected bond lengths (Å) and angles (°).P(1)-N(1): 1.699(3), P(1)-C(1): 1.721(3), C(1)-N(3): 1.357(4), N(3)-N(2): 1.295(3), N(2)-N(1): 1.362(3), N(1)-C(2): 1.428(4), Cu(1)-N(2): 1.977(3), Cu(1)-N(4): 1.989(2), C(11)-C(12) 1.225(4), N(1)-P(1)-C(1): 86.0(1), N(4)-Cu(1)-N(2): 81.31(9) C(13)-C(12)-C(11): 161.7(3), C(12)-Cu(1)-C(11): 36.3(1), C(12)-Cu(1)-N(4)-C(2): 178.9(2), N(2)-N(1)-C(2)-N(4): 9.1(3).

The metric parameters of the complex show only a slight contraction of the inter-ring distance between the pyridyl and the triazaphosphole unit compared to the free ligand and complex **C24**. As expected, the C^{11}-C^{12}-C^{13} angle decreased by 20 ° and the triple bond of the acetylene units is elongated by 0.02 Å upon coordination. The overall structure is almost perfectly planar. Copper triflate was chosen as reference compound and the catalytic reaction was stopped after 6 h showing 61% conversion (Table 14, Entry 1). The reaction time of the catalysis using **C27** showed full conversion after 235 min, which is a notable enhancement of the reaction towards the free copper(I) triflate. Most striking, using the triazaphosphole-based complex **C24**, the reaction was complete within 5 min. The triazole-based complex was treated during the aggregation phase with 10 mol-% DABCO in order to improve the catalyst transformation (Entry 4). Indeed the reaction time was reduced by the addition of the base. But in contrast to the previous results, the experiment and the control experiment showed significant differences in their conversion times, as the control experiment took 5 times longer. Since compound **C24** yielded full conversion within 5 min in a solvent free environment, NMR samples were taken every 30 s (Figure 69). During the catalysis violent boiling of the reaction mixture was noticed when **C24** was used. Enhancement of the catalysed cycloaddition was obtained by using 10 mol-% DABCO with reliable results and already

90% conversion was detected after 60 seconds after violently boiling occurred. However, 99% conversion of the starting material was observed after 5 min (Entry 5).

Entry	Cu-Source	Additive	Conversion [%]*	Time [min]
1	CuOTf	-	61	335
2	C24	-	100	5
3	C27	-	100	235
4	C27	DABCO	100	5/25**
5	C24	DABCO	90	1
			99	5

* Yields obtained by referencing ^{1}H NMR spectra. ** Inhomogeneous results in the performed catalysis.

Remarkably, monitoring the CuAAC performed with **C24**, in 30 second-steps point out, that full conversion after the violent boiling occurred was always observed after a critical amount of conversion (ca. 35–40%). This was further investigated and the reaction mixture was treated with 10 mol-% triazole. A clear referencing was made possible by using compound triazole **34**, due to the lack of the methylene bridge. Indeed, the violent boiling occurred faster and 96% conversion were achieved after 225 sec. During this violent boiling, it was impossible to obtain samples for this time interval, causing gaps in the conversion/time plot (Figure 69).
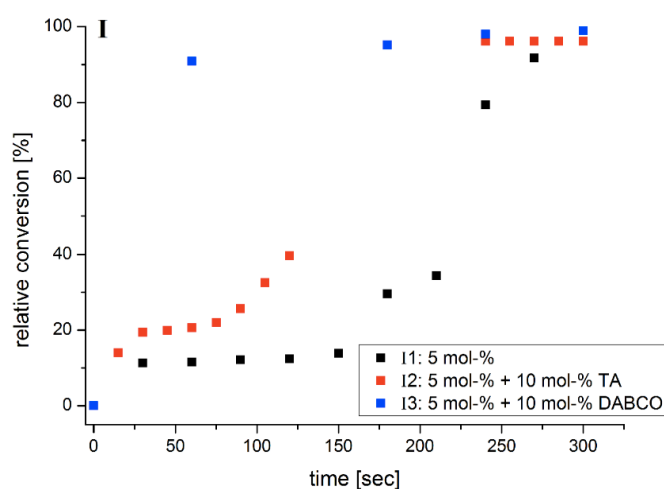
Figure 69: Conversion [%]/time [s] plot of the CuAAC, using **C24** as catalyst.

To receive further information about the effect of the triazole on the reaction, the triazole **34** was added to **C24** and phenylacetylene in a 2:1:2 ratio. Analysing the reaction mixture by means of ^{1}H and ^{31}P{^{1}H} NMR spectroscopy revealed the formation of a different complex **C29**. The acetylene proton is shifted $\Delta\delta = 0.5$ ppm to higher field (Figure 70).
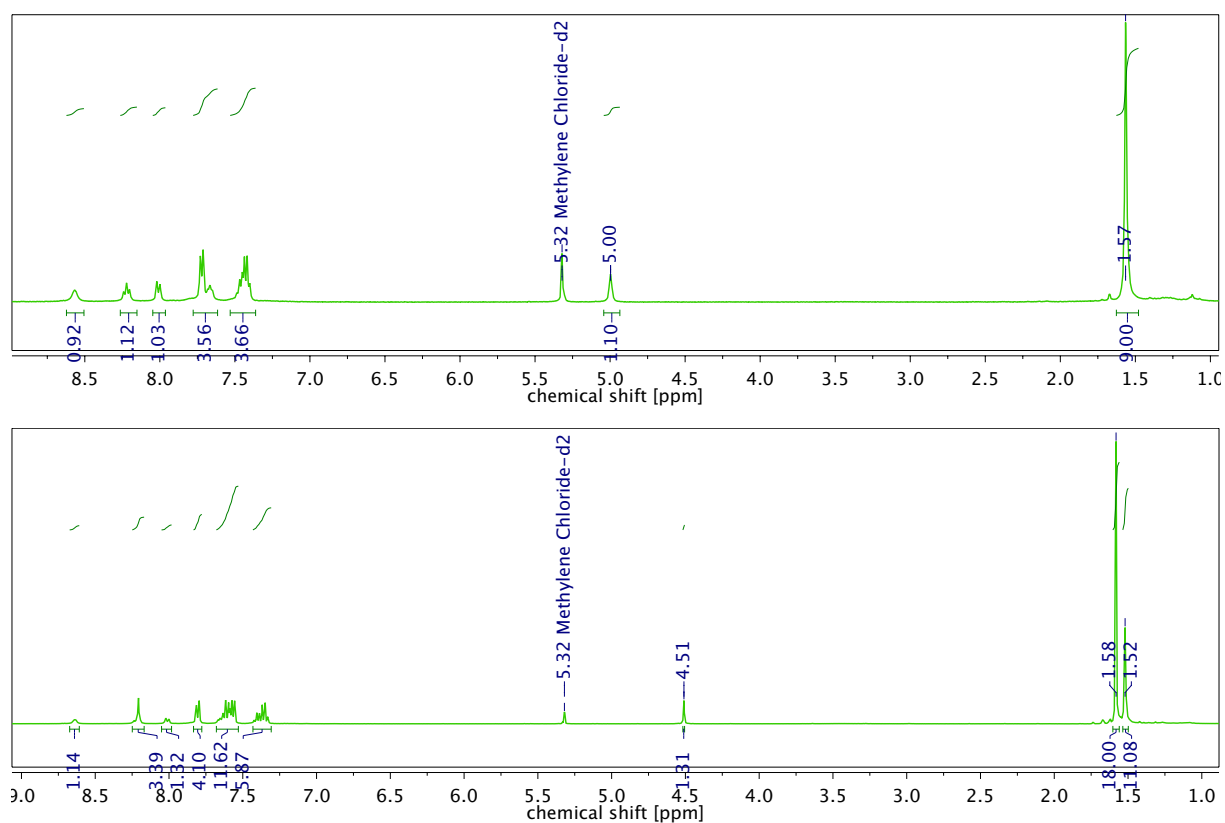
Figure 70: ^{1}H NMR spectra of acetylene complex **C28** (**top**) and **C29** (**bottom**). Acetylene proton is shifted from $\delta = 5.00$ ppm to $\delta = 4.51$ ppm by the addition of triazole. This might indicate hydrogen bonding *via* the acidified proton.

The observed chemical shift in the ^{1}H NMR spectrum (DCM-d$_2$) of the acetylene proton in complex **C29** neither corresponds to the free phenyl acetylene nor to the η^2-coordination complex observed in coordination compound **C28**. Furthermore, ^{31}P{^{1}H} NMR spectroscopy revealed a small upfield shift of the complex resonance from δ(DCM-d$_2$) = 175.1 to 172.4 ppm. Both upfield shifts indicate the formation of a new species. Due to the lack of the molecular structure in the crystal suitable crystals, no valid statement about the structure can be given. To give a rough estimation about the structure it is necessary to have a closer look to the one of **C28**. Here, the phenylacetylene is bound weakly to the copper ion (*vide supra*) and the η^2-coordination causes a strong chemical shift of the acetylene proton. This proton can be assumed to be

sufficiently acidic to undergo hydrogen bonding with the nitrogen atom of the triazole **34**. Whether the triazole coordinates the **Cu**(I) ion as well or even directs a second copper complex towards a supramolecular structure is still under investigation.
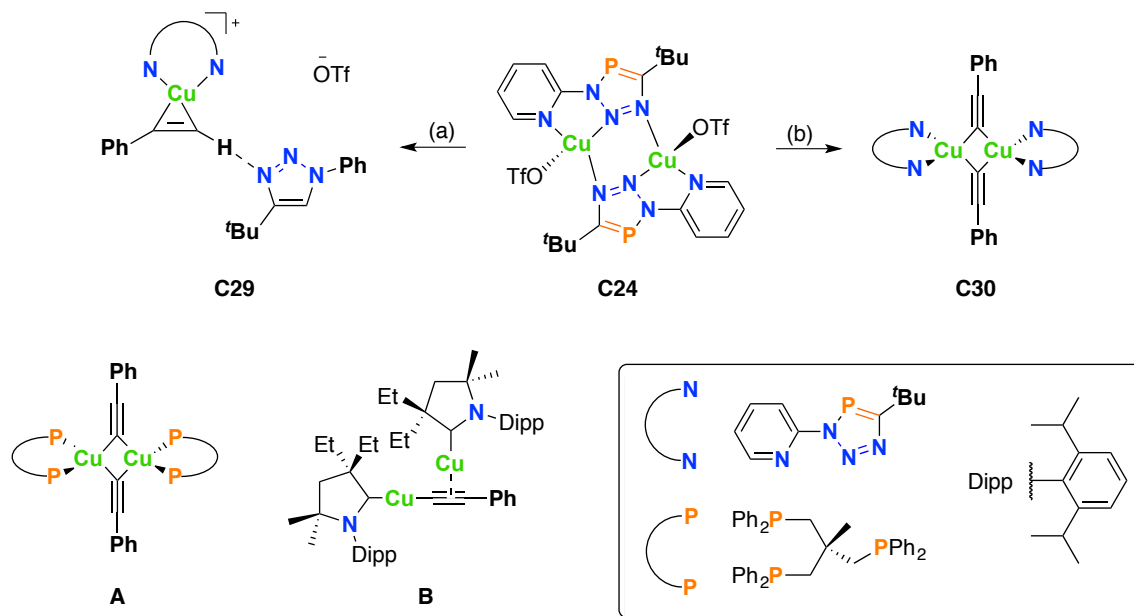
Scheme 59: Synthesis of complexes **C29** and **C30**. The structures are not verified and only a suggestion. Reaction conditions (a): 2 eq. phenyl acetylene, 2 eq. **34**, DCM, 10 min, r.t.; 2 eq. phenyl acetylene, 2 eq. DABCO, DCM, 10 min r.t..

Different types of copper-acetylyl-based structures are known, but one example is quite interesting regarding the determination of compound **C30**. Allen White *et al.* reported the structure of a dinuclear copper ethynyl complex containing a chelating ligand of type **A** (Scheme 59).

In order to assign a structure for **C30**, the triazaphosphole-based catalyst was converted with two equivalents of phenyl acetylene as well as two equivalents of DABCO. From the proton NMR spectrum obtained from the reaction mixture, a resonance next to activated or free acetylene proton was found. Only the signal of the DABCO protons appears in the eligible area (Figure 71). The back-reaction to the starting complex can be excluded, both for the missing acetylenic resonance and the shifted high field ^{31}P{^{1}H} NMR resonance of the **C30** ($\Delta\delta$ = 9 ppm).
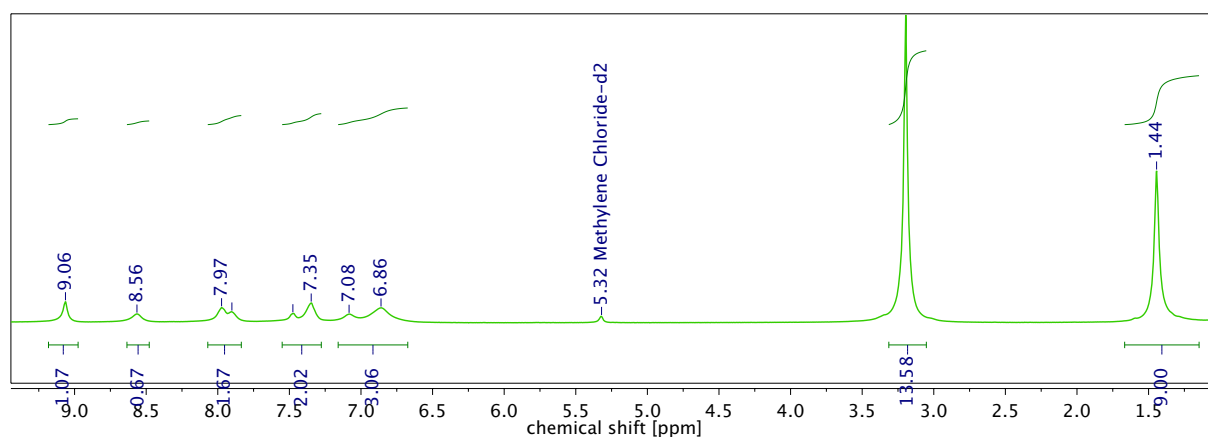
Figure 71: ^{1}H NMR spectrum of complex **30**. The addition of DACBO leads to deprotonating, only the hydrogen atoms from the DABCO are found.

Each copper atom is thereby bridged by two phenylethyn-1-ide ligands bond through the terminal carbon atom.[121] This structure slightly resembles the dinuclear copper acetylene complex **B** reported by Bertrand *et al.*,[122] but differences in the structures are quite obvious. The fact that only one of two possible η^1- and η^2-copper acetylene bonds are present is caused by the reduced number of acetylenic ligands But also the difference in the arrangement (square planar *vs.* linear) and the steric demand of the ligands might contribute to the reported structures. Further, the binding mode in Bertrand's **NHC** copper complex is quite clear, while in White's structure some differences prevail. Even though the distance of the carbon-carbon triple bond is only slightly elongated two different C-C$_{acetylene}$-Cu angles were found (158° *vs.* 129°). However, to compensate for the lack of the molecular structures in the solid state, kinetic measurements were set up.

From the initial rates the dependency of the reactions on the additives can be determined. The reactions were carried out in a sealed NMR tube. An overview of the experiments is given in Table 15. From the results several information can be deduced. Starting with catalyst **C24**, the overall reaction times indicate a strong influence of the additive on the reaction time. From the conversion/time profile (Figure 72, top left), a small impact is noticeable and the largest difference is found between entries 1 and 2. Nevertheless, the reactions carried out with the addition of triazole proceed, but the variation of the amount (Entries 2 to 7) of triazole **34** did not show a trend in the results.

Table 15: Overview of the catalytic reactions. All reactions were performed in 1 M solution of ethynyl benzene and benzyl azide (1:1) in DCM-d$_2$. For better referencing, triazole **34** was used.

Entry	Catalyst	Mol-% Cu	34 [mol-%]	DABCO [mol-%]	Time [min]	NMR Yield %	Rate [mmol/ mL*min]
1	**C24**	1.0	-	-	241.4	99	0.004
2	**C24**	1.0	1	-	191.7	100	0.005
3	**C24**	1.0	2	-	207.3	100	0.295 [b]
4	**C24**	1.0	2.5	-	203.2	98	0.005
5	**C24**	1.0	4	-	200.6	99	0.004
6	**C24**	1.0	5	-	222.3	100	0.004
7	**C24**	1.0	10	-	222.2	100	0.004
8	**C24**	2.5	-	-	195.7	100	0.005
9	**C24**	2.5	2.5	-	124.5	100	0.008
10	**C24**	2.5	5	-	128.3	100	0.009
11	**C24**	2.5	10	-	149.4	99	0.009
12	**C24**	5.0	-	-	88.4	98	0.012
13	**C24**	5.0	5	-	61.3	100	0.019
14	**C24**	5.0	10	-	49.7	99	0.022
15	**C27**	5.0	-	-	579.6	70.4	0.329
16	**C27**	5.0	5	-	578.3	47.6	0.146
17	**C27**	5.0	10	-	578.5	50.0	0.163
18	**C24**	2.5	-	2.5	27.7	99	[c]
19	**C24**	5.0	-	5	21.7	100	[c]
20	**C24**	5.0	-	10	33.5	99	[c]
21	**C24**	5.0	5	5	27.8	100	[c]
22	**C27**	5.0	-	5	310.3	99	0.594
23	**C27**	5.0	-	10	71.8	100	[c]
24	**C27**	5.0	5	5	75.8	100	1.009
25[a]	**C27**	5.0	-	5	85.5	99	2.082
26[a]	**C27**	5.0	-	10	68.1	99	[c]

[a] Aggregation time over night; [b] experimental error expected; [c] too few measurement points

Increasing the concentration of catalyst **C24** from c = 1.0 mol-% to 2.5 mol-% showed a stronger dependency of the rates towards the additive concentration. The reaction performed without any triazole (entry 8) has the lowest rate, which is also obvious from the conversion/time profile (Figure 72, top right). The reaction rates were increased by the addition of **34** (Entries 9 and 10), but the amount of **34** is only slightly affecting the rate of the reactions. Additionally, the initial rate (Entry 11) decreased again below the value of Entry 10. At around 85% turnovers, the reaction speed decreased again (Figure 72, top right, purple line).
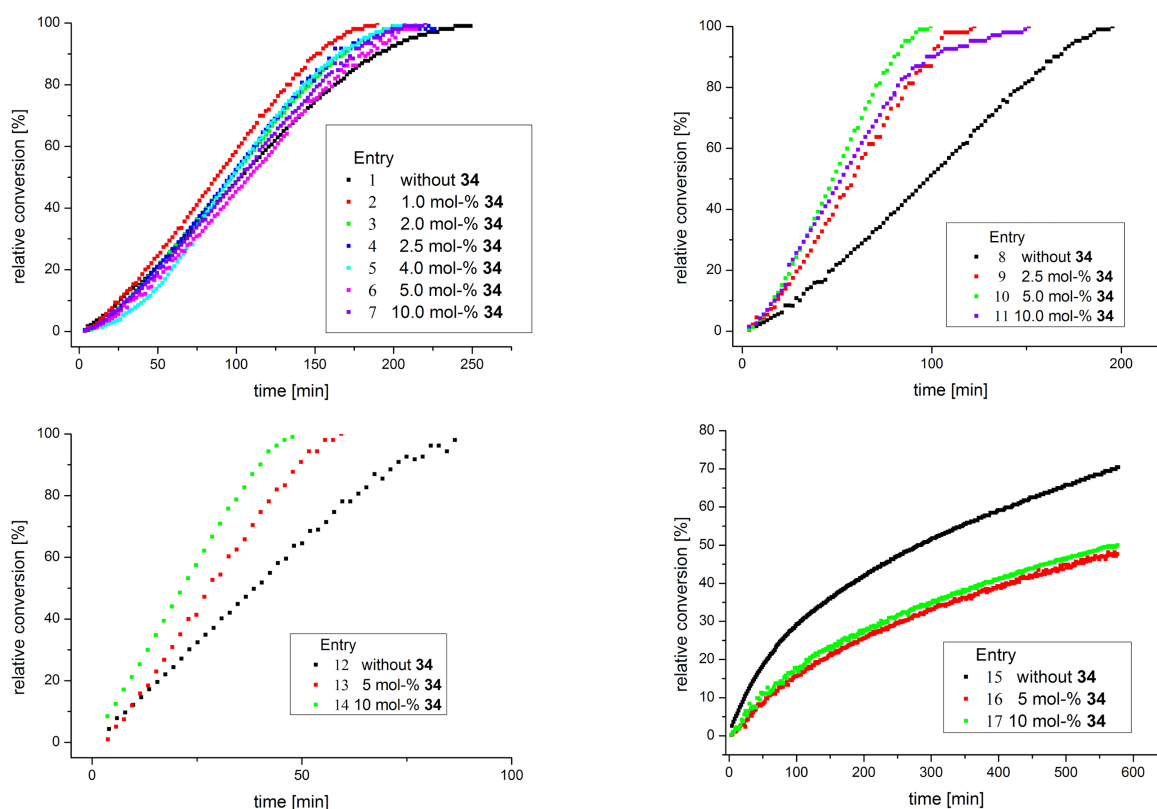
Figure 72: Conversion/time plots of CuAAC with triazole additive. (**Top left**) catalysed with 1 mol-% **C24** (**Top right**) catalysed with 2.5 mol-% **C24** (**bottom left**) catalysed with 5 mol-% **C24** and (**bottom right**) catalysed with 5 mol-% **C27**.

Using 5 mol-% catalyst **C24**, an enhancement between Entries 12 and 13 (no additive and 5 mol-% **34**) as well as entries 13 and 14 (5 mol-% and 10 mol-%) is found. Again, the influence of additive is lower by increasing the additive/catalyst ratio. Further, these results indicate an additive/catalyst ratio dependency, rather than an influence of the overall amount of the additive.

For the triazole based catalysis reactions (Entries 15-17) a contrary picture is obtained. The addition of **34** significantly reduces the catalyst activity. Furthermore, the reaction

was stopped after 600 min at less than 75% conversion (Figure 72, bottom right) suggesting that the catalyst is poisoned by the triazole. With the continuous formation of the product, the reaction speed thus decreased.

Also reactions using DABCO as additive were performed. For catalyst **C24**, some striking results were obtained. First of all, the reactions using 2.5 mol-% catalyst with an equal amount of additive showed similar rates as the catalysis with 5 mol-% copper and DABCO (Entries 18 and 19). This might be due to the diffusion limit in the reaction mixture. Supported is this finding by the Entry 20, as no effect by an additive/catalyst ratio of two is observed, besides a slightly earlier flattening of the conversion/time curve at around 85%. Further, the triazole **34** obviously does not have a noticeable effect anymore, as Entry 21 indicates (Figure 73).
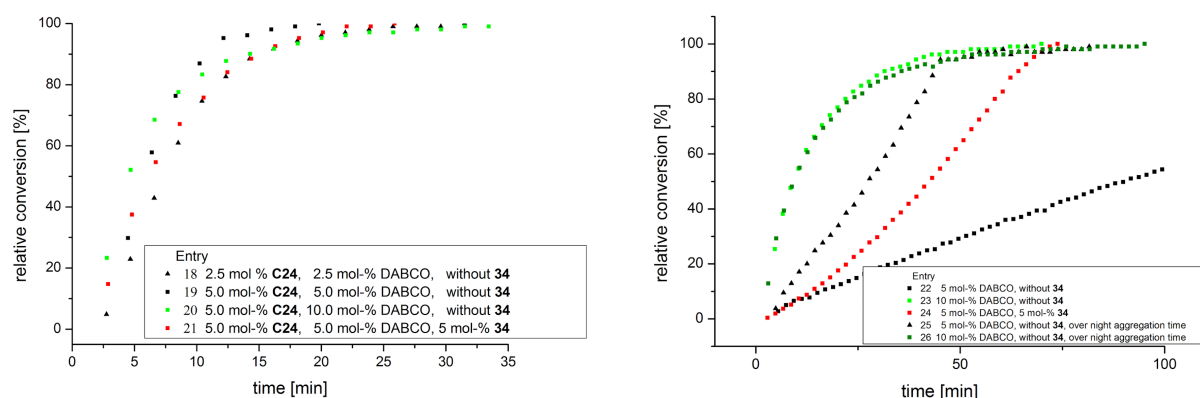
Figure 73: Conversion/time plots of CuAAC with DABCO additive. (Left) Results of catalysis with **C24**. (Right) results for catalyst **C27**.

The last set of the performed reactions consisted of the catalysis with triazole based **Cu** complex **C27** and DABCO. Entry 22 shows the longest reaction time and the lowest initial rate. Treating the reaction with the double amount of DABCO, a significantly shorter reaction time and much higher reaction rate was observed (Entry 23). The reaction of DABCO and triazole **34** in equimolar amount to the copper concentration (Entry 24) shows also an enhancement comparable to the reaction with only DABCO. But allowing the **C27** and DABCO to aggregate over night (Entry 25) the reaction without triazole shows better results than observed in Entry 24. The need for a long aggregation time might be attributed the low solubility observed for catalyst **C27** and the excess of DABCO might help in the aggregation. This is nicely demonstrated in the uniform reaction times of the over night aggregated mixture (Entry 26) and without (Entry 23).

Concerning the initial rates of the catalysis for the catalyst load of 1 mol-% no change is observed, except for Entry 3 (Table 15). But this significant large value is assigned to an experimental error. The positive effect of the triazole additive became obvious in the experiments that were conducted with 2.5 mol-% **C24**, as the rate is doubled. In this process the catalyst/additive ratio changes only slightly between 1:1, 1:2 and 1:4 (Entries 12-14). Also for the higher catalyst concentration of 5 mol-% this relation is found, as shown in Entries 15-17. The most striking result is found in the comparison of the triazaphosphole (**C24**) and triazole (**C27**) based Cu(I) complexes with 5 mol-% catalyst load. The rate values of the triazole-based catalyst are one magnitude larger than the ones of the triazaphosphole-based complex. Further, while the addition of the additive **34** causes higher rates in **C24** as already mentioned, in **C27** they become lower by the addition of the additive. In both cases they alternate around a factor of two (Entries 12-17). Although the **C27** has the highest initial rates, full conversion was not achieved within 578 min.

The initial rates for the catalytic reactions with DABCO, could not be determined, because within only one or two measurement points the 20% conversion limit for the initial rates was already crossed. They all might be in an area of 5-10 mmol*mL^{-1}*min^{-1} or even higher. Therefore, only the Entries 22, 24 and 25 can be discussed. The comparison of Entries 22 and 24 shows an enhancement of the reaction rate by a factor of two in the initial rates, but using a longer aggregation time and no **34** as additive, on enhancement by a factor of four is found.

In order to investigate the relationship between the rates and the copper as well as triazole additive dependency the corresponding rate/concentration graphs were plotted (Figure 74). The initial rates of the catalysis performed without any additive shows an exponential curve progression, indicating a binuclear copper mechanism (Chapter 1). The initial rates obtained with 2.5 mol-% additive are approximately in a linear relation. The same counts for the ones with 5 mol-%, indicating a 1:1 ratio of the active species, while for 10 mol-% might almost become exponential again. However, for a meaningful plot more measurement points are needed.
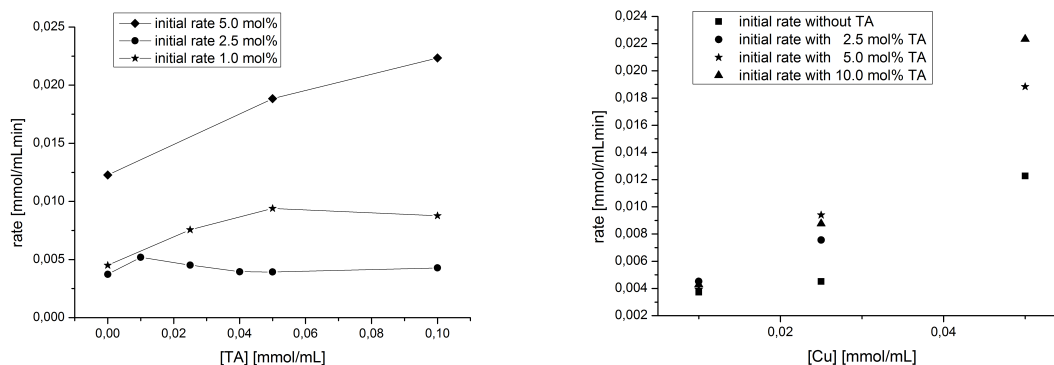
Figure 74: (**Left**) initial rate/triazole concentration plot. The effect of the triazole abate with increasing triazole concentration. This effect is proportional to the concentration of catalyst **C24**. (**Right**) initial rate/triazole concentration plot: significant enhancement on the reaction by triazole additive is noticeable.

This performed catalysis shows an enhancement of the reactions rate by triazole addition and therefore supports the previous made assumption that the catalysis with copper complex **C24** proceeds *via* an autocatalytic pathway. Binder *et al.* reported autocatalysis on this type of reaction, but in their case the ligand was a polymer, directing or accumulating the **Cu** atoms.[123] In the present case, the product/additive assistance might be attributed to weak interactions of the nitrogen lone pair of the triazole and the acidified acetylene proton in **C28**, as the shift in ^{1}H NMR spectrum revealed. Using this concept of weak interactions, the long reaction time in a solvent is also plausible, besides the lack of reaction heat. Furthermore, the different reaction speeds using the deprotonated form also support this assumption. Fokin *et al.*[124] reported the need of two copper nuclei for the catalysis to proceed (Chapter 1), while Bertrand *et al*. relativised this assumption, demonstrating the dependency of the reaction speed on the presence/absence of a second copper core.[122] Under the assumption that complex **C30** has a similar structure to either White's enthnylide complex **A** or to Bertrand-related binuclear copper complex **B** or an in-between arrangement, the extraordinarily short reaction time compared to the triazole-assisted reactions would be in line with the assumed mechanism of both a mono- and binuclear pathway. This can also be supported by the rates and the rate/concentration plots. The obtained data support the assumption of the catalytic active species **C29**, formed (undefined) copper:phenylacetylene:triazole complex with an assumed 1:1:1 ratio and therefore supporting the hints for an autocatalytic CuAAC. Although the rates for the complex **C27** are one magnitude higher compared to the once of **C24**, the reactions speed decreased radically.

From the data, the reaction mechanism can be concluded on basis of Bertrand's latest investigations.[122] The catalyst dimer **C24** is split due to η^2-coorination of the ethynyl benzene forming complex **C28** by weak interactions. In solution this equilibrium is more flexible due to dilution effects. For reactions without triazole additive, a mononuclear pathway is assumed (Chapter 1) and is obvious in the conversion/time plot of the solvent free reactions (Figure 69) as their relative concentration does not significantly change for a certain time period. As ^{1}H NMR spectroscopy revealed, triazoles are able to interact with the acidified proton in **C28** and the chemical shift of $\Delta\delta = 0.5$ ppm is attributed to a hydrogen bond in a similar arrangement as proposed for structure **C29**. From this activated and polarised acetylene, a triazole is generated according to the literature know pathway (Chapter 1).[122,124] From this, an intermediate similar to **C** (Scheme 59) is expected and that can be transferred by ligand exchange into the starting complex **C29**. A complex like **C** has to be present, either in this or a similar fashion since the reaction slows down at high concentrations of the additive and in an advanced reaction progress. The differences in the concentration ratios of phenylacetylene and the triazole the predominantly formation of **C** rather than the ligand exchange. This might also be the reason for the low reaction times with catalyst **C27**, as the reaction is inhibited by the triazole.

The acidified proton in complex **C28** can also be deprotonated by a stronger base, such as DABCO, as it can be derived from the ^{1}H NMR spectrum. The formed complex is less soluble than the **C28**, and by this as well as the report White's complex[121] the structure of **C30** was concluded. Hence, the exact binding situation remains unclear. However, whether the Cu-(μ-CC-Ph)(Cu-η^2) arrangement like in structure **B** is needed or if the binding situation in [Cu-(μ-CC-Ph)] provides a sufficient reactivity of the catalyst remains unclear. The observed low reaction times are in line with the latest investigation on mechanistic studies of binuclear copper complexes.[122,124] In contrast to these reports, the structure **D** is assumed to be unequal to the current investigations. The main reason for this is attributed to the dimer species **C30** including two phenylethyn-1-ide units. Also to what extent the different binding sites included in the ligand **L12** influence the final structure of **D** is unclear and the simplest assumable arrangement was chosen, related to an intermediate obtained by Straub *et al.*

Figure 75: Preliminary assumed mechanism, formulated for the triazaphosphole based complex. Compounds in blue boxes were characterised by X-ray diffraction analysis, in black boxes were observed and characterised by multicore NMR spectroscopy, while compounds in the red boxes are only proposed.

The mechanism for **C27** is assumed to proceed in an analogous way, but the formation of the triazole derivative of **C28** might be less favoured due to the longer aggregation times needed. But this might also be attributed the low solubility of **C27**. Furthermore, higher concentration of triazole reduces the rates and the catalytic process. This might indicate that complex **C** is more stable towards ligand exchange by a phenylacetylene. Especially the high initial rates together with the extreme long reaction times point strongly in this direction.

An error occurred somewhere during this study, making the previous results irreproducible in the beginning. In a last experiment, it could be shown that the atmosphere in the solvent glovebox changes the activity of the catalyst.

However, Figure 76 visualises nicely this effect, since the samples on the left side (II, III and IV) have the same compound ratios as the ones on the right side (V, VI and VII). This demonstration is based on chemical shifts in the $^{31}P\{^1H\}$ NMR spectra, showing independent from the composition of the reaction mixture a shift at δ (DCM-d$_2$) = 164 ppm. This signal might be attributed to the free ligand, but the ^1H NMR spectra do not correlate. Therefore, the formation of a different compound inside of the

glovebox atmosphere can be concluded. Later, Selina Kaiser could reproduce the results again.
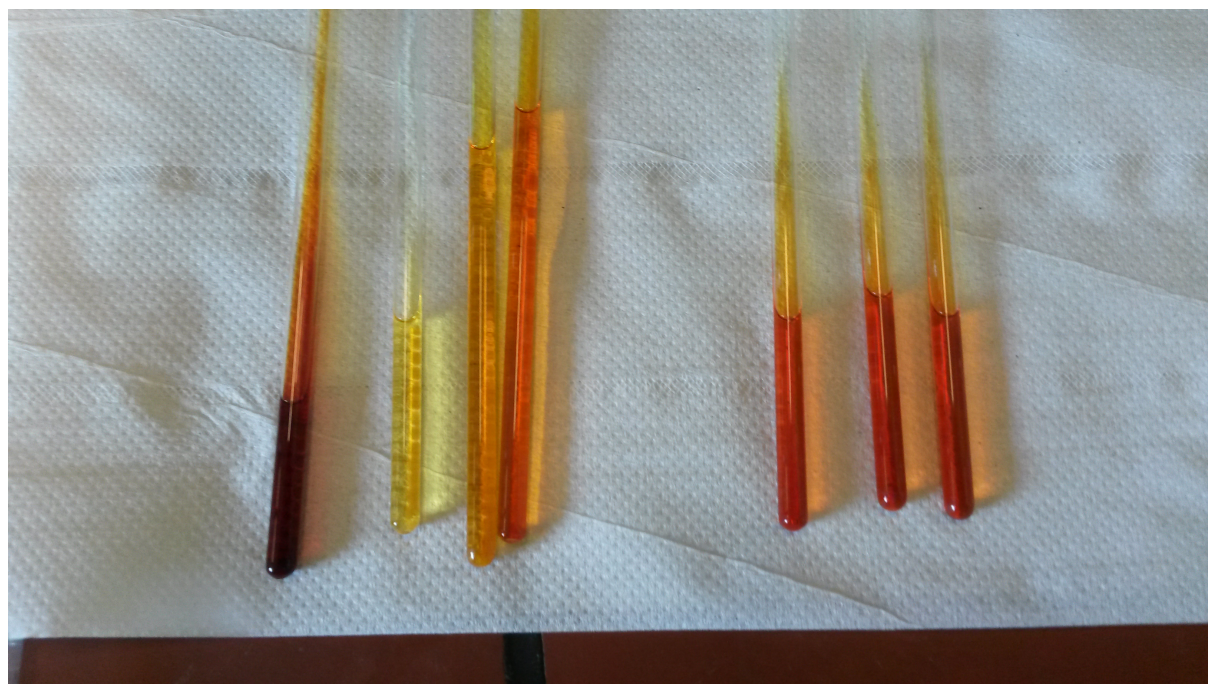
Figure 76: Visible effect of the catalyst decomposition. From left to right: catalyst **C24**, ethynyl complex **C28,** ethynyl complex **C28** with triazole **34** in 2:1 ratio and ethynyl complex **C28** with triazole **34** in 1:4 ratio. Right reaction mixtures to generate **C28**, ethynyl complex **C28** with triazole **34** in 2:1 ratio and ethynyl complex **C28** with triazole **34** in 1:4 ratio.

However, further experiments can still be planned. For instance the catalytic reactions should be investigated with stoichiometric amounts of **C28** and benzyl azide in the presence and absence of triazole **34**. The hydrogen bond could further be proven by NMR spectroscopy using ^{15}N-enriched triazole [15N]**34**. Also more experiments are needed for the catalysis to determine the saturated concentration in the catalysis with 5 mol-% catalyst, which is expected to be around 15 to 20 mol-% **34**. For reactions with catalyst **C30**, similar experiments as with **C28** should be performed.

Experimental Details of Conjugated Triazaphospholes and Triazoles

General Synthesis Procedure of Aryl Azides:

Aryl azides were synthesized following a reported procedure[31] 10 mmol of the corresponding aryl bromide was dissolved in 100 mL of a degased water/EtOH mixture (7:3 *v:v*). Sodium azide (2 eq.), copper iodide (10 mol %), N,N'-Dimethylethylenediamine (30 mol %) were added. The reaction mixture was refluxed under argon atmosphere for 2 h, cooled to r.t. and diluted with 50 mL H_2O. The organic compounds were extracted by washing with Et_2O (3x 100 mL), the combined organic phased were washed with Brine solution and dried afterwards over $MgSO_4$, concentrated and filtrated on a SiO_2 plug (ø = 6,5 cm × 3 cm). The solvent was removed in vacuum and the crude products were used without additional purifications. *Exception (vide infra)*: Tetrazolo[1,5-a]pyridine **F** ("2-azido pyridine" *vide supra*) was purified by column chromatography (SiO_2, dichloromethane/ethylacetate 9:1 *v:v*).

Synthesis of azidobenzene (*20*):
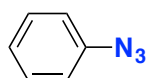
The compound was obtained as yellow oil in 21% yield.

¹H NMR (400 MHz, $CDCl_3$): δ = 7.00-7.04 (m, 2 H), 7.11-7.15 (m, 1 H), 7.32-7.37 (m, 2 H) ppm.

Spectroscopic data are consistent with the literature data. [125]

Synthesis of 4-azidopyridine (*21*):
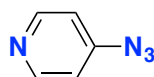
The product was obtained as slightly yellow oil in 59% yield.

¹H NMR (400 MHz, $CDCl_3$): δ = 6.87 (dd, *J* = 1.6, 4.6 Hz, 2 H), 8.46 (dd, *J* = 1.6, 4.6 Hz, 2 H)

ppm.

Spectroscopic data are consistent with the literature data.[126]

Synthesis of 3-azidopyridine (*22*):
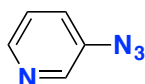
The compound was obtained as slightly yellow oil in 62% yield.

¹H NMR (400 MHz, CDCl₃): δ = 8.85 (1 H, dd, J = 6.9, 0.4 Hz, H$_{Ar}$), 8.07 (1 H, dd, J = 9.0, 0.4 Hz, H$_{Ar}$), 7.72 – 7.66 (1 H, m, H$_{Ar}$), 7.24 (1 H, d, J = 6.8 Hz, H$_{Ar}$) ppm.
Spectroscopic data consist with the literature.[127]

Synthesis of tetrazolo[1,5-a]pyridine (*23*)
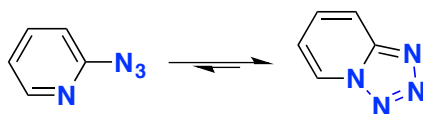
The compound was obtained in 71% yield as white solid.

¹H NMR (400 MHz, CDCl₃): δ = 8.85 (1 H, dd, J = 6.9, 0.4 Hz, H$_{Ar}$), 8.07 (1 H, dd, J = 9.0, 0.4 Hz, H$_{Ar}$), 7.72 – 7.66 (1 H, m, H$_{Ar}$), 7.24 (1 H, d, J = 6.8 Hz, H$_{Ar}$) ppm.
Spectroscopic data are consistent with the literature data.[128]

General Synthesis Procedure of 5-^{t}Bu Substituted Triazaphospholes:[31]

Aryl and benzyl azides (3.75 mmol) was placed with a stirring bar in a 100 mL Normag flask, the azide was freezed and the flask evacuated, followed by the addition of around 50 mL dry toluene as well as (dimethyllidyne)phosphine (412.9 mg, 4.13 mmol, 1.5 eq.). The reaction solution was allowed to warm to r.t. and stirred for 24 h. The solvent and the excess of alkyne was removed in vacuum. The resulting solid was recrystallized from a hot saturated *n*-pentane solution.

*Synthesis of 5-(tert-butyl)-3-phenyl-3H-1,2,3,4-triazaphosphole (**28**):*
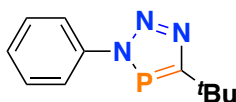
White crystalline solid (87% yield).

¹H NMR (400 MHz, methylene chloride-d_2): δ = 1.49 (d, $^4J_{\text{H-P}}$ = 1.5 Hz, 9H, Me-H9, Me-H10, Me-H11), 7.42 (m, 1H, Ar-H5), 7.48 (m, 2H, Ar-H4, Ar-H6), 7.76 (m, 2H, Ar-H3, Ar-H7) ppm.

¹³C NMR (176 MHz, methylene chloride-d_2) δ = 31.80 (d, $^3J_{\text{C-P}}$ = 7.6 Hz, Me-C9, Me-C10, Me-C11), 35.85(d, $^2J_{\text{C-P}}$ = 16.2 Hz, ^{t}Bu-C8), 122.83 (d, $^3J_{\text{C-P}}$ = 7.3 Hz, Ar-C3, Ar-C7), 129.03 (s, Ar-C5), 130.13 (s, Ar-C4, Ar-C6), 141.59 (d, $^2J_{\text{C-P}}$ = 10.4 Hz, Ar-C2), 198.99 (d, $^1J_{\text{C-P}}$ = 55.5 Hz, Ar-C1) ppm.

³¹P{¹H} NMR (162 MHz, methylene chloride-d_2): δ = 174.3 (s) ppm.

ESI-TOF-MS (+, 200.0 V)**:** [M+H]$^+$ = 220.1013 m/z (calc.: 220.0998 m/z).

EA(NCH): N: 18.59%, C: 60.06%, H: 6.456%; calc.: N: 19.17%, C: 60.27%, H: 6.44%.

*Synthesis of 4-(5-(tert-butyl)-3H-1,2,3,4-triazaphosphole-3-yl)pyridine (**29**):*
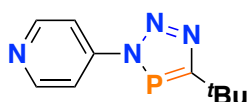
White crystalline needles (83% yield).

¹H NMR (500 MHz, methylene chloride-d_2): δ = 1.51 (d, $^4J_{\text{H-P}}$ = 1.7 Hz, 9H, Me-H8, Me-H9, Me-H10,), 7.79 (dt, $^3J_{\text{H-H}}$ = 4.6 Hz, $^4J_{\text{H-P}}$ = 1.4 Hz, 2H, Ar-H4, Ar-H5), 8.70 (m, 2H, Ar-H3, Ar-H6) ppm.

¹³C NMR (176 MHz, methylene chloride-d_2): δ = 31.64 (d, $^3J_{\text{C-P}}$ = 8.1 Hz, Me-C8, Me-C9, Me-C10), 36.00 (d, $^2J_{\text{C-P}}$ = 15.5 Hz, ^{t}Bu-C7), 116.08 (d, $^3J_{\text{C-P}}$ = 8.3 Hz, Ar-C3, Ar-C6), 147.80 (d, $^2J_{\text{C-P}}$ = 11.4 Hz, Ar-C2), 152.05 (s, Ar-C4, Ar-C5), 199.77 (d, J = 55.4 Hz, Ar-C1) ppm.
³¹P{¹H} NMR (162 MHz, methylene chloride-d_2): δ = 174.7 (s) ppm.

ESI-TOF-MS (+, 150.0 V)**:** [M+H]$^+$ = 221.0965 m/z (calc.: 221.0951 m/z).

EA(NCH): N: 24.80%, C: 54.50%, H: 6.066%; calc.: N: 25.44%, C: 54.54%, H: 5.95%.

*Synthesis of 3-(5-(tert-butyl)-3H-1,2,3,4-triazaphosphole-3-yl)pyridine (**30**):*
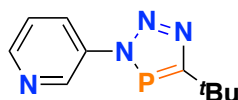
White crystalline needles (81% yield).

^{1}H NMR (400 MHz, methylene chloride-d$_2$): δ = 1.51 (d, $^4J_{H\text{-}P}$ = 1.5 Hz, 9H, ^{t}Bu), 7.47 (ddd, $^3J_{H\text{-}H}$ = 8.2 Hz, $^3J_{H\text{-}H}$ = 4.8 Hz, $^4J_{H\text{-}H}$ = 0.8 Hz, 1H, Ar-H4), 8.12 (dddd, $^3J_{H\text{-}H}$ = 8.2 Hz, $^4J_{H\text{-}P}$ = 2.5, $^4J_{H\text{-}H}$ = 1.5 Hz, $^5J_{H\text{-}H}$ = 1.0 Hz, 1H, Ar-H3), 8.65 (dd, $^3J_{H\text{-}H}$ = 4.8 Hz, $^4J_{H\text{-}H}$ = 1.5 Hz, 1H, Ar-H5), 9.03 (dt, $^4J_{H\text{-}P}$ = 2.3 Hz, $^4J_{H\text{-}H}$ = 1.0 Hz, 1H, Ar-H6) ppm.

^{13}C NMR (101 MHz, methylene chloride-d$_2$): δ = 31.20 (d, $^3J_{C\text{-}P}$ = 7.9 Hz, Me-C8, Me-C9, Me-C10), 35.41 (d, $^2J_{C\text{-}P}$ = 15.5 Hz, ^{t}Bu-C7), 124.12 (s, Ar-C4), 129.41 (d, $^3J_{C\text{-}P}$ = 6.0 Hz, Ar-C3), 137.54 (d, $^2J_{C\text{-}P}$ = 9.4 Hz, Ar-C2), 143.37 (d, $^3J_{C\text{-}P}$ = 8.6 Hz, Ar-C7), 149.68 (s, Ar-C5), 199.03 (d, $^1J_{C\text{-}P}$ = 56.5 Hz, Ar-C1) ppm.

^{31}P{^{1}H} NMR (162 MHz, methylene chloride-d$_2$): δ = 170.9 (s) ppm.

ESI-TOF-MS (+, 250.0 V)**:** [M+H]$^+$ = 221.0969 m/z (calc.: 221.0951 m/z).

EA(NCH): N: 23.75%, C: 53.78%, H: 6.11%; calc.: N: 25.44%, C: 54.54%, H: 5.95%.

*Synthesis of 2-(5-(tert-butyl)-3H-1,2,3,4-triazaphosphole-3-yl)pyridine (**L12**):*
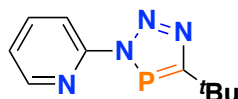
Tetrazolo[1,5-*a*]-pyridine (450.0 mg, 3.75 mmol, 1 eq.) was added to a solution of (2,2-dimethyllidyne)phosphine (412.9 mg, 4.13 mmol, 1.5 eq.) in 30 mL of toluene. The reaction mixture was heated for 1 week at T = 80°C. After full conversion of compound the solvent and the excess of (2,2-dimethylpropylidyne)phosphine was removed in

vacuum. The crude product was dissolved again in toluene at r.t. and crystallized by slowly cooling down to T = -20°C. The title compound was obtained as slightly yellow needles (53% yield).

¹H NMR (400 MHz, methylene chloride-d₂): δ = 1.48 (d, $^4J_{H-P}$ = 1.6 Hz, 9H, Me-H9, Me-H10, Me-H11), 7.31 (ddd, $^3J_{H-H}$ = 7.5 Hz, $^3J_{H-H}$ 4.9 Hz, $^4J_{H-H}$ 1.1 Hz, 1H, Ar-H5), 7.88 (td, $^3J_{H-H}$ = 7.8 Hz, $^4J_{H-H}$ 1.9 Hz, 1H, Ar-H4), 8.08 (dt, $^3J_{H-H}$ = 8.3 Hz, $^4J_{H-H}$ 1.0 Hz, 1H), 8.44 (ddd, $^3J_{H-H}$ = 4.9 Hz, $^4J_{H-H}$ = 1.9 Hz, $^5J_{H-H}$ = 0.9 Hz, 1H, Ar-H6).

¹³C NMR (176 MHz, methylene chloride-d₂): δ = 31.11(d, $^3J_{C-P}$ = 8.3 Hz, Me-C8, Me-C9, Me-C10), 35.27 (d, $^2J_{C-P}$ = 15.3 Hz, ^tBu-C7), 113.42 (d, $^3J_{C-P}$ = 2.6 Hz, Ar-C3), 123.45 (s, Ar-C5), 139.06 (s, Ar-C4), 148.51 (s, Ar-C6), 153.27 (d, $^2J_{C-P}$ = 8.4 Hz, Ar-C2), 199.00 (d, $^1J_{C-P}$ = 57.2 Hz, Ar-C1) ppm.

³¹P{¹H} NMR (162 MHz, methylene chloride-d₂): δ = 167.51 ppm.

ESI-TOF-MS (+, 150.0 V)**:** [M+H]⁺ = 221.0967 m/z (calc.: 221.0951 m/z).

EA(NCH): N: 25.36%, C: 54.56%, H: 5.965%; calc.: N: 25.44%, C: 54.54%, H: 5.95%.

General Synthesis Procedure of 5-TMS Substituted Triazaphospholes:

Aryl and benzyl azides (3.75 mmol) were placed with a stirring bar in a 250 mL Normag flask, the azide was freezed and the flask evacuated, followed by the addition of around 100 mL dry ((trimethylsilyl)methylidyne)phosphine in toluene (large excess). The reaction solution was allowed to warm to r.t. and stirred for 24 h. The solvent and the access of alkyne were removed in vacuum.

*Synthesis of 3-(5-(trimethylsilyl)-3H-1,2,3,4-triazaphosphole-3-yl)pyridine (**33**):*
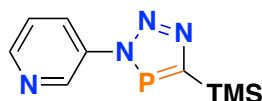
Orange solid, 93% yield.

¹H-NMR (400 MHz, CD$_2$Cl$_2$): δ = 9.14 – 8.99 (1 H, m, H$_{Ar}$), 8.66 (1 H, dd, J = 4.8, 1.4 Hz, H$_{Ar}$), 8.17 – 8.12 (1 H, m, H$_{Ar}$), 7.48 (1 H, ddt, J = 8.2, 4.8, 0.8 Hz, H$_{Ar}$), 0.45 (9 H, s, CH$_3$) ppm.

¹³C-NMR (101 MHz, CD$_2$Cl$_2$): δ = 186.35 (d, $^1J_{P-C}$ = 75.5 Hz, C=P), 150.28 (d, $^4J_{P-C}$ = 1.2 Hz, C$_{5, Ar}$), 144.12 (d, $^2J_{P-C}$ = 7.7 Hz, C$_{3, Ar}$), 130.21 (d, $^3J_{P-C}$ = 5.3 Hz, C$_{4, Ar}$), 124.68 (s, C$_{6, Ar}$), -0.21 (d, $^3J_{P-C}$ = 3.6, CH$_3$) ppm.

³¹P{¹H}-NMR (162 MHz, CD$_2$Cl$_2$): δ = 213.7(s) ppm.

ESI-TOF-MS (+, 330 V): [M+Na]$^+$ 259.1177 m/z (calc. 259.0539 m/z).

*Synthesis of 2-(5-(trimethylsilyl)-3H-1,2,3,4-triazaphosphole-3-yl)pyridine(**L13**):*
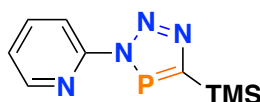
Orange oil, 91% yield.

¹H-NMR (400 MHz, CD$_2$Cl$_2$): δ = 8.49 (1 H, ddd, J = 4.9, 1.8, 0.9 Hz, H$_{Ar}$), 8.14 (1 H, dt, J = 8.2, 0.9 Hz, H$_{Ar}$), 7.95 – 7.89 (1 H, m, H$_{Ar}$), 7.35 (1 H, ddd, J = 7.4, 4.9, 1.0 Hz, H$_{Ar}$), 0.44 (9 H, d, J = 0.6, CH$_3$) ppm.

¹³C-NMR (101 MHz, CD$_2$Cl$_2$): δ = 186.38 (d, $^1J_{P-C}$ = 74.0 Hz, C=P), 153.62 (d, $^2J_{P-C}$ = 7.1 Hz, C$_{2, Ar}$), 149.22, 139.76 (s, C$_{Ar}$), 124.17 (d, $^4J_{P-C}$ = 1.1 Hz, C$_{4, Ar}$), 114.55 (d, $^3J_{P-C}$ = 2.2 Hz, C$_{3, Ar}$), -0.19 (d, $^3J_{P-C}$ = 3.8, CH$_3$) ppm.

³¹P{¹H}-NMR (162 MHz, CD$_2$Cl$_2$): δ = 211.6 (s) ppm.

*Synthesis of 3-phenyl-5-(trimethylsilyl)-3H-1,2,3,4-triazaphosphole (**31**):*
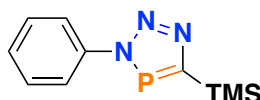
Red oil, 91% yield.

¹H NMR (400 MHz, CD₂Cl₂): δ = 7.82 (2 H, dt, J = 8.4, 1.2 Hz, H$_{Ar}$), 7.55 – 7.50 (2 H, m, H$_{Ar}$), 7.48 – 7.42 (1 H, m, H$_{Ar}$), 0.46 (9 H, d, J = 0.6 Hz, Me) ppm.

¹³C NMR (101 MHz, CD₂Cl₂): δ = 185.71 (d, $^1J_{P\text{-}C}$ = 74.7 Hz, C=P), 141.30 (d, $^2J_{P\text{-}C}$ = 9.3 Hz, C$_{1,\,Ar}$), 130.17 (s, C$_{4,\,Ar}$), 129.12 (d, $^4J_{P\text{-}C}$ = 1.1 Hz, C$_{3,3',}$ Ar), 123.13 (d, $^3J_{P\text{-}C}$ = 6.5 Hz, C$_{2,2'\,Ar}$), -0.13 (d, $^3J_{P\text{-}C}$ = 3.6, Me) ppm.

³¹P{¹H} NMR (162 MHz, CD₂Cl₂): δ = 213.0 (s) ppm.

General Synthesis of 1,2,3-Triazoles: [34]

In a 20 mL microwave reaction vessel 188.7 mg (0.375 mmol, 10 mol %) copper(I) trifluoromethansulfonate benzene complex were added to 450 mg (3.75 mmol) of tetrazolo[1,5-a]pyridine (**F**). 20 mL of dry toluene were added as well as 4.125 mmol (1.1 eq) of substituted alkyne. The mixture was heated at T = 140°C for 4 h in the microwave. After cooling the reaction vessel to r.t., the solvent was removed in vacuum and column chromatography (SiO₂, DCM/EE 9:1 *v:v*) yielded the pure title compounds.

2-(4-(tert-butyl)-1H-1,2,3-triazol-1-yl)pyridine (L14):
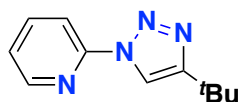
White solid, 77% yield.

¹H NMR (500 MHz, CDCl₃): δ = 1.41 – 1.38 (s, 9H, Me-H12, Me-H13, Me-H14), 7.29 (ddd, $^3J_{H\text{-}H}$ = 7.4 Hz, $^3J_{H\text{-}H}$ = 4.9 Hz, $^4J_{H\text{-}H}$ = 1.0 Hz, 1H, Ar-H6), 7.87 (ddd, $^3J_{H\text{-}H}$ = 8.2 Hz, $^3J_{H\text{-}H}$ = 7.4 Hz, $^4J_{H\text{-}H}$ =1.8 Hz, 1H, Ar-H5), 8.16 (dt, $^3J_{H\text{-}H}$ = 8.2 Hz, $^4J_{H\text{-}H}$ = 1.0 Hz, 1H, Ar-H4), 8.27 (s, 1H, Ar$_{Triazol}$-H2), 8.46 (ddd, $^3J_{H\text{-}H}$ = 4.9 Hz, $^4J_{H\text{-}H}$ = 1.9 Hz, $^5J_{H\text{-}H}$ = 0.9 Hz, 1H, Ar-H7) ppm.

¹³C NMR (126 MHz, CDCl₃): δ = 30.31 (s, Me-C12, Me-C13, Me-C14), 30.95 (s, ^{t}Bu-C11), 113.87 (s, Ar-C4), 116.14 (s, Ar$_{Triazol}$-C2), 123.28 (s, Ar-C6), 139.15 (s, Ar-C5), 148.47 (s, Ar-C7), 149.57 (s, Ar-C3), 158.18 (s, Ar$_{Triazol}$-C1) ppm.

ESI-TOF-MS (+, 100.0 V)**:** [M+Na]⁺ = 225.1126 m/z (calc.: 225.11107 m/z).

EA(NCH): N: 26.97%, C: 64.93%, H: 6.98%: calc.: N: 27.7%, C: 65.32%; H: 6.98%.
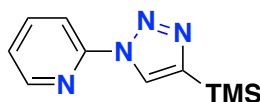
White solid, 59% yield.

¹H NMR (500 MHz, CDCl₃): δ = 0.37(s, 9H, Me-H11, Me-H12, Me-H13), 7.32 (ddd, $^3J_{H\text{-}H}$ = 7.4 Hz, $^3J_{H\text{-}H}$ = 4.9 Hz, $^4J_{H\text{-}H}$ = 1.0 Hz, 1H, Ar-H6), 7.90 (ddd, $^3J_{H\text{-}H}$ = 8.2 Hz, $^3J_{H\text{-}H}$ = 7.4 Hz, $^4J_{H\text{-}H}$ = 1.8 Hz, 1H, Ar-H5), 8.20 (dt, $^3J_{H\text{-}H}$ = 8.2 Hz, $^4J_{H\text{-}H}$ = 1.0 Hz, 1H, Ar-H4), 8.49 (ddd, $^3J_{H\text{-}H}$ = 4.9 Hz, $^4J_{H\text{-}H}$ = 1.9 Hz, $^5J_{H\text{-}H}$ = 0.9 Hz, 1H, Ar-H7), 8.55 (s, 1H, Ar$_{Triazol}$-H2) ppm.

¹³C NMR (126 MHz, CDCl₃): δ = -1.06 (s, Me-C12, Me-C13, Me-C14), 114.41 (s, Ar-C4), 123.42 (s, Ar-C6), 126.52 (s, Ar$_{Triazol}$-C2), 139.27 (s, Ar-C5), 147.29 (s, Ar-C3) 148.61 (s, Ar-C7), 149.49 (s, Ar$_{Triazol}$-C1) ppm.

ESI-TOF-MS (+, 150.0 V)**:** [M+Na]⁺ = 241.0881 m/z (calc.: 241.08799 m/z).

EA(NCH): N: 25.593%, C: 54.923%, H: 6.521%: calc.: N: 25.66%, C: 55.01%; H: 6.46%.

General Synthesis Procedure of Re(I) Complexes:

In a J. R. Young NMR tube 50 mg (0.1231 mmol) Re(CO)₅Br were mixed with 0.1231 mmol (1 eq.) of the ligand **L12** to **L15** and suspended in 0.5 mL dry DCM-d₂. The reaction mixture was heated for 8 h at T = 80°C, leading to full conversion (¹H/³¹P NMR). Cooling a hot saturated solution of the complex in DCM, yielding single crystalline pure compounds, recrystallized the precipitating product.

Synthesis of Rhenium(I) tris(carbonyl) 2-(5-(tert-butyl)-3H-1,2,3,4-triazaphosphol-3-yl)pyridyl bromide (*C12*):
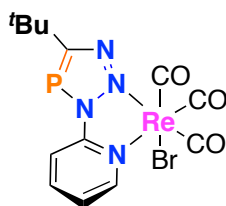
Red needles, 63% yield.

¹H NMR (700 MHz, methylene chloride-d_2): δ = 1.57 (d, $^4J_{\text{H-P}}$ = 1.5 Hz, 9H, Me-H11, Me-H12, Me-H13), 7.35(ddd, $^3J_{\text{H-H}}$ = 7.3 Hz, $^4J_{\text{H-H}}$ = 5.6 Hz, $^5J_{\text{H-H}}$ = 1.1 Hz, 1H, Ar-H5), 8.06 (d, $^3J_{\text{H-H}}$ = 8.2 Hz, 1H, Ar-H3), 8.16 (ddd, $^3J_{\text{H-H}}$ = 8.2 Hz, $^4J_{\text{H-H}}$ = 7.6 Hz, $^5J_{\text{H-H}}$ = 1.7 Hz, 1H, Ar-H4), 8.92 (dd, $^3J_{\text{H-H}}$ = 5.4 Hz, $^4J_{\text{H-H}}$ = 1.4 Hz, 1H, Ar-H6) ppm.

¹³C NMR (176 MHz, methylene chloride-d_2): δ = 31.37 (d, $^3J_{\text{C-P}}$ = 9.1 Hz, Me-C11, Me-C12, Me-C13), 36.73 (d, $^2J_{\text{C-P}}$ = 14.6 Hz), 116.74 (d, $^3J_{\text{C-P}}$ = 13.5 Hz, Ar-C3), 126.15 (s, Ar-C5), 142.30 (s, Ar-C4), 152.90 (s, Ar-C6), 153.01 (d, $^2J_{\text{C-P}}$ = 10.0 Hz), 188.08 (s, CO), 195.15 (s, CO), 197.11 (s, CO), 201.62 (d, $^1J_{\text{C-P}}$ = 60.9 Hz) ppm.

³¹P NMR (162 MHz, methylene chloride-d_2): δ = 184.1 (s) ppm.

ESI-TOF-MS(+, 200 V)**:** [M-Br+MeCN]⁺: 532.0583 m/z (calc.: 532.05428).

EA(NCH): N: 7.524%, C: 24.92%, H: 2.244%; calc.: N: 7.57%, C: 24.34%, H: 2.31%.

Attempts in the synthesis of Rhenium(I) tris(carbonyl) 2-(5-(trimethylsilyl-butyl)-3H-1,2,3,4-triazaphosphol-3-yl)pyridyl bromide (*C13*):
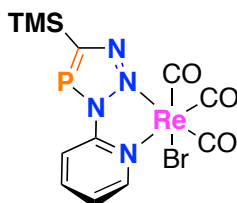
The title compound could not be isolated. The reaction mixture showed in the ³¹P{¹H} NMR spectrum a major and several minor products, while the ¹H NMR spectrum revealed three different products.

$^{31}\textbf{P NMR}$ (162 MHz, methylene chloride-d$_2$): δ = 224.0 (s) ppm.

*Synthesis of Rhenium(I) tris(carbonyl) 2-(4-(tert-butyl)-1H-1,2,3-triazol-1-yl)pyridyl bromide (**C14**):*
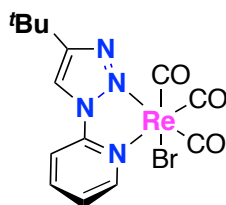
Yellow needles, 57% yield.

$^{1}\textbf{H NMR}$ (700 MHz, CDCl$_3$): δ = 1.45 (s, 9H, Me-H12, Me-H13, Me-H14), 7.35 (ddd, *J* = 7.6, 5.6, 1.0 Hz, 1H, Ar-H5), 7.81 (d, $^3J_{\text{H-H}}$ = 8.2 Hz, 1H, Ar-H4), 8.15 (s, 1H, Ar$_{\text{Triazol}}$-H2), 8.19 (ddd, $^3J_{\text{H-H}}$ = 8.3, $^4J_{\text{H-H}}$ = 7.6 Hz, $^5J_{\text{H-H}}$ = 1.6 Hz, 1H, Ar-H6), 8,97 (ddd, $^3J_{\text{H-H}}$ = 5.5 Hz, $^4J_{\text{H-H}}$ = 1.5 Hz, $^5J_{\text{H-H}}$ = 0.6 Hz, 1H, Ar-H7) ppm.

$^{13}\textbf{C NMR}$ (176 MHz, CDCl$_3$): δ = 30.05 (s, Me-C12, Me-C13, Me-C14), 31.74 (s, ^{t}Bu-C11), 113.18 (s, Ar-C4), 117.99 (s), 125.65 (s, Ar-C5), 141.96 (s, Ar-C6), 147.72 (s, Ar-C3), 153.30 (s, Ar-C7), 161.67 (s, Ar-C1), 187.63 (s, CO), 193.90 (s, CO), 195.91 (s, CO) ppm.

ESI-TOF-MS (+, 150.0 V)**:** [M+Na]$^+$ = 574.9704 m/z (calc.: 574.9699 m/z).

EA(NCH): N: 9.76%, C: 30.08%, H: 2.67%: calc.: N: 10.14%, C: 30.44%; H: 2.55%.

*Synthesis of Rhenium(I) tris(carbonyl) 2-(4-(trimethylsilyl)-1H-1,2,3-triazol-1-yl)pyridyl bromide (**C15**):*
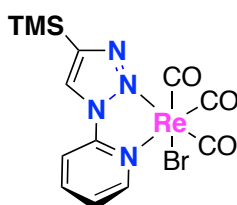
Neon yellow needles, 11% yield.

¹H NMR (700 MHz, CDCl₃): δ = 0.41 (s, 9H, Me-H), 7.50-7.59 (m, 1Ar-H), 7.90 (dt, $J_{\text{H-H}}$ = 1.0, 8.3 Hz, 1H, Ar-H), 8.20 (dddd, $J_{\text{H-H}}$ = 1.6, 6,8, 7,6, 8.4 Hz 1H, Ar-H), 8.45 (s, 1H, Ar$_{\text{Triazol}}$-H), 8,96 (dddd, $J_{\text{H-H}}$ = 0.7, 1.6, 5.5, 8.1 Hz, 1H, Ar-H) ppm.

¹³C NMR (176 MHz, CDCl₃): δ = -1.3 (s, Me-C), 113.5 (s, Ar-C), 125.8 (s), 127.7 (s, Ar-C), 141.9 (s, Ar-C), 147.5 (s, Ar-C), 152.3 (s, Ar-C), 153.3 (s, Ar-C), 187.63 (s, CO), 194. 0 (s, CO), 195.9 (s, CO) ppm.

ESI-TOF-MS (+, 300.0 V)**:** [M+Na]⁺ = 590.9446 m/z (calc.: 590.9468 m/z).

*Attempts in the Synthesis of Rhodium(III) [2-(4-(tert-butyl)-1H-1,2,3-triazol-1-yl)1,2-phenylene] [(1,2,3,4,5-η)-1,2,3,4,5-pentamethyl-2,4-cyclopentadien-1yl)] chlorid (**C16**):*
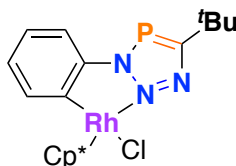
In a J. R. Young NMR tube 30 mg (0.137 mmol, 2 eq.) **28** were suspended together with 42.29 mg (0.068 mmol, 1 eq.) [**Rh**(Cp*)Cl₂]₂ and 11.23 (0.137 mmol, 2 eq.) sodium acetate in 0.5 ml DCM-d₂. The reaction was heated for 60 d in an T = 80 °C hot oil bath. The reaction was stopped since no further progress was noticeable. No product was obtained.

*Attempts in the Synthesis of Iridium(III) [2-(4-(tert-butyl)-1H-1,2,3-triazol-1-yl)1,2-phenylene] [(1,2,3,4,5-η)-1,2,3,4,5-pentamethyl-2,4-cyclopentadien-1yl)] chlorid (**C17**):*
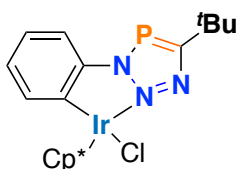
In a J. R. Young NMR tube 30 mg (0.137 mmol, 2 eq.) **28** were suspended together with 54.51 mg (0.068 mmol, 1 eq.) [**Ir**(Cp*)Cl₂]₂ and 11.23 (0.137 mmol, 2 eq.) sodium acetate in 0.5 ml DCM-d₂. The reaction was heated for 60 h in an T = 80 °C hot oil bath.

The reaction was stopped since no further progress was noticeable. No product was obtained.

*Synthesis of 4-(tert-butyl)-1-phenyl-1H-1,2,3-triazole (**34**)*
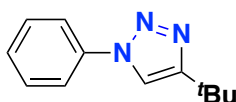
White solid, 68% yield.

1H NMR (700 MHz, CDCl$_3$): δ = 1.41 (s, 9H, Me-H), 7.39 (tt, $J_{\text{H-H}}$ = 1.2, 7.3 Hz, 1H, Ar-H), 5.51 - 7.46 (m, 2H, Ar-H), 7.70 – 7.73 (m, 2H, Ar-H) ppm.

13C NMR (176 MHz, CDCl$_3$): δ = 30.4 (s, Me-C), 31.0 (s, C$_{\text{CH3}}$), 116.9 (s, Triazol-C), 120.5 (s, Ar-C), 128.4 (s, Ar-C), 129.7 (s, Ar-C), 137.5 (s, Ar-C), 158.4 (s, Triazole-C) ppm.

ESI-TOF-MS (+, 300.0 V)**:** [M+Na]$^+$ = 240.0906 m/z (calc.: 240.0898 m/z).

General Synthesis Procedure of Mn(I) Complexes:

In a J. R. Young NMR tube 50 mg (0.181 mmol) Mn(CO)$_5$Br were mixed with 0.181 mmol (1 eq.) of the ligand **L12** or **L13** and suspended in 0.5 mL dry DCM-d$_2$. The reaction mixture was heated for 8 h at T = 40°C, leading to full conversion (^{1}H/^{31}P NMR), yielding pure products.

*Synthesis of Manganese(I) tris(carbonyl) 2-(5-(tert-butyl)-3H-1,2,3,4-triazaphosphol-3-yl)pyridyl bromide (**C18**):*
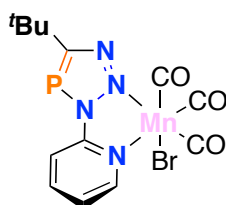
Red crystalline solid, 63% yield.

¹H NMR (700 MHz, CDCl₃): δ = 1.57 (s, 9H, Me-H), 7.41 - 7.60 (m, 1H, Ar-H), 7.83 – 7.89 (m, 1H, Ar-H), 8.02 – 8.18 (m, 1H, Ar-H), 9.04 (d, $J_{H\text{-}H}$ = 9.9 Hz, 1H, Ar-H) ppm.

¹³C NMR (176 MHz, CDCl₃): δ = 31.3 (d, $^3J_{C\text{-}P}$ = 8.1 Hz, Me-C), 36.6 (d, $^3J_{C\text{-}P}$ = 14.8 Hz, C_{CH3}), 116.2 (d, d, $^2J_{C\text{-}P}$ = 12.0 Hz, Ar-C), 125.3 (s, Ar-C), 141.5 (s, Ar-C), 152.6 (d, $^4J_{C\text{-}P}$ = 9.8 Hz, Ar-C), 152.6 (s, Ar-C), 153.4 (s, Ar-C), 202.4 (d, $^1J_{C\text{-}P}$ = 58.9 Hz, $C_{triazaphosphole}$), 219.9 (s, CO), 221.6 (s, CO), 222.8 (s, CO) ppm.

³¹P NMR (162 MHz, methylene chloride-d₂): δ = 195.5 (s) ppm.

ESI-TOF-MS (+, 200.0 V)**:** [M-Br]⁺ = 359.0158 m/z (calc.: 359,1000 m/z).

EA(NCH): N: 12.76%, C: 35.36%; H: 2.98%; calc.: N: 12.76%, C: 35.56%, H: 2.98%.

*Synthesis of Manganese(I) tris(carbonyl) 2-(4-(tert-butyl)-1H-1,2,3-triazol-1-yl)pyridyl bromide (**C19**):*
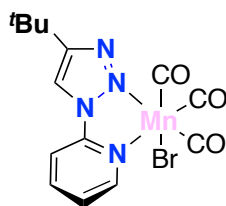
Yellow-brown crystalline solid, 57% yield.

¹H NMR (700 MHz, CDCl₃): δ = 1.46 (s, 9H, Me-H), 7.55 (s, Ar-H), 7.75 (s, 1H, Ar-H), 8.13 (s, 1H, Ar-H), 8.24 (s, 1H, Ar-H), 8.92-9.16 (m, 1H, Ar-H) ppm.

¹³C NMR (176 MHz, CDCl₃): δ = 30.3 (s, Me-C), 32.1 (s, C_{CH3}), 113.3 (s, Triazol-C), 118.9 (s, Ar-C), 125.4 (s, Ar-C), 141.8 (s, Ar-C), 147.9 (s, Ar-C), 153.9 (S, Ar-C), 162.9 (s, Triazole-C), 220.1 (s, CO), 221.7 (s, CO), 223.7 (s, CO) ppm.

ESI-TOF-MS (+, 200.0 V)**:** [M-Br]⁺ = 341.0495 m/z (calc.: 341,0441 m/z).

EA(NCH): N: 12.36%, C: 37.62%; H: 3.22%; calc.: N: 12.36%, C: 36.88%, H: 3.23%.

Attempts in the Synthesis of Rhodium(III) [(1,2,3,4,5-η)-1,2,3,4,5-pentamethyl-2,4-cyclopentadien-1yl)] chlorid {Rhenium(I) tris(carbonyl) 2-(5-(tert-butyl)-3H-1,2,3,4-triazaphosphol-3-yl)pyridyl} bromide (C20):
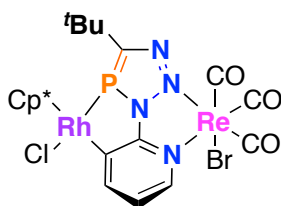
In a J. R. Young NMR tube 80 mg (0.14 mmol, 2 eq.) **C12** were suspended together with 43.3 mg (0.07 mmol, 1 eq.) [**Rh**(Cp*)Cl$_2$]$_2$ and 11.23 (0.137 mmol, 2 eq.) sodium acetate in 0.5 ml DCM-d$_2$. The reaction was heated for 1424 h in an 80 °C hot oil bath. The reaction was stopped since no further progress was noticeable. No pure product could be obtained.

^{31}P NMR (162 MHz, methylene chloride-d$_2$): δ = 133.1 (d, of $^1J_{\text{P-Rh}}$ = 137.1 Hz) ppm.

Attempts in the Synthesis of Iridium(III) [(1,2,3,4,5-η)-1,2,3,4,5-pentamethyl-2,4-cyclopentadien-1yl)] chlorid {Rhenium(I) tris(carbonyl) 2-(5-(tert-butyl)-3H-1,2,3,4-triazaphosphol-3-yl)pyridyl} bromide (C20):
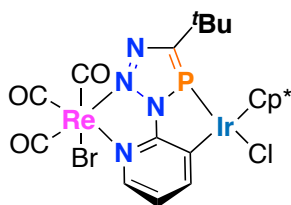
In a J. R. Young NMR tube 80 mg (0.14 mmol, 2 eq.) **C12** were suspended together with 55.9 mg (0.07 mmol, 1 eq.) [**Ir**(Cp*)Cl$_2$]$_2$ and 11.5 (0.14 mmol, 2 eq.) sodium acetate in 0.5 ml DCM-d$_2$. The reaction was heated for 743 h in an T = 80 °C hot oil bath. Monitoring the reaction by means of ^{31}P{^{1}H} NMR showed the formation of several by-products and therefore stopped.

General Procedure for the Attempts in Cu(I) Complexation Reactions:

In a J. R. Young NMR tube 20 mg (0.09 mmol) of **L12** and 0.09 mmol of the copper precursor were dissolved in 0.5 mL dry DCM. (a) The reaction progress was monitored by means of ^{31}P{^{1}H} NMR spectroscopy. (b) If no significant shift in the ^{31}P{^{1}H} NMR was

observed, the reaction was sonicated in an ultrasonic bath over night. (c) If still no complexation was detected, the reaction was heated for 8 h at T = 80°C.

Each significant shift was further investigated by means of ^{1}H NMR spectroscopy in a deuterated solvent.

*Attempts in the synthesis of Copper(I) 2-(5-(tert-butyl)-3H-1,2,3,4-triazaphosphol-3-yl)pyridyl bromide (**C22**):*
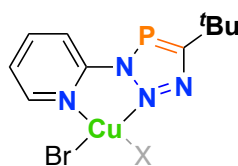
Procedures (a) to (c). No indication for any product formation.

*Attempts in the synthesis of Copper(I) 2-(5-(tert-butyl)-3H-1,2,3,4-triazaphosphol-3-yl)pyridyl iodide dimethyl sulfide (**C23**):*
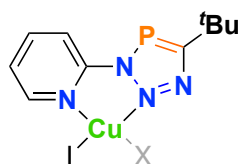
Procedures (a) to (c). No indication for any product formation.

*Synthesis of Copper(I) 2-(5-(tert-butyl)-3H-1,2,3,4-triazaphosphol-3-yl)pyridyl trifluoromethanesulfonate dimer (**C24**):*
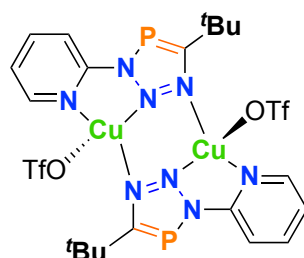
Procedure (a). Purification: Isolation of the crystalline material or complex solution in DCM was decanted and precipitated by pentane, resulted in either blood red platelets in 65 % yield or in a dark red solid (85% yield). Drying the solids in high vacuum led to brightening of the color.

¹H NMR (400 MHz, acetonitrile-d₃): δ = 1.45 (d, $^4J_{H\text{-}P}$ = 1.6 Hz, 9H, Me-H), 7.40(ddd, $^3J_{H\text{-}H}$ = 7.3 Hz, $^4J_{H\text{-}H}$ = 4.9 Hz, $^5J_{H\text{-}H}$ = 1.2 Hz, 1H, Ar-H), 7.93 - 8.01 (m, 1H, Ar-H), 8.04 (dt, $^3J_{H\text{-}H}$ = 8.2 Hz, $^5J_{H\text{-}H}$ = 1.0 Hz, 1H, Ar-H), 8.45 (ddd, $^3J_{H\text{-}H}$ = 5.0 Hz, $^4J_{H\text{-}H}$ = 1.8 Hz, $^5J_{H\text{-}H}$ = 0.9 Hz, 1H, Ar-H) ppm.

¹³C NMR (176 MHz, methylene chloride-d₂): δ = 31.37 (d, $^3J_{C\text{-}P}$ = 9.1 Hz, Me-C11, Me-C12, Me-C13), 36.73 (d, $^2J_{C\text{-}P}$ = 14.6 Hz), 116.74 (d, $^3J_{C\text{-}P}$ = 13.5 Hz, Ar-C3), 126.15 (s, Ar-C5), 142.30 (s, Ar-C4), 152.90 (s, Ar-C6), 153.01 (d, $^2J_{C\text{-}P}$ = 10.0 Hz), 188.08 (s, CO), 195.15 (s, CO), 197.11 (s, CO), 201.62 (d, $^1J_{C\text{-}P}$ = 60.9 Hz) ppm.

³¹P{¹H} NMR (162 MHz, acetonitrile-d₃): δ = 175.9 (s) ppm.

ESI-TOF-MS(+, 200 V)**:** [1/2 M +MeCN]⁺: 324.0437 m/z (calc.: 324.0439).

*Synthesis of Copper(I) 2-(5-(tert-butyl)-3H-1,2,3,4-triazaphosphol-3-yl)pyridyl tetrafluoroborate (dimer) (**C25**):*
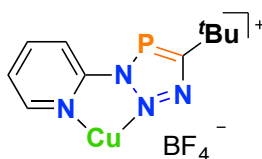
Procedures (a) to (c). No indication for any product formation.

*Synthesis of Copper(I) 2-(5-(tert-butyl)-3H-1,2,3,4-triazaphosphol-3-yl)pyridyl hexafluorophosphate (dimer) (**C26**):*

Procedures (a) to (c). No indication for any product formation.

Red needles, 63% yield.

^{1}H NMR (400 MHz, methylene chloride-d$_2$): δ = 1.61 (s Me-H), 7.76(s, 1H, Ar-H), 8.07 (s,

ESI-TOF-MS(+, 200 V)**:** [1/2 M + MeCN]$^+$: 306.0776 m/z (calc.: 306.0780).

*Synthesis of Copper(I) (2-(5-(tert-butyl)-3H-1,2,3,4-triazaphosphol-3-yl)pyridyl)-(η^2-ethynylphenyl) trifluoromethanesulfonate (**C28**):*
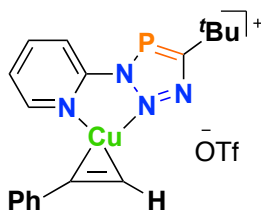
In a Y. R. Young NMR tube 10.0 mg (0.1 mmol, 1 eq.) phenylacetylene and 84.8 mg (0.1 mmol, 1 eq.) **C24** were dissolved in 0.5 mL DCM-d$_2$. Reaction yields quantitative (^{1}H and ^{31}P{^{1}H} NMR) a yellow compound.

^{1}H NMR (400 MHz, methylene chloride-d$_2$): δ = 1.56 (s, 9H, Me-H), 5.00 (s, 1H, CC-H),7.49 (m, 3H, Ar-H), 7.67 (t, J_{H-H} = 5.8 Hz, 1H, Ar-H), 7.72 (d, J_{H-H} = 8.1 Hz, 2H, Ar-H), 8.01 (d, J_{H-H} = 8.2 Hz, 1H, Ar-H), 8.22 (t, J_{H-H} = 8.0 Hz, 1H, Ar-H), 8.56 (s, 1H, Ar-H) ppm.

^{13}C NMR (176 MHz, methylene chloride-d$_2$): δ = 31.49 (s, Me-C), 36.49 (d, $^2J_{C-P}$ = 14.6 Hz), 78.2 (s, Ar-C), 89.1 (s, Ar-C), 116.6 (s, Ar-C), 120.0 (s, Ar-C), 122.1 (s, Ar-C), 126.9 (s, Ar-C), 129.2 (s, Ar-C), 130.1 (s, Ar-C), 132.65 (s, Ar-C), 143.1 (s, Ar-C), 150.4 (s, Ar-C), 200.6 (d, $^1J_{C-P}$ = 61.2 Hz, Ar-C) ppm.

^{31}P{^{1}H} NMR (162 MHz, methylene chloride-d$_2$): δ = 175.9 (s) ppm.

ESI-TOF-MS(+, 200 V)**:** [M-OTf]⁺: 385.0583 m/z (calc.: 385.0638).

*Synthesis of Copper(I) (2-(5-(tert-butyl)-3H-1,2,3,4-triazaphosphol-3-yl)pyridyl)-(η²-ethynylphenyl) trifluoromethanesulfonate 4-(tert-butyl)-1-phenyl-1H-1,2,3-triazole adduct (**C29**):*
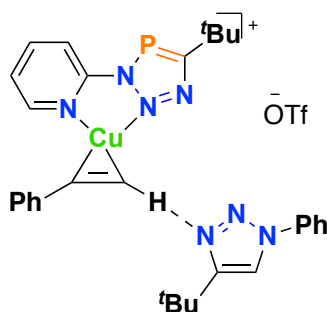
In a Y. R. Young NMR tube 10.0 mg (0.1 mmol, 1 eq.) phenylacetylene and 84,8 mg (0.1 mmol, 1 eq.) **C24** and 19.7 mg (0.1 mmol, 1 eq.) **34** were dissolved in 0.5 mL DCM-d₂. Reaction yielded quantitative (¹H and ³¹P{¹H} NMR) an orange compound.

¹H NMR (400 MHz, methylene chloride-d₂): δ = 1.53 (s, 9H, Me-H), 1.58(s, 9H, Me-H), 4.57 (s, 1H, CC-H), 7.38 (dq, J_{H-H} = 6.6, 14.3 Hz, 3H, Ar-H), 7.54-7.71 (m, 5H, Ar-H), 7.81 (d, J_{H-H} = 7.3 Hz, 2H, Ar-H), 8.02(d, J_{H-H} = 8.0 Hz, 1H, Ar-H), 8.22 (s, 2H, Ar-H), 8.63 (d, J_{H-H} = 4.4 Hz, 1H, Ar-H) ppm.

³¹P {¹H}NMR (162 MHz, methylene chloride-d₂): δ = 172.2 (s) ppm.

*Synthesis of {Cu(μ-CC-Ph)(2-(5-(tert-butyl)-3H-1,2,3,4-triazaphosphol-3-yl)pyridyl)}₂ (**C30**):*
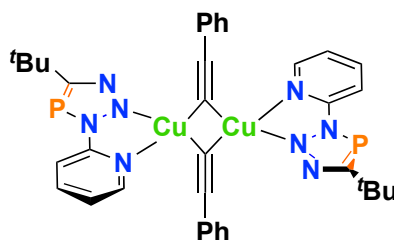
In a Y. R. Young NMR tube 10.0 mg (0.1 mmol, 1 eq.) phenylacetylene and 84,8 mg (0.1 mmol, 1 eq.) **C24** and 11.0 mg (0.1 mmol, 1 eq.) DABCOwere dissolved in 0.5 mL DCM-d$_2$. Reaction yielded quantitative (^{1}H and ^{31}P{^{1}H} NMR) an red compound.

^{1}H NMR (400 MHz, methylene chloride-d$_2$): δ = 1.47 (d, $^4J_{\text{H-P}}$ = 1.5 Hz, 9H, Me-H), 7.36(t, $^3J_{\text{H-H}}$ = 6.2 Hz, 1H, Ar-H), 7.87 - 7.99 (m, 1H, Ar-H), 8.07 (d, $^3J_{\text{H-H}}$ = 8.4 Hz, 1H, Ar-H), 8.48 (d, $^3J_{\text{H-H}}$ = 4.9 Hz, 1H, Ar-H) ppm.

^{19}F NMR (162 MHz, methylene chloride-d$_2$): δ = 78.9 (s) ppm.
^{31}P{^{1}H} NMR (162 MHz methylene chloride-d$_2$): δ = 167.7 (s) ppm.

Bibliography of Chapter 3.2

(1)   Sklorz, J. A. W.; Hoof, S.; Rades, N.; Derycke, N.; Könczöl, L.; Szieberth, D.; Weber, M.; Wiecko, J.; Nyulászi, L.; Hissler, M.; Müller, C. *Chem. Eur. J.* **2015**, *21* (31), 11096.

(2)   Botiz, I.; Astilean, S.; Stingelin, N. *Polym. Int.* **2016**, *65*, 157.

(3)   Cheng, Y.-J.; Yang, S.-H.; Hsu, C.-S. *Chem. Rev.* **2009**, *109* (11), 5868.

(4)   Priegert, A. M.; Rawe, B. W.; Serin, S. C.; Gates, D. P. *Chem. Soc. Rev.* **2016**, *45*, 922.

(5)   Zhao, Y.; Zhu, K. *Chem. Soc. Rev.* **2015**, *45* (Li), 655.

(6)   Harris, K. D.; Elias, A. L.; Chung, H. J. *J. Mater. Sci.* **2016**, *51* (6), 2771.

(7)   Zhao, G.-W.; Zhao, J.-H.; Hu, Y.-X.; Zhang, D.-Y.; Li, X. *Synth. Met.* **2016**, *212*, 131.

(8)   Omae, I. *Coord. Chem. Rev.* **2015**, *310*, 154.

(9)   Kim, S.; Kim, B.; Lee, J.; Shin, H.; Park, Y. Il; Park, J. *Mater. Sci. Eng. R Reports* **2016**, *99*, 1.

(10)   Lamansky, S.; Djurovich, P.; Murphy, D.; Abdel-Razzaq, F.; Lee, H.-E.; Adachi, C.; Burrows, P. E.; Forrest, S. R.; Thompson, M. E. *J. Am. Chem. Soc.* **2001**, *123* (18), 4304.

(11)   Lo, W. K. C.; Huff, G. S.; Cubanski, J. R.; Kennedy, A. D. W.; McAdam, C. J.; McMorran, D. A.; Gordon, K. C.; Crowley, J. D. *Inorg. Chem.* **2015**, *54* (4), 1572.

(12)   Deligonul, N.; Browne, A. R.; Golen, J. A.; Rheingold, A. L.; Gray, T. G. *Organometallics* **2014**, *33* (3), 637.

(13)   Hu, Y.; Maclennan, A.; Sham, T. K. *J. Lumin.* **2015**, *166*, 143.

(14)   Juris, A.; Balzani, V.; Barigelletti, F.; Campagna, S.; Belser, P.; von Zelewsky, A. *Coord. Chem. Rev.* **1988**, *84* (C), 85.

(15)   Stoeffler, H. D.; Thornton, N. B.; Temkin, S. L.; Schanze, K. S. *J. Am. Chem. Soc.* **1995**, *117* (22), 7119.

(16)   Evans, R. C.; Douglas, P.; Winscom, C. J. *Coord. Chem. Rev.* **2006**, *250* (15-16), 2093.

(17)   Cocchi, M.; Kalinowski, J.; Virgili, D.; Fattori, V.; Develay, S.; Williams, J. A. G. *Appl. Phys. Lett.* **2007**, *90* (16), 77.

(18)   Chi, Y.; Chou, P.-T. *Chem. Soc. Rev.* **2007**, *36* (9), 1421.

(19)   Argazzi, R.; Bertolasi, E.; Chiorboli, C.; Bignozzi, C. A.; Itokazu, M. K.; Murakami Iha, N. Y. *Inorg. Chem.* **2001**, *40* (27), 6885.

(20)   Leitl, M. J.; Küchle, F. R.; Mayer, H. A.; Wesemann, L.; Yersin, H. *J. Phys. Chem. A* **2013**, *117* (46), 11823.

(21)   Zhang, Q.; Komino, T.; Huang, S.; Matsunami, S.; Goushi, K.; Adachi, C. *Adv. Funct. Mater.* **2012**, *22* (11), 2327.

(22)   Zhong, C.; Guo, R.; Wu, Q.; zhang, H. *React. Funct. Polym.* **2007**, *67* (5), 408.

(23)   Deaton, J. C.; Switalski, S. C.; Kondakov, D. Y.; Young, R. H.; Pawlik, T. D.; Giesen, D. J.; Harkins, S. B.; Miller, A. J. M.; Mickenberg, S. F.; Peters, J. C. *J. Am. Chem. Soc.* **2010**, *132* (27), 9499.

(24)   Hissler, M.; Dyer, P. W.; Réau, R. *Coord. Chem. Rev.* **2003**, *244* (1-2), 1.

(25)   Baumgartner, T.; Réau, R. *Chem. Rev.* **2006**, *106*, 4681.

(26)   Su, H.-C.; Fadhel, O.; Yang, C.-J.; Cho, T.-Y.; Fave, C.; Hissler, M.; Wu, C.-C.; Reau, R. *J. Am. Chem. Soc.* **2006**, *128* (3), 983.

(27)   Chen, H.; Delaunay, W.; Yu, L.; Joly, D.; Wang, Z.; Li, J.; Wang, Z.; Lescop, C.; Tondelier, D.; Geffroy, B.;

Duan, Z.; Hissler, M.; Mathey, F.; Réau, R. *Angew. Chem. Int. Ed.* **2012**, *51*, 214.

(28)   Broeckx, L. E. E.; Delaunay, W.; Latouche, C.; Lutz, M.; Boucekkine, A.; Hissler, M.; Müller, C. *Inorg. Chem.* **2013**, *52* (19), 10738.

(29)   Roesch, P.; Nitsch, J.; Lutz, M.; Wiecko, J.; Steffen, A.; Müller, C. *Inorg. Chem.* **2014**, *53* (18), 9855.

(30)   de Krom, I. 2-(2'-Pyridyl)-4,6-diphenylphosphinine Synthesis, charakterization, and reactivity based on aromatic phosphorus heterocycles, Dissertation Eindhoven University of Technology Library, 2015.

(31)   Andersen, J.; Madsen, U.; Björkling, F.; Liang, X. *Synlett* **2005**, No. 14, 2209.

(32)   Lowe-Ma, C.; Nissan, R. A.; Wilson, W. S. *J. Org. Chem.* **1990**, *55* (12), 3755.

(33)   Evans, R. A.; Wentrup, C. *J. Chem. Soc., Chem. Commun.* **1992**, No. 1062, 1062.

(34)   Chattopadhyay, B.; Vera, C. I. R.; Chuprakov, S.; Gevorgyan, V. *Org. Lett.* **2010**, *12* (9), 2166.

(35)   Roncali, J. *Chem. Rev.* **1997**, *97* (1), 173.

(36)   Roncali, J. *Macromol. Rapid Commun.* **2007**, *28* (17), 1761.

(37)   Grimsdale, A. C.; Chan, K. L.; Martin, R. E.; Jokisz, P. G.; Holmes, A. B. *Chem. Rev.* **2009**, *109* (3), 897.

(38)   Yamamoto, T.; Fukumoto, H.; Koizumi, T. *J. Inorg. Organomet. Polym. Mater.* **2009**, *19* (1), 3.

(39)   Scarborough, C. C.; Wieghardt, K. *Inorg. Chem.* **2011**, *50* (20), 9773.

(40)   Choua, S.; Sidorenkova, H.; Geoffroy, M.; Rosa, P.; Ricard, L.; Floch, P. Le. *J. Am. Chem. Soc.* **2000**, 12227.

(41)   LeFloch, P. e; Ricard, L.; Mathey, F.; Jutand, A.; Amatore, C. *Inorg. Chem.* **1995**, *34* (1), 11.

(42)   Breque, A.; Santini, C. C.; Mathey, F.; Fischer, J.; Mitschler, A. *Inorg. Chem.* **1984**, *23* (22), 3463.

(43)   Procedure, E.; Echegoyen, L.; Decian, A.; Fischer, J.; Lehn, J. *Angew. Chem. Int. Ed.* **1991**, *30* (7), 838.

(44)   Müller, C.; Broeckx, L. E. E.; de Krom, I.; Weemers, J. J. M. *Eur. J. Inorg. Chem.* **2013**, 187.

(45)   Kleiman, J. P.; Dubeck, M. *J. Am. Chem. Soc.* **1963**, *85*, 1544.

(46)   Ho, C. L.; Li, H.; Wong, W. Y. *J. Organomet. Chem.* **2014**, *751*, 261.

(47)   Yersin, H.; Rausch, A. F.; Czerwieniec, R.; Hofbeck, T.; Fischer, T. *Coord. Chem. Rev.* **2011**, *255* (21-22), 2622.

(48)   Chi, Y.; Tong, B.; Chou, P. T. *Coord. Chem. Rev.* **2014**, *281*, 1.

(49)   Dumur, F. *Org. Electron. physics, Mater. Appl.* **2015**, *21*, 27.

(50)   Williams, J. A. G. *Chem. Soc. Rev.* **2009**, *38* (6), 1783.

(51)   You, Y.; Park, S. Y. *Dalton Trans.* **2009**, *9226* (8), 1267.

(52)   Wong, W.-Y.; Ho, C.-L. *J. Mater. Chem.* **2009**, *19* (26), 4457.

(53)   Suzuri, Y.; Oshiyama, T.; Ito, H.; Hiyama, K.; Kita, H. *Sci. Technol. Adv. Mater.* **2014**, *15* (5), 054202.

(54)   Broeckx, L. E. E.; Lutz, M.; Vogt, D.; Müller, C. *Chem. Commun.* **2011**, *47* (7), 2003.

(55)   de Krom, I.; Lutz, M.; Müller, C. *Dalton Trans.* **2015**, *44* (22), 10304.

(56)   Stoessel, P. WO2010086089A1.pdf. WO 2010086089, 2010.

(57)   Beyer, B.; Ulbricht, C.; Escudero, D.; Friebe, C.; Winter, A.; González, L.; Schubert, U. S. *Organometallics* **2009**, *28* (18), 5478.

(58)   Choong, S. L.; Nafady, A.; Stasch, A.; Bond, A. M.; Jones, C. *Dalton Trans.* **2013**, *42* (21), 7775.

(59)   Vliegenthart, A. B.; Müller, C. *Chelating Synthesis and Coordination Chemistry of Novel Bidentate Ligands Based on Low - Coordinated Phosphorus Heterocycles*; 2016.

(60)   Valeur, B.; Berberan-Santos, M. N. *J. Chem. Educ.* **2011**, *88* (6), 731.

(61)   Anderson, C. B.; Elliott, A. B. S.; McAdam, C. J.; Gordon, K. C.; Crowley, J. D. *Organometallics* **2013**, *32* (3), 788.

(62)   Modelli, A.; Hajgatá, B.; Nixon, J. F.; Nyulászi, L. *J. Phys. Chem. A* **2004**, *108* (36), 7440.

(63)   Bock, H.; Mollère, P. D. *J. Chem. Ed.* **1972**, 506.

(64)   James, T. L. *J. Chem. Educ.* **1971**, *48* (11), 712.

(65)   von Nagy-Felsobuki, E. I. *J. Chem. Educ.* **1989**, *66* (10), 821.

(66)   Lacombe, S.; Gonbeau, D.; Cabioch, J.; Pellerin, B.; Denis, J.; Pfister-Guillouzo, G. *J. Am. Chem. Soc.* **1988**, *110*, 6964.

(67)   Veszprkmi, T.; Nyulhszi, L.; Nagy, J. *J. Organomet. Chem.* **1987**, *331*, 175.

(68)   Nyulászi, L.; Veszpremi, T.; Reffy, J.; Burkhardt, B.; Regitz, M. *J. Am. Chem. Soc.* **1992**, *114* (23), 9080.

(69)   Liu, S. Y.; Alnama, K.; Matsumoto, J.; Nishizawa, K.; Kohguchi, H.; Lee, Y. P.; Suzuki, T. *J. Phys. Chem. A* **2011**, *115* (14), 2953.

(70)   Palmer, M. H.; Hoffmann, S. V.; Jones, N. C.; Head, A. R.; Lichtenberger, D. L. *J. Chem. Phys.* **2011**, *134* (8).

(71)   Qiao, J.; Liu, Y.; Hong, F.; Zhang, J. *A review of catalysts for the electroreduction of carbon dioxide to produce low-carbon fuels.*; 2006; Vol. 37.

(72)   Grice, K. A.; Kubiak, C. P. *Recent Studies of Rhenium and Manganese Bipyridine Carbonyl Catalysts for the Electrochemical Reduction of CO2*, 1st ed.; Elsevier Inc., 2014; Vol. 66.

(73)   Yamazaki, Y.; Takeda, H.; Ishitani, O. *J. Photochem. Photobiol. C Photochem. Rev.* **2015**, *25*, 106.

(74)   Benson, E. E.; Grice, K. A.; Smieja, J. M.; Kubiak, C. P. *Polyhedron* **2013**, *58*, 229.

(75)   Schneider, J.; Jia, H.; Muckerman, J. T.; Fujita, E. *Chem. Soc. Rev.* **2012**, *41* (6), 2036.

(76)   Bakan, S.; Raschke, E. *Promet* **2002**, *28* (3/4), 85.

(77)   Meserole, C. a.; Mulcahy, F. M.; Lutz, J.; Yousif, H. A. *J. Chem. Educ.* **1997**, *74* (3), 316.

(78)   Pletcher, D. *Electrochem. Commun.* **2015**, *61*, 97.

(79)   Reithmeier, R.; Bruckmeier, C.; Rieger, B. *Catalysts* **2012**, *2* (4), 544.

(80)   Windle, C. D.; Perutz, R. N. *Coord. Chem. Rev.* **2012**, *256* (21-22), 2562.

(81)   Kumar, B.; Llorente, M.; Froehlich, J.; Dang, T.; Sathrum, A.; Kubiak, C. P. *Annu. Rev. Phys. Chem.* **2012**, *63*, 541.

(82)   Hawecker, J.; Lehn, J.-M.; Ziessel, R. *J. Chem. Soc. Chem. Commun.* **1984**, *984* (6), 328.

(83)   Johnson, F. P. A.; George, M. W.; Hartl, F.; Turner, J. J. *Organometallics* **1996**, *15* (15), 3374.

(84)   Scheiring, T.; Klein, A.; Kaim, W. *J. Chem. Soc., Perkin Trans. 2* **1997**, 2569.

(85)   Benson, E. E.; Kubiak, C. P. *Chem. Commun.* **2012**, *48* (59), 7374.

(86)   Sullivan, B. P.; Bolinger, C. M.; Conrad, D.; Vining, W. J.; Meyer, T. J. *J. Chem. Soc., Chem. Commun.* **1985**, 1414.

(87)   Benson, E. E.; Sampson, M. D.; Grice, K. A.; Smieja, J. M.; Froehlich, J. D.; Friebel, D.; Keith, J. A.; Carter, E. A.; Nilsson, A.; Kubiak, C. P. *Angew. Chem. Int. Ed.* **2013**, *52* (18), 4841.

(88)   Riplinger, C.; Sampson, M. D.; Ritzmann, A. M.; Kubiak, C. P.; Carter, E. A. *J. Am. Chem. Soc.* **2014**, *136* (46), 16285.

(89)   Smieja, J. M.; Benson, E. E.; Kumar, B.; Grice, K. A.; Seu, C. S.; Miller, A. J. M.; Mayer, J. M.; Kubiak, C. P. *Proc. Natl. Acad. Sci. U.S.A.* **2012**, *109*, 15646.

(90)   Kaim, W.; Kohlmann, S. *Chem. Phys. Lett.* **1987**, *139* (3-4), 365.

(91)   Kaim, W.; Kohlmannt, S. *Inorg. Chem.* **1990**, *29*, 2909.

(92)   Kleverlaan, C. J.; Stufkens, D. J. *Chem. Commun.* **1999**, No. 15, 1411.

(93)   Gibson, D. H.; Sleadd, B. A.; Vij, A. *J. Chem. Crystallogr.* **1999**, *29* (5), 619.

(94)   Gibson, D. H.; Yin, X.; He, H.; Mashuta, M. S. *Organometallics* **2003**, *22* (2), 337.

(95)   Slater, S.; Wagenknecht, J. H. *J. Am. Chem. Soc.* **1984**, *106*, 5367.

(96)   Wong, K.; Chung, W.; Lau, C. *Jounal Electroanal. Chem.* **1998**, *453*, 161.

(97)   Yaroshevsky, a. a. *Geochemistry International* **2006**, *44* (1), 48.

(98)   Bourrez, M.; Molton, F.; Chardon-Noblat, S.; Deronzier, A. *Angew. Chem. Int. Ed.* **2011**, *50* (42), 9903.

(99)   Smieja, J. M.; Sampson, M. D.; Grice, K. A.; Benson, E. E.; Froehlich, J. D.; Kubiak, C. P. *Inorg. Chem.* **2013**, *52* (5), 2484.

(100)   Sampson, M. D.; Nguyen, A. D.; Grice, K. A.; Moore, C. E.; Rheingold, A. L.; Kubiak, C. P. *J. Am. Chem. Soc.* **2015**, *137* (10), 3718.

(101)   Sampson, M. D.; Kubiak, P. *Inorg. Chem.* **2015**, *54*, 6674.

(102)   Hoffert, M. I.; Caldeira, K.; Jain, A. K.; Haites, E. F.; Harvey, L. D. D.; Potter, S. D.; Schlesinger, M. E.; Schneider, S. H.; Watts, R. G.; Wigley, T. M. L.; Wuebbles, D. J. *Nature* **1998**, *395* (6705), 881.

(103)   Blakemore, J. D.; Crabtree, R. H.; Brudvig, G. W. *Chem. Rev.* **2015**.

(104)   Rabten, W.; Kärkäs, M. D.; Åkermark, T.; Chen, H.; Liao, R. Z.; Tinnis, F.; Sun, J.; Siegbahn, P. E. M.; Andersson, P. G.; Åkermark, B. *Inorg. Chem.* **2015**, *54* (10), 4611.

(105)   Chen, Z.; Concepcion, J. J.; Jurss, J. W.; Meyer, T. J. *J. Am. Chem. Soc.* **2009**, *131* (43), 15580.

(106)   Concepcion, J. J.; Jurss, J. W.; Templeton, J. L.; Meyer, T. J. *J. Am. Chem. Soc.* **2008**, *130* (49), 16462.

(107)   Hull, J. F.; Balcells, D.; Blakemore, J. D.; Incarvito, C. D.; Eisenstein, O.; Brudvig, G. W.; Crabtree, R. H. *J. Am. Chem. Soc.* **2009**, *131*, 8730.

(108)   Cueto, L. F.; Hirata, G. a.; Sánchez, E. M. *J. Sol-Gel Sci. Technol.* **2006**, *37* (2), 105.

(109)   Huckaba, A. J.; Sharpe, E. A.; Delcamp, J. H. *Inorg. Chem.* **2016**, *55* (2), 682.

(110)   Hartl, F.; Mahabiersing, T.; Le Floch, P.; Mathey, F.; Ricard, L.; Rosa, P.; Záliš, S. *Inorg. Chem.* **2003**, *42* (14), 4442.

(111)   Walsh, J. J.; Smith, C. L.; Neri, G.; Whitehead, G. F. S.; Robertson, C. M.; Cowan, A. J. *Farad. Discuss.* **2015**, *183*, 147.

(112)   Smieja, J. M.; Kubiak, C. P. *Inorg. Chem.* **2010**, *49* (20), 9283.

(113)   Sklorz, J. A. W.; Hoof, S.; Sommer, M. G.; Weißer, F.; Weber, M.; Wiecko, J.; Sarkar, B.; Müller, C. *Organometallics* **2014**, *33* (2), 511.

(114)   Roesch, P. Synthese, Charakterisierung und Eigenschaften von Phosphininkomplexen der Münzmetalle, Freie Universität Berlin, 2014.

(115)   Urankar, D.; Pinter, B.; Pevec, A.; De Proft, F.; Turel, I.; Kosmrlj, J. *Inorg. Chem.* **2010**, *49* (11), 4820.

(116)   Richardson, C.; Steel, P. J. *Dalton Trans.* **2003**, 992.

(117)   Jahromi, E. Z.; Gailer, J. *Dalton Trans.* **2010**, 329.

(118) Bai, S.-Q.; Jiang, L.; Sun, B.; Young, D. J.; Hor, T. S. A. *Cryst. Eng. Comm.* **2015**, *17*, 3305.

(119) Bai, S.-Q.; Jiang, E. L.; Zuo, B. J.; Yan, C. C.; A, T. S. A. H. *Aust. J. Chem.* **2013**, *66*, 1029.

(120) Hohloch, S.; Suntrup, L.; Sarkar, B. *Inorg. Chem. Front.* **2016**, *3* (1), 67.

(121) Bruce, M. I.; Zaitseva, N. N.; Skelton, B. W.; Somers, N.; White, A. H. *Inorganica Chim. Acta* **2007**, *360* (2), 681.

(122) Jin, L.; Tolentino, D. R.; Melaimi, M.; Bertrand, G. *Sci. Adv.* **2015**, *1* (5), e1500304.

(123) Döhler, D.; Michael, P.; Binder, W. H. *Macromolecules* **2012**, *45* (8), 3335.

(124) Worrell, B. T.; Malik, J. a.; Fokin, V. V. *Science* **2013**, *340*, 457.

(125) Pardin, C.; Roy, I.; Lubell, W. D.; Keillor, J. W. *Chem. Biol. Drug Des.* **2008**, *72* (3), 189.

(126) Galli, U.; Mesenzani, O.; Coppo, C.; Sorba, G.; Canonico, P. L.; Tron, G. C.; Genazzani, A. A. *Eur. J. Med. Chem.* **2012**, *55*, 58.

(127) Alvarez, S. G.; T., A. M. *Synthesis* **1997**, *1997* (4), 413.

(128) Stengel, I.; Mishra, A.; Pootrakulchote, N.; Moon, S.-J.; Zakeeruddin, S. M.; Grätzel, M.; Bäuerle, P. *J. Mater. Chem.* **2011**, *21* (11), 3726.

3.3 Chemical Modification of Triazaphospholes

3.2.1 Methylated Triazaphospholes – the Isoelectronic Analogues of the 1*H*-1,2,3-Triazolylidenes

In coordination chemistry, N-heterocyclic carbenes (nNHCs)[1,2] of type **A** (Figure 77) were extensively investigated and discovered to be useful ligands in different catalytic reactions. To mention some examples, nNHCs were used in metathesis reactions,[3] polymerisation reactions[4] or even as organocatalyst[5] as well as other reactions.[6–8] The broad application of these compounds originates from their binding strength and tuneability towards redox activity.[9] Besides this normal binding mode *via* the carbon in 2-position, Crabtree *et al.* observed an "abnormal" binding mode of type **B**,[10] where the term of the abnormal carbenes was derived from later. Bertrand was finally able to isolate a non-coordinated compound.[11]However, in the context of triazaphosphole chemistry, the subgroup of the 1,2,3-triazolyidenes[12] **C** are the most interesting because they are the isoelectronic counterpart to the 1,2,3,4-triazaphosphol-1-ium salts **D**. Due to the unique properties of 1,2,3-triazolydenes, the modular construction owned by their "click"-chemical approach and donor ability is filling the donation ability gap between nNHCs **A** and aNHCs **B**.[13] These compounds were also extensively investigated as catalysts for condensation,[14] hydroamination[15], hydrosilation,[16] oxidation reactions[17], as is can be shown by these review articles.

The following part will deal with the synthesis of the unknown 1,2,3,4-triazaphosphol-1-ium analogues.
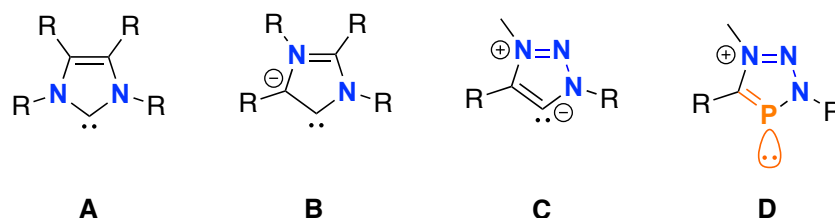
Figure 77: Structures of selected carbene types and one triazaphospholium cation.

As shown before (Chapter 3.1), the triazaphospholes preferentially bind as a chelating ligand to metal centres. The functionalization of abnormal chelates is not trivial because the additional binding side is alkylated as well. Kǒsmrlj *et al.* developed an elegant pathway to form selectively pyridyl substituted 1,2,3-triazolium salts.[18] The key step in

this approach is the oxidation of the pyridyl nitrogen to a pyridine-*N*-oxide (Scheme 60, **F**). During the methylation, the methoxide **G** is formed and subsequently reduced by hexacarbonyl manganese(0) to the pyridyl functionalized salt **H**. Using this strategy, picolyl and pyridyl substituted triazolium species can be obtained, as well as their inverse click products.
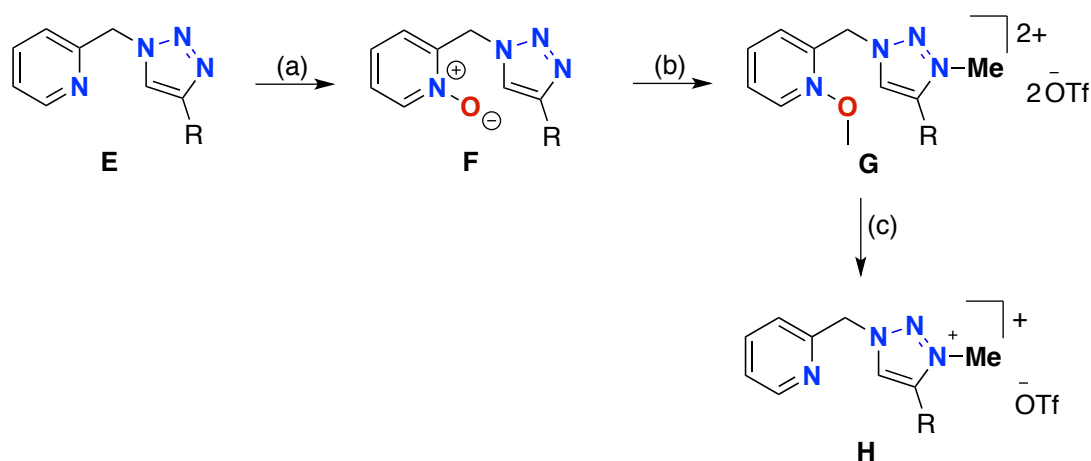
Scheme 60: Synthesis strategy for selective methylated triazolium salts. Reaction conditions: (a) 1.1 eq. *m*-CPBA, CHCl$_3$, 30 min reflux; (b) 1 eq. MeOTf, DCM, 30 min, T = 0 °C; 2 eq. **Mo**(CO)$_6$, EtOH, 1 h reflux.[18]

Attempt in the Synthesis of Pyridyl-N-oxide with Triazaphospholes

The synthesis strategy in Scheme 60 was adopted for triazaphospholes. At first, the same procedure was used for the selective oxidation of the picolyl-functionalized triazaphosphole **L4**, showing no product formation, but decomposition of the starting material. A slight change in the protocol using hydrogen peroxide urea as the oxidative agent did not improve the results (Scheme 61).
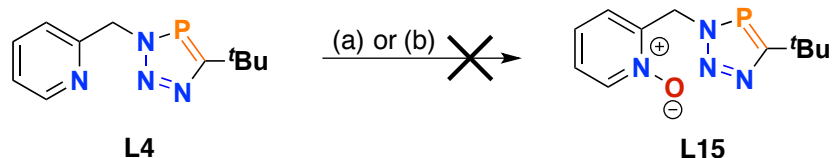
Scheme 61: N-oxide formation for selective methylation. Reaction conditions (a): *m*-CPBA (1.1 eq.), DCM, 30 min r.t., (b): hydrogen peroxide/hydrogen peroxide urea (1.1 eq.), DCM, 30 min, r.t..

Methylation of 3H-1,2,3,4-Triazaphospholes

The compounds **L1** and **L2** were selected for the methylation reactions to investigate the general reactivity and stability of triazaphospholium salts. Initial test reactions were done with equimolar amounts of Meerwein reagent,[19] resulted in multiple resonances in the ^{31}P{^{1}H} NMR spectrum. Consequently, the reaction temperature was lowered to T = -78 °C, but no product formation was observed as well as when the reaction was performed at T = -20 °C.

For further investigations, dimethyl sulfate was used, which is a more soft methylation reagent. However, this reagent was obviously too weak to generate the triazaphospholium salt. In the last attempt, the usage of methyl triflate revealed the formation of two resonances in the ^{31}P{^{1}H} NMR spectrum. The more high field shifted resonance at δ = 206.5 ppm was attributed to the starting material (**L1**), while the signal located at δ = 243.2 ppm was assigned to the triazaphospholium salt. Further addition of methyl triflate up to 2.2 equivalents resulted in a full conversion of the starting material (Scheme 62).
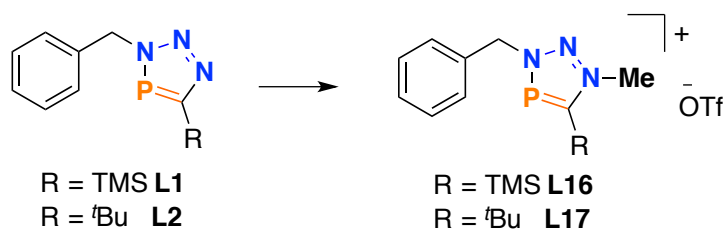
Scheme 62: Synthesis of triazaphospholium salts **L16** and **L17**. Reaction conditions: Methyl triflate (2.2 eq.), MeCN, T = 0 °C, 2h.

Due to the decomposition of the product, all further reactions were performed at T = 0°C. The chemical shift of the *tert*-butyl substituted triazaphosphonium **L17** in ^{31}P{^{1}H} NMR spectroscopy was determined at δ = 203.5 ppm. Further, a solvent dependency was discovered as product formation occurred in acetonitrile exclusively. From reactions in diethyl ether and DCM, no product was obtained. A further important point was the usage of freshly distilled methyl triflate, as the ^{1}H NMR spectra (Figure 78) showed fewer signals. The compounds have been recrystallized from dichloromethane, but no single crystals suitable for X-ray diffraction analysis were obtained. Besides the ^{31}P{^{1}H} NMR spectrum indicating a strong downfield shift for the alkylated compounds **L16** and **L17** and signifying a strong decrease in electron density in the heterocycle,

clear evidence for the product formation can be derived from the ^{1}H NMR spectrum. The additional resonance located at $\delta = 4.45$ ppm corresponds to the introduced methyl group. This data is in line with the signal splitting to a double, showing a coupling constant of $^4J_{\text{H-P}} = 1.0$ Hz. This value is a bit below the usual values for a $^4J_{\text{H-P}}$ coupling *via* a nitrogen atom but connected to electron withdrawing groups similarities are noticeable.[20] From the coupling constant, no information regarding the position of the methyl group can be obtained. However, most likely, methylation would occur at the N[1] atom, as previous metal coordination had shown (Chapter 1 & 3). Furthermore, all signals are shifted to the downfield, which might be attributed to the lower shielding.
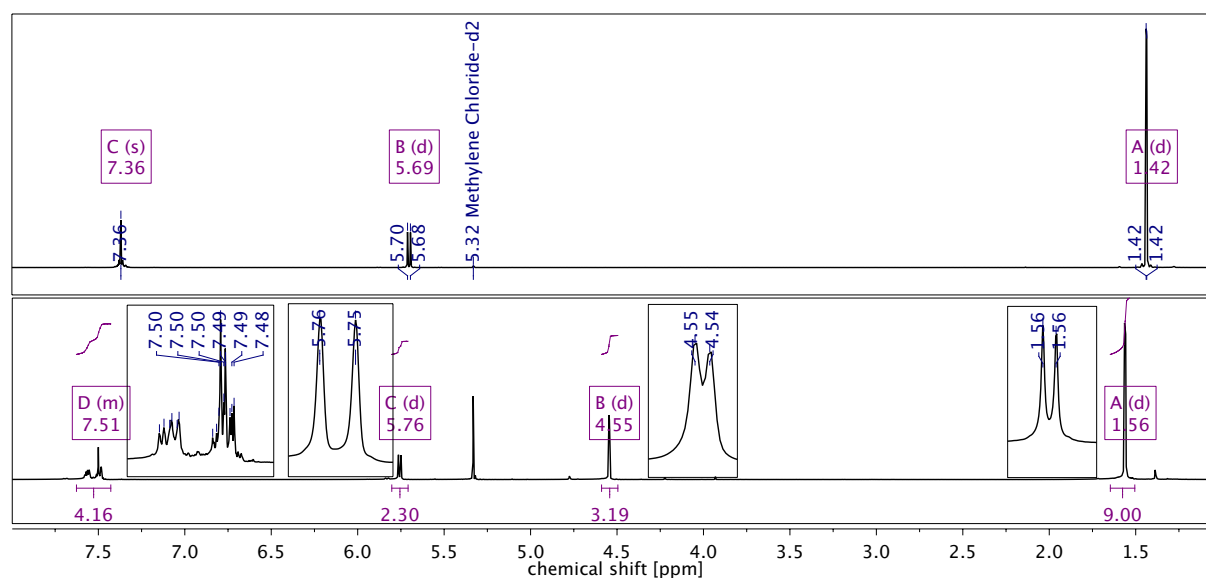
Figure 78: (top) ^{1}H NMR spectrum of **L2**, referenced to DCM-d[2]. (**bottom**) ^{1}H NMR spectrum of **L17**, referenced to DCM-d[2]. Traced of side product are visible. Product resonances are highlighted.

Investigations towards Stabilization of 3H-1,2,3,4-Triazaphospholium Salts

Further evidence for product formation was obtained from the ^{13}C NMR spectra. The additional carbon atom verifies the findings observed by ^{1}H NMR spectroscopy, as an extra resonance is found at δ(DCM-d[2]) = 35.7 ppm. The coupling constant of $^3J_{\text{C-P}} = 11.4$ Hz is slightly larger than the other assignments, but might be attributed to the vinylic position of the N[1] to the phosphorus atom. Moreover, compared to the coupling constants in the **L2**, all values are enlarged in the methylated species and correspond with previous reports on coupling constant enlargement.[21] The same results also apply to the modification of ligand **L1**. The stabilization of the methylated compound was also investigated with metal coordination towards Cu(I), but no

213

coordination could be detected. Silylation with trimethylsilyl triflate, assuming that it would provide a higher stability due to the increased steric bulk, did not show any product formation (Scheme 63).
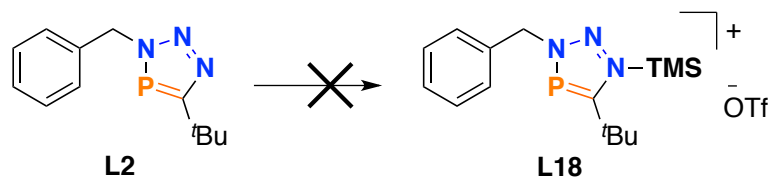
Scheme 63: Attempts in silylation with TMS triflate. Reaction conditions: TMS triflate (2.2 eq.), MeCN, 2h, r.t..

Based on the instability of the triaza phosphonium salt, the project was discontinued.

3.2.2 Modification by Diels-Alder Reactions

Pericyclic reactions are well established in the low-coordinate phosphorus chemistry and are a useful tool for ligand synthesis. For example, the so-called phosphabarrelenes (Figure 79, **A**) are the cycloaddition products of a carbon-carbon triple bond with phosphinines. While the synthesis of the parent compound was to this point not reported, the synthesis and characterization of the barrelene tungsten pentacarbonyl complex are described,[22] as well as several substituted phosphabarrelenes. The interest in these compounds is set to catalysis reactions due to their steric demand. Bulky phosphorus compounds provide an adequate stabilization of highly active species by kinetic shielding[23–25] and their suitability as ligands have been demonstrated in cycloisomerization, hydroformylation, and cross-coupling reactions.[26-32]

However, similar reaction behaviour shown by phosphinines was also reported for azaphospholes, forming the phosphaazanorbornadienes of type **B**.[33]
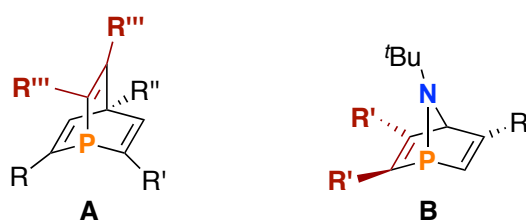
Figure 79: Selected examples of products obtained from cycloaddition. Attached groups are highlighted in red.

The pathway of the reactions strongly depends on the number and position of the nitrogen atoms. In case nitrogen atoms can form a leaving group, the barrelene or norbornadiene is a reactive intermediate, and else wise the (intermediate) product can be isolated. This result might be attributed to the lower electron density in five-membered heterocycles.[13] DFT calculations (B3LYP) performed on aza-, diaza- and phosphinines showed an increased destabilisation in the relative energy values with increasing number of nitrogen atoms.[34] Further, a dependency of the stabilisation on the position of the nitrogen atom(s) in the heterocycle is found. The *meta*-diaza-phosphinine is reported to be about 12 kcal/mol less stable than the *ortho* derivative. The successive N-CH exchange yield for the 5 kcal/mol more stable *ortho*-aza-phosphinine, while the difference in the stability to the parent phosphorus heterocycle is still 35 kcal/mol higher (Scheme 64). The lower stability can also be connected with a

decrease of aromaticity of these compounds, as bond length and NICS derived from calculations are in line with findings from synthetic approaches by Le Floch *et al.*.[35]

Nitrile expulsion is not necessary for that process. Rickert and Alder reported a cycloreversion, with ethylene eliminated from benzene. Insofar, it is interesting since the addition-elimination reaction does not proceed with cyclopenta-1,3-diene.[36] However, the transformation of substituted cyclohexa-1,3-diene was reported by the same authors.[37] From these findings inspired, Huisgen demonstrated the CO_2 elimination from five-membered heterocycles[38] and the nitrile expulsion was reported by Neunhoeffer *et al.*.[39] In connection with theses studies, the substitution of phosphaalkynes from the heterocycle was also observed.[40]

The transformation of triazaphospholes into diazaphospholes was done, but so far only for the 2*H*-1,2,4,3-triazaphospholes **H**. These compounds contain a N=P double bond and undergo cycloreversion reactions with dimethyl but-2-ynedioate **35** (Scheme 65).[41]
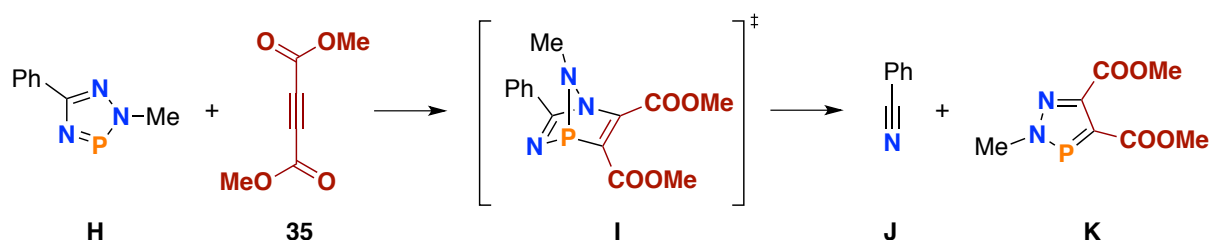
The intermediate **I** was neither isolated nor observed, but benzonitrile **J** and diazaphospholes **K** were identified.

Diels-Alder Reactions of 3H-1,2,3,4-Triazaphospholes

The constitutional isomers of **H**, the 3*H*-1,2,3,4-triazaphospholes, however, were not investigated so far towards their behaviour in cycloaddition and elimination reactions. At first, the reactions were performed with alkyne **35** in toluene. After 108 h of heating at T = 65 °C, a resonance with minor intensity was observed in the ^{31}P{^{1}H} NMR spectrum at δ = 235.2 ppm, assigned to the desired product **L19**. Heating the reaction mixture for additional 28 days showed an increase of intensity for the presumed product signal, but also several new signals appeared (Scheme 66).
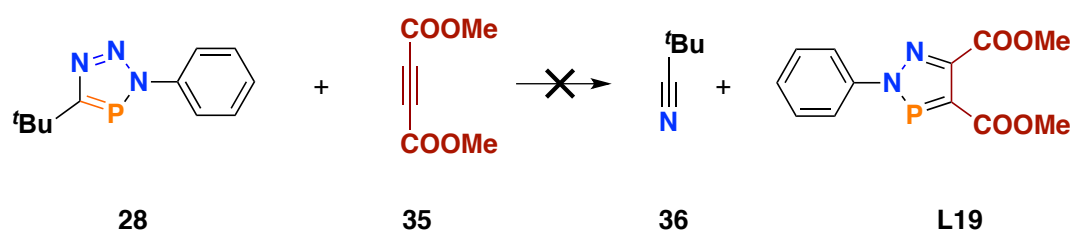
Scheme 66: Assumed product formation by cycloreversion of **28** and **35**.

The impure reaction pathway might be attributed to the presence of an ester functionality. Consequently, this type of electron withdrawing group got substituted by perfluorobutyne (**37**) and toluene was used as a solvent. An overview of the performed reactions is given in Scheme 67. The reactions were first carried out in a sealed NMR tube. All reactions appeared to be quantitative by the NMR spectra, since no resonances, neither of the starting material nor of any by-product, were observed besides the product signal. Further, this experiments exhibited about 25 days longer reaction times for the non-conjugated systems, than for the conjugated compounds. For preparative approaches, the methylene bridged molecules were neglected.

The long reaction times of 95 days for the compounds **L2** and **L4** and 70 days for **28** and **L12** might be caused by the solvent effect observed in Diels-Alder reactions, as reactions that are carried out in an aromatic solvent have longer reaction times.[42]
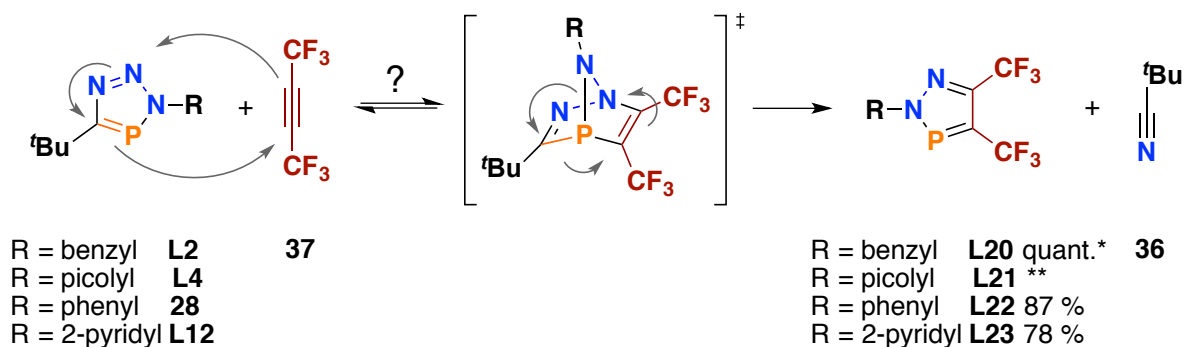
Scheme 67: Cycloreversion reactions performed with perfluorobutyne in a sealed NMR tube. Reaction conditions: 4 eq. Perfluorobutyne, benzene-d_6, T = 65 °C. Reaction times: **L2** and **L4** 95 d. Reaction times: **28** and **L12** 70 d. * NMR yield. ** decomposition.

However, the reaction times of the reported triaza- and diazaphospholes, performed in toluene did not have such long reaction times, although less activated alkynes than the perfluorobutyne were used in fewer equivalents.[43,44] For the long reaction times, either an equilibrium between the starting material and the transition state or a high activation barrier between these two states, might be considered. By this, the formation of the transition state becomes the rate-determining step. Nyulászi and co-workers currently do quantum mechanic investigations concerning these assumptions.

The reactions were also performed with **L2** and **28** in toluene at T = 65 and 110 °C to optimize the reaction parameters. In all cases, the $^{31}P\{^1H\}$ and ^{19}F NMR spectra revealed the formation of by-products. During these investigations, a barrelene-like resonance was observed by $^{31}P\{^1H\}$ NMR spectroscopy during the cycloreversion reaction of **L4** (Figure 80). However, this compound was not isolated because several side-products were formed. The intensity of this signal decreased over the time, indicating the presence of an intermediate. Whether this resonance can be attributed to an intermediate in the pathway towards the product or to the formation of side-products remains unclear. The coupling constant of $^3J_{P-F}$ = 20.8 Hz is below the observed ones for hexafluorobut-2-enyl containing phosphabarrelenes (type **A**, $^3J_{P-F}$ = 38.4 Hz)[45] and a bit larger than the values for hexafluorobut-2-enyl containing aza-phospham norbornadienes (type **B**, $^3J_{P-F}$ = 15.8 Hz)[33].
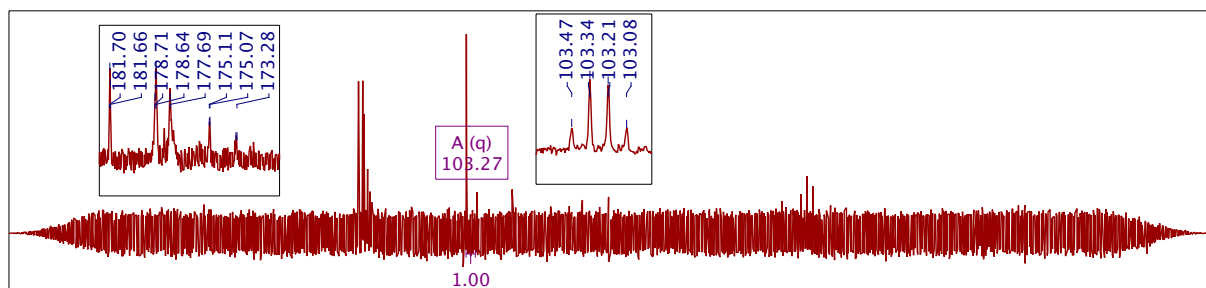
Figure 80: $^{31}P\{^1H\}$ NMR spectrum of the transformation of **L4** in **L21**.

To investigate these findings further, the cycloreversion reactions carried out in a sealed NMR vessel were monitored using ^1H NMR spectroscopy. Using this methodology, the formation of pivalonitrile **36** was observed. During the reaction process, the formation of a new resonance without any coupling to the phosphorus was observed. After the reaction was complete, an equivalent of **36** was added to the sealed NMR tube, resulting in an increase of intensity and integral of the new-formed species.

After the reaction was complete, all volatile compounds were removed under vacuum, and the remaining solids of **L20** and **L22** were redissolved in benzene-d$_6$. A large excess of **36** was added to the sealed NMR tube and heated at T = 65 °C for several days to rule out any retro-cycloreversion reaction (Scheme 68). Neither the starting material of the compounds **L20** and **L22** nor their *cis* products **L2_cis** and **28_cis** could be observed. These results are in line with the previously made assumption that the nitrile eliminations yielded a more stable product.
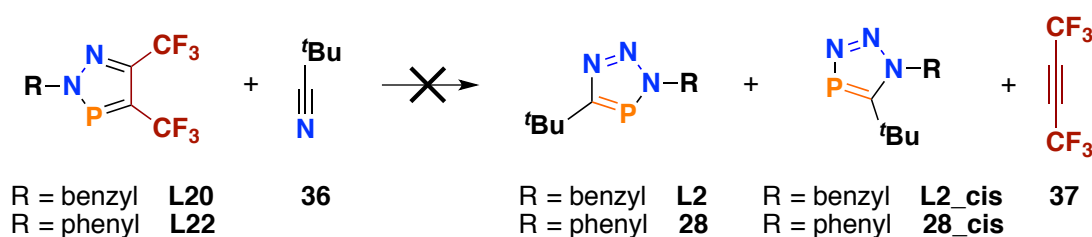
Scheme 68: Attempts in retro-cycloreversion reactions of **L20** and **L22**.

Single crystals of **L22** suitable for X-ray diffraction analysis were obtained by slow evaporating off the DCM solvent and cooling down the mixture slowly down to T = -21 °C and warming back up to room temperature. The first solid state structure of a CF$_3$-subsituted diazaphospholes (Figure 81), it is evident that the exchange of the pivaloyl nitrile by a perfluorobutyne does not cause significant changes in the remaining system. The C^1-P^1 and N^1-N^2 bond distances in the heterocycle are the same as in **28**. The

same holds true for the inter-ring distance of the C^3-N^1 bond. Also, the N^1-P^1-C^1 and the P^1-N^1-N^2, as well as the torsion angle N^2-N^1-C^3-C^4, are not affected by the cycloreversion.
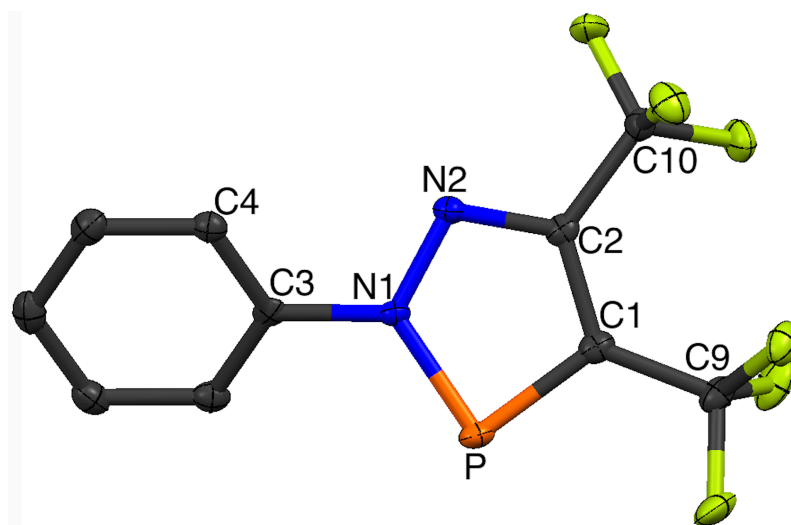
Figure 81: Molecular structure of **L22** in the crystal. Displacement ellipsoids are shown at the 50% probability level. Hydrogen atoms are omitted for clarity. Selected bond lengths (Å) and angles (°). P(1)-C(1): 1.712(2), C(1)-C(2): 1.406(3), C(2)-N(2): 1.323(3), N(2)-N(1): 1.349(2), N(1)-P(1): 1.693(2), N(1)-C(3): 1.436(3). N(1)-P(1)-C(1): 88.14(9), N(2)-N(1)-C(3) C(4): -34.5(3).

For the purpose of exploring the coordination properties of this diazaphospholes, coordination attempts were carried out with **Rh**(I) and **Au**(I) (Scheme 69). For both reactions, the solvent was added to the previously mixed solids in a sealed NMR vessel. In case of the assumed formation of **C31,** a strong gas evolution was observed. No signal could be detected by ^{31}P{^{1}H} NMR spectroscopy, while the ^{19}F NMR spectrum showed several signals. In contrast to that, the attempts in the synthesis of **Au**(I) complex **C32** did not show any change in the chemical shift or shape of the ligand resonance. Also, from the ^{1}H and ^{19}F NMR spectra neither product formation could be concluded, nor decomposition as in **C31** was observed. Further coordination chemistry with different metals is outstanding since the compounds **L22** and **L23** were obtained in the very late phase of this thesis.
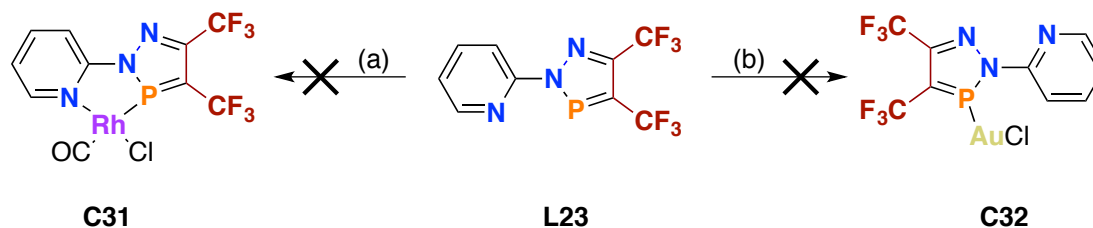
Scheme 69: Efforts in metal coordination towards **L23**. Reaction conditions (a): 1 eq. [Rh(CO)$_2$Cl]$_2$, DCM, 5 min, r.t.; (b): 1 eq. AuCl•SMe$_2$, DCM, 7 d, r.t..

*Synthesis of 3-benzyl-1-methyl-5-(trimethylsilyl)-3H-1,2,3,4-triazaphosphol-1-ium trifluoromethanesulfonate (**L16**)*
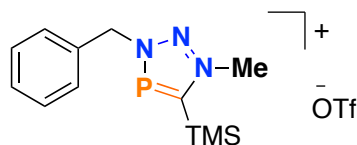
In a 15 mL Schlenk-flask 100 mg (0.40 mmol) of **L2** were dissolved in 6 mL acetonitrile and cooled to T = 0 °C. The solution was treated with 132 mg (0.80 mmol, 2 eq.) methyl triflate. The reaction mixture was stirred for 1.5 h at T = 0 °C and afterwards the solvent was removed in vacuum. Recrystallization from DCM yielded clean product. Quantitative reaction.

¹H NMR (500 MHz, Methylene Chloride-d₂): δ = 0.35 (d, $^4J_{H-P}$ = 1.3 Hz, 9H, Si(CH₃)₃) 4.51 (s, 3H, CH₃), 5.82 (d, $^3J_{H-P}$ = 5.7 Hz, 2H, CH₂), 7.54 (m, 5H, Phenyl-H) ppm.

¹³C{¹H} NMR (176 MHz, Methylene Chloride-d₂): δ = -1.0 (d, $^3J_{C-P}$ = 5.8 Hz, CH₃)₃), 44.6 (CH₃), 60.3 (d, $^2J_{C-P}$ = 9.3 Hz, CH₂), 130.3 (Ar-C), 130.7 (Ar-C), 130.9 (Ar-C) 133.2 (d, $^3J_{C-P}$ = 3.2 Hz, Ar-C), 181.4 (d, $^1J_{C-P}$ = 79.4 Hz, C$_{triazaphosphole}$) ppm.

¹⁹F{¹H} NMR (376 MHz, Methylene Chloride-d₂): δ = -78.6 (s) ppm.

³¹P{¹H} NMR (162 MHz, Methylene Chloride-d₂): δ = 240.2 (s) ppm.

*Synthesis of 3-benzyl-5-(tert-butyl)-1-methyl-3H-1,2,3,4-triazaphosphol-1-ium trifluoromethanesulfonate (**L17**)*
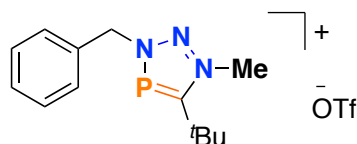
In a 15 mL Schlenk-flask 100 mg (0.43 mmol) **L2** were dissolved in 6 mL acetonitrile and cooled to T = 0 °C. The solution was treated with 176 mg (1.10 mmol, 2.1 eq.) methyl triflate. The reaction mixture was stirred for 1.5 h at T = 0 °C and afterwards the solvent was removed in vacuum. Some purification was obtained by recrystallization from DCM. Recrystallization from DCM yielded clean product. Quantitative reaction.

¹H NMR (500 MHz, Methylene Chloride-d₂): δ = 1.50 (d, *J* = 2.4 Hz, 9H, C(CH₃)₃) 4.45 (d, *J*

= 1.0 Hz, 3H, CH$_3$), 5.73 (d, J = 6.2 Hz, 2H, CH$_2$), 7.47 (m, 5H, Phenyl-H) ppm.

^{13}C{^{1}H} NMR (126 MHz, Methylene Chloride-d$_2$): δ = 30.0 (d, $^3J_{C-P}$ = 10.9 Hz, CH$_3$)$_3$), 30.9 (d, $^2J_{C-P}$ = 7.7 Hz, C$_{tBu}$), 35.6 (d, J = 11.4 Hz, CH$_3$), 60.7 (d, $^2J_{C-P}$ = 10.4 Hz, CH$_2$), 130.2 (Ar-C), 130.7 (Ar-C), 130.8 (Ar-C), 130.84 (Ar-C) 132.96 (d, $^3J_{C-P}$ = 3.6 Hz, Ar-C), 191.2 (d, $^1J_{C-P}$ = 63.8 Hz, C$_{triazaphosphole}$) ppm.

^{19}F{^{1}H} NMR (376 MHz, Methylene Chloride-d$_2$): δ = -78.7 (s) ppm.

^{31}P{^{1}H} NMR (162 MHz, Methylene Chloride-d$_2$): δ = 202.9 (s) ppm.

*Attempts in the synthesis of 3-benzyl-5-(tert-butyl)-1-(trimethylsilyl)-3H-1,2,3,4-triazaphosphol-1-ium trifluoromethanesulfonate (**L18**)*
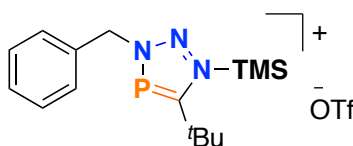
In a 15 mL Schlenk-flask 100 mg (0.43 mmol) **L2** were dissolved in 6 mL acetonitrile and cooled to T = 0 °C. The solution was treated with 244 mg (1.10 mmol, 2.1 eq.) methyl triflate. The reaction mixture was stirred for 1.5 h at T = 0 °C, no reaction was observed, wherefore the mixture was allowed to warm up to r.t. but no product formation was observed.

*Synthesis of 2-benzyl-4,5-bis(trifluoromethyl)-2H-1,2,3-diazaphosphole (**L19**)*
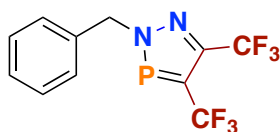
Into a sealed NMR tube 20 mg (0.09 mmol, 1 eq.) **28** was placed, evacuated and 0.45 mmol (5 eq.) perfluorobutyne **36** were condensed in, followed by the addition of 0.5 mL benzene-d$_6$. The reaction mixture was allowed to warm up over night and heated at T = 60 °C for eight weeks. The reaction progress was monitored regularly. Quantitative reaction.

¹H NMR (400 MHz, benzene-d₆): δ = 4.58 (d, $^2J_{H-P}$ = 7.7 Hz, 2H, CH₂) 6.78-6.83 (m, 2H, Ar-H), 6.92-6.98 (m, 2H, Ar-H), 7.08-7.11 (m, 1H, Ar-H) ppm.

¹⁹F{¹H} NMR (376 MHz, benzene-d₆): δ = -52.2 (dq, $^3J_{F-P}$ = 25.1, $^5J_{F-F}$ = 7.3 Hz), -60.74 (q, $^4J_{F-F}$ = 7.3) ppm.

³¹P{¹H} NMR (162 MHz, benzene-d₆): δ = 237.5 (q, $^3J_{P-F}$ = 20.7 Hz).

*Attempts in the synthesis of 2-((4,5-bis(trifluoromethyl)-2H-1,2,3-diazaphosphol-2-yl)methyl)pyridine (**L20**)*
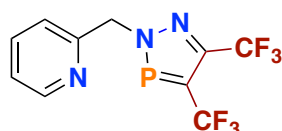
Into a sealed NMR tube 20 mg (0.09 mmol, 1 eq.) **L4** was placed, evacuated and 0.45 mmol (5. eq.) perfluorobutyne **36** were condensed in, followed by the addition of 0.5 mL benzene-d₆. The reaction mixture was allowed to warm up over night and heated at T = 60 °C for eight weeks. And the reaction progress was regularly monitored. Product showed decomposition.

*2-phenyl-4,5-bis(trifluoromethyl)-2H-1,2,3-diazaphosphole (**L21**)*
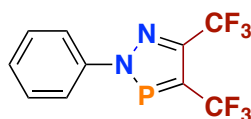
Into a pressure tube 500 mg (2.28 mmol, 1 eq.) **28** was placed, evacuated and 11 mmol (5 eq.) perfluorobutyne **36** were condensed in, followed by 10 mL toluene. The reaction mixture was allowed to warm up over night and heated at T = 60 °C for eight weeks. The excess of **36** as well as the solvent were removed in vacuum and the compound was crystalized from DCM. The compound was obtained as a light brown crystalline material in 87% yield (1.98 mmol).

¹H NMR (700 MHz, Methylene Chloride-d₂): δ = 7.48 (t, $^3J_{H-H}$ = 7.4 Hz, 1H, Ar-H) 7.52 (d, $^3J_{H-H}$ = 7.0, 8.7 Hz, 2H, Ar-H), 7.79 (d, $^3J_{H-H}$ = 8.5 Hz, 2H, Ar-H) ppm.

¹³C{¹H} NMR (126 MHz, Methylene Chloride-d₂): δ = 121.6 (d, $^3J_{C-P}$ = 9.2 Hz, Ar-C), 123.0 (d, $^1J_{C-F}$ = 24.2 Hz, CF₃), 124.5 (d, $^1J_{C-F}$ = 24.4 Hz, CF₃), 129.8 (d, $^4J_{C-P}$ = 1.1 Hz, Ar-C), 130.5

(Ar-C), 142.8 (d, $^2J_{C\text{-}P}$ = 11.5 Hz, phenyl-C), 144.5 (ddd, $^2J_{C\text{-}F}$ = 73.6, $^2J_{C\text{-}P}$ = 42.7, $^3J_{C\text{-}F}$ = 37.0 Hz, C$_{diazolphosphole\text{-}N}$), 145.9 (ddddd, $^1J_{C\text{-}P}$ = 40.7, $^3J_{C\text{-}F}$ = 38.0, $^4J_{C\text{-}F}$ = 35.5, $^3J_{C\text{-}F/P}$ = 4.6, $^4J_{C\text{-}F/P}$ = 2.6 Hz, C$_{diazolphosphole\text{-}P}$) ppm.

^{19}F{^{1}H} NMR (376 MHz, Methylene Chloride-d$_2$): -53.5 (dq, $^3J_{F\text{-}P}$ = 25.4, $^5J_{F\text{-}F}$ = 7.4 Hz), -61.9 (qd, $^5J_{F\text{-}F}$ = 7.4, $^4J_{F\text{-}P}$ = 1.2 Hz) ppm.

^{31}P{^{1}H} NMR (162 MHz, Methylene Chloride-d$_2$): 234.4 (q, $^3J_{P\text{-}F}$ = 25.5 Hz).

*Synthesis of 2-(4,5-bis(trifluoromethyl)-2H-1,2,3-diazaphosphol-2-yl)pyridine (**L22**)*
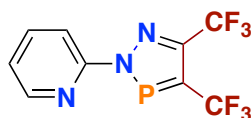
Into a pressure tube 500 mg (2.27 mmol, 1 eq.) **L12** was placed, evacuated and 11 mmol (5 eq.) perfluorobutyne **36** were condensed in, followed by 10 mL toluene. The reaction mixture was allowed to warm up over night and heated at T = 60 °C for eight weeks. The excess of **36** as well as the solvent were removed in vacuum and the compound was crystalized from DCM. The compound was obtained as light brown crystalline material in 78% yield (1.77 mmol).

^{1}H NMR (700 MHz, C$_6$D$_6$): δ = 6.53 (ddd, $^3J_{H\text{-}H}$ = 7.4 Hz, $^3J_{H\text{-}H}$ = 4.7 Hz, $^3J_{H\text{-}H}$ = 1.0 Hz, 1H, Ph-H3), 7.00 (td, $^3J_{H\text{-}H}$ = 7.8, $^3J_{H\text{-}H}$ = 1.8 Hz, 1H Ph-H2), 7.46 (td, $^3J_{H\text{-}H}$ = 8.2, $^3J_{H\text{-}H}$ = 1.0 Hz, 1H, Ph-H1), 7.89 (ddd, $^3J_{H\text{-}H}$ = 4.8, $^3J_{H\text{—}H}$ = 1.8, $^3J_{H\text{-}H}$ = 0.9 Hz, 1H, Ph-H4) ppm.

^{13}C{^{1}H} NMR (126 MHz, C$_6$D$_6$): δ = 111.6 (d, $^3J_{C\text{-}P}$ = 3.8 Hz, Phenyl-C2), 123.4 (d, $^1J_{C\text{-}F}$ = 24.5 Hz, CF$_3$), 123.8 (d, $^4J_{C\text{-}P}$ = 1.3 Hz, Phenyl-C3), 124.9 (d, $^1J_{C\text{-}F}$ = 24.4 Hz, CF$_3$), 139.1 (s, Phenyl-C4), 145.2 (dq, $^2J_{C\text{-}P}$ = 44.8, $^2J_{C\text{-}F}$ = 35.9 Hz, diazaphospholes$_N$-C2), 145.5 – 146.4 (m, diazaphospholes$_P$-C1), 148.0 (s, phenyl-C5), 153.3 (d, J = 8.6 Hz, phenyl-C1) ppm.

^{19}F{^{1}H} NMR (377 MHz, C$_6$D$_6$): -52.6 (dq, $^3J_{F\text{-}P}$ = 27.4, $^5J_{F\text{-}F}$ = 7.4 Hz), -61.2 (qd, $^5J_{F\text{-}F}$ = 7.4, $^4J_{F\text{-}P}$ = 1.2 Hz) ppm.

^{31}P{^{1}H} NMR (162 MHz, C$_6$D$_6$): 236.2 (q, $^3J_{P\text{-}F}$ = 26.8 Hz).

Attempts in the synthesis of rhodium(I) (2-(4,5-bis(trifluoromethyl)-2H-1,2,3-diazaphosphol-2-yl)pyridyl) carbonyl chloride (C31)
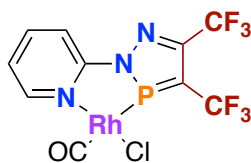
In a sealed NMR vessel 20 mg (0.067, 1 eq.) **L22** and 13 mg (0.034, 0.5 eq.) [**Rh**(CO)$_2$Cl]$_2$ were dissolved in 0.5 ml DCM-d$_2$. With the addition of the solvent a strong gas evolution was observed. No resonance could be detected by ^{31}P{^{1}H} NMR spectroscopy, while the ^{19}F NMR spectrum revealed multiple signals. No optimization of the reaction parameters was done.

Attempts in the synthesis of gold(I) 2-(4,5-bis(trifluoromethyl)-2H-1,2,3-diazaphosphol-2-yl)pyridyl) chloride (C32)
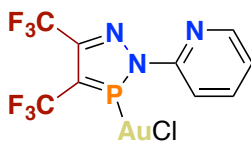
In a sealed NMR vessel 20 mg (0.067, 1 eq.) **L22** and 19.8 mg (0.067, 1 eq.) **Au**Cl•SMe$_2$ were dissolved in 0.5 ml DCM-d$_2$. Although all components were dissolved immediately, no change of the chemical shift and of the signal shape was observed in the ^{1}H, ^{19}F and ^{31}P{^{1}H} NMR spectra.

Bibliography of Chapter 3.3

(1)   Wanzlick, H.-W.; Schönherr, H.-J. *Angew. Chem. Int. Ed. Engl.* **1968**, *7* (2), 141.

(2)   Öfele, K. *J. Organomet. Chem.* **1968**, *12*, P42.

(3)   Sattely, E. S.; Meek, S. J.; Malcolmson, S. J.; Schrock, R. R.; Hoveyda, A. H. *J. Am. Chem. Soc.* **2009**, *131* (3), 943.

(4)   Naumann, S.; Dove, A. P. *Polym. Int.* **2016**, *65* (1), 16.

(5)   Fèvre, M.; Pinaud, J.; Gnanou, Y.; Vignolle, J.; Taton, D. *Chem. Soc. Rev.* **2013**, *42* (5), 2142.

(6)   Chinchilla, R.; Najera, C. *Chem. Soc. Rev.* **2011**, *40* (10), 5084.

(7)   Wang, S.; Wang, X. *Angew. Chem. Int. Ed.* **2016**, *55* (7), 2308.

(8)   Marion, N.; Nolan, S. P. *Chem. Soc. Rev.* **2008**, *37* (9), 1776.

(9)   Praneeth, V. K. K.; Ringenberg, M. R.; Ward, T. R. *Angew. Chem. Int. Ed.* **2012**, *51* (41), 10228.

(10)   Gründemann, S.; Kovacevic, A.; Albrecht, M.; Faller, J. W.; Crabtree, R. H. *Chem. Commun.* **2001**, *4* (21), 2274.

(11)   Aldeco-Perez, E.; Rosenthal, A. J.; Donnadieu, B.; Parameswaran, P.; Frenking, G.; Bertrand, G. *Science (80-.).* **2009**, *326*, 556.

(12)   Mathew, P.; Neels, A.; Albrecht, M. *J. Am. Chem. Soc.* **2008**, *130*, 13534.

(13)   Donnelly, K. F.; Petronilho, A.; Albrecht, M. *Chem. Commun.* **2013**, *49* (12), 1145.

(14)   Canseco-Gonzalez, D.; Petronilho, A.; Mueller-Bunz, H.; Ohmatsu, K.; Ooi, T.; Albrecht, M. *J. Am. Chem. Soc.* **2013**, *135* (35), 13193.

(15)   Schaper, L.-A.; Wei, X.; Hock, S. J.; Pöthig, A.; Öfele, K.; Cokoja, M.; Herrmann, W. a; Kühn, F. E. *Organometallics* **2013**, *32*, 3376.

(16)   Hohloch, S.; Duecker, F. L.; Van Meer, M. Der; Sarkar, B. *Molecules* **2015**, *20* (4), 7379.

(17)   Bolje, A.; Hohloch, S.; Urankar, D.; Pevec, A.; Gazvoda, M.; Sarkar, B.; Košmrlj, J. *Organometallics* **2014**, *33* (10), 2588.

(18)   Bolje, A.; Košmrlj, J. *Org. Lett.* **2013**, *15* (19), 5084.

(19)   Meerwein, H.; Hinz, G.; Hofmann, P.; Kroning, E.; Pfeil, E. *J. Prakt. Chemie* **1937**, *147* (10-12), 257.

(20)   Klehr, K. K. H.; Schmidpeter, A.; Karaghiosoff, K.; Klehr, H. *Chem. Ber.* **1986**, *119*, 410.

(21)   Olah, G.; Baker, E.; Evans, J.; Tolgyesi, W.; Mcintyre, J.; Bastien, I. *J. Am. Chem. Soc.* **1964**, *86* (110), 1360.

(22)   Märkl, G.; Beckh, H. J. *Tetrahedron Lett.* **1987**, *28* (30), 3475.

(23)   Paul, F.; Patt, J.; Hartwig, J. F. *J. Am. Chem. Soc.* **1994**, *116* (14), 5969.

(24)   Otsuka, S.; Yoshida, T.; Matsumoto, M.; Nakatsu, K. *J. Am. Chem. Soc.* **1976**, *98* (19), 5850.

(25)   Reid, S. M.; Boyle, R. C.; Mague, J. T.; Fink, M. J. *J. Am. Chem. Soc.* **2003**, No. 0, 7816.

(26)   Rigo, M.; Müller, C. *unpubl. results.*

(27)   Jongsma, T.; Challa, G.; van Leeuwen, P. W. N. M. *J. Organomet. Chem.* **1991**, *421* (1), 121.

(28)   van Leeuwen, P. W. N. M.; Roobeek, C. F. *J. Organomet. Chem.* **1983**, *258* (3), 343.

(29)   van Rooy, A.; Orij, E. N.; Kamer, P. C. J.; van Leeuwen, P. W. N. M. *Organometallics* **1995**, *14* (1), 34.

(30)   Wolfe, J. P.; Buchwald, S. L. *Angew. Chem., Int. Ed. Engl.* **1999**, *38* (16), 2413.

(31)   Littke, A. F.; Dai, C.; Fu, G. C. *J. Am. Chem. Soc.* **2000**, *122* (17), 4020.

(32)   Mann, G.; Incarvito, C.; Rheingold, A. L.; Hartwig, J. F. *J. Am. Chem. Soc.* **1999**, *121* (13), 3224.

(33)   Peters, C.; Tabellion, F.; Schroder, M.; Bergstrasser, U.; Preuss, F.; Regitz, M. *Synthesis* **2000**, No. 3, 417.

(34)   Frison, G.; Sevin, A.; Avarvari, N.; Mathey, F.; Le Floch, P. *J. Org. Chem.* **1999**, *64* (15), 5524.

(35)   Avarvari, N.; Le Floch, P.; Ricard, L.; Mathey, F. *Organometallics* **1997**, *16* (19), 4089.

(36)   Alder, K.; Rickert, H. F. *Justus Liebigs Ann. Chem.* **1936**, *524*, 180.

(37)   Alder, K.; Rickert, H. F. *Chem. Ber.* **1937**, *70*, 1364.

(38)   Huisgen, R.; Gotthavdt, H. *Chem. Ber.* **1968**, *101*, 536.

(39)   Werner, H. N. G.; N, R. V. P.; Neunhoefler, H. *Liebigs Ann. Chem.* **1974**, *1974*, 1190.

(40)   Asmus, S.; Nyulászi, L.; Regitz, M. *J. Chem. Soc. Perkin Trans. 2* **2001**, 1968.

(41)   Schmidpeter, A.; Klehr, H. *Z. Naturforsch.* **1983**, *38 b*, 1484.

(42)   Desimoni, G.; Faita, G.; Garau, S.; Righetti, P. *Tetrahedron* **1996**, *52* (17), 6241.

(43)   Märkl, G.; Heier, K. H. *Tetrahedron Lett.* **1974**, No. 49-50, 4369.

(44)   Märkl, G.; Lieb, F. *Angew. Chem.* **1968**, *17*, 702.

(45)   Bruce, M. Phosphabarrelenes, Dissertation Freie Universität Berlin, 2016.

Summary and Outlook

Summary of Chapter 3.1

The "click" reaction of the stable TMS (**A1**)- and ^{t}Bu (**A2**)-phosphaalkynes with azides proceeded quantitatively and within only a few minutes based upon ^{1}H and ^{31}P{^{1}H} NMR spectroscopy. The synthesis of **A2** requested larger amounts of the phosphorus (III) source **P**(TMS)$_3$. The reaction time for the synthesis was found to be much longer as reported in the original procedure. Investigations dealing with this detriment revealed a fast passivation of the lithium surface as cause of this increase in reaction time. A remedy was found in either the handling of the compounds or mechanical ablation of the passivated surface. However, significant shorter reaction times were achieved with lithium foil, exclusively handled under argon atmosphere. During these investigations an upscaling of the reaction and the development of a reproducible and reliable synthetic procedure of **P**(TMS)$_3$ was achieved.

Three monodentate ligands were subsequently developed and presented in this chapter. Initial attempts for the substitution of the TMS group were investigated, with minor success. However, their molecular structure in the crystal was determined and no changes in the basic framework of the heterocycle caused by the different substituents were noticed. Considering the chemical shift of the ^{31}P NMR spectra exhibits an influence of the position of the substituent. The substituent in 5-position caused a stronger shifts than the one in 3-position. This behaviour is in line with 1,2,3-triazoles. While a TMS group originating from phosphaalkyne **A1** causes a strong downfield shift relative to the shift of the *tert*-butyl group (**A2**), no significant influence is observed with the strong electron-withdrawing tosyl group in 3-position. Crowley and co-workers deemed 1,2,3-triazoles as being electronically insulated between the N$_3$ and the HC=C-R subunits.

Coordination chemistry attempts using these three ligands show that the 3*H*-1,2,3,4-triazaphosphole framework itself is a poor ligand in metal coordination. One exception is the tosyl substituted compound **L3**. Here, the reaction with an electron rich metal caused a severe rearrangement of the triazaphosphole core. It is assumed, that the pathway towards this compound contains a zwitterionic diazo species, from which an N$_2$

elimination is possible. The resulting zwitterion rearranges and charge equilibration yields a carbene, from which an iminophosphane is obtained by methyl migration. However, the iminophosphine undergoes cyclodimerisation, as the crystallographic characterization of the Au(I) complex verifies. Obviously, the strong electron-withdrawing tosyl group destabilises the aromatic system. From corresponding 1*H*-1,2,3-triazoles similar behaviour is known, albeit using much harsher reaction conditions and without the formation of dimers.

For further investigations, the 3*H*-1,2,3,4-triazaphosphole framework was functionalized with a picolyl group to determine the influence of a TMS- and *tert*-Bu-substituent in 5-position. Therefore, these desired compounds as well as their corresponding Re(I) carbonyl complexes were synthesised, analysed by means of DFT calculation and cyclic voltammetry and opposed to their 1*H*-1,2,3-triazole analogues. In all cases, the metal centre ion is bond to the N^2 nitrogen atom lone pair of the heterocycle. Additional information about the ligand properties was obtained from the IR spectra shifts of the carbonyl complexes. While no strong shift was observed in the IR bands within the change of the substitution pattern, the oxidation could not proceed within the solvent window of DCM for the TMS-substituted ligands **L5** and **L7**. As previously demonstrated, similarities are found in the coordination mode as well as in the properties of the heterocycle. The comparison of both heterocycles highlighted a rather stronger π-donation ability of the 3*H*-1,2,3,4-triazaphospholes than of the 1*H*-1,2,3-triazoles.

The picolyl substituted ligands were also used for the synthesis of Cu(I) complexes. The obtained $^{31}P\{^1H\}$ NMR spectra indicated the formation of the desired complexes, but the molecular structures in the crystal remained undetermined, since no single crystals suitable for X-ray characterisation were obtained. Most interestingly, differences in the coordination chemistry of TMS- and *tert*-Bu-substituted triazaphospholes were observed.

With the introduction of an alkoxy-substituent, a second chelate was designed, synthesized and crystallographically characterized. The TMS-ether cleaved alkoxide could, however, not be isolated. *In situ* cleavage followed by metal coordination as well as a *vice versa* protocol showed no homogeneous results at all and thus were discontinued.

Summary of Chapter 3.2

In order to establish a new class of phosphorus-containing molecular emitters based on 3*H*-1,2,3,4-triazaphospholes, a set of *tert-Bu-* and TMS-substituted derivatives were synthesised and characterised, most of them by X-ray crystal structure determination. Additionally, selected representatives of the 1,2,3-triazoles and **Re**(I) carbonyl complex with the chelating ligands **L12**, **L14** and **L15** were chosen. Complexation using the TMS-substituted triazaphosphole ligand **L13** did not yield a clean product and purification was not possible due to decomposition. Most interestingly, from the obtained stretch vibrations of the carbonyl complex a π-accepting property could be derived for the conjugated 3*H*-1,2,3,4-triazaphospholes. This marks a strong contrast to the non-conjugated triazaphosphole ligands. Cyclometalation of phenyl triazaphosphole derivative **28** with **Rh**(III) and **Ir**(III) precursors failed. Interestingly, the conjugated phosphorus containing heterocycles indeed emitted light - albeit in the UV spectral range - with high quantum yields, while no emission was detected for the triazoles at all. As TD-DFT calculations revealed, this contrary behaviour is caused by the 180° twisted geometry of the first excited state of the triazole, while the ground state and the first excited state of the triazaphospholes remain the same.

Investigating the 3*H*-1,2,3,4-triazaphospholes and 1*H*-1,2,3-triazoles by means of photoelectron spectroscopy, another triazole was included for a better comparison. The compound was synthesised and characterised by means of X-ray diffraction analysis. Preliminary photoelectron spectroscopy measurements were performed, although at the time of writing insufficient information was available.

The previously synthesised **Re**(I) carbonyl complexes were assumed to be suitable for electrochemical carbon dioxide reduction. Additionally, the corresponding triazaphosphole and triazole **Mn**(I) complexes were considered. From all complexes the molecular structure could be obtained by means of single crystal X-ray diffraction. From the molecular structures, no differences between the triazaphosphole and triazole ligand could be found in terms of π-donation or π-accepting properties. Underpinning this assumption, the comparison of the values of the carbonyl stretch vibrations is in line with the observations made. The cyclic voltammetry measurements performed with 10 mmol catalyst in acetonitrile under argon, carbon dioxide saturated solution and carbon dioxide saturated solution with 5% water additive revealed that the two reductive events proceed at an insufficient current for carbon dioxide reduction.

Furthermore, the triazole Mn(I) complex appeared to be the least stable one. No current enhancement was observed for the second reduction wave of any inserted metal complex. Nonetheless, both Re(I) complexes showed a current enhancement over a broad area. In case of the triazaphospholes, additional reduction waves at low potential could be detected, while no changes were observed for the corresponding triazole. This investigation demonstrated nicely the accessibility of Mn(I) carbonyl complexes, while the influence of the phosphorus atom became smaller by the use of a lighter metal. A poor orbital overlap is assumed. This work does not include any ligand optimisation by varying the substitution pattern of the heterocycle. Admittedly, the results from the previous chapters could allow a possible modification of the pyridyl subgroup caused by the insulating properties in the triaza-heterocycles. However, the ligands act as a capacitor and thus the variation on the (phospha)alkene subgroup has to be considered, although the synthesis might be more challenging.

The conjugated, chelating ligand **L12** did not form any metal complex with Cu(I) sources, except with Cu(I)OTf, as a interesting and rare dimer formation was observed. The bond lengths between nitrogen atoms and the metal centre as well as between metal centre and counter ion are very similar to those in the corresponding triazole-based metal complex. Furthermore, the inter-ring distances remained unchanged in both cases. From both indications, it can be concluded that no back bonding occurred. Both metal complexes were investigated regarding their suitability in CuAAC, first in neat reactions. Initial test reactions indicate an aggregation step. Splitting of the dimer with phenylacetylene leads to a square planar mononuclear Cu(I)-complex, containing η^2-coordinated alkyne ligand, as crystallographic characterisation of **C28** revealed. During catalysis, the triazaphosphole-based complex **C24** outclasses the triazole-based ligand **C27** significantly with a reaction time of 5 min, versus 235 min. Attempts with additives to support the reaction with a strong base, DABCO (10 mol-%), showed inhomogeneous results. The poorer results in the catalysis might be explained by the low solubility of **C27**. However, the reaction mixture of **C24** was also treated with DABCO (10 mol-%), yielding 96% conversion after only 1 min. It is also worth monitory that the conversion-time plot of the CuAAC using **C24** as a catalyst might indicate an autocatalytic process. Consequently, triazole **34** (10 mol-%) was used as an additive, whereby the reaction time decreased to 225 s. Subsequently, equimolar mixtures of catalyst **C24** and ethynyl benzene (Cu:PhCCH 1:1) as well as **C24**, ethynyl benzene and triazole **34** were prepared and analysed by means of ^{1}H NMR spectroscopy, resulting in

a chemical shift of the acetylene proton of $\Delta\delta = 0.5$ ppm. Assuming a hydrogen bond would explain this shift. Further reactions using a 1 M solution in a sealed NMR tube showed that the catalysis with triazaphosphole-based ligand **C24** is enhanced by triazole additive **34**, although higher amounts reduced the activity again. On the other hand, the reaction time of the antagonist is strongly enlarged by the additive. Even the *in-situ* formed triazole significantly lowers the activity, as it is obvious from the conversion-time plot. At last the reactions with DABCO as an additive were performed and - like in the neat reactions - their reaction times were significantly shorter. The similarity of the conversion times obtained with 2.5 mol-% and 5 mol-% catalysts might indicate that the reaction proceeds close to the diffusion limit. From the ^{1}H NMR spectra and according to the literature, it was concluded that the differences in the reaction times might be caused by the two known pathways, namely mononuclear and dinuclear CuAAC. In case of the mononuclear mechanism, it is assumed that polarisation due to a hydrogen bond between the triazole nitrogen lone pair and acetylene proton assisted the reaction. Therefore, the acidification of the proton by the formation of an **Cu**(I) η^2-acetylyl complex is critical. Especially in the neat reactions, the high excess of the phenyl acetylene and the absence of any solvent effect shift the (proposed) equilibrium between **C24** and **C28** to the η^2-complex. However, the catalysis reactions with DABCO are not influenced by the addition of triazole. Here, it is assumed that the mechanism proceeds in a binuclear way, as similar structures were reported to undergo dimerisation.

Summary of Chapter 3.3

The first part of the last chapter comprised the chemical modification of 3*H*-1,2,3,4-triazaphosphole to generate the 1*H*-1,2,3-triazolium analogues. The isoelectronic counterpart is a common ligand. The modification of chelating ligands following a literature-known procedure proved impossible, because the synthesis of the required pyridyl N-oxide resulted in decomposition of the starting material. The attempts with a slightly modified protocol also did not yield the desired product. Using different methylation agents and varying the reaction parameters exhibited the best conditions. Selective product formation was observed, when the triazaphospholes were treated with freshly distilled methyl triflate in DCM at T = 0°C and afterwards

recrystallized from the same solvent. During the investigations with compounds **L1** and **L2**, the tolerance of the TMS group was shown. The changes in the chemical shift of both products were in the same range. In case of the *tert*-Bu substituted triazaphospholium salt **L17**, the methyl group showed a H-P coupling in the ^{1}H NMR spectrum, while the corresponding TMS compound **L16** only showed a similar chemical shift for the CH_3 group. Both compounds lack (thermal) stability and proved to be much more sensitive towards air and moisture. However, neither a mass peak could be assigned nor could a single crystal X-ray structure be obtained for any 3*H*-1,2,3,4-triazaphospholium salts. The compound could not be stabilized by complex formation, as no coordination towards Cu(I) precursor occurred. The use of a higher kinetic stabilisation by alkylation with TMS triflate did not proceed as well.

The second part dealt with cycloreversion reactions. Several aza-phospha heterocycles had been reported to undergo either Diels-Alder reactions or cycloreversion reactions, including 2*H*-1,2,4,3-triazaphospholes. The missing building block was the 3*H*-1,2,3,4-triazaphospholes. Adopting the procedures from those previously reported, no conversion was observed by means of NMR spectroscopy. By using the highly reactive perfluorobut-2-yne and optimised reaction conditions, selective product formation was observed in extreme long reaction times of 95 d for the non-conjugated (benzyl **L20**, picolyl **L21**) and 70 d for the conjugated (phenyl **L22**, pyridyl **L23**) compounds. Consequently, only the biaryls were used in the preparative approaches. From the NMR spectroscopic experiments, the loss of pivalonitrile was already determined and slow evaporation of the DCM yielded single crystals of **L22**, suitable for X-ray diffraction. As expected, the compound was the cycloreversion product. Given that no aza-phospha-norbornadiene intermediate was observed during the NMR spectroscopic experiments, either the rate-determining step is assumed to be the formation of the intermediate or the addition of the perfluorobut-2-yne is an equilibrium. The cycloreversion itself is not reversible, because no change of the chemical shifts was observed, as the **L20** and **L22** were heated in the absence of the perfluorobut-2-yne with an excess of pivalonitrile. The group of Nyulászi currently performs quantum chemical calculations to investigate the reaction pathway. The coordination chemistry of pyridyl compound **L23** was explored with Rh(I) and Au(I) and in case of the lighter metal the ligand immediately underwent decomposition, while for gold no coordination could be detected.

Conclusion and Outlook

The phosphorus atom undoubtedly has a strong influence on the heterocycle, as the C^1-P-N^1 angle was determined to be around 86°, indicating a non-hybridised phosphorus atom. This would mean, that the phosphorus atom lone pair has almost exclusively *s*-orbital character (see Figure 31 or Figure 44). Further, this would result in a more diffuse and energetically low lying lone pair that consequently is energetically more disfavoured than the nitrogen atom lone pair(s). The corresponding N^1-C^1-C^2 angle is enlarged with an average value of 105°. Consequently, the N^2-C^1-C^X angle (C^X: carbon atom of the substituent in 5-position) enlarges around 3° and might cause different steric aspects for the system. The values of the inter-ring distance are only slightly affected and in case of the triazaphospholes with an average value of 0.008 Å they are negligibly larger.

Whether these structural aspects cause the differences e.g. in the catalytic activity of the Cu(I) complexes by increasing the solubility or if this is caused by the lesser number of intermolecular interactions can only be speculated. Electronic effects were excluded (Chapter 3.2).

From the comparison of 3*H*-1,2,3,4-triazaphospholes and 1*H*-1,2,3-triazoles, it is most obvious that the metal coordination in all cases proceed *via* the nitrogen lone pair rather than by the phosphorus lone pair. Although the first example of metal coordination with triazaphospholes as ligands - reported by Cameron Jones *et al.* (see Chapter 1) – show a coordination to two **Pt**(0) centres *via* the phosphorus lone pairs, this might be attributed to either the high electron density of the uncharged metal centre or the perfect fitting of the platinum atom into the coordination plane, or both. To date, no other metal (ion) has been reported to coordinate *via* the phosphorus atom lone pair of a 3*H*-1,2,3,4-triazaphosphole. Especially the transition metals in low oxidation states - known from the phosphinine chemistry to bind to phosphorus - were all located at the nitrogen atoms. Consequently, it can be concluded that in terms of metal coordination, the 3*H*-1,2,3,4-triazaphospholes act more as tuned triazoles.

The direction of the electron density flow varies depending on whether a non-conjugated (π-donating, **L4**) or a conjugated system is present (π-accepting, **L12**). This behaviour might be critical in coordination chemistry, since no other Cu(I) complexes were obtained with **L12** compared to **C24**, while $^{31}P\{^1H\}$ NMR spectroscopy

indicated that **L4** formed metal complexes with all employed **Cu**(I) precursors in all cases.

It was also shown during the investigations of **Cu**(I) and **Mn**(I) as well as **Re**(I) carbonyl complexes that the impact of this electronic tuning strongly depends on the size of the metal centre. This simply refers to the orbital overlap needed for the π-accepting properties. The exploration of this decency of the π-donating properties in **I** and **II** with the non-conjugated compounds **L4** and **L6** remains open (Scheme 70).
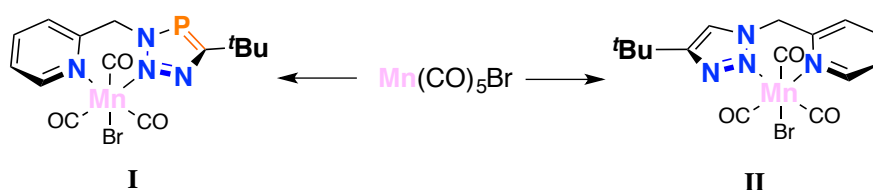
Scheme 70: Proposed complexes for investing π-donating properties subjecting to the metal ion size.

Besides the coordination chemistry, there are also more general aspects to mention. The most striking advantage of the 3*H*-1,2,3,4-triazaphospholes is their photo electronic emission, since the 1*H*-1,2,3-triazaphospholes remained silent. Customising the wavelength might enhance the suitability of these compounds for further light emitting applications. Furthermore, the phosphorus containing heterocycle obviously became more reactive than the presented antagonist, although it is still more stable than the 2*H*-1,2,4,3-triazaphospholes. This property was derived from the much longer reaction times with the high reactive perfluorobut-2-yne, although for a detailed analysis it is necessary to perform DFT calculations.

In addition, the phosphorus atom in 3*H*-1,2,3,4-triazaphospholes provides the ability to be further tuned by a nucleophilic addition of organolithium compounds. These reactions are known from phosphinines yielding the λ^4-phosphorus anionic compounds (Chapter 1). This can be adopted to generate more electron rich triazaphospholes. Initial reactions, which are not included in this work showed that *tert*-butyl substituted triazaphospholes form stable λ^4-triazaphosphole anions. Scheme 71 shows a suggestion for this type of chemical modification based upon the example of a metal complex.

Scheme 71: Modification of 3*H*-1,2,3,4-triazaphosphole-based metal complexes by nucleophilic attack.

This work contains the synthesis, characterisation and coordination chmistry of the "inverse" 3*H*-1,2,3,4-triazaphospholes. This is mainly attributed to the "click" reaction between organo azides and phosphaalkynes as well as the limited access of stable phosphaalkynes. Concerning the obtained results, the interest in the properties of "normal" 3*H*-1,2,3,4-triazaphospholes emerges. Chelating ligands like the "normal" variant of **L12** can also be taken into account (Scheme 72). The most interesting question in terms of investigating the "normal" 3*H*-1,2,3,4-triazaphospholes is how much and in what way the insulating property - found by Crowley for the 1*H*-1,2,3-triazoles - influences the coordination chemistry of these compounds.

Scheme 72: Retrosynthesis of "normal" **L12**.

Although this study has shown fascinating properties of these triazaphospholes, no rank of the "better" compound will be assessed. Besides the stability, reactivity or any other chemical interesting property, nowadays the most important characteristic is the sustainability. However, here the preliminary impression might favour the 3*H*-1,2,3,4-triazaphospholes over the 1*H*-1,2,3-triazoles due to their synthesis proceeding without any copper catalyst and thus appearing to be greener. Nonetheless, one undeniable fact must be considered, namely that phosphorus is a quite limited

resource and according to a study it will become rare within this century, despite its role as an energy carrier in biological systems being an essential element on Earth.

5 Appendix

5.1 General Experimental Information

All reactions were performed in an argon atmosphere by using Schlenk techniques, unless stated otherwise. All the glassware was dried prior to use by heating under vacuum. All the common chemicals were commercially available and purchased from AldrichChemical Co., ABCR, Alfa Aesar or Acros as well as Eurisol and were used as received. All solvents were dried and degased using standard techniques or used from Braun Solventsystems.

The ^{1}H, ^{13}C{^{1}H}, and ^{31}P{^{1}H} **NMR spectra** were recorded on a Fa. JEOL ECX400 (400 MHz), Fa. JEOL ECP500 (500 MHz) or on Fa. BRUKER AVANCE500 (500 MHz), Fa. BRUKER AVANCE700 (700 MHz) spectrometers, and all the chemical shifts are reported relative to the residual resonance in the deuterated solvents.

Infra-Red-spectra were obtained from Nicolet iS10 MIR FT-IR Spectrometer.

ESI-TOF-Mass spectrometry was performed on Agilent 6210 ESI-TOF, Agilent Technologies, Santa Clara, CA, USA, (5 µL/min, 4 kV, 15 psi.). The voltage was optimized during the measurements for the max. abundance of [M+X] signal (X: H, Na, K).

EI-TOF-Mass spectrometry AT 711, von der Firma Varian MAT.

FTIRC-MS spectrometry measurements were performed on an Ionspec QFT-7 von Varian Inc.

Cyclic voltammetry measurements Cyclic Voltammetry measurements were performed with VersaSTAT 4 Princeton Applied Research potentiostat and a three electrode system with a Classic-Carbon working electrode (WE), platinum counter electrode (CE) and silver pseudo-reference electrode (RE). Conducting salt tetrabutylammonium hexafluorophosphat (NBu$_4$PF$_6$, Fulka) was used for electrochemical analysis (≥99.0%). As reference ferrocene (Fc, 98 %, Aldrich) was used.

THF was predried over calcium hydride and distilled from sodium/benzophenone, methylene chloride (DCM, H_2O ≤ 0.005 %, ≥99.5% GC) was obtained from Aldrich was distilled from calcium hydride.

X-Ray Analysis was performed by Stoe IPDS 2T diffractometer with a rotating anode and D8 Venture, Bruker Photon CMOS diffractometer.[1] The reflections were corrected for absorption and scaled on the basis of multi-scan measured reflections by using the SADABS program (0.15–0.53 correction range).[1] The structures were solved with SHELXL-2014[2] by using direct methods and refined with SHELXS-2014[2] on F^2 for all reflections. Using anisotropic displacement parameters refined non-hydrogen atoms. The positions of the hydrogen atoms were calculated for idealized positions. Geometry calculations and checks for higher symmetry were performed with the PLATON program.[3] Structures were displayed with Mercury.

Determination of optical data were performed at room temperature on a Varian Cary 5000 UV-Vis-NIR spectrophotometer. Luminescence spectra were recorded at room temperature with a FS920 Steady State Fluorimeter (M300, UC920, CD920/CD930, S900) using a xenon lamp (Xe900). All spectra were recorded in CH_2Cl_2 (SDS, HPLC grade) stabilized with ethanol, with concentrations of 5.10^{-6}, 10^{-5}, 5.10^{-5} and 10^{-4} M. Quantum yields were calculated relative to quinine sulfate (ϕ = 0.55 in H_2SO_4 0.1N)[29] or to $[Ru(bpy)]_3^{2+}$ in H_2O, $ϕ[Ru(bpy)_3]^{2+}$ = 4.2%.,[29] using the following equation $Q_x/Q_r = [A_r(\lambda)/A_x(\lambda')][n_x^2/n_r^2][D_x/D_r]$ where A is the absorbance at the excitation wavelength (λ), n the refractive index and D the integrated luminescence intensity. "r" and "x" stand for reference and sample. Excitations of references and samples compounds were performed at the maximum wavelength of the molecules.

Microwave reactions were performed with Anton Paar Monowave 300.

Density functional calculations were carried out with the Gaussian 09 suite of programs.[4–6] Geometry optimization was performed at the ωB97xD/aug-cc-pVTZ level,[5] to account for the dispersion effects, which are likely to contribute significantly to the interactions influencing the rotational energy surface. The complexes were calculated at the ωB97xD/6-31+G* (on the transition metals def2-TZVP basis was used) level.

Geometries were fully optimized and at the minima second derivatives were calculated to ensure that real minima were obtained. To find the rotational energy surfaces relaxed scan calculations were carried out, at 30 degree steps. The computed molecular structures and orbitals were visualized by the MOLDEN program.[6] Orbitals were visualized with Chemcraft (version 1.7).

5.2 Optical Data
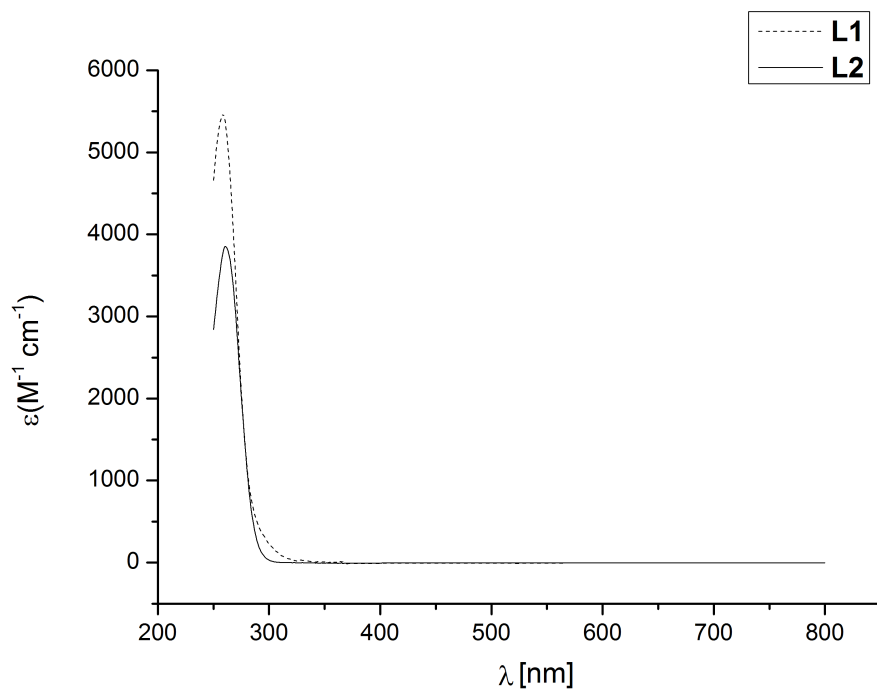
Figure 82: UV/Vis spectra of non-conjugated 3*H*-1,2,3,4-triazaphospholes.
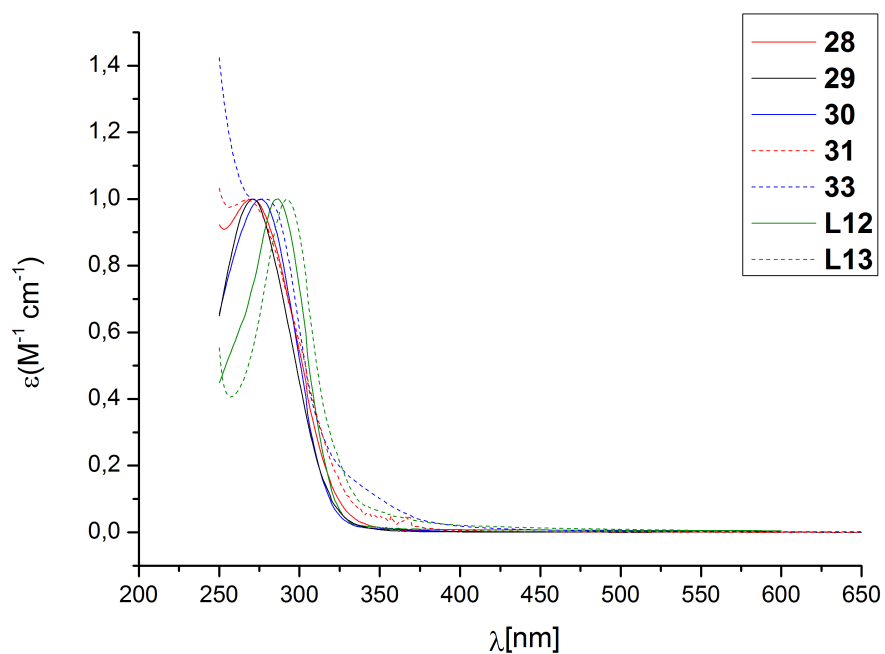
Figure 83: UV/Vis spectra of conjugated 3*H*-1,2,3,4-triazaphospholes.
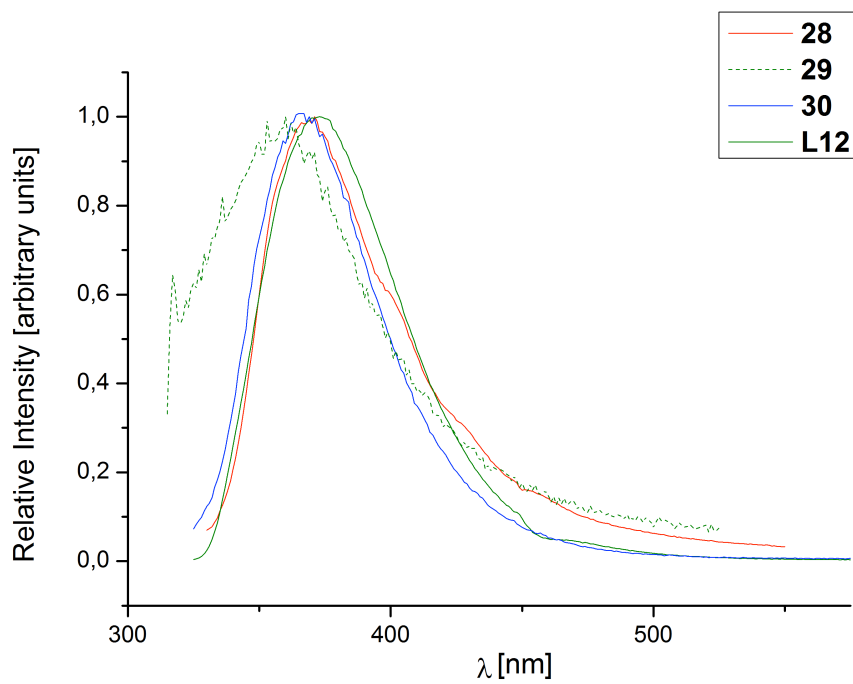
Figure 84: Emission spectra of 3*H*-1,2,3,4-trazaphospholes.
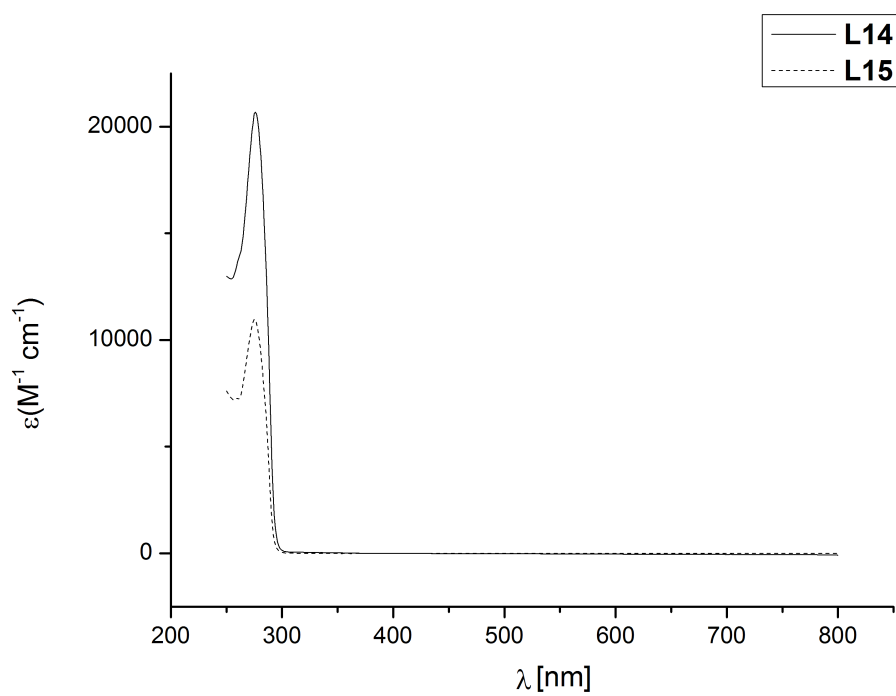
Figure 85: UV/Vis spectra of conjugated 1*H*-1,2,3-triazoles.

5.3   Crystallographic Information

Table 16: Crystallographic information of compounds **L1**, **L2**, **L3** and **C1**.

	L1	L2	L3	C1
Chemical formula	$C_{11}H_{16}N_3PSi$	$C_{12}H_{16}N_3P$	$C_{24}H_{32}N_6O_4P_2S_2$	$C_{12}H_{16}AuClNO_2PS$
Mr [g mol^{-1}]	249.33	233.25	594.61	501.70
Crystal system	Monocline	Monocline	Triclinic	Monocline
Space group	P2(1)/c	P2(1)/c	P-1	P1 21/n 1
a [Å]	11.031(2)	10.6292(19)	10.077(3)	8.8016(5)
b [Å]	5.8615(12)	5.7408(7)	11.221(3)	9.8055(4)
c [Å]	21.475(4)	21.165(4)	12.849(3)	17.4622(9)
α [°]	90	90	90.472(19)	90
β [°]	99.85(3)	100.691(14)	94.79(2)	96.710(2)
γ [°]	90	90	90.122(19)	90
V [Å³]	1268.2(5)	1269.1(4)	1447.8(6)	1496.74(13)
Z	4	4	2	4
Density [g mol^{-1}]	1.210	1.221	1.364	2.226
F [000]	528.0	496	624	952
Radiation type	Mo K$_\alpha$	Mo K$_\alpha$	Mo K$_\alpha$	Mo K$_\alpha$
μ [mm^{-1}]	0.268	0.194	0.335	10.250
Crystal size [mm]	0.11 x 0.05x 0.02	0.47 x 0.09 x 0.08		0.115 x 0.035 x 0.02
Meas. Refl.	6352	8291	15721	18922
Indep. Refl.	2366	3384	7780	3072
Observd. [I > 2σ(I)] refl.	1592	1392	1685	2653
R$_{int}$	0.0682	0.1512	0.3202	0.0434
R [F^2 > 2σ(F^2)], wR(F^2)	0.0362, 0.0757	0.0476, 0.0803	0.0929	0.0335, 0.0582
S	0.875	0.776	0.2632	1.186
Δρ$_{max}$, Δρ$_{min}$ [e Å^{-3}]	0.151, -0.225	0.242, -0.233	1.203, -0.425	1.832, -1.617

Table 17: Crystallographic information of compounds **C3** to **C6**.

	C3	C4	C5	C6
Chemical formula	$C_{14}H_{15}BrN_4O_3PRe$	$C_{14}H_{16}BrN_4O_3ReSi$	$C_{15}H_{16}BrN_4O_3Re$	$C_{26}H_{28}Br_2N_8O_6Re_2Si_2$
Mr [g mol^{-1}]	584.38	582.51	566.43	1136.96
Crystal system	Monocline	Orthorhombic	Triclinic	Monocline
Space group	P 21/n	Pca21	P-1	P2(1)/c
a [Å]	10.4019(6)	14.1775(16)	7.6834(7)	11.141(2)
b [Å]	7.6938(5)	12.6712(18)	10.3540(9)	23.330(5)
c [Å]	25.6897(15)	10.9575(13)	13.0783(11)	13.880(3)
α [°]	90	90	79.260(7)	90
β [°]	100.823(5)	90	76.666(7)	93.47(3)
γ [°]	90	90	86.164(7)	90
V [Å³]	2019.4(2)	1968.5(4)	994.34(15)	3601.3(12)
Z	4	4	2	4
Density [g mol^{-1}]	1.922	1.966	1.892	2.097
F [000]	1104	1104	536	2144
Radiation type	Mo K$_\alpha$	Mo K$_\alpha$	Mo K$_\alpha$	Mo K$_\alpha$
µ [mm^{-1}]	8.093	8.282	8.138	9.051
Crystal size [mm]	0.28 x 0.233 x 0.15	0.34 x 0.06 x 0.02	0.5 x 0.247 x 0.05	0.3 x 0.133 x 0.04
Meas. Refl.	13397	7508	11855	26308
Indep. Refl.	5418	4925	5328	6339
Observd. [I > 2σ(I)] refl.	4186	2720	4512	2980
R$_{int}$	0.0548	0.1098	0.0397	0.1251
R [F^2 > 2σ(F^2)], wR(F^2)	0.0410, 0.1078	0.0491, 0.1264	0.0313, 0.0764	0.0467, 0.0889
S	0.938	0.884	0.955	0.749
Δρ$_{max}$, Δρ$_{min}$ [e Å^{-3}]	1.750, -2.679	1.369, -2.042	1.314, -1.284	1.218, -1.711

Table 18: Crystallographic information of compounds **L8**, **L9**, **28** and **29**.

	L8	**L9**	**28**	**29**
Chemical formula	$C_{17}H_{28}N_3OPSi$	$C_{16}H_{28}N_3OPSi_2$	$C_{11}H_{14}N_3P$	$C_5H_{6.5}N_2P_{0.5}$
Mr [g mol^{-1}]	349.48	365.56	219.22	110.11
Crystal system	Monocline	Monocline	Monocline	Monocline
Space group	P1 21/c1	P 21/n	P 21	P 21/m
a [Å]	6.2652(2)	6.1929(5)	6.5047(15)	6.8490(7)
b [Å]	16.0712(5)	23.452(3)	11.314(3)	7.0770(12)
c [Å]	20.0483(6)	15.0751(12)	8.1640(17)	12.248(4)
α [°]	90	90	90	90
β [°]	96.0580(17)	97.705(6)	96.415(18)	106.236(13)
γ [°]	90	90	90	90
V [Å³]	2007.38(11)	2169.7(3)	597.1(2)	570.0(2)
Z	4	4	2	4
Density [g mol^{-1}]	1.156	1.119	1.219	1.283
F [000]	752	784	232	232
Radiation type	Cu K$_\alpha$	Mo K$_\alpha$	Mo K$_\alpha$	Mo K$_\alpha$
μ [mm^{-1}]	1.837	0.244	0.202	0.215
Crystal size [mm]	0.35 x 0.04 x 0.02	0.35 x 0.1 x 0.1	0.26 x 0.07 x 0.06	0.34 x 0.09 x 0.08
Meas. Refl.	12965	14570	4489	4004
Indep. Refl.	3499	5783	3036	1627
Observd. [I > 2σ(I)] refl.	2991	2736	1926	1154
R$_{int}$	0.0611	0.1353	0.0924	0.0636
R [F^2 > 2σ(F^2)], wR(F^2)	0.0497, 0.1254	0.0500, 0.1016	0.0496, 0.1163	0.0395, 0.0940
S	1.112	0.881	0.906	0.947
Δρ$_{max}$, Δρ$_{min}$ [e Å^{-3}]	0.453, -0.295	0.212, -0.201	0.195, -0.231	0.262, -0.245

Table 19: Crystallographic information of compounds **30**, **L12**, **L13**, **C12**.

	30	L12	L13	C12
Chemical formula	$C_{10}H_{13}N_4P$	$C_5H_{6.5}N_2P_{0.5}$	$C_{11}H_{14}N_4$	$C_{28}H_{30}Br_2Cl_4N_8O_6P_2Re_2$
Mr [g mol^{-1}]	220.21	110.11	202.26	1310.56
Crystal system	Monocline	Orthorhombic	Orthorhombic	Triclinic
Space group	P 21	P n m a	P b c a	P-1
a [Å]	6.2161(13)	7.9500(10)	9.2269(3)	13.4120(11)
b [Å]	11.251(3)	6.8020(8)	11.3942(5)	18.0785(18)
c [Å]	8.1840(19)	20.732(3)	20.5459(9)	8.6707(8)
α [°]	90	90	90	89.999(8)
β [°]	92.885(18)	90	90	91.816(7)
γ [°]	90	90	90	89.998(7)
V [Å^3]	571.7(2)	1121.1(3)	2160.06(15)	2101.3(3)
Z	2	8	8	2
Density [g mol^{-1}]	1.279	1.305	1.244	2.071
F [000]	232	464	864	1240
Radiation type	Mo K$_\alpha$	Mo K$_\alpha$	Mo K$_\alpha$	Mo K$_\alpha$
μ [mm^{-1}]	0.214	0.218	0.079	8.035
Crystal size [mm]	0.45 x 0.09 x 0.09	0.5 x 0.37 x 0.29	0.67 x 0.45 x 0.28	0.11 x 0.06 x 0.03
Meas. Refl.	6489	3647	16063	22878
Indep. Refl.	3082	1607	2214	11254
Observd. [I > 2σ(I)] refl.	1796	1136	1859	4608
R$_{int}$	0.1141	0.0587	0.0495	0.1743
R [F^2 > 2σ(F^2)], wR(F^2)	0.0702, 0.1883	0.0368, 0.0974	0.0393, 0.1015	0.0539, 0.0820
S	0.906	0.937	1.062	0.774
Δρ$_{max}$, Δρ$_{min}$ [e Å^{-3}]	0.581, -0.504	0.195, -0.260	0.260, -0.240	1.025, -1.309

Table 20: Crystallographic information of compounds **C14**, **C15** and **34**.

	C14	C15	34
Chemical formula	$C_{15}H_{16}BrCl_2N_4O_3Re$	$C_{26}H_{28}Br_2N_8O_6Re_2Si_2$	$C_{12}H_{15}N_3$
Mr [g mol^{-1}]	637.33	1136.96	201.27
Crystal system	Monocline	Monocline	Monocline
Space group	P 2$_1$/c	P 2$_1$/c	P$_1$2/n$_1$
a [Å]	12.5797(10)	11.141(2)	12.4663(9)
b [Å]	8.8545(5)	23.330(5)	5.8838(4)
c [Å]	19.1529(15)	13.880(3)	15.8387(12)
α [°]	90	90	90
β [°]	106.658(6)	93.47(3)	108.765(3)
γ [°]	90	90	90
V [Å³]	2043.9(3)	3601.3(12)	1100.00(14)
Z	4	4	4
Density [g mol^{-1}]	2.071	2.097	1.215
F [000]	1208	2144	432
Radiation type	Mo K$_\alpha$	Mo K$_\alpha$	Mo K$_\alpha$
μ [mm^{-1}]	8.183	9.051	0.075
Crystal size [mm]	0.13 x 0.1 x 0.08	0.3 x 0.133 x 0.04	0.59 x 0.12 x 0.1
Meas. Refl.	15327	26308	22245
Indep. Refl.	5482	6339	2268
Observd. [I > 2σ(I)] refl.	3653	2980	2118
R$_{int}$	0.0654	0.1251	0.5834
R [F^2 > 2σ(F^2)], wR(F^2)	0.0339, 0.0689	0.0467, 0.0889	0.5697, 0.8832
S	0.856	0.749	1.069
Δρ$_{max}$, Δρ$_{min}$ [e Å^{-3}]	1.178, -1.331	1.218, -1.711	4.741, -2.807

	C18	C19	C24
Chemical formula	$C_{14}H_{15}BCl_2MnN_4O_3P$	$C_{14.5}H_{15}BrClMnN_4O_3$	$C_{11}H_{13}CuF_3N_4O_3PS$
Mr [g mol^{-1}]	524.02	463.60	432.82
Crystal system	Monocline	Triclinic	Triclinic
Space group	P 1 2$_1$/c 1	P -1	P -1
a [Å]	8.6638(5)	12.4172(8)	8.7446(3)
b [Å]	17.7912(13)	17.7265(12)	10.0149(3)
c [Å]	13.1073(10)	17.7270(12)	12.1471(4)
α [°]	90	88.727(2)	82.6640(11)
β [°]	91.379(3)	72.382(2)	86.4850(11)
γ [°]	90	83.586(2)	66.8690(11)
V [Å³]	2019.8(2)	3695.4(4)	970.20(6)
Z	4	8	2
Density [g mol^{-1}]	1.723	1.667	1.482
F [000]	1040	1848	436
Radiation type	Mo K$_\alpha$	Cu K$_\alpha$	Mo K$_\alpha$
μ [mm^{-1}]	2.997	9.863	1.358
Crystal size [mm]	0.6 x 0.09 x 0.02	0.36 x 0.32 x 0.21	0.13 x 0.07 x 0.02
Meas. Refl.	24586	82996	16890
Indep. Refl.	4144	15050	3962
Observd. [I > 2σ(I)] refl.	3508	12656	3619
R$_{int}$	0.0388	0.0457	0.0431
R [F^2 > 2σ(F^2)], wR(F^2)	0.0279, 0.0713	0.0354, 0.0830	0.0399, 0.1084
S	1.038	1.032	1.154
Δρ$_{max}$, Δρ$_{min}$ [e Å^{-3}]	0.431, -0.843	0.584, -0.840	1.409, -0.565

Table 22: Crystallographic information of compounds **C27**, **C28** and **L22**.

	C27	C28	L22
Chemical formula	$C_{24}H_{28}Cu_2F_6N_8O_6S_2$	$C_{20}H_{21}Cl_2CuF_3N_4O_3PS$	$C_{10}H_5F_6N_2P$
Mr [g mol^{-1}]	829.74	619.88	298.13
Crystal system	Monocline	Triclinic	Orthorhombic
Space group	C 1 2/c 1	P -1	P b c a
a [Å]	19.0940(13)	10.2039(11)	7.5247(5)
b [Å]	16.2511(9)	10.7901(11)	12.9354(9)
c [Å]	11.8108(8)	12.6708(15)	22.6658(15)
α [°]	90	65.494(4)	90
β [°]	102.377(3)	82.290(4)	90
γ [°]	90	80.769(4)	90
V [Å³]	3579.7(4)	1249.4(2)	2206.2(3)
Z	4	2	8
Density [g mol^{-1}]	1.540	1.648	1.795
F [000]	1680	628	1184
Radiation type	Mo K$_\alpha$	Mo K$_\alpha$	Mo K$_\alpha$
μ [mm^{-1}]	1.383	1.289	0.318
Crystal size [mm]	0.42 x 0.28 x 0.17	0.42 x 0.2 x 0.13	0.2 x 0.149 x 0.06
Meas. Refl.	19993	22955	18484
Indep. Refl.	3686	5115	2444
Observd. [I > 2σ(I)] refl.	3017	4084	2187
R$_{int}$	0.0461	0.0539	0.0514
R [F^2 > 2σ(F^2)], wR(F^2)	0.0331, 0.0758	0.0365, 0.0802	0.0440, 0.1047
S	1.040	1.025	1.171
Δρ$_{max}$, Δρ$_{min}$ [e Å^{-3}]	0.339, -0.338	0.615, -0.557	0.519, -0.366

5.4 Time-Dependent DFT Data

DFT calculations were performed with ωB97xD/aug-cc-PVDZ TD DFT for the vertical excitation wavelength (λ in nm), oscillator strength (f) and assignment with significant electron configuration.

Compound 29 (minimum energy structure non planar)

λ (nm)	f (oscillator strength)	Assignment	Significant Electron Configuration
278	0.0056	π*- n	LUMO- HOMO-2 (+LUMO- HOMO)
254	0.0469	π*- π	LUMO- HOMO
250	**0.2675**	π*- π	LUMO- HOMO-1 (LUMO- HOMO)
249	0.0457	π*- n	LUMO- HOMO-4

Compound 30 (minimum energy structure non planar)

λ (nm)	f (oscillator strength)	Assignment	Significant Electron Configuration
271	0.0230	π*- n	LUMO- HOMO-2
251	**0.2397**	π*- π	LUMO- HOMO (+LUMO- HOMO-1)
248	0.0583	π*- π	LUMO- HOMO-1 (+LUMO- HOMO)
244	0.0676	π*- n	LUMO+1 - HOMO-2

Compound 32 (minimum energy structure non planar)

λ (nm)	f (oscillator strength)	Assignment	Significant Electron Configuration
285	0.0058	π*- n	LUMO- HOMO-1
254	0.0856	π*- π	LUMO- HOMO-2 (+LUMO- HOMO)
250	0.0752	π*- n	LUMO- HOMO-4(+LUMO- HOMO-1)
248	**0.1821**	π*- π	LUMO- HOMO (LUMO- HOMO-2)

Compound 33 (minimum energy structure non planar)

λ (nm)	f (oscillator strength)	Assignment	Significant Electron Configuration
279	0.0207	π*- n	LUMO-HOMO-2 (+LUMO- HOMO)
252	**0.2289**	π*- π	LUMO- HOMO
246	0.0272	π*- π	LUMO- HOMO-1
243	0.0996	π*- π	LUMO-HOMO-1(+LUMO+1-HOMO-4)

Compound L12

λ (nm)	f (oscillator strength)	Assignment	Significant Electron Configuration
282	0.0023	π*- n	LUMO- HOMO-2
259	**0.3478**	π*- π	LUMO- HOMO-1 (+LUMO- HOMO)
255	0.0764	π*- π	LUMO- HOMO (+LUMO- HOMO-1)
245	0.0003	π*- n	LUMO- HOMO-3

Compound L13

λ (nm)	f (oscillator strength)	Assignment	Significant Electron Configuration
290	0.0018	π*- n	LUMO- HOMO-2
260	**0.3151**	π*- π	LUMO- HOMO-1 (+LUMO- HOMO)
252	0.1156	π*- π	LUMO- HOMO
248	0.0004	π*- n	LUMO- HOMO-3

5.5 Cartesian Coordinates (Å) and Total Energies of Optimized Structures

L4
B3LYP/def2-TZVP
E: -988.3430037

6	8.69532	3.25953	4.12375
6	4.95202	3.95113	3.82491
1	4.75819	4.95581	4.22884
1	4.40319	3.21482	4.42736
6	4.52430	3.86510	2.37580
6	4.19309	5.01472	1.64862
1	4.23555	5.99626	2.12335
6	3.82105	4.88087	0.30970
1	3.55970	5.75853	-0.28336
6	3.79593	3.60507	-0.25196
1	3.51440	3.44965	-1.29393
6	4.14074	2.51654	0.55727
1	4.12809	1.50017	0.15286
6	10.20435	3.09657	4.10506
6	10.83386	3.96127	3.00056
1	11.92618	3.83232	2.99796
1	10.62370	5.03057	3.15725
1	10.46165	3.67653	2.00428
6	10.53884	1.60993	3.85094
1	11.62931	1.46167	3.86283
1	10.15540	1.28509	2.87263
1	10.08803	0.97479	4.62471
6	10.76652	3.52495	5.47881
1	11.85854	3.38964	5.49785
1	10.32262	2.92353	6.28291
1	10.54560	4.58382	5.67854
7	6.37569	3.62613	3.99511
7	6.68920	2.76534	4.98658
7	7.97217	2.56928	5.04980
7	4.49540	2.63056	1.84299
15	7.69778	4.23217	3.07860

L6
B3LYP/def2-TZVP
E: -685.7119139

6	3.71324	9.29648	8.22274
6	3.20704	10.33406	8.98569
1	2.60900	10.36432	9.88818
6	3.39150	12.85702	8.72051
1	2.38164	13.13738	8.38364
1	4.12693	13.44792	8.15873
6	3.54411	13.09670	10.20738
6	2.43640	13.39637	11.00948
1	1.44191	13.47307	10.56644

```
6    2.62835    13.59081    12.37919
1    1.78452    13.82599    13.02955
6    3.91811    13.47503    12.89547
1    4.11840    13.61670    13.95791
6    4.96155    13.17286    12.01275
1    5.98760    13.07765    12.37986
6    3.58995     7.80053     8.39277
6    2.71756     7.47571     9.61641
1    3.15729     7.88055    10.54059
1    2.62674     6.38642     9.73714
1    1.70274     7.88731     9.50584
6    2.94886     7.20086     7.12267
1    2.88010     6.10589     7.21067
1    3.54913     7.44547     6.23622
1    1.93511     7.59964     6.96942
6    5.00029     7.20209     8.58719
1    5.64245     7.44341     7.72965
1    4.94003     6.10740     8.68561
1    5.47535     7.60585     9.49339
7    3.65062    11.46463     8.37082
7    4.39458    11.15679     7.27849
7    4.42975     9.85022     7.19180
7    4.79147    12.98711    10.69806
```

J
wb97xd/aug-cc-pvtz
E: -791.9720502
```
 6    -3.332649   -0.141176   -0.000140
 6    -2.766391    1.124606   -0.000017
 6    -1.391882    1.256958    0.000093
 6    -0.643258    0.086966   -0.000065
 7    -1.160521   -1.126142    0.000074
 6    -2.485257   -1.234264    0.000039
 7     0.777387    0.125727    0.000031
15     1.817974   -1.224269    0.000010
 6     3.071433   -0.069049   -0.000047
 7     2.647995    1.217703   -0.000059
 7     1.372697    1.321794    0.000027
 1     4.133716   -0.255579   -0.000154
 1    -2.879618   -2.242757    0.000193
 1    -4.403614   -0.279948   -0.000272
 1    -3.391561    2.006862   -0.000093
 1    -0.903412    2.217623    0.000493
```

J-*trans*
wb97xd/aug-cc-pvtz
E: -791.9641428
```
 6     2.581118   -1.102753   -0.481667
 7     1.253166   -1.119762   -0.447027
 6     0.647802   -0.056410    0.043691
```

```
6     1.304132    1.071649    0.513376
6     2.685678    1.082785    0.450570
6     3.341982   -0.026448   -0.054657
7    -0.779752   -0.093361    0.066383
7    -1.363899   -1.174908    0.590720
7    -2.640569   -1.095101    0.528982
6    -3.081904    0.044208   -0.051355
15   -1.831511    1.088008   -0.551119
1    -4.144836    0.193119   -0.154461
1     0.748655    1.901480    0.924805
1     3.238876    1.942012    0.803148
1     4.419674   -0.062527   -0.117679
1     3.054838   -1.990461   -0.882174
```

K
wb97xd/aug-cc-pvtz
E: -791.9632703
```
6    -2.739493    1.089049   -0.335839
6    -1.361686    1.186765   -0.328512
6    -0.634591    0.063522    0.030382
6    -1.311272   -1.099468    0.371080
7    -2.632939   -1.197694    0.347385
6    -3.328585   -0.120562   -0.000267
7     0.785838    0.096738    0.049413
7     1.365885    1.243181    0.421944
7     2.643657    1.166226    0.376167
6     3.092879   -0.039859   -0.035110
15    1.851533   -1.151139   -0.396132
1     4.157112   -0.197335   -0.107287
1    -0.761295   -1.981381    0.680594
1    -4.406169   -0.229416   -0.008611
1    -3.351098    1.936950   -0.608249
1    -0.852147    2.102423   -0.589247
```

K *-trans*
wb97xd/aug-cc-pvtz
E: -791.9624412
```
7     2.683743   -1.164743   -0.394723
6     1.359930   -1.150555   -0.351442
6     0.634196   -0.032196    0.043786
6     1.311880    1.118196    0.405464
6     2.693582    1.106502    0.346555
6     3.332639   -0.055061   -0.054411
7    -0.786008   -0.078440    0.062889
7    -1.357462   -1.218465    0.466336
7    -2.635745   -1.154380    0.410174
6    -3.093525    0.034381   -0.040217
15   -1.859876    1.145599   -0.426731
1    -4.158688    0.179491   -0.123769
1     0.772484    1.995599    0.735807
```

```
 1    3.265909   1.980951   0.619791
 1    4.413661  -0.099093  -0.105748
 1    0.840866  -2.056335  -0.636242
```

L
wb97xd/aug-cc-pvtz
E: -791.9643028

```
 6   -2.745091   1.090553  -0.238117
 6   -1.365015   1.198977  -0.226463
 6   -0.628484   0.054342   0.032693
 6   -1.297243  -1.135908   0.267605
 6   -2.681370  -1.126921   0.220046
 7   -3.407261  -0.042485  -0.025766
 7    0.791363   0.096412   0.046730
 7    1.369985   1.275023   0.307281
 7    2.645910   1.199184   0.265682
 6    3.099530  -0.039581  -0.034521
15    1.864066  -1.184304  -0.281954
 1    4.164126  -0.197850  -0.098130
 1   -0.765667  -2.049300   0.492885
 1   -3.229139  -2.044654   0.396730
 1   -3.348085   1.968386  -0.436611
 1   -0.876166   2.142260  -0.410512
```

L12
wb97xd/aug-cc-pvdz
E:-949.0989802

```
 6   -4.742390   0.259516   0.000004
 6   -4.236037  -1.040112  -0.000006
 6   -2.861885  -1.239554  -0.000008
 6   -2.053178  -0.100625   0.000001
 7   -2.512087   1.143359   0.000011
 6   -3.836061   1.314617   0.000011
 7   -0.634756  -0.207577  -0.000001
15    0.483176   1.108049  -0.000017
 6    1.698879  -0.115190  -0.000003
 6    3.204630   0.057006   0.000003
 6    3.781482  -0.614168   1.258240
 7   -0.094269  -1.428701   0.000004
 7    1.191014  -1.381027   0.000004
 6    3.781494  -0.614203  -1.258208
 6    3.569378   1.546308  -0.000017
 1   -4.183362   2.349012   0.000019
 1   -5.813654   0.452394   0.000005
 1   -4.909148  -1.897340  -0.000012
 1   -2.417250  -2.230267  -0.000015
 1    4.660824   1.665785  -0.000068
 1    3.176817   2.055935  -0.891540
 1    3.176893   2.055940   0.891537
 1    4.874809  -0.504110   1.273104
```

1	3.375817	-0.151061	2.167895
1	3.536376	-1.682836	1.276535
1	4.874823	-0.504155	-1.273059
1	3.536380	-1.682870	-1.276485
1	3.375848	-0.151116	-2.167882

L14
wb97xd/aug-cc-pvdz
E:-1200.5183811

6	-3.223349	-1.233264	0.000001
6	-2.406111	-0.100544	0.000001
7	-2.855887	1.146897	0.000001
6	-4.178421	1.327975	0.000002
6	-5.092690	0.279551	0.000003
6	-4.596187	-1.023703	0.000002
7	-0.987936	-0.217643	-0.000002
15	0.148114	1.080730	-0.000006
6	1.356370	-0.142832	-0.000001
14	3.240321	0.052683	0.000002
6	3.632521	1.895175	0.000001
7	-0.456197	-1.446044	-0.000005
7	0.829325	-1.411878	-0.000002
6	3.916465	-0.777671	1.546228
6	3.916470	-0.777674	-1.546221
1	-4.518015	2.364935	0.000003
1	-6.162501	0.480383	0.000003
1	-5.275621	-1.875893	0.000002
1	-2.785956	-2.227200	0.000000
1	4.720043	2.055356	0.000003
1	3.222488	2.393911	-0.889600
1	3.222484	2.393913	0.889598
1	5.013061	-0.706411	1.583373
1	3.513552	-0.310153	2.455161
1	3.641040	-1.841092	1.561262
1	5.013066	-0.706414	-1.583363
1	3.641045	-1.841095	-1.561254
1	3.513560	-0.310157	-2.455156

29
wb97xd/aug-cc-pvdz
E:-949.0923336

7	4.832989	0.140372	-0.054723
6	4.211185	-1.028130	-0.235849
6	2.829510	-1.194982	-0.207075
6	2.043669	-0.069945	0.035979
6	2.669701	1.158229	0.238135
6	4.060100	1.203630	0.175790

7	0.625736	-0.167489	0.069690
15	-0.512747	1.098825	-0.205922
6	-1.719750	-0.107961	0.026432
7	-1.192983	-1.337912	0.281698
7	0.092167	-1.371554	0.301482
6	-3.226109	0.045189	-0.025348
1	2.100215	2.061696	0.449407
1	4.575452	2.153833	0.327502
1	4.853130	-1.890887	-0.423141
1	2.375401	-2.168956	-0.367277
6	-3.600737	1.494744	-0.354636
6	-3.782271	-0.891999	-1.110954
6	-3.809395	-0.341656	1.344760
1	-4.692703	1.600614	-0.395442
1	-3.227780	2.191652	0.409821
1	-3.199341	1.802132	-1.331052
1	-4.875606	-0.796039	-1.161973
1	-3.367660	-0.638528	-2.095978
1	-3.532397	-1.936519	-0.890350
1	-4.904054	-0.249266	1.323034
1	-3.550770	-1.376248	1.599782
1	-3.423464	0.317509	2.134063

30
wb97xd/aug-cc-pvdz
E:-949.0910158

6	4.745890	0.214762	-0.040593
6	4.198137	-1.029442	-0.352123
6	2.818010	-1.184271	-0.319710
6	2.049008	-0.079791	0.039863
6	2.688144	1.120760	0.353931
7	4.010562	1.273474	0.305973
7	0.629830	-0.167195	0.085382
15	-0.501788	1.067014	-0.319631
6	-1.714207	-0.106677	0.038994
7	-1.191918	-1.304390	0.415940
7	0.095544	-1.339153	0.440176
6	-3.220280	0.045481	-0.030708
1	2.104029	1.991176	0.660696
1	5.826215	0.366750	-0.069604
1	4.845410	-1.861180	-0.626371
1	2.337385	-2.129962	-0.561536
6	-3.589425	1.469006	-0.464193
6	-3.772099	-0.964258	-1.051741
6	-3.814961	-0.241116	1.358594
1	-4.680798	1.573864	-0.521209
1	-3.219687	2.216150	0.252722
1	-3.179829	1.705760	-1.456779
1	-4.865314	-0.873241	-1.114269
1	-3.352936	-0.778460	-2.049974
1	-3.522142	-1.990965	-0.758839

```
1    -4.909078   -0.146230   1.322091
1    -3.561952   -1.255498   1.688996
1    -3.431913    0.470758   2.102352
```

32
wb97xd/aug-cc-pvdz
E:-1200.5117283
```
 6      4.407317   1.214361   0.174196
 7      5.185034   0.156492  -0.065010
 6      4.569163  -1.014768  -0.248179
 6      3.188541  -1.189582  -0.213177
 6      2.397472  -0.070124   0.038380
 6      3.017573   1.160627   0.243230
 7      0.979829  -0.175158   0.077112
 7      0.453591  -1.385690   0.311823
 7     -0.831500  -1.362837   0.296378
 6     -1.376170  -0.129411   0.040144
14     -3.264043   0.041680  -0.024077
 6     -3.948698  -0.437987   1.659678
15     -0.174623   1.075276  -0.194603
 6     -3.663374   1.835757  -0.434051
 6     -3.902748  -1.114511  -1.361354
 1      2.443816   2.059869   0.461056
 1      4.918118   2.166752   0.327555
 1      5.215158  -1.873012  -0.442164
 1      2.739114  -2.165502  -0.374718
 1     -4.751235   1.979991  -0.496519
 1     -3.281429   2.522539   0.334648
 1     -3.233999   2.132908  -1.401400
 1     -5.046986  -0.387604   1.665512
 1     -3.651585  -1.464390   1.914575
 1     -3.573207   0.230650   2.446359
 1     -4.998424  -1.061352  -1.435520
 1     -3.482060  -0.856389  -2.342842
 1     -3.624456  -2.152932  -1.135735
```

33
wb97xd/aug-cc-pvdz
E:-1200.5104483
```
 6      5.097533   0.229147  -0.048477
 6      4.555343  -1.017026  -0.361842
 6      3.176217  -1.179354  -0.325122
 6      2.402356  -0.079858   0.039686
 6      3.036318   1.123071   0.355274
 7      4.357679   1.282919   0.303617
 7      0.983517  -0.173999   0.089119
15     -0.164197   1.047249  -0.303120
 6     -1.371054  -0.125517   0.053739
 7     -0.830740  -1.328755   0.425296
 7      0.456445  -1.353703   0.442829
```

14	-3.257865	0.042434	-0.027403
1	2.448579	1.989453	0.666607
1	6.176932	0.386891	-0.080497
1	5.206119	-1.844684	-0.640062
1	2.700000	-2.127193	-0.567206
6	-3.657116	1.820965	-0.500651
6	-3.889576	-1.156472	-1.331072
6	-3.954390	-0.384906	1.665402
1	-4.744561	1.961898	-0.576534
1	-3.280891	2.532752	0.247784
1	-3.220614	2.086504	-1.474051
1	-5.052969	-0.341100	1.660874
1	-3.652566	-1.400507	1.955505
1	-3.588792	0.310782	2.433055
1	-4.984585	-1.104551	-1.415510
1	-3.460980	-0.931022	-2.317277
1	-3.614704	-2.187556	-1.069875

29 dimer
wb97xd/6-311+g(d,p)
E: -1898.375025

6	-0.095784	-1.868387	0.152333
7	-1.442821	-1.440709	0.006856
15	-2.462430	-0.776982	1.211848
6	-3.655857	-0.687291	-0.017466
7	-3.212287	-1.154892	-1.214416
7	-1.999496	-1.565983	-1.204613
6	-5.088959	-0.214885	0.104332
6	0.658505	-1.464205	1.246900
6	1.965721	-1.919598	1.344243
7	2.545671	-2.716736	0.449098
6	1.807038	-3.085560	-0.595884
6	0.490316	-2.698344	-0.797182
1	-0.065697	-3.029993	-1.662347
1	2.290921	-3.734672	-1.319823
1	2.582147	-1.601635	2.179271
1	0.262772	-0.790649	1.996900
6	-5.295896	0.502188	1.443018
6	-6.002528	-1.451566	0.028056
6	-5.423113	0.747601	-1.046273
1	-4.819242	1.655891	-0.980028
1	-5.248651	0.272456	-2.013510
1	-6.478052	1.031827	-0.986383
1	-5.867205	-1.971478	-0.923135
1	-7.050302	-1.147781	0.111318
1	-5.782101	-2.153482	0.837573
1	-6.335795	0.826521	1.535630
1	-5.081098	-0.155117	2.292849
1	-4.659565	1.389359	1.513193
6	0.095739	1.868276	-0.152835

6	-0.658636	1.463237	-1.247041
6	-1.965706	1.918922	-1.344843
7	-2.545422	2.717096	-0.450451
6	-1.806716	3.086730	0.594167
6	-0.490080	2.699349	0.795836
1	-0.263062	0.788733	-1.996280
1	-2.582286	1.600345	-2.179522
1	-2.290393	3.736707	1.317470
1	0.066023	3.031699	1.660676
7	1.442660	1.440374	-0.006901
15	2.462845	0.777512	-1.211842
6	3.655742	0.687126	0.017978
7	3.211624	1.153991	1.214988
7	1.998793	1.565035	1.204865
6	5.088942	0.214906	-0.103504
6	6.002337	1.451674	-0.026482
6	5.422843	-0.747955	1.046845
6	5.296416	-0.501674	-1.442370
1	4.660699	-1.389266	-1.512786
1	5.081195	0.155690	-2.292052
1	6.336559	-0.825202	-1.535046
1	5.782501	2.153586	-0.836164
1	7.050211	1.147998	-0.108889
1	5.866218	1.971561	0.924612
1	4.818940	-1.656194	0.980204
1	6.477777	-1.032229	0.987028
1	5.248274	-0.273099	2.014205

L14
6-31+G* / def2tzvp (Re)
E: -646.5322981

6	-2.800801	-1.145931	-0.000167
6	-1.908427	-0.076484	0.000131
7	-2.261932	1.197002	0.000271
6	-3.567312	1.470104	0.000118
6	-4.549983	0.493082	-0.000197
6	-4.150047	-0.839745	-0.000319
7	-0.512959	-0.316207	0.000281
6	0.495001	0.594885	-0.000138
6	1.635996	-0.160247	-0.000226
7	1.264135	-1.476881	0.000107
7	-0.019834	-1.566513	0.000369
6	3.086623	0.248080	-0.000157
6	3.763629	-0.320004	1.257688
6	3.200850	1.775841	-0.003395
6	3.765579	-0.325575	-1.254377
1	-2.431731	-2.161918	-0.000337
1	-4.885152	-1.636174	-0.000541
1	-5.597079	0.768060	-0.000372
1	-3.829022	2.523567	0.000186

```
 1     3.669120   -1.413002   -1.282317
 1     4.829712   -0.070053   -1.258091
 1     4.827783   -0.064563    1.261936
 1     3.311840    0.080380   -2.163099
 1     3.667061   -1.407303    1.290341
 1     3.308525    0.090014    2.163901
 1     2.731215    2.212874    0.883103
 1     2.731904    2.209080   -0.892105
 1     4.253685    2.071258   -0.003545
 1     0.299634    1.651938   -0.000029
```

C12-K
6-31+G* / def2tzvp (Re)
E: -3938.8984735
```
 6    -0.088980    2.190142   -0.279558
 6     0.002738    3.577367   -0.241208
 6    -1.174881    4.308694   -0.247908
 6    -2.394506    3.637563   -0.301567
 6    -2.388892    2.254711   -0.345006
 7    -1.254249    1.533168   -0.338347
 1     0.968209    4.068410   -0.198230
 1    -1.138418    5.392521   -0.210531
 1    -3.337319    4.171850   -0.304811
 1    -3.309090    1.683997   -0.380867
75    -1.161165   -0.680153   -0.254926
35    -0.773173   -0.186329    2.304769
 6    -1.365050   -0.911960   -2.138486
 8    -1.492770   -1.049964   -3.285111
 6    -0.755342   -2.556037   -0.068813
 8    -0.484519   -3.672507    0.037224
 6    -3.024708   -1.074785   -0.001856
 8    -4.155546   -1.271918    0.144293
 7     1.070601    1.382559   -0.271944
 7     0.882857    0.053293   -0.366067
 7     1.977085   -0.614291   -0.327299
 6     3.075744    0.165243   -0.182395
15     2.712972    1.843838   -0.095643
 6     4.429153   -0.505011   -0.094526
 6     4.413364   -1.474756    1.102334
 6     5.531205    0.543680    0.103151
 6     4.679674   -1.284898   -1.398563
 1     3.902575   -2.037988   -1.560063
 1     5.648403   -1.794113   -1.343183
 1     5.384488   -1.976283    1.182762
 1     4.694655   -0.611863   -2.263551
 1     3.637695   -2.236379    0.980810
 1     4.222412   -0.941327    2.039937
 1     5.392060    1.104897    1.035751
 1     5.573045    1.254300   -0.732266
 1     6.506657    0.049696    0.162198
```

C12-J
6-31+G* / def2tzvp (Re)
E: -3938.8830868
```
 6      4.134842  -0.307472  -0.058881
 6      2.949019   0.625751  -0.121456
 7      3.115283   1.981651  -0.057534
 7      2.042296   2.682589  -0.094563
 7      0.959616   1.884101  -0.194867
15      1.299824   0.236362  -0.234390
 6     -0.346033   2.402424  -0.218520
 7     -1.326243   1.484697  -0.308540
 6     -2.593174   1.942109  -0.332546
 6     -2.914781   3.285945  -0.272864
 6     -1.883340   4.217956  -0.179602
 6     -0.571696   3.773230  -0.153764
 1      0.272669   4.447386  -0.079909
 1     -2.097179   5.280493  -0.124927
 1     -3.955394   3.588242  -0.294050
 1     -3.369885   1.191092  -0.398542
75     -0.898627  -0.788207  -0.279814
 6     -2.766061  -1.299622  -0.139248
 8     -3.876373  -1.596072  -0.061920
 6     -0.971815  -0.942742  -2.188074
 8     -1.026001  -1.034164  -3.342396
 6     -0.383675  -2.635693  -0.132090
 8     -0.054621  -3.737741  -0.042870
35     -0.799868  -0.378659   2.319909
 6      4.839744  -0.112532   1.296115
 1      4.165808  -0.353416   2.125598
 1      5.178237   0.921255   1.415513
 1      5.712332  -0.772966   1.358039
 6      5.099284   0.028919  -1.209426
 1      5.446752   1.064063  -1.137972
 1      5.971540  -0.633450  -1.168093
 1      4.612793  -0.105696  -2.182165
 1      4.503090  -2.444716  -0.133666
 6      3.651314  -1.758672  -0.187082
 1      2.962419  -2.030005   0.623296
 1      3.149429  -1.934190  -1.147397
```

C14
6-31+G* / def2tzvp (Re)
E: -3636.2638399
```
 7      2.065460  -0.751294  -0.347532
 6      3.108481   0.118548  -0.212530
 6      2.595293   1.392023  -0.178510
 7      1.250232   1.235064  -0.296470
 7      0.970053  -0.079715  -0.390683
 6      0.187201   2.156584  -0.295406
 7     -1.030110   1.602079  -0.358237
```

```
 6   -2.094981   2.420607  -0.361913
 6   -1.976655   3.799290  -0.308508
 6   -0.703464   4.359580  -0.247611
 6    0.406516   3.526510  -0.246701
75   -1.136716  -0.625232  -0.253221
 6   -3.025923  -0.832651   0.011444
 8   -4.170496  -0.916988   0.163859
 6    4.526663  -0.378271  -0.100047
 6    5.487334   0.808707   0.042009
 6    4.875808  -1.187585  -1.361686
 6    4.624794  -1.282854   1.142512
35   -0.695912  -0.123083   2.297311
 6   -1.370196  -0.858731  -2.132102
 8   -1.518337  -0.995068  -3.276734
 6   -0.916206  -2.527240  -0.044150
 8   -0.760132  -3.664013   0.076685
 1    1.409886   3.931862  -0.199234
 1   -0.572070   5.435574  -0.200339
 1   -2.867943   4.415818  -0.308499
 1   -3.061678   1.933391  -0.403355
 1    4.185552  -2.026938  -1.490112
 1    5.892748  -1.587286  -1.277673
 1    5.644446  -1.672681   1.240683
 1    4.826094  -0.561576  -2.260171
 1    3.936213  -2.129533   1.064458
 1    4.377554  -0.728765   2.054731
 1    5.270321   1.395637   0.942968
 1    5.441747   1.473429  -0.829739
 1    6.516398   0.443995   0.126614
 1    3.065623   2.355908  -0.075443
```

Bibliography of Chapter 5.1

(1)   Bruker (2010). APEX2, SAINT, SADABS and XSHELL. Bruker AXS Inc., Madison, Wisconsin, USA.

(2)   Sheldrick, G. M. *Acta Cryst.* **2008**, *A64*, 112.

(3)   Spek, A. L. *Acta Cryst.* **2009**, *D65* (2), 148.

(4)   Frisch, M. J.; Trucks, G. W.; Schlegel, H. B.; Scuseria, G. E.; Robb, M. A.; Cheeseman, J. R.; Scalmani, G.; Barone, V.; Mennucci, B.; Petersson, G. A.; Nakatsuji, H.; Caricato, M.; Li, X.; Hratchian, H. P.; Izmaylov, A. F.; Bloino, J.; Zheng, G.; Sonnenberg, J. L.; Hada, M.; Ehara, M.; Toyota, K.; Fukuda, R.; Hasegawa, J.; Ishida, M.; Nakajima, T.; Honda, Y.; Kitao, O.; Nakai, H.; Vreven, T.; Montgomery, J. A.; Peralta, J. E., J.; Ogliaro, F.; Bearpark, M.; Heyd, J. J.; Brothers, E.; Kudin, K. N.; Staroverov, V. N.; Keith, T.; Kobayashi, R.; Normand, J.; Raghavachari, K.; Rendell, A.; Burant, J. C.; Iyengar, S. S.; Tomasi, J.; Cossi, M.; Rega, N.; Millam, J. M.; Klene, M.; Knox, J. E.; Cross, J. B.; Bakken, V.; Adamo, C.; Jaramillo, J.; Gomperts, R.; Stratmann, R. E.; Yazyev, O.; Austin, A. J.; Cammi, R.; Pomelli, C.; Ochterski, J. W.; Martin, R. L.; Morokuma, K.; Zakrzewski, V. G.; Voth, G. A.; Salvador, P.; Dannenberg, J. J.; Dapprich, S.; Daniels, A. D.; Farkas, O.; Foresman, J. B.; Ortiz, J. V.; Cioslowski, J.; Fox, D. J. *Gaussian, Inc., Wallingford CT*. 2010,.

(5)   Chai, J.-D.; Head-Gordon, M. *Phys. Chem. Chem. Phys.* **2008**, *10*, 6615.

(6)   Schaftenaar, G.; Noordik, J. H. *J. Comput. Aided Mol. Des.* **2000**, *14* (2), 123.

Der Lebenslauf ist in der Online-Version aus Gründen des Datenschutzes nicht enthalten.

For reasons of data protection, the curriculum vitae is not published in the electronic version.

Der Lebenslauf ist in der Online-Version aus Gründen des Datenschutzes nicht enthalten.

For reasons of data protection, the curriculum vitae is not published in the electronic version.

Der Lebenslauf ist in der Online-Version aus Gründen des
Datenschutzes nicht enthalten.

For reasons of data protection, the curriculum vitae is not
published in the electronic version.